



City Research Online

City, University of London Institutional Repository

Citation: Patel, Z (2019). Development of an intraluminal photoplethysmography sensor for the assessment of bowel viability. (Unpublished Doctoral thesis, City, University of London)

This is the accepted version of the paper.

This version of the publication may differ from the final published version.

Permanent repository link: <https://openaccess.city.ac.uk/id/eprint/23776/>

Link to published version:

Copyright: City Research Online aims to make research outputs of City, University of London available to a wider audience. Copyright and Moral Rights remain with the author(s) and/or copyright holders. URLs from City Research Online may be freely distributed and linked to.

Reuse: Copies of full items can be used for personal research or study, educational, or not-for-profit purposes without prior permission or charge. Provided that the authors, title and full bibliographic details are credited, a hyperlink and/or URL is given for the original metadata page and the content is not changed in any way.

City Research Online:

<http://openaccess.city.ac.uk/>

publications@city.ac.uk

Development of an intraluminal photoplethysmography sensor for the assessment of bowel viability



Zaibaa Patel

Supervisor: Professor Panicos Kyriacou

School of Mathematics, Computer Science and Engineering
Research Centre for Biomedical Engineering

This dissertation is submitted for the degree of
Doctor of Philosophy

City, University of London

27th September 2019

*One life I'm going to live it up.
"I'm takin", I said, "I'll never get enough".
Stand tall. I'm young and kind of proud.
I'm on top, but as long as [you are around].*

Rob Halford & Glenn Tipton, "You've got another thing comin'"
Judas Priest (Screaming for Vengeance)

Table of contents

List of figures	ix
List of tables	xiii
Notations & Symbols	xxi
1 Introduction	1
1.1 Overview	1
1.2 Motivation and relevance	1
1.3 Aim and objectives	2
1.4 Contributions	3
1.5 Outline and thesis structure	4
2 Gastro-intestinal tract: Anatomy, physiology and pathology	7
2.1 Overview of the gastrointestinal anatomy	7
2.2 Anatomy and physiology of the large intestine	8
2.3 Colorectal vascular supply	11
2.4 Colorectal ischaemia	15
2.5 Colorectal cancer	16
2.6 Summary	21
3 Current state of the art for assessing intestinal viability	23
3.1 Mechanical patency	25
3.2 Tonometry	36
3.3 Imaging modalities	44
3.4 Optical	58
3.5 Summary	73

Table of contents

4	Photoplethysmography and pulse oximetry	75
4.1	Principles of light-tissue interaction	76
4.2	Principles of photoplethysmography	80
4.3	Principles of pulse oximetry	85
4.4	Summary	88
5	Assessing light-tissue interactions using Monte Carlo simulations	89
5.1	Principles of Monte Carlo modelling for light-tissue interactions	90
5.2	Development of multi-layer colon model	96
5.3	Modelling the effects of colonic perfusion states and light propagation	105
5.4	Modelling the effects of sensor-tissue distance and light propagation	110
5.5	Summary	115
6	Design and development of the intraluminal PPG system	117
6.1	Specifications of the intraluminal PPG sensor	118
6.2	Electrical design of the intraluminal sensor	120
6.3	Intraluminal PPG sensor casing	121
6.4	Reflectance finger PPG sensor	125
6.5	Specifications of the processing system	126
6.6	Instrumentation unit	127
6.7	Data acquisition, control and user interface	128
6.8	Data processing	132
6.9	Summary	142
7	Evaluation of the reflectance PPG system	143
7.1	Hardware and software integration	144
7.2	<i>In-vitro</i> and <i>in-vivo</i> thermal testing	146
7.3	Validation of acquiring photoplethysmography signals	148
7.4	Summary	155
8	The effects of optical sensor-tissue separation	157
8.1	Materials and methods	158
8.2	Data analysis and statistics	161
8.3	Summary	172

9	Clinical evaluation on healthy tissue regions within the colorectum	173
9.1	Materials and methods	174
9.2	Data analysis and statistics	178
9.3	Summary	189
10	Discussion	191
11	Conclusions and future work	201
11.1	Major contributions	201
11.2	Major conclusions	202
11.3	Limitations	204
11.4	Suggestions for further research	205
	References	207
	Appendix A Instrumentation unit and data acquisition	231
A.1	Instrumentation unit	231
A.2	Data acquisition, control and user interface	237
	Appendix B Access for research documentation	241
	Appendix C Clinical physics documentation	245
	Appendix D Health Research Authority (HRA) documentation	261
	Appendix E Clinical trial approval and protocol	269

List of figures

1.1	Graphical representation of the outline and thesis structure.	4
2.1	Macroscopic and microscopic anatomy of the large intestine.	9
2.2	Overview of arterial and venous circulation of the large intestine.	12
2.3	Cross section microvascular of the human rectum.	13
2.4	Progression of blood vessel from artery to capillaries.	14
2.5	Pathway of cancer spreading and the percentage of cancer occurrence.	17
2.6	Types of bowel resections.	18
2.7	Types of anastomosis joining and the process of angiogenesis.	20
3.1	Taxonomy of techniques assessing bowel tissue viability.	24
3.2	Example of colour change of bowel.	26
3.3	Principle of arterial pulsation.	27
3.4	Principle of bowel wall contractility.	28
3.5	Electronic contractility meter applied to the bowel.	29
3.6	Air leak test within the lumen of the bowel.	31
3.7	Example of the Doppler effect.	33
3.8	Doppler Ultrasound applied on the bowel.	34
3.9	Principle of a modified Clark electrode.	37
3.10	Principle of gastric tonometry.	40
3.11	Principle and geometries of microdialysis.	43
3.12	Principle of fluorescence.	46
3.13	Visibility of fluorescein dye in intestine.	47
3.14	Quantifying fluorescence imaging.	49
3.15	Difference between single photon and multi-photon excitation.	50
3.16	Principle of sidestream dark-field imaging.	53
3.17	Parts and accessories of a colonoscope.	56

List of figures

3.18	Process of C-reactive protein binding to bacteria.	59
3.19	Set-up for nephelometry and turbidimetry	60
3.20	Schematic diagram of Laser Doppler flowmetry.	62
3.21	Principle of flow cytometry.	65
3.22	Understanding the measurement of oxygen saturation.	70
3.23	Types of photoplethysmography configurations.	70
3.24	Pulsatile signal arising from the change in the artery vessel diameter.	71
3.25	Transanal pulse oximeter.	72
4.1	Reflection and refraction.	76
4.2	Optical path through a scattering and non-scattering medium.	79
4.3	Absorbed and transmitted light in biological tissue.	82
4.4	Components of a photoplethysmographic waveform.	83
4.5	Absorption coefficient spectra for oxyhaemoglobin and deoxyhaemoglobin.	86
5.1	Relationship between the Cartesian and polar co-ordinate systems.	90
5.2	Illustration of a photon undergoing a scattering event.	92
5.3	The steps of sampling a random variable.	93
5.4	Illustration of the geometry and tissue structure of the colorectum	97
5.5	Wavelength selection for the dual-wavelength intraluminal optical sensor.	98
5.6	2D illustration of an optical path in a reflectance geometry.	107
5.7	Light image in multi-layer colon model	108
5.8	Mean absorbance and weight within the colon.	109
5.9	Simplified representation of the source-tissue separation method.	111
5.10	Light image when varying the sensor-tissue separation.	113
5.11	Light image in tissue when varying the sensor-tissue separation.	114
5.12	Mean optical quantities within the colon.	115
6.1	Overall block diagram for the development of the sensors and processing system.	118
6.2	Illustration of the intraluminal sensor design.	119
6.3	Intraluminal reflectance sensor circuit board design.	122
6.4	Development of the intraluminal optical sensor.	123
6.5	Mechanical drawing of the modified intraluminal PPG sensor.	125
6.6	The modified intraluminal PPG sensor.	126
6.7	Detailed block diagram of the data acquisition, control and user interface.	128

6.8	Front panel of the virtual instrument.	130
6.9	Naming scheme for the data storage.	131
6.10	Format of stored data within a file.	132
6.11	Detailed block diagram of the offline analysis module.	132
6.12	Data columns required for offline signal analysis.	133
6.13	Short-time Fourier transforms on simulated PPG signals.	134
6.14	Signal extraction of raw PPG signals.	135
6.15	Graphical user interface of interval acquisition.	137
6.16	Process for amplitude measurements from a PPG recording.	138
6.17	Signal-to-noise ratio method for PPG signals.	139
6.18	Example of a Bland-Altman representation.	141
7.1	Results from altering the light emitter driving current.	145
7.2	<i>In-vitro</i> thermal evaluation set-up using a pig's intestine.	147
7.3	<i>In-vitro</i> thermal evaluation using a section of a pig's intestine.	149
7.4	<i>In-vivo</i> thermal evaluation on the buccal mucosa.	150
7.5	PPG pre-processing procedure.	152
7.6	Typical ac PPG signals from the buccal mucosa and finger.	153
8.1	Simplified representation of the signal acquisition method.	158
8.2	Adjustable distance apparatus achieving five separation distances.	159
8.3	Twenty seconds of typical infrared ac PPG traces from the buccal mucosa.	162
8.4	Twenty seconds of typical red ac PPG traces from the buccal mucosa.	163
8.5	Twenty seconds of typical infrared ac PPG traces from the finger.	164
8.6	Twenty seconds of typical red ac PPG traces from the finger.	165
8.7	Example of noisy signals from both wavelengths.	166
8.8	Overall mean of the ac PPG amplitudes from the mouth.	166
8.9	Overall mean of the ac PPG amplitudes from the finger.	167
8.10	Overall mean of the SNR for red and infrared at different sensor-tissue separations.	168
9.1	Illustration of measurement setup of the clinical pilot study.	174
9.2	Clinical trolley set-up.	175
9.3	Comparison of spectrogram of two studies.	179
9.4	Overview of all consented and exclusion studies.	180
9.5	Oxygen saturation represented as box plots.	182

List of figures

9.6	First reported colorectum PPG signals.	184
9.7	Overall mean of the ac PPG amplitudes at different depths within the colorectum.	185
9.8	Overall mean of the signal-to-noise ratio within the colorectum	186
9.9	Comparisons of oxygen saturation values from the intraluminal sensor and the commercial pulse oximeter.	187
A.1	Photographs of the instrumentation unit	232
A.2	Detailed block diagram of the instrumentation unit.	232
A.3	Functional diagram of the multiplexer module.	234
A.4	Functional diagram of the demultiplexer module.	235
A.5	Pin configuration for the D-Sub 9 connector.	236

List of tables

2.1	Postoperative signs and symptoms of anastomotic leakage.	21
5.1	Colon optical properties.	98
5.2	Optical parameters for model validation.	103
5.3	Total reflectance and total transmittance values.	104
5.4	Comparison of experimental results to the accepted validation results. .	105
5.5	Optical properties for blood.	106
5.6	Mean penetration depth and optical path of photons propagating through the colon.	109
6.1	Light source specifications for the intraluminal sensor.	120
6.2	Light detector specifications for the intraluminal sensor.	120
6.3	Definitions of statistical variables within the offline analysis module. . .	139
7.1	Voltage adjustments and the corresponding driving current.	144
7.2	Overall mean peak-to-peak amplitude and standard deviation.	153
7.3	Comparison of blood oxygen saturation.	154
8.1	Overall mean of blood oxygen saturation at each sensor-tissue separation.	168
8.2	One-way analysis of variance between the overall mean ac PPG signals.	169
9.1	Recruited patient statistics.	177
9.2	Overall mean of the SNR of excluded patients.	181
9.3	Overall mean of the blood oxygen saturation estimated at different depths within the colorectum.	183
9.4	One-way analysis of variance between the overall mean of ac PPG signals.	188
A.1	Pin configuration of the data acquisition card.	238

Acknowledgements

This work was carried out within the Research Centre for Biomedical Engineering (RCBE) at City, University of London, with the support of a PhD Studentship provided by City, University of London.

I am very grateful to my supervisor, Professor Panicos Kyriacou, for selecting me to receive the PhD Studentship. I am also grateful for his guidance, wisdom and support throughout my time as a student. Thank you for all the encouragement and opportunities for my work to reach a large audience.

I would like to thank Mr Mohammad Thaha at the Royal London Hospital for his generous support and assistance. The clinical trials could not have been possible without him and his surgical team. Special thanks are due to Ms. Arti Garg for recruiting the patients and Mr. Anthony Ramsanahie for his enthusiasm and co-operation whilst carrying out the studies. I would especially like to thank the patients who participated in the clinical trials for their invaluable contribution.

I would like to acknowledge all the members, academic and researchers of RCBE. José Alonso, James, Tomas, Michelle H, Subhasri, Michelle N, Ananda, Abdullah and Zaheer, other than support, you have all contributed to memorable moments.

I am grateful to have my group of friends like Ashish, Lauren and Harriett. I aspire to be enthusiastic about science and research like Radmila, Theodora and Theofanis. Thank you for appreciating and supporting my research, and for all the teaching experience and the stacks of marking!

Most importantly, I dedicate this thesis and achievements to my parents (A & B). I thank my mother for all the love, support, motivation, and most importantly, the delicious food and warm roti's I come home to. My father worked extremely hard for my education. His jokes, laughter and his unconditional love were always in mind - I know he is very proud. I also want to thank my sisters for their company and support. Finally, I want to thank José Alonso for being there, every step of the way. Thank you for all the fun, the adventures and simply being the amazing you. Thank you for everything; you are my best friend, my *ghost*.

Declaration

I hereby declare that the work presented in this thesis is my own work. Any idea, result, or illustration originating from other subject's work has been acknowledged in the text by referencing to the original author. This thesis has never been published or submitted elsewhere for obtaining an academic degree or professional qualification. This dissertation is my own work and contains nothing which is the outcome of work done in collaboration with others, except as specified in the text and Acknowledgements.

I grant power of discretion to the Librarian at City, University of London to allow the thesis to be copied in whole or in part without further reference. This permission covers only single copies made for study purposes, subject to normal conditions of acknowledgement.

Zaibaa Patel
27th September 2019

Abstract

Intestinal anastomotic complications that occur mainly due to ischaemia are a serious risk in colorectal cancer patients undergoing surgery. Surgeons continue to rely on subjective methods such as visual inspection, due to the lack of assessment tools. Continuously and quantitatively monitoring bowel viability is therefore essential to minimise postoperative complications, which are currently not being identified efficiently.

A novel intraluminal optical sensor and processing system, have been designed and developed to overcome the limitations in bowel viability assessments. Within the lumen of the colon, the sensor uses the techniques of photoplethysmography (PPG) and pulse oximetry (PO). Advanced Monte Carlo modelling was also utilised for a better understanding of the light-tissue interaction occurring within the lumen of the bowel. The sensor specifications were reinforced by *in-silico* evaluations of contact and non-contact geometries between the sensor and colon. Prior to clinical pilot studies, the sensor was evaluated in twenty healthy volunteers on the buccal mucosa, as a surrogate for the colon mucosa. Furthermore, *in-vivo* measurements were made in twenty patients prior to bowel resection surgeries.

The *in-silico* evaluations revealed, for the first time, the behaviour of photons within the colon. Contact and non-contact modelling have shown that photons penetrated no further than the muscularis layer, where a large detection of photons could still be achieved in a non-contact instance. These results correlated with the *in-vivo* study within the buccal mucosa. Non-contact distances up to 5 mm were the most optimal, producing signals of high quality with a maximum signal-to-noise ratio (SNR) of 26 dB, resulting in reliable estimations of blood oxygen saturation (S_pO_2).

The first in-human colorectum results demonstrated the ability to continuously acquire good quality PPG signals at different depths with a SNR ranging between 30 dB and 37 dB. A multiple comparison of the colorectal S_pO_2 at each depth indicated no significant difference was found [ANOVA, $F = 0.43$, $p = 0.7847$ ($p < 0.05$)]. The intraluminal PPG sensor could be used as an assessment tool for bowel viability.

Notations & Symbols

General notation

A	Absorbance
ϕ	Azimuthal angle
$CDF_X(\cdot)$	Cumulative distribution function of variable X .
CO_2	Carbon dioxide
HHb	Deoxygenated haemoglobin or deoxyhaemoglobin
$\mu_{x,y,z}$	Directional cosines
$p_X(\cdot)$	Probability distribution of variable X .
DPF	Differential pathlength factor
G	Scattering factor
μ_a	Absorption coefficient
μ_s	Scattering coefficient
n_i	Incidence refractive index
n_t	Transmitted refractive index
OP	Optical pathlength
$\overline{M}_q \pm \overline{SD}_q$	Overall mean and standard deviation which is the mean of the means of a signal parameter of interest (q)
HbO_2	Oxygenated haemoglobin or oxyhaemoglobin

Notations & Symbols

P_aO_2	Arterial partial pressure of oxygen
PCO_2	Partial pressure of carbon dioxide
PD	Photon penetration depth
PO_2	Partial pressure of oxygen
P_tO_2	Partial pressure of tissue oxygen
R	Reflectance or reflected intensity
R_{OS}	Ratio of ratios
θ	Scatter angle
ϵ	Extinction coefficient
S_mO_2	Mucosal blood oxygen saturation
T	Transmittance or transmitted intensity
$totalHb$	Summation of oxygenated and deoxygenated haemoglobin
θ_i	Angle of incidence with respect to the normal
θ_r	Angle of reflection with respect to the normal
θ_t	Angle of refraction with respect to the normal
W	Photon weight detected
W_A	Photon weight absorbed
λ	Wavelength

Acronyms / Abbreviations

ac	Alternating component from a photoplethysmography waveform
dc	Relative constant component from a photoplethysmography waveform
AI	Analogue input

AL	Anastomotic leak
ANOVA	One-way analysis of variance
AO	Analogue output
ASA	American society of anaesthesiologists
BA	Bland Altman
CI	Colorectal ischaemia or colonic ischaemia
CRF	Case report form
CRP	C-reactive protein
DAQ	Data acquisition card
EMG	Electromyography
FA	Fluorescent angiography
FG	French gauge
GCP	Good clinical practice
GIT	Gastrointestinal tract
Hct	Haematocrit, proportion of red blood cells in total blood volume
HRA	Health research authority
ICG	Indocyanine green
IMA	Inferior mesenteric artery
IMV	Inferior mesenteric vein
IVM	Intravital microscopy
KS	Kolmogorov-Smirnov test
LDF	Laser Doppler flowmetry
LED	Light emitting diode

Notations & Symbols

LoA	Limits of agreement
L/P ratio	Lactate to pyruvate ratio
HG	Henyey-Greenstein
MC	Monte Carlo
MFI	Micro-vascular flow index
MPM	Multiphoton microscopy
NHS	National Health Service
NIR	Near infrared
PCB	Printed circuit board
PD	Photodetector
pHi	Gastric mucosal pH
PPV	Proportion of perfused villi
PVD	Perfused vessel density
RBC	Red blood cell
RCBE	Research centre for biomedical engineering
REC	Research ethics committee
RLH	Royal London Hospital
ROC	Receiver operating characteristic
SDF	Sidestream dark-field
SMA	Superior mesenteric artery
SNR	Signal-to-noise ratio
STFT	Short-time Fourier transforms, also known as spectrograms
STL	Stereolithography

TIVA	Total intravenous anaesthesia
TVD	Total vessel density
ui	User interface
U/S	Ultrasound
VI	Virtual instrument
VLS	Visible light spectroscopy
VR	Venous return
WBC	White blood cell
WLS	White light spectroscopy

List of publications

Journal publications:

- S. Chatterjee, **Z. Patel**, M. A. Thaha, and P. A. Kyriacou, ‘*In silico* and *In vivo* investigation of tissue viability monitoring using an endocavitary photoplethysmography sensor’, *Biomedical Optics Express*, (submitted).
- **Z. Patel**, M. A. Thaha, and P. A. Kyriacou, ‘The Effects of Optical Sensor-Tissue Separation in Endocavitary Photoplethysmography’, *Physiological Measurement*, vol. 39, no. 7, 2018.

Conference publications:

- **Z. Patel**, M. A. Thaha, and P. A. Kyriacou, ‘Can the Human Colorectum Give Adequate PPG signals for the Assessment of Bowel Viability Using an Indwelling Optical Sensor’, in *Biomedical Engineers, Medical Engineers and Bioengineers Conference (BioMedEng19)*, 2019.
- **Z. Patel**, S. Chatterjee, M. A. Thaha, and P. A. Kyriacou, ‘A Multilayer Monte Carlo Model for the Investigation of Optical Path and Penetration Depth at Different Perfusion States of the Colon’, in *Proceedings of the Annual International Conference of the IEEE Engineering in Medicine and Biology Society (EMBC 2019)*, 2019.
- **Z. Patel**, M. A. Thaha, and P. A. Kyriacou, ‘Development of an Intraluminal Intestinal Photoplethysmography Sensor’, in *Proceedings of the Annual International Conference of the IEEE Engineering in Medicine and Biology Society (EMBC 2017)*, 2017, pp. 1840-1843.

Chapter 1

Introduction

1.1 Overview

The large bowel or large intestine, composed of the colon and rectum, colorectum (CR), holds important functions within the gastrointestinal tract, such as processing indigestible food and absorbing water and vitamins back into the body [1]. The function and survival of the bowel, also known as bowel viability, is dependent on a continuous blood supply. In various diseases, the CR blood supply is the first to be compromised, due to a variable extent of systemic illnesses and is commonly triggered by the fight or flight response. Sudden reductions of the blood supply, known as colon ischaemia, result in the dysfunction of the bowel. This consequently leads to significant medical complications and an impairment to an individuals' quality of life [2].

1.2 Motivation and relevance

Colorectal cancer (CRC) is the fourth most common cause of cancer death in the UK [3]. Surgery for CRC is the only curative treatment which often involves excision of the tumour bearing intestine followed by an intestinal anastomosis to restore intestinal continuity. The blood supply to the CR is a major contributing factor in the most feared complication of CRC surgeries. In 2–10% of patients, anastomotic failure occurs due to colon ischaemia and inadequate vascularity surrounding the anastomosis [4]. The blood supply to the anastomosis is one factor that surgeons have some influence over. Early diagnosis of colon ischaemia would be the key to a successful outcome, due to supportive measures and timely interventions.

The problem Despite the clinical awareness, identifying colon ischaemia is often observed late. The current gold standards to assess the adequacy of bowel viability intraoperatively are based on visual inspections of the colour, arterial pulsation and the presence of peristalsis [5]. There are no advancements in monitoring and identifying early signs of colon ischaemia in the past 50 years. Attempted techniques such as oxygen tension [6], fluorescence [7] and laser Doppler flowmetry [8] have not been adopted into mainstream clinical practice and have remained as research tools. Significantly, none of the techniques allow continuous monitoring of bowel viability, especially in the postoperative period [2]. Additionally, most techniques are operator dependent, resulting in inter-observer inconsistency and unreliable technological performance. To increase the rate of survival and success of CRC surgeries following a resection, there is an urgent need for a routine monitoring technique to aid clinicians in the assessment of bowel viability. The monitoring technique should aim to provide continuous, quantitative measurements and enabling the tool to be used both intraoperatively and postoperatively.

1.3 Aim and objectives

The aim of this thesis is to develop an intraluminal optical sensor that can be used to continuously monitor bowel tissue viability. The proposal is to utilise the techniques of photoplethysmography (PPG) and pulse oximetry (PO), to obtain blood oxygen saturation (S_pO_2) within the inner walls of the colorectum. The proposed technique could aid as an additional clinical tool for the assessment of bowel tissue viability. To achieve the aim, the objectives are the following:

1. Design and develop an intraluminal, two wavelength, reflectance PPG sensor for the colorectum. In addition, develop the instrumentation unit for acquiring the PPG signals and the relevant packages for the processing and analysis of the signals obtained.
2. Develop a computational optical model simulating the colon to facilitate in the understanding of light-tissue interactions whilst using an intraluminal reflectance optical sensor.
3. Perform *in-vitro* and *in-vivo* technical feasibility studies for the evaluation of the intraluminal PPG system. This includes studies validating the system's

safety and capability of providing S_pO_2 values, by comparing to a commercial PO device.

4. Perform *in-vivo* investigations on healthy volunteers to acquire PPG signals within a surrogate environment, closely resembling the colorectum tissue properties.
5. Conduct an *in-vivo* clinical pilot study on healthy regions of the colorectum, in patients before undergoing a colorectal cancer surgery. This is to evaluate the intraluminal PPG system in a clinical setting and demonstrate the possibility of using such a method to aid with continuous quantitative monitoring of the bowel tissue viability.

1.4 Contributions

The original contributions of this thesis are:

1. Development of the first custom-made, intraluminal reflectance PPG sensor, incorporating a co-contributed sensor instrumentation. In addition, an online and semi-automated offline signal analyser was programmed. All modules combined creates a system which has the capability of interrogating the colorectum for real-time, continuous measurements of bowel tissue viability.
2. Model the colorectum and intraluminal PPG sensor through computational simulations to understand the possible light-tissue interactions. This includes *in-silico* evaluations during contact and non-contact geometries between the sensor and colorectum tissue.
3. Demonstrate the feasibility of acquiring PPG signals within the walls of the colorectum by leading the clinical pilot study and to enable the estimation of S_pO_2 .

1.5 Outline and thesis structure

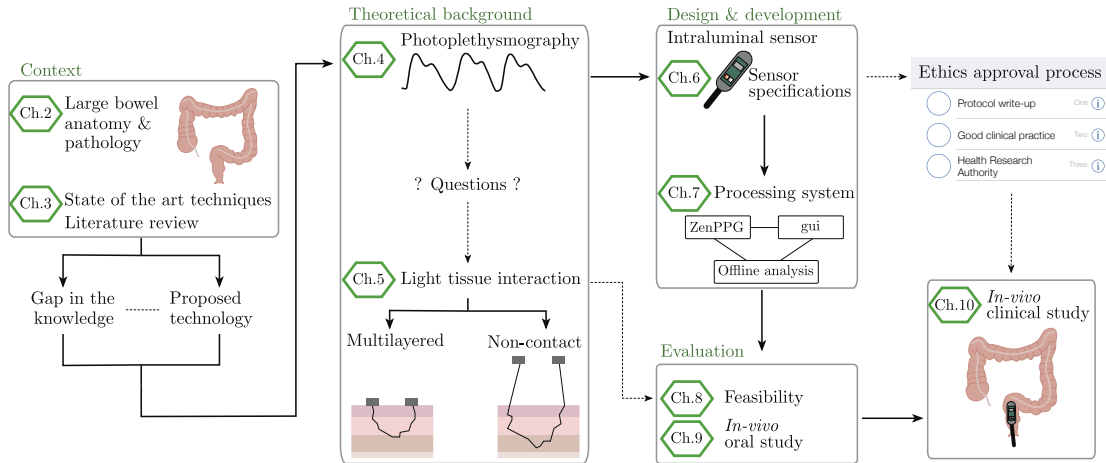


Figure 1.1 Graphical representation of the outline and thesis structure.

Chapter 2 The anatomy and physiology of the intestine will be introduced, where the main research area focuses on the large intestine, consisting of the colon and rectum. Pathologies commonly occurring within the colorectum will be presented, such as colon ischaemia and colorectal cancer. The chapter aims to provide context to readers about the research area and understand the normal and abnormal physiology.

Chapter 3 A review of attempted techniques used for assessing bowel tissue viability will be presented. The chapter aims to provide an overview of the current state of the art and techniques used in both research and clinical settings. The chapter provides context to readers about the working principle of each technique, their application within the colorectum and the limitations.

Chapter 4 Once understanding the gap in the knowledge, theoretical background on photoplethysmography will be presented. As photoplethysmography (PPG) is the proposed technique to aid in monitoring bowel viability, the aim of the chapter is to provide readers a detailed description on the principles of PPG and its application in pulse oximetry.

Chapter 5 The principles of light-tissue interaction, followed by computational modelling of the colon will be presented. Modelling of a multi-layered colon with the use of Monte Carlo simulations will be presented, where light-tissue interactions will

be evaluated during contact and non-contact geometries between the proposed sensor and tissue. The aim of this chapter is to provide readers a further understanding on how PPG can be obtained within the colon.

Chapter 6 The design and development of the intraluminal photoplethysmography sensor and PPG processing system will be presented. The proposed sensor consists of electronic components, encapsulated in a sensor casing; all which will be presented. The aim of this chapter is to justify the design specifications of the custom-made sensor and include the manufacturing process. The development of the PPG processing system will allow the acquisition of PPG signals from the developed sensor and process the signals through hardware and software. The processing system consists of three modules: (i) the instrumentation unit, (ii) the graphical user interface (gui) and (iii) a semi-automated offline signal analyser. The aim of this chapter is to explain the working principle of each module and the development process.

Chapter 7 Feasibility studies for the performance of the intraluminal sensor and the PPG processing system will be presented. *In-vitro* and *in-vivo* technical evaluations such as thermal emission will be presented. The aim of this chapter is to evaluate the sensor and the processing system's performance and safety.

Chapter 8 An *in-vivo* investigation on the effects of variable distances between the sensor and tissue surface to the quality of signals will be presented. The investigation is an extension to the work presented in Chapter 5, thus the aim of this chapter is to relate the *in-silico* evaluations to an *in-vivo* environment.

Chapter 9 The first *in-vivo* clinical study using a custom-made intraluminal PPG sensor will be presented. The aim of this chapter is to assess the feasibility in acquiring adequate signals within the lumen of a healthy colorectum. The study is conducted on twenty colorectal cancer patients at the Royal London Hospital, prior to a bowel resection and away from the surgical site.

Chapter 10 and 11 The thesis will be concluded by discussing the main findings from all investigations performed, the limitations and the suggestions for future work.

Chapter 2

Gastro-intestinal tract: Anatomy, physiology and pathology

In this chapter, the anatomy and physiology of the gastrointestinal tract (GIT) will be presented, where the lower GIT is the key focus. As the main research area focuses on the large intestine, consisting of the colon and rectum, this region will be discussed in further detail. Pathologies commonly occurring within the colorectum such as colon ischaemia and colorectal cancer (CRC) will be presented.

Motivation The anatomical physiology of the large intestine must be well understood to successfully develop a tool in monitoring tissue viability. Thus, the structure of the large intestine, the tissue layers and the blood supply should be reviewed. The chapter aims to provide context to readers about the large intestine and understand the normal and abnormal physiology.

2.1 Overview of the gastrointestinal anatomy

The bowel, or intestine, is part of the digestive system, including all structures beginning from the mouth, through the oesophagus and the stomach. This continuous pathway is known as the GIT which is a long, muscular tube, having an approximate length of 9 m for an adult [9]. Controlled by the autonomous nervous system, each specialised organ is functioned to breakdown food, extract useful components from the food by absorption and excrete waste products [9]. The lower GIT is the main region of interest, therefore discussed further in the remainder of this chapter.

The intestine consists of two subdivisions: (i) the small intestine and (ii) the large intestine. The small intestine has an average length of 7 m, responsible for breakdown and absorption of nutrients that are needed for the body [10].

2.2 Anatomy and physiology of the large intestine

As a continuation from the small bowel, the distal end of the GIT is the large intestine, also known as the colon. Unlike the small intestine, the large intestine has a shorter length of approximately 1.5 m, making up one-fifth of the length of the GIT [1]. The large intestine is responsible for processing the remaining food after most nutrients are absorbed by the small intestine. The remaining food is the indigestible watery material known as chyme, where the large intestine performs the essential role of absorbing water, vitamins and electrolytes from the waste material, before being excreted [1]. Below is a summary of the four major functions of the colon.

(i) Movement The large intestinal wall is made up of multiple layers, which will be discussed further in Section 2.2.2. The intestinal wall includes a muscular layer which contributes to the motility of the colon. There are two types of motility: (i) haustral contraction and (ii) mass movement. As the name suggests, haustral contraction occurs within small sacs, known as the haustrums, which gives a visual appearance of segmented sections of the colon due to the arrangement of the muscle fibres supporting the colon [11, 12]. Haustral contractions initiate with the presence of chyme, allowing the water residue to mix and move from one haustra to the next; resulting in the formation of soft, manageable faeces [1]. Mass movements are stronger contractions allowing the chyme to move towards the rectum quickly, to be excreted.

(ii) Productions and absorption of vitamins With the presence of bacteria, digestion continues in the large bowel, where indigestible compounds are broken down. Through the process of fermentation, various gases and vitamins are released, where vitamins such as K and B are absorbed into the blood.

(iii) Absorption of water and electrolytes Water absorption takes place via osmosis, based on the osmotic gradient created by the electrolytes. Electrolytes such as sodium (Na^+) is actively absorbed through sodium channels. Additional electrolytes such as Chloride (Cl^-) and Potassium (K^+) are also absorbed.

2.2 Anatomy and physiology of the large intestine

(iv) **Defecation** Once absorption no longer occurs, the remaining indigestible material, known as faeces, reaches the rectum. A defecation reflex is initiated which causes the faeces to exit the body via the back passage known as the anus.

2.2.1 Macroscopic intestinal anatomy

The large intestine is divided into five structural sections, which begins at the terminal ileum of the small intestine. Beginning with the ascending colon till the rectum, each structural section will be summarised and visually presented in Figure 2.1(a).

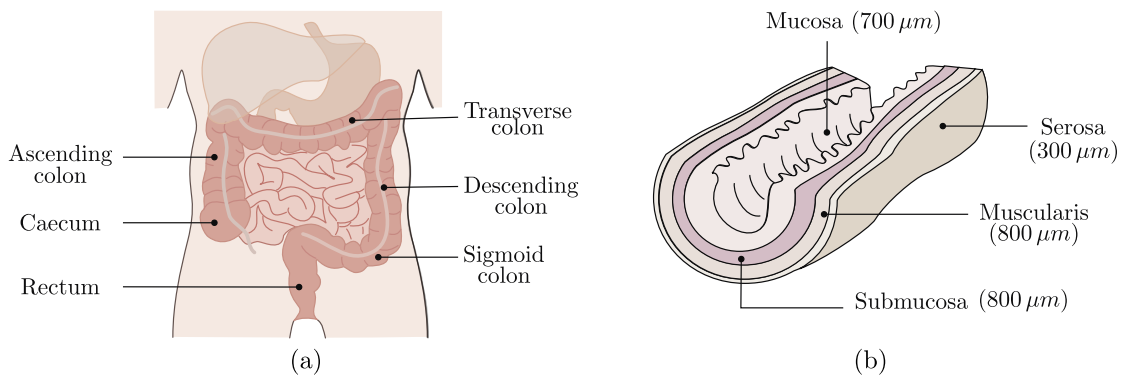


Figure 2.1 Macroscopic and microscopic anatomy of the large intestine. (a) illustrates macroscopic structure of the large intestine, whilst indicating the regions of the large intestine, starting from the caecum and ending at the rectum. (b) illustrates the microscopic structure of the large intestine, specifying the tissue layers and their corresponding thickness.

(i) **Ascending colon** Beginning with the caecum and including the appendix, the ascending colon runs on the right side of the abdomen. Identified as the widest structure and entrance to the large bowel, the main function is to control the chyme entering [12].

(ii) **Transverse colon** The longest section of the large intestine runs horizontally across the abdomen. The main function is to absorb fluid and salts.

(iii) **Descending colon** Parallel to the ascending colon, the descending colon allows the waste to travel down towards the sigmoid colon. The descending colon allows a slow movement of the chyme via haustral contractions, to allow the formation of manageable faeces.

(iv) **Sigmoid colon** Linking the descending colon to the rectum, the sigmoid colon is characteristically identified by its S-shaped loop [9]. With an approximate length of 40 cm, the function of the slow movement of chyme is shared between the descending and sigmoid colon [9].

(v) **Rectum** In conjunction with the anus, which is the external opening of the rectum, the rectum is approximately 15 cm long [9]. The main function is to temporarily store the faeces, from twelve to twenty-four hours, until the defecation reflex is initiated.

The large intestine is distinguishable from the small intestine by the macroscopic structures [13]. This includes the omental appendices, haustra and the teniae coli. The omental appendices are small sacs of adipose tissue mostly found on the transverse and sigmoid colon, are small sacs of peritoneum filled with adipose tissue. The sacs are attached to the surfaces of the two regions of the colon. The teniae coli are smooth muscles orientated longitudinally on the extraluminal region of the large bowel [14, 9]. Previously mentioned in Section 2.2, the haustra aids in the function of mechanical movement. Due to the teniae coli contracting to shorten the wall of the bowel, small sacs are formed known as haustrums [9]. Additionally, the haustral contractions allows the water residue to mix and move from one haustra to the next; resulting in the formation of faeces to occur slowly, producing soft and manageable stool [11, 12].

2.2.2 Microscopic intestinal anatomy

Looking closer to the anatomy of the large colon, there are four layers forming the intestinal wall. Beginning with the mucosa, which is the inner most layer with respect to the lumen of the colon, this section summarises each layer of the colon till the outer layer which is visible when the abdomen is open. Figure 2.1(b), presents each layer of the colon, including their thickness.

Mucosa The innermost layer of the colon which is divided into three sub-layers: (i) epithelial lining, (ii) lamina propria and (iii) muscularis mucosae. With the epithelial lining being the innermost surface with respect to the lumen of the colon, the lamina propria is a loose connective tissue rich in blood and lymph vessels. The muscularis mucosae consists of a thin inner circular layer and outer longitudinal layer of smooth muscle cells separating the mucosa from the second major layer called the submucosa.

Submucosa This layer is made of connective tissue, with a dense network of blood and lymph vessels and submucosal nerve plexus.

Muscularis The layer contains the myenteric nerve plexus and two sublayers of smooth muscle cells, defined as internal and external sublayers. The internal layer, close to the lumen, orientates its smooth muscles circular. In comparison to the external sublayer, the smooth muscle is orientated longitudinally.

Serosa The final outermost layer is a squamous epithelium layer, which has a thin layer of loose connective tissue and vessels.

2.3 Colorectal vascular supply

The importance of the knowledge of the colonic vascular anatomy cannot be overstated [15]. Referring to the arteries which supply the oxygenated blood to areas of the body, the descending aorta passes blood to the abdominal aorta. The blood supplied to all the abdominal GIT organs is the splanchnic circulation, whereas the mesenteric circulation refers to the intestinal portion, which receives one-quarter of the cardiac output at rest. As the colorectum (CR) region of the large intestine is of interest, which is the lower end of the GIT where the descending, sigmoid colon and rectum join, the mesenteric circulation will be discussed further in this section.

Superior and inferior mesentery artery Within the mesenteric circulation, the main arteries supplying the colon are the superior mesenteric artery (SMA) and the inferior mesenteric artery (IMA) [13]. Both arteries are distinguishable based on their internal diameters, where SMA is 1 cm in diameter and IMA is 0.5 cm [9]. Two-thirds of the transverse colon is supplied by branches of the SMA, whereas the descending colon receives oxygenated blood from the IMA. More specifically, the arteries supplying the CR are derived from the left colic artery and sigmoid branches as shown in Figure 2.2. In order to communicate between the SMA and IMA, the main arteries branch repeatedly and anastomose to form an additional artery known as the marginal artery. The marginal artery runs parallel to the outer surface of the bowel wall which forms a continuous arterial loop [13].

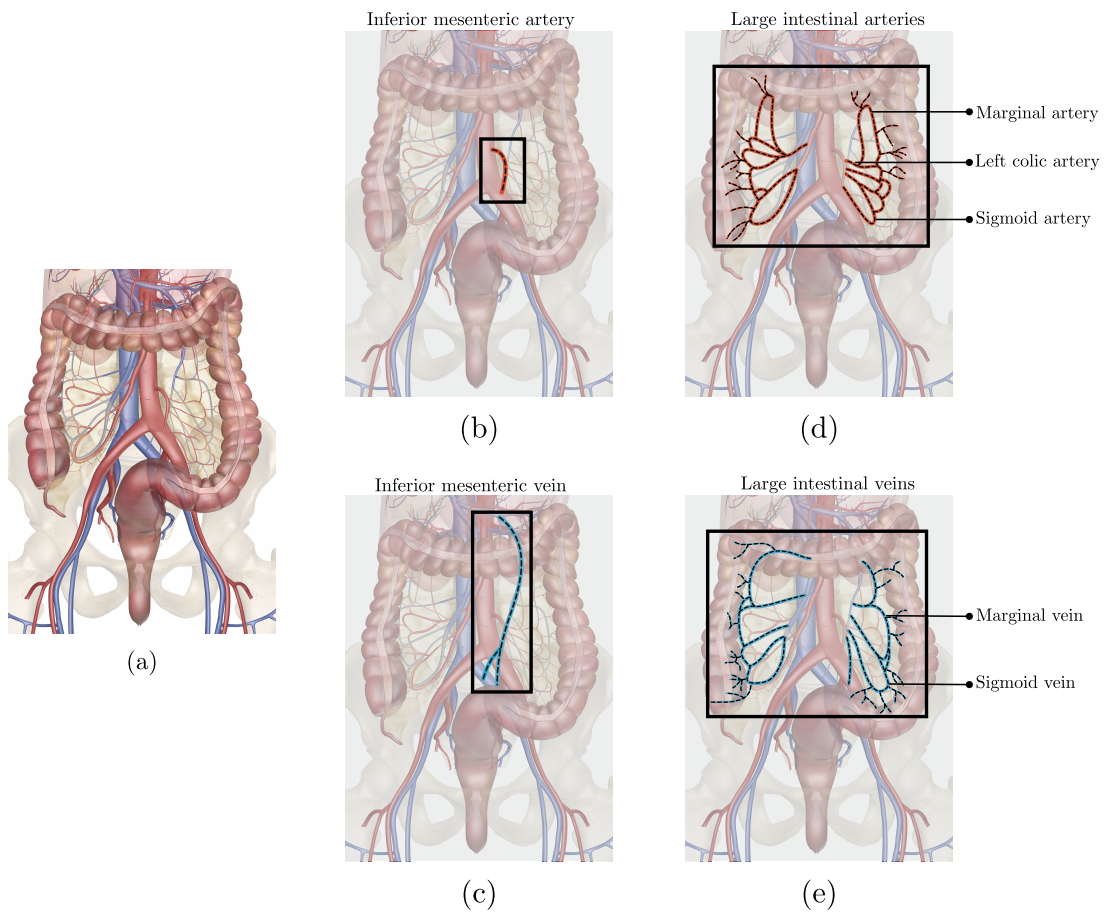


Figure 2.2 Overview of arterial and venous circulation of the large intestine illustrated in (a). Important regions of the circulation have been highlighted and encased a bold black box for easier visualisation where, (b) is the inferior mesenteric artery supplying oxygenated blood to the left side of the large intestine; (c) is the inferior mesenteric vein collecting deoxygenated blood; (d) are the intestinal arteries supplying oxygenated blood to the left side of the intestine, with three major arteries called the marginal, left colic and sigmoid artery; (e) are the intestinal veins removing deoxygenated blood.

2.3 Colorectal vascular supply

Arterioles and capillaries Penetrating the bowel wall, arterioles, which have an approximate diameter ranging between $5\mu\text{m}$ to $10\mu\text{m}$ [16], are found within the muscular and submucosal layers of the colon. There are several arteriole branches which anastomose to ensure the evenness of blood flow to reduce the risk of regional reduction of blood flow, also known as hypoperfusion or ischaemia [9]. As shown in Figure 2.3(a), arterioles progress into extensive networks of capillaries, found within the mucosal layer. At the end of the arterioles, precapillary sphincters regulate the blood flow through the capillaries [9, 17]. Capillaries are thin walled and lack smooth muscles to allow efficient exchange of gases, nutrients and waste products within the tissue [18]. Referring to Figure 2.3(b), the drainage of the capillaries occurs within the venules at the luminal surface of the mucosa which passes into the submucosa veins. Figure 2.4 can be visualised as a simplified illustration of the progression of blood vessels starting from the outer layer of the intestine, to the inner layer of the intestine.

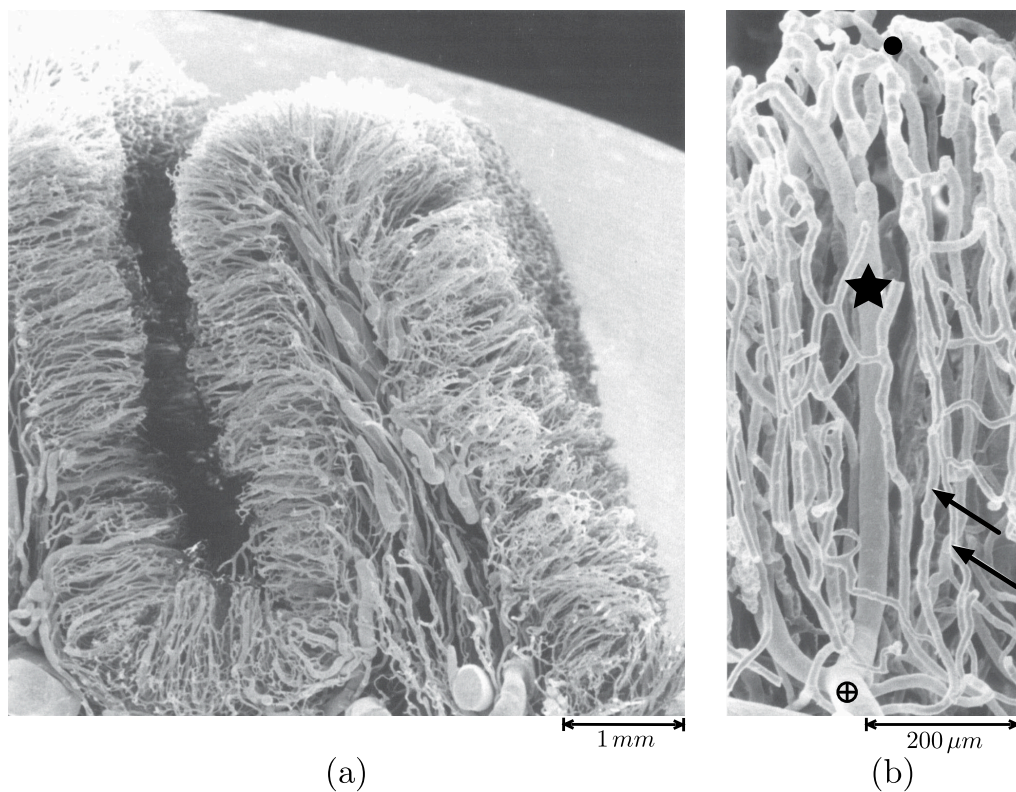


Figure 2.3 Cross section microvascular of the human rectum. Arteries and veins from the muscularis and microvessels within (a) mucosa and (b) submucosa are presented. Within the submucosa (b), the arrows indicate the arterioles whom supply the mucosal capillary network (●). The capillaries drain into venules (★) at the luminal surface of the mucosa which then pass to the submucosal veins (⊕) [17].

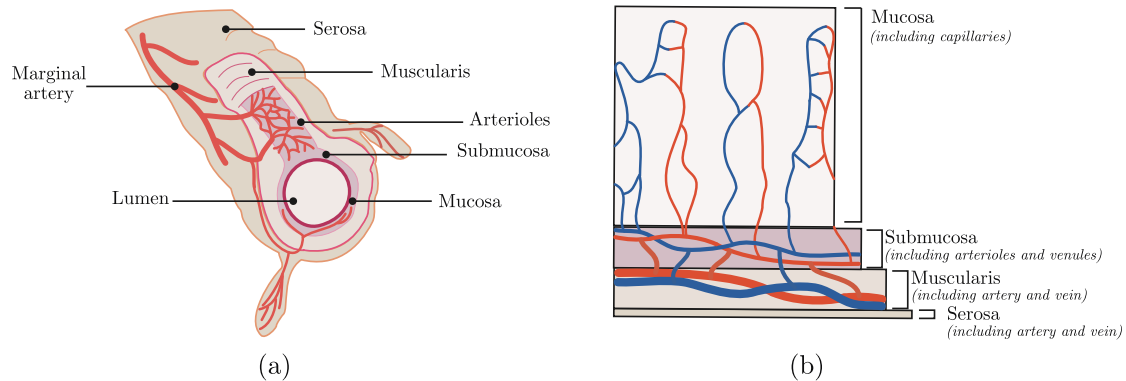


Figure 2.4 Progression of blood vessel from artery to capillaries surrounding and entering the large intestine is illustrated in (a). Internal tissue structures are illustrated to visualise the types of blood vessels within each of the four intestinal tissue layers.

Inferior mesentery vein Waste products including deoxygenated blood from the capillaries, drain through the venous circulation [13]. There are two routes where the deoxygenated blood is drained: (i) the portal venous system and, (ii) the systemic venous system. The portal venous system transports venous blood enriched with nutrients, extracted from the digested food, to the liver for additional processing via the portal vein [9]. The systemic venous system returns blood from the CR region which follows a similar path of the arterial supply, where the inferior mesenteric vein (IMV) situates to the left of the IMA [19]. The IMV leads to the inferior vena cava, which transports the deoxygenated blood to the heart. The systemic blood pressure is maintained by the venous return (VR), where the heart can only circulate blood it receives. Therefore, if the VR decreases, the ventricular systole decreases as the cardiac muscle fibres do not extend, therefore resulting in a lower blood pressure [20]. Similar to the arteriole branches, venous branches have similar interlinks via vessel anastomosis to ensure the evenness of blood flow.

2.4 Colorectal ischaemia

The function and survival of the colon is dependent on a continuous blood supply. The marginal artery provides the availability of collateral blood flow. The mesenteric circulation has an extensive collateral network, where arterial branches anastomose. This is advantageous as the collateral communication allows the colon to remain viable when 1 – 3 main supplying arterial trunks are occluded [21]. However, if there is an inadequate collateral communication, the blood supply could be compromised, resulting in colorectal ischaemia, also known as colonic ischaemia (CI).

CI is defined as a sudden reduction in blood flow which is most apparent when two or more smaller arterial trunks are occluded. Prominent areas vulnerable to disastrous ischaemia occurs at the Griffiths' and Sudek's point, due to marginal artery defects. CI can occur during several stresses, such as exercise and pathological conditions including thrombosis and arterial embolism [21]. Arteriosclerotic occlusions within the IMA are the general causes of CI due to the small arterial calibre.

Severe reduction in blood flow or supply of oxygenated blood can have adverse effects on the gastrointestinal function, where structural and metabolic changes occur [21]. These changes are first visible through microscopic changes within the antimesenteric mucosal lining, being the furthest tissue layer from the supplying artery [22]. Following ischaemia, injury or necrosis of the mucosal wall can occur due to hypoxia, as there is a deficiency of oxygen reaching the tissues. As a result of tissue damage or death, neutrophils accumulate and numerous inflammatory substances. As a devastating consequence, the loss of mucosal barrier function results in bacterial translocation and endotoxin absorption into the portal blood. The release of bacteria and toxic by-products not only cause injury to the intestinal mucosa but can lead to multiple organ dysfunction [23].

Early clinical features of CI are non-specific, therefore the diagnosis is often delayed until full infarction has occurred, by which surgical intervention is severely delayed [23]. The CR typically has a lower blood flow compared to other parts of the GIT, due to the distribution of the collateral networks. For surgical procedures resulting in the formation of colonic anastomoses, where local vasculature is disrupted and re-joined, the healing process becomes vulnerable due to the poor blood supply. CI plays a major contributing factor for the success of CRC surgeries; therefore, the following section and research focuses in an area where assessing viability within the CR is crucial.

2.5 Colorectal cancer

Colorectal cancer (CRC) is the fourth most common cause of cancer death in the UK; where approximately 100 new cases every day are diagnosed [3]. CRC is a form of cancer which occurs within the large intestine; specifically the colon and rectum [24]. Like all types of cancer, CRC begins when tissue lining of the specific organ becomes abnormal and replicates uncontrollably, resulting in the formation of a cancerous tumour. If left untreated, the cancer could spread into the surrounding organs via the lymphatic or systemic circulation. As shown in Figure 2.5, cancer could potentially spread into the abdomen via the lymphatic system. In comparison, cancer commonly spreads to the liver via the systemic circulation as blood flows via the liver through the portal vein[3].

The CR is the main focus of this research, as a large population of cancer cases are diagnosed at the regions within the rectum and sigmoid colon, as shown in Figure 2.5. With reference to the gender, the proportion of cases occurring in the rectum and sigmoid colon are higher in men, 31.5 % and 23.1 %, compared to women, 23.1 % and 20.4 %, respectively.

There are various risk factors for CRC, where 54 % of CRC cases are linked to lifestyle [3]. There are a number of factors, one which has been addressed previously, gender; additionally, diet, obesity, alcohol and most commonly known, age [3]. Data suggests that there are a high incidence rate of CRC occurring in older men. For both genders, the average ages where individuals are diagnosed are aged 70 and above [3].

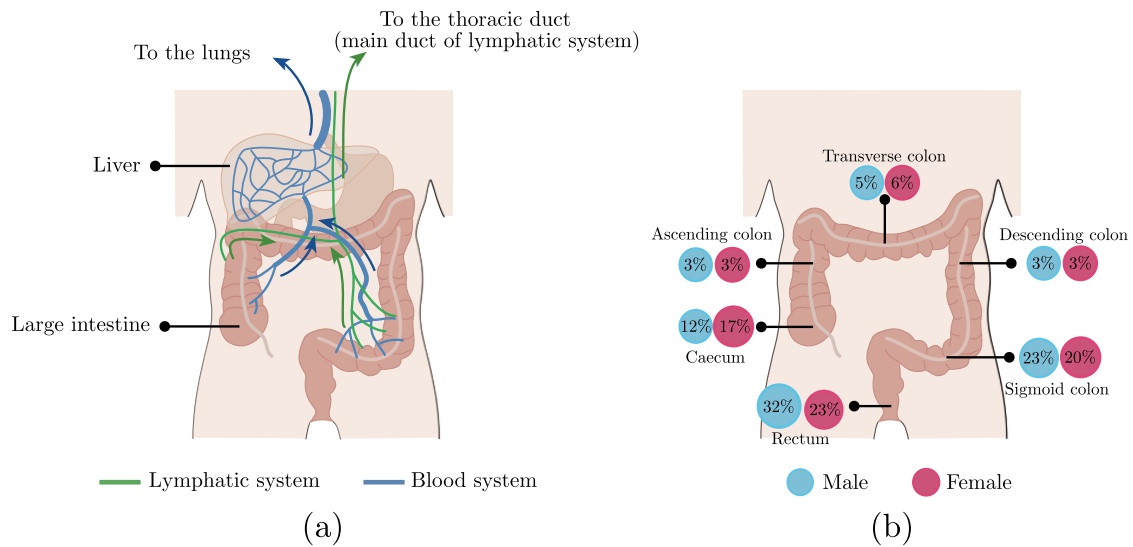


Figure 2.5 The pathway of cancer spreading and the percentage of cancer occurrence. (a) Untreated cancer may spread into the surrounding organs via lymphatic (green) or systemic blood circulation (blue) [3]. (b) The percentage distribution of cancer occurrence is illustrated and annotated based on the anatomical site. The percentages are based on the diagnosis within the UK and summarised by gender during 2010 – 2012 [3]. It is noticeable that cancer occurring in the colorectum, consisting of the sigmoid colon and rectum are highly diagnosed in men.

2.5.1 Surgical treatment for colorectal cancer

Depending on the type, size of the cancer and the general wellbeing of the individual, the appropriate type of treatment is chosen. There are several treatments including chemotherapy and radiotherapy, however, surgery remains the main curative treatment for CRC. The objective of curative surgery is to remove the tumour and re-join the bowel for continuous GIT functionality.

There are two types of surgery methods which can be undertaken during a bowel resection: (i) laparotomy, which is a long incision in the middle of the abdomen allowing open surgery and (ii) laparoscopy, which is a minimally invasive surgery requiring multiple keyhole incisions to allow the insertion of surgical tools. With advancing technologies, laparoscopic assisted resection of the bowel has become the most common technique. This is due to the faster restoration of the GIT function, reduction in postoperative pain and shorter lengths of hospital stay [25].

Patients undergoing an elective resection often undergo bowel preparation, either as an outpatient preparation or inpatient. Bowel cleansing is an important factor de-

ing the likelihood of septic complications and considered a high priority. Outpatient cleansing involves patients consuming liquids twenty-four hours before the surgery and/or provided a laxative. Inpatient cleansing involves a saline washout immediately before surgery. However, if patients experience complete obstruction or there are signs of perforation, mechanical bowel preparation are not to be followed.

With patients typically within the Lloyd-Davies position for simultaneous access to the abdomen and perineum, the tumour is removed with a minimal proximal and distal margin ranging between 2 cm to 5 cm [9]. Removal of the intestine is known as a colectomy, where a partial colectomy involves a section of the intestine to be removed depending on the location of the tumour as shown in Figure 2.6. Tumours within the cecum and ascending colon are treated by a right-hemicolectomy, where the ileocolic, right colic and right branch of the middle colic vessels are clamped or ligated to terminate blood flow within the operating region. An extended right-hemicolectomy involves the removal of tumours within the distal ascending colon and hepatic flexure, where the ileocolic, right colic, middle colic and ascending branch of the left colic vessels are ligated. Tumours within the descending and sigmoid colon are treated by a left-hemicolectomy, where the IMA is ligated.

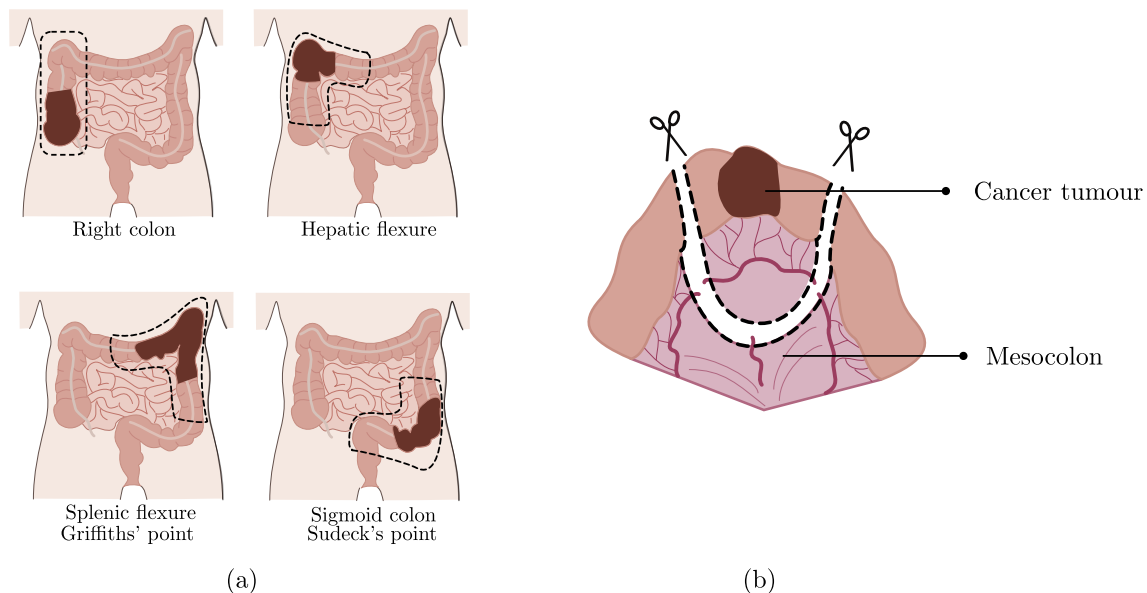


Figure 2.6 Types of bowel resections, where the dark regions represents a cancer tumour (a). The dotted lines corresponds to the suggested excision to remove the tumour. (b) illustrates the procedure to remove the cancerous section, through the cutting of either sides of the intestine, including the blood circulation. Once removed, the two healthy ends of the intestine would be joined to form an intestinal anastomosis.

Once the tumour has been removed, the remaining healthy ends of the bowel are joined together to form an anastomosis. The next section will explain the requirements for a successful anastomotic formation.

2.5.2 Anastomotic formation

An anastomosis restores the GIT continuity with complete avoidance of tension, avoidance of contamination and being well-vascularised. Anastomotic healing success is related to pathological and surgical variables. Creating an anastomosis is a meticulous technique, where surgical variables depend on the surgeons' technique to perform a joining with minimal bowel tension. A successful anastomosis requires a vasculature of a rich blood supply, which is affected by the patients' pathological factors and constantly questioned by surgeons.

Determining intestinal viability, including the adequacy of blood supply, is essential during and after the surgery. Intraoperatively, distal vascularity within the CR is almost never questionable, due to the visual colour indication of the intestinal surface. An inadequate blood supply is a major factor causing the disruption to the healing process. This disruption results in a fatal anastomotic leak which is the leakage of bowel content into the surrounding abdomen, which is fatal. Scientifically, the definition of an anastomosis leak is an integrity defect at the anastomotic site, leading to a communication between the intraluminal and extraluminal compartments [26, 27].

Colon ischaemia is considered to be the source of origin, causing anastomotic leaks [26]. When an anastomosis is created, the local vasculature is disrupted, due to vessel injuries and tissue compressions from the staples or sutures used for the joining. As a result, the operation activates a series of events, resulting in a higher metabolic activity, consequently increasing the oxygen demand for angiogenesis to occur, as shown in Figure 2.7. As the oxygen demand increases in an area of deprived blood supply, due to the decrease in vascular networks, the anastomosis becomes hypoxic, compared to normal tissue [26].

2.5.3 Postoperative care and complications

Anastomotic leakage (AL) is the most serious and devastating postoperative complication. Once completing the operation and the incision has been closed, the assessment of the anastomosis is no longer available [29, 30]. Postoperatively, over 80% of patients

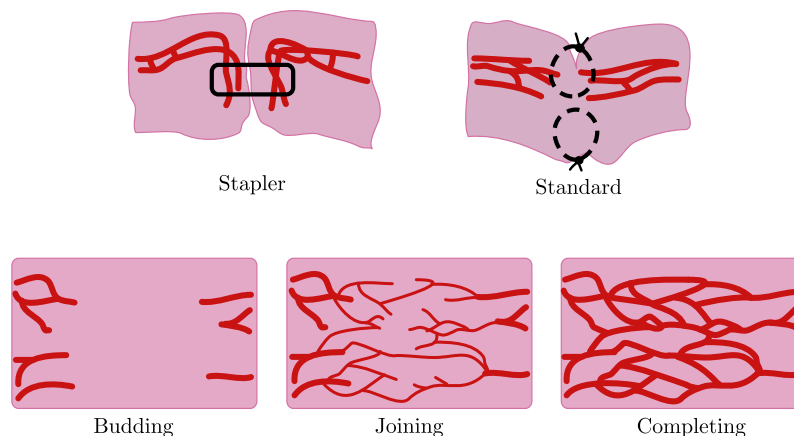


Figure 2.7 Types of anastomosis joining and the process of angiogenesis. Two healthy ends of the intestine can be joined using staples or standard stitching, to form an intestinal anastomosis. Once an anastomosis is created, the process of angiogenesis begins on each side of the anastomosis by capillary budding. The vascular buds join across the anastomosis, where angiogenesis terminates once all vascular channels have reconnected. Redrawn from Wheelless and Smith [28].

encounter undiagnosed anastomotic leaks. Furthermore, the remaining 20% who are diagnosed, still have a high mortality rate of 32% [29, 30].

Identifying a postoperative complication is challenging, as a leak is clinically indicated days after surgery via various signs and symptoms the individuals reflect. The first clinical indicator is pyrexia, which is associated with tachycardia and the signs and symptoms of sepsis and peritonitis [5, 2]. Therefore, the assessment of the patient would include a general examination for the signs and symptoms of sepsis and peritonitis. As the signs and symptoms are common for all surgical procedures, the observations are not immediately considered to be early presentations of an anastomotic leak [2]. Table 2.1 summarises the duration after the operation when observations of certain signs and symptoms are made [31, 32]. There are severe concerns for identifying anastomotic leaks, as there is a delayed diagnosis, where in the best-case scenario, found six days postoperatively [25].

Referring to Table 2.1, it is understandable to why mortality rates increase postoperatively as the implications occur due to patients not being within the managed care environment. As patients are discharged earlier, based on their capability of maintaining enteral nutrition and signs of a functioning bowel, patients are no longer

Table 2.1 Postoperative signs and symptoms of anastomotic leakage. The time taken, in days, for the first sign and symptom of a failed surgery has been tabulated.

Signs and Symptoms	Duration after operation for observation [days]
Fever ($> 38^{\circ}C$)	2
Absence of bowel activity	4
Diarrhoea	7
Renal failure	7
Leukocytosis	4

under the direct care of the hospital, whom are able to identify the likeliness of a leak and intervene accordingly [25].

Other than relying on systemic parameters, which are providing confirmation of the common signs and symptoms, there are requirements of tests to carry out intraoperatively and postoperatively, to easily acquire and interpret the changes of the body, to intervene early if there are high chances of an anastomotic leak [33]. It has been suggested that the most suitable test is to measure the bowel viability before and after the creation of an anastomosis, which would take into account the pathophysiological mechanism of the leak [33].

2.6 Summary

Reviewing the anatomical physiology of the colorectum is required, in order to develop a monitoring tool for tissue viability. A good understanding of the mesenteric circulation is needed to correctly interpret the changes when CI occurs and the successful surgical interventions. An oxygen rich blood supply to the colorectum is a major contributing factor affecting the healing success during colorectal cancer surgeries. Early identification of healing complications can be observed in the inner lining of the colorectum, corresponding to the mucosal layer. To assess bowel tissue viability and identify early indicators of colon ischaemia, there are currently several techniques available, including research techniques, all attempting to reduce post-surgical complications. Chapter 3 will discuss in detail the techniques, principles and uses for monitoring bowel tissue viability.

Chapter 3

Current state of the art for assessing intestinal viability

As seen in Chapter 2, the splanchnic circulation is the first to be compromised when the oxygen demand of other vital organs such as the heart and brain are higher. As a consequence, the intestine has become a focal point for monitoring viability over several years, as twenty-five percent of the cardiac output is directed to the splanchnic region, causing vital organs within this region to be easily susceptible to viability inadequacy [34].

Tissue viability Often referred as *tissue perfusion*, results to several definitions, where two are worth noting: (i) tissue perfusion is associated with blood oxygenation and blood flow, where perfusion is defined as the process of delivering oxygenated arterial blood to the capillaries surrounding biological tissue, and (ii) tissue perfusion is considered as a global observation based on different evaluations, such as the nature of the tissue, partial pressures of gases and anaerobic metabolism products [35].

For an organ or tissue to be viable, it is important to maintain adequate perfusion, otherwise if compromised, cell death or tissue necrosis would occur. Inadequate perfusion may lead to pathological conditions such as ischaemia, septic shock and multiple organ failure [36]. Colon ischaemia is the most common resultant of inadequate bowel perfusion, resulting in the dysfunction of the mucosal barrier. The consequence of the mucosal barrier abnormality allows bacterial translocation and endotoxin absorption into the portal blood, resulting in the amplification of the systemic inflammatory response [36].

Current state of the art for assessing intestinal viability

Motivation There are several techniques attempting to assess bowel viability, where the ideal technique should have the capability in indicating early signs of ischaemia. Complications from colorectal cancer (CRC) surgeries such as anastomotic leaks (AL) has been a great interest for many researchers. This chapter presents current techniques including the gold standard and research-based methods studied throughout the years. All techniques will include the following: (i) type of measurements with reference to their medical importance, (ii) technology principle, (iii) use for the assessment of bowel viability and (iv) advantages and limitations.

Figure 3.1 summarises the techniques discussed in this chapter. Each technique has been divided into categories based on their fundamental principle, ranging from gross structural inspection (mechanical patency), to the use of light (optical).

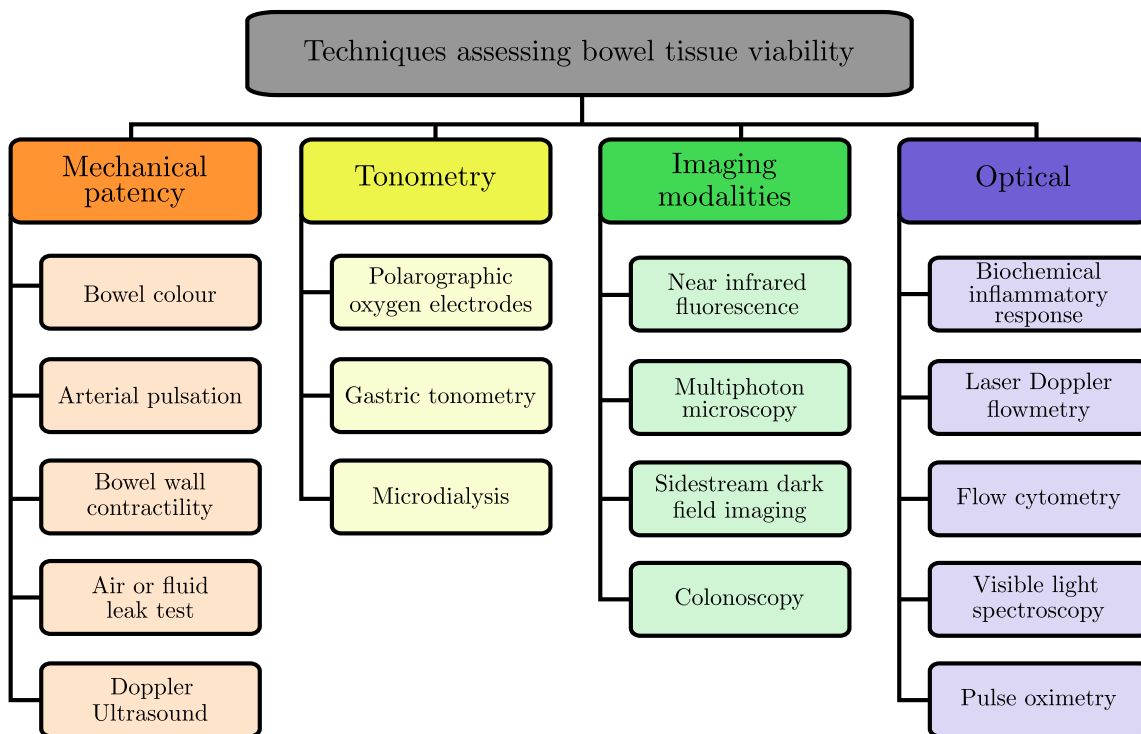


Figure 3.1 Taxonomy of techniques assessing bowel tissue viability. Each technique has been categorised into four fundamental principle. Each will be reviewed further within this chapter.

3.1 Mechanical patency

Mechanical patency assessments refers to the gross inspection for obstruction. These assessments are the gold standard techniques for clinicians to assess bowel viability [32]. As stated by Nachiappan et al. [32], three techniques are routinely undertaken to minimise inadequate viability based on visual inspection of different characteristics: bowel colour, arterial pulsation and bowel wall contractility. This section includes two additional assessments of mechanical patency: leak tests and Doppler ultrasound.

3.1.1 Visual inspection of bowel colour

Changes in the tissue colour occur based on the presence of oxygen in blood. To determine the health of a tissue in surgeries, such as free flap reconstruction and wound checks, the gold standard method surgeons use intraoperatively to assess the tissue colour is by using their eyes [37]. As a method of assessment, visual inspection suffers from several forms of noise, ranging from the lighting conditions in the operating theatre to the surgeon's own perspective.

Principle of operation During bowel resection, surgeons assess the tissue colour of the outer surface of the bowel to determine viability. A poorly perfused region of tissue compared to an adequately perfused area is distinguishable in colour, where it is seen either blue or red respectively [38, 39]. Assessing the colour of the regional tissue would indicate the ability of blood circulation [39, 40].

Use of technique for monitoring bowel viability Visual inspection of the bowel colour is the gold standard technique for intraoperative assessments of bowel viability. Animal studies have been performed by introducing graded ischaemia via mesenteric artery occlusion. Orland et al. [41] and Strand-Amundsen et al. [39] commented on the colour observed, where both studies noticed colour changes during ischaemia. Several colour changes were observed proportionally to the duration of ischaemia as shown in Figure 3.2. Contrasting from both researchers, the colour observations varied, where Orland et al. [41] categorised the colours as “dusky, blue and black”, whereas Strand-Amundsen et al. [39] colours ranged from shades of purple to black. When initiating reperfusion, the time taken for colour restoration was associated with the duration of ischaemia; indicating the time taken was affected by the level of tissue injury [39].

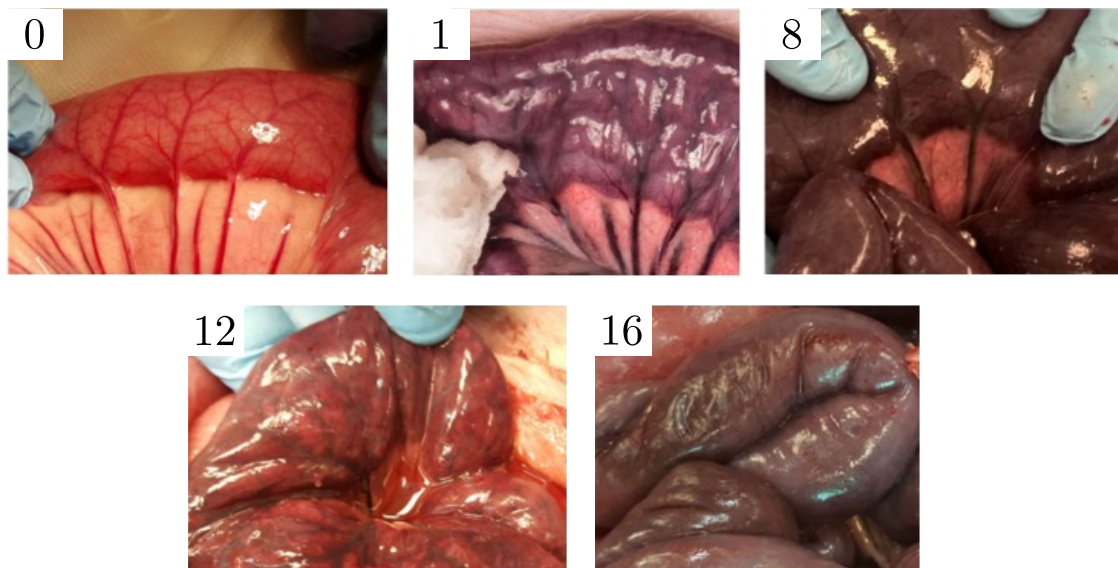


Figure 3.2 Example of colour change of bowel caused by increased duration of ischaemia. Numbers on each figure indicate the duration of colon ischaemia. Figure taken from Strand-Amundsen et al. [39].

Limitations Although determining a colour change is instantaneous to the human eye, the most prominent drawback of the gold standard technique is subjectivity. Colour is a highly complex sensation requiring input from variety of sources and determining colour varies due to each brain processing the information differently. Subjectivity within a study was minimised in the work by Orland et al. [41], using the same observer in all experiments. However, the reported colours remain inconsistent amongst the observers.

Ischaemia is not the only reason identified by a dark blue tissue, as venous insufficiency whilst the bowel is viable is an alternative suggestion [30, 42]. Furthermore, the surface of the bowel can appear to be normal during early arterial occlusion [30, 42]. As there are several reasons causing the bowel colour to change and the lack of quantitative results, colour assessments invites surgeons to assume bowel viability.

The accuracy of visually inspecting the bowel colour heavily depends on the surgeon experience. Colour is perceived by the brains' interpretation which is prone to personal experience; although this does not correlate with the rate of survival and bowel viability [41, 40]. To confidently determine bowel viability, surgeons require techniques to provide continuous, consistent, qualitative measurements [43].

3.1.2 Visual inspection of arterial pulsation

An arterial pulse remains to be the most accessible and important indication of a patient's health [44]. Identifying a pulse via palpitations immediately indicates function of the cardiovascular system.

Principle of operation A pulse occurs when oxygenated blood ejects from the heart through the aorta and travels throughout the systemic circulation [45]. Elastic fibres within the arteries aid in maintaining a high-pressure gradient by expanding, increasing vessel diameter to accommodate the blood, followed by recoiling to the original vessel diameter, as shown in Figure 3.3.

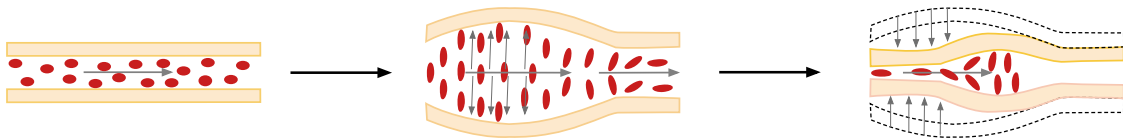


Figure 3.3 Principle of arterial pulsation, where the elastic fibres within the arteries aid in maintaining a high-pressure gradient. The high-pressure is maintained by increasing the vessel diameter and recoiling to its original state.

As the large bowel wall is formed by four thin layers, where the outermost layers are translucent, arterioles can be visually observed by surgeons intraoperatively. By visually inspecting the arteries and arterioles surrounding the colonic anastomosis, the absence of a pulse could suggest arterial occlusion or anastomotic complications, where the joining of blood vessels were unsuccessful [45].

Use of technique for monitoring bowel viability Intraoperative assessments for the presence of arterial pulsations is performed by visually assessing the colon. Once a bowel resection has been performed, the occluded mesenteric artery is released to allow blood flow to the newly formed anastomosis. This provides the surgeons an opportunity to determine continuity of blood flow incoming towards the anastomosis.

Limitations Visually inspecting for a pulse may indicate systemic circulation, however, there is a lack of information on the blood flow, volume and the composition of blood [46]. Adequate bowel viability does not only rely on arterial pulsation, but could also be compromised by venous occlusion. Without quantitative measurements of the blood flow or composition, such as the carbon dioxide concentration, observing a pulse

remains qualitative and a deficient technique [47]. There is a requirement for a reliable method in monitoring intestinal blood flow to determine bowel viability by obtaining quantitative measurements as a pulse remains present with low volume or flow [48, 45].

3.1.3 Visual inspection of bowel wall contractility

Muscles function optimally when receiving sufficient oxygenated blood to allow aerobic activities [49, 50]. A muscle deprived from oxygen enters anaerobic muscle activity, causing it to tire, and to accumulate lactic acid. If left in this state for longer, it would ultimately result in muscle dysfunction and irreversible muscle cell damage [51–53]. For colonic ischaemia, an insufficient blood supply leads to the damage of the muscularis propria and muscularis mucosa, resulting in the absence of muscle contractions within the bowel wall [39]. Although there is a possibility of reperfusion, where the pulse and colour of the bowel is restored, these assessments do not provide information on the intestinal muscles ability to recover [40].

Principle of operation Intraoperative assessments for the presence of peristalsis is an additional gold standard technique performed to assess bowel viability by visualising the movement of the bowel [30, 54, 39, 55]. The rhythmic contraction of the muscularis propria found within the bowel wall is known as peristalsis. It allows the movement of bowel content towards the rectum for waste removal [56]. Visual inspection of muscle contractility provides an indication of muscle function, where the absence of movement suggests tissue necrosis due to bowel ischaemia as seen in Figure 3.4.

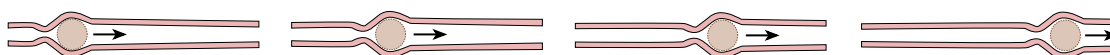


Figure 3.4 Principle of bowel wall contractility. The rhythmic contraction known as peristalsis allows the movement of bowel content towards the rectum.

Use of technique for monitoring bowel viability Monitoring the presence of peristalsis has been undertaken in animal studies [57]. For example, the studies by Strand-Amundsen et al. [39] and Glotzer et al. [58], where ischaemia was initiated via mesenteric artery occlusion. Whilst increasing the duration of ischaemia, studies visually observed overactive peristalsis, also known as hyper-peristalsis, lasting up to 40 minutes post initiating ischaemia [39, 58]. Although bowel wall contractility may

be a good indicator of muscle functionality, the presence of peristalsis was observed in areas of probable irreversible damage due to ischaemia [40, 39, 30].

Limitations Inconsistencies in the assessment suggests bowel wall contractility is a qualitative method for evaluating bowel viability. Visual inspections for the presence of bowel wall contractility is believed to indicate muscle functionality, indicating bowel viability. However, studies observed the continuation or mimicking likeness of peristalsis due to hypoxic spasms after the release of occlusion, with over ten minutes required for signs of peristalsis to be evident [59, 40].

To distinguish peristalsis quantitatively, electromyography (EMG) has been used as a research tool to indicate bowel viability [40, 60]. Improvement of the electronic contractility meter, first introduced by Brolin et al. [61], surface electrodes such as Figure 3.5 are clipped on the serosa, allowing quantitative measurements of external bowel wall contractions by analysing slow wave contractility [41, 40, 62]. Furthermore, Hegde et al. [63] recorded EMG before and during ischaemia, followed by reperfusion to the jejunum in 20 rabbits. As expected, the amplitude and frequency, which corresponds to the level of muscle activity, fell significantly after 15 minutes of ischaemia and became undetectable by 90 minutes for all participants.

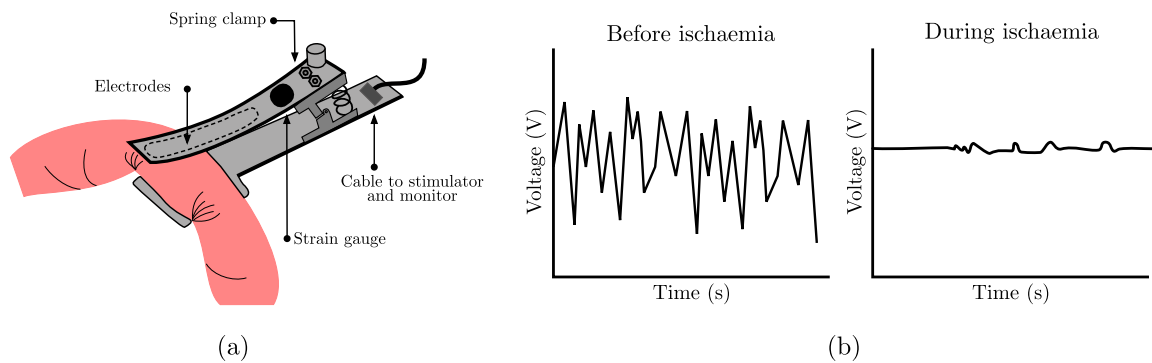


Figure 3.5 Electronic contractility meter applied to the bowel. (a) A clip on surface electrodes clamped onto the bowel with a strain gauge to measure the applied pressure to the bowel. (b) Illustration of the expected contractility signal to be obtained before and during ischaemia, where an amplitude decrease and absence of contractility suggests muscle necrosis. Image redrawn from Brolin et al. [61].

Having the ability to measure quantitatively bowel wall contractility compared to visual inspection has provided valuable information. From the studies recording EMG signals, the likelihood of peristalsis returning was found to be highly correlated with the duration of ischaemia [63]. Whilst an improvement has been made, the technique

cannot be used postoperatively, as the outer surface of the bowel is not easily accessible; additional to the inability of inserting and removing the device without further incision.

3.1.4 Air or fluid insufflation leak test

Intraoperative air or fluid leak test has been frequently performed since the 1960 within other surgical fields, such as bariatric surgeries [64–66]. Once forming an anastomosis, by either stitching or stapling the joining ends, surgeons can test for potential leaks by detecting a mechanically inadequate anastomosis [67, 68]. The intraoperative test could lead surgeons to immediately repair the anastomosis within the operating theatre, decreasing the incidence of clinical leakage [69, 67, 68]. By injecting either air or fluid into the lumen, an unsuccessful anastomosis would be visually identified by the leakage of the injected content on the outer surface of the lumen or the presence of air bubbles.

Principle of operation The procedure of the test is marginally altered depending of the injection material [69]. A common procedure for both techniques involves occluding the bowel proximal to the anastomosis using a soft clamp to maintain intraluminal pressure [67, 69]. An air leak test is performed by filling the abdomen with saline, ensuring trapped air is dislodged by moving the intestine [67]. As shown in Figure 3.6, a syringe or an endoscope with an integrated air pump is used to insufflate the distended rectum whilst the anastomosis is under the pool of saline [70, 65, 67, 71, 72]. By injecting air, surgeons inspect the anastomosis where immediate apparent bubbles would be visible in the saline, denoting air is escaping through a defective anastomosis [67].

A fluid leak test is performed by inserting a rectal balloon catheter, allowing the balloon to be inflated within the rectum with the intention to occlude the distal bowel [73]. The rectum is occluded by gently withdrawing the inflated balloon towards the internal anal sphincter to prevent leakage of the chosen test fluid [73]. Before introducing the test fluid, such as methylene blue, the anastomosis is surrounded by clean gauze. This aids surgeons to inspect the resection, where a defective anastomosis would be visible due to the spillage of blue dye on the sponges [73]. With indications of a defective anastomosis from the leak test, surgeons can revise their joining technique and repeat the test to ensure mechanical defects are absent before completing the surgery [67].

Use of technique for monitoring bowel viability The leak test is a standard procedure for many surgeons during bowel resection [74–76], where several studies have

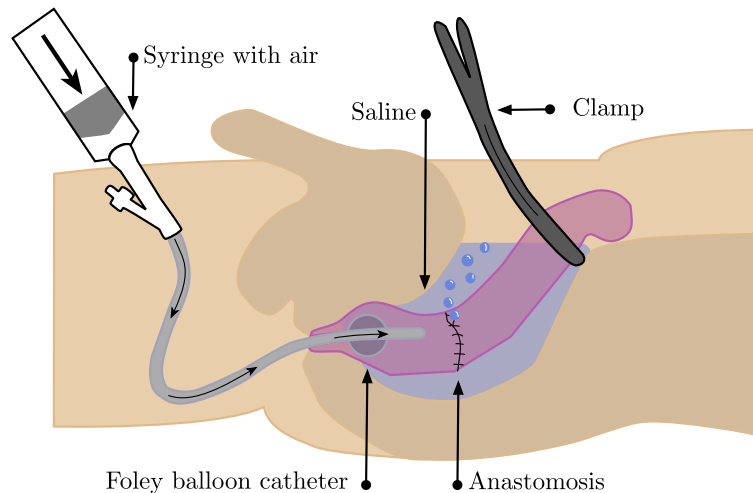


Figure 3.6 Air leak test within the lumen of the bowel. The newly developed anastomosis is submerged in saline, where air is injected into the lumen. The presence of bubbles indicates an anastomotic mechanical disruption, requiring revision of the anastomosis. Image redrawn from Davies et al. [67].

been conducted to determine whether such tests aid in the reduction of anastomotic failures [77–81].

In particular, Beard et al. [74] conducted a randomised study of 143 patients undergoing bowel resection, evaluating the effectiveness of air leak test in reducing postoperative leaks. In the study, a significant reduction was found. Seventy-four patients were tested with the technique and compared to the remaining seen as a control group. Based on the air leakage test, 18 (25%) intraoperative anastomotic corrections were performed. Postoperatively, radiological leaks were detected in eight individuals (11%) compared to twenty individuals (29%) from the control group. Speculations arise with the technique integrity as patients achieving a negative leak test developed postoperative anastomotic complications [70].

Wu et al. [68] performed a systematic review where 45% of the patients participated in a leak test with positive result, where the total number of participants accounted to be 5283; accumulated from several studies. However, a significant difference was not found from the participants not undergoing the test, thus reduction in postoperative complications could not be conclusively proved [68, 82].

Limitations Studies reporting the use of a leakage test in assessing bowel viability were found to have extensive risks of bias due to the lack of study randomisation and the absence of thorough methodology [68]. With the minority reporting, variability

in the method such as the volume of the inflated gas or dye were seen, where the volume ranged from 60 mL to 1000 mL due to variation the patients' anatomy [83, 68]. The intraluminal pressure is a known factor contributing to a leak whilst performing the leakage test [68]. The burst pressure for a newly constructed anastomosis has been reported to range between 70 mmHg to 184 mmHg, however no leak test study has mentioned obtaining intraluminal pressures, which could be valuable [84]. The ambiguous methodology calls for technique standardisation to validate the effectiveness of the leakage test [68].

Whilst comparing air and fluid leak tests, an apparent benefit in utilising a dye fluid offers the ability to identify the area of the defected anastomosis due to the precise locations of the gauze [79]. However, for a lower bowel resection, where the anastomosis is within 6 cm of the anal verge, a fluid leak test was shown to be a poor choice, as the balloon catheter could not be positioned [73].

Leak tests do not guarantee the continuation of an intact anastomosis after surgery, as observed with participants encountering postoperative complications even when showing negative leak test results [79, 74, 70, 83]. An intraoperative leak test more appropriately examines the performance of the surgeon constructing an anastomosis than evaluating bowel viability [83]. This strengthens the hypothesis where bowel viability incorporating physiological measurements such as blood flow, volume and saturation may be more relevant [70].

3.1.5 Doppler Ultrasound

Doppler ultrasound is a widely used technique for evaluating peripheral blood flow as a predictor of viability for cardiology [60]. Ultrasound (U/S) is sound at a high frequency which is used to estimate blood velocity through an artery, commonly on the limbs, and can be associated with vessel obstruction or occlusion [85, 60]. The technique has been adopted to monitor the flow within the bowel to assess its viability [86].

Principle of operation U/S is a sound wave above the audible range (> 20 kHz) [85]. Commonly used by bats [87], dolphins and man-made objects like submarines for echolocation, the Doppler effect is the result of the alteration of frequency caused by the interaction of U/S with moving objects. An example of the principle is shown in Figure 3.7, used by emergency services.

Considering the example of the siren of a passing emergency ambulance in Figure 3.7, the change in the siren's pitch can be observed due the change in sound frequency.

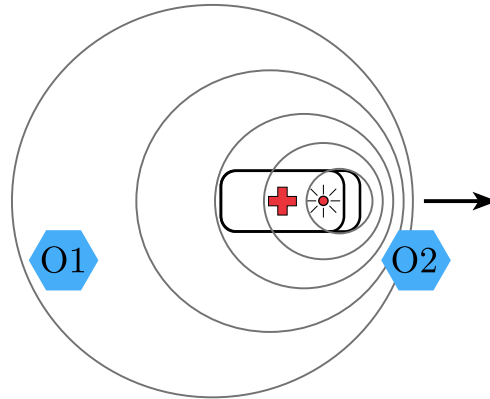


Figure 3.7 Example of the Doppler effect with a siren of a passing emergency ambulance. The change in the siren’s pitch can be observed due the change in sound frequency. The Doppler effect results in the siren to sound higher in pitch when approaching the observer, compared to when it is receding due to the change in wavelength. Image redrawn from Middleton [85].

The Doppler effect results in the siren to sound higher in pitch when approaching the observer, compared to when it is receding due to the change in wavelength.

The Doppler principle can be used to estimate blood flow by emitting U/S into a tissue to interact with moving structures, such as the red blood cells (RBC) within an artery. By measuring the Doppler shift as shown in Equation (3.1), which is the frequency difference (Δf) between the source (f_o) and detected reflection (f_r), the velocity of the moving object (v) can be estimated, where cs and θ refer to the ultrasound speed and the angle between the ultrasound beam with a travelling red blood cell, respectively [85],

$$\Delta f = f_r - f_o = 2 \cdot f_o \cdot v \cdot \cos(\theta/cs). \quad (3.1)$$

The technique is commonly implemented with the use of a handheld, pencil-like transducer [85]. The main component of the transducer are piezoelectric crystals which generate continuous U/S due to the crystal structure resonating when an alternating current is applied [85, 88]. Referring to Equation (3.1), the orientation of the transducer should not be perpendicular to the flowing RBCs (*i.e.* the tissue) as no Doppler shift would be detected [85, 36]. The angled orientation causes extraneous reflections between the transducer and the surface of the tissue, which can be minimised with water-soluble gels matching the acoustic impedance. The transducer connects to an audio output allowing the operator to audibly identify the blood velocity, similar to the Korotkoff

Current state of the art for assessing intestinal viability

principle [89]. Fast moving RBCs are identified by a high pitch audio, compared to slow or no movement identified by a lower or absent pitch [36].

Use of technique for monitoring bowel viability Doppler U/S has been reported as a research tool for monitoring bowel viability in animals, commonly in small samples of dogs [90, 61, 60], and human participants [91]. For blood flow monitoring, sections of the bowel are isolated and exposed via surgical incisions. The tip of the transducer is coated with water-soluble gel before applying direct contact to the tissue at an angle of approximately 45° [92, 93], as illustrated in Figure 3.8. The transducer is placed on the serosal surface of the bowel [92], where light pressure is applied, minimising the compression of small vessels on the bowel wall [93].

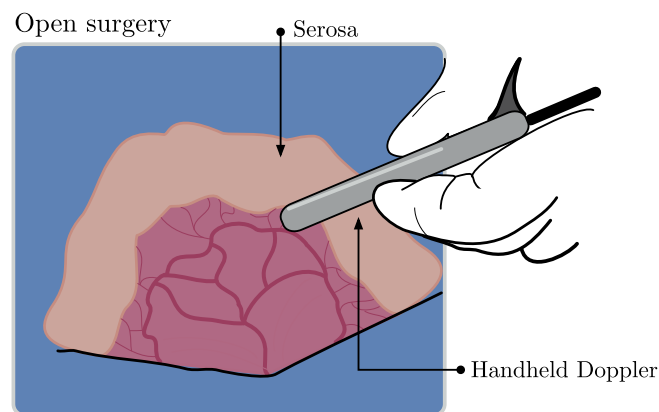


Figure 3.8 Doppler Ultrasound applied on the bowel. During an open surgery, a handheld Doppler ultrasound transducer can be placed directly on serosal surface for blood flow measurements. The transducer is placed at an angle of 45° with minimal compression of the arteries on the bowel wall.

Assessment for bowel ischaemia was first reported by Hobson et al. [94] during aortic reconstruction of 25 patients. The colonic blood flow was examined from the serosa via audible Doppler flow before and after the occlusion of the mesenteric artery. With collateral flow audible in eighteen patients, Doppler U/S was recommended as a technique to be used to determine bowel viability during reconstructive vascular procedures.

Similar studies to Hobson et al. [94] were performed, where the mesenteric artery or vein were occluded with the use of clamps to understand the relationship of blood flow and intestinal ischaemia [60, 95, 86]. Consistently audible flow would refer to a viable bowel, in comparison to the absence of an audible output referring to inadequacy [60]. Rather than two possible outcomes, Lynch et al. [88] evaluated the blood flow by

scoring the presence of audio, with a scale ranging from 1 – 4, depending on subjective interpretation of the audio at the mesenteric and antimesenteric borders. The use of Doppler U/S as an assessment of colonic blood flow was successful for Shah and Andersen [60] who consistently heard mesentery flow in 13 dogs, similar to the outcome for various studies comparing measurements of occluded and re-perfused mesentery arteries or vessel to baseline assessments [93, 55, 86].

Limitations Doppler U/S appears to be an attractive intraoperative monitoring technique for bowel viability due its rapid measurement and relative non-invasiveness [60]. Unfortunately, the technique is outweighed by several limitations. The technique is known to be non-invasive, as the U/S probe does not require penetration into the bowel wall. However, for reliable measurements, the region of interest must be exposed for direct contact between the transducer and tissue, in addition to the presence of pulsatile blood flow [36, 30].

Reliable monitoring heavily depends on the operator, where experience is required to hold the transducer correctly and lightly applied to the bowel to obtain consistent results without impairing the local blood flow [86, 36, 96, 30]. Technical difficulties such as incorrect positioning of the probe and sub-optimal contact could result in identifying an inadequate segment as viable [92, 36]. Blood flow monitoring with Doppler U/S results in a subjective and qualitative audio, making the technique undesirable [97]. In comparison to the previously mentioned mechanical patency assessments, authors such as Bulkley et al. [92] question the techniques contribution to clinical decisions, as no additional advantages were found. Tracing the recorded audio as a waveform has been attempted, however proved to be less reliable [92].

Identifying the blood flow on the serosal surface does not relate to microscopic evidence of ischaemia, where early identification is found in the mucosal and muscular lining [95]. Although mucosal assessment would be the ideal monitoring region, solely utilising Doppler U/S would be insufficient, as blood flow does not indicate bowel functionality. Blood flow alone does not provide information on the blood composition such as the concentration of gases [97, 60].

3.2 Tonometry

Tonometry refers to monitoring the concentration of natural movement of particles within a cavity as an indication of blood flow to the specific area of measurement. It can be measured through (i) polarographic oxygen electrodes, (ii) gastric tonometry, or (iii) microdialysis, which respectively measures the concentration of oxygen, carbon dioxide and metabolites such as glucose and lactate.

3.2.1 Polarographic oxygen electrodes

Monitoring the partial pressure of tissue oxygen (P_tO_2) provides measurements of the oxygen availability at a cellular level. Maintaining adequate tissue oxygenation is fundamental for tissue survival. Similar to oxygen diffusion within the alveoli, providing sufficient oxygen from the arterial blood to the tissue requires a partial pressure gradient, where gaseous particles from an area of higher pressure move to an area where its pressure is lower [85]. Deprivation of oxygen within a tissue promotes the release of oxygen from the arterial blood, thus reducing the partial pressure of oxygen (PO_2) within the tissue as the plasma PO_2 decreases [36].

Polarographic electrodes, known as the modified Clark electrodes, are used to measure P_tO_2 , based on the principles of amperometric measurements. As shown in Figure 3.9, the modified Clark electrodes are composed of an anode and a cathode which undergo electrochemical reactions when in contact with oxygen, resulting in the change of electrical current with an external voltage supply [98].

Principle of operation Figure 3.9 presents a typical polarographic oxygen electrode used for measuring the P_tO_2 in a liquid medium. The sensing chamber, consisting of the electrodes, is isolated from the sample chamber by a thin permeable membrane. The membrane allows the diffusion of oxygen from the high-pressure environment (sample chamber) to the zero-pressure environment (sensing chamber) [99]. A silver anode and platinum cathode are suspended in a chloride electrolyte in addition to an external voltage of 0.7 V applied to the electrodes. The fixed voltage allows oxygen to be reduced at the cathode and oxidation of silver at the anode.

For reduction to occur at the cathode, the reaction requires oxygen, water and the transfer of electrons, as seen in Equation (3.2). The current is dependent on the supply of oxygen molecules to produce hydroxide ions; therefore, the current is proportional to the partial pressure of oxygen in the sample.

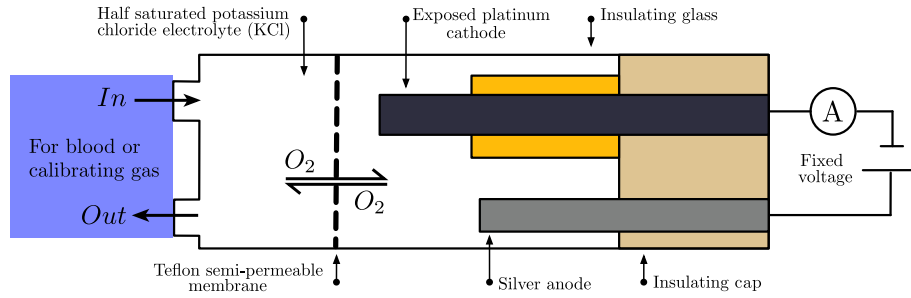


Figure 3.9 Principle of a modified Clark electrode, for the measurement of the partial pressure of oxygen in a medium. There is a platinum (Pt) cathode and a reference silver/silver chloride (Ag/AgCl) anode suspended in a chloride electrolyte. The sample chamber and sensing chamber is isolated by a semi-permeable membrane, allowing the movement of oxygen between the two chambers. A fixed voltage is supplied to the electrodes and an ammeter to measure the output current. Image redrawn from Middleton [85].



Clark electrodes are available as needle electrodes, implantable catheter electrodes or transcutaneous surface electrodes [99]; where the latter is commonly used for bowel P_tO_2 measurements. By placing the Clark electrode on the surface of the tissue, transcutaneous P_tO_2 measurements require vasodilation to increase the blood flow within the area for oxygen to diffuse through the arteries to the outer surface of the tissue [100]. Such diffusion from the inner to outer surface is achieved by heating the measurement site, promoting oxygen to enter the Clark electrode for the electrochemical reaction to take place. The heating technique allows P_tO_2 to be correlated to the arterial partial pressure of oxygen (P_aO_2) [101, 102, 100].

Use of technique for monitoring bowel viability Polarographic oxygen electrodes have been reported as research tools for monitoring intestinal viability on animal and human participants [103, 104, 36]. Several animal studies, mainly researched on small samples of anaesthetised dogs and pigs, have been reported [105, 104, 106–110].

For P_tO_2 monitoring, sections of the small intestine, either the ileum or jejunal were isolated and exposed via surgical incisions. This allowed the polarographic

oxygen electrodes to be placed on the surface of the intestine to obtain serosal P_tO_2 measurements [105, 104, 106]. Direct measurements of mucosal P_tO_2 is uncommon [107], however Vallet et al. [104] and Haisjackl et al. [107] demonstrated the possibility of measuring mucosal P_tO_2 within the small intestine. These studies were conducted by exposing the mucosal tissue via an antimesenteric enterotomy, an incision allowing entry into the intestine. The incision is used for the polarographic oxygen electrode to be directly positioned on the mucosal surface. For accurate monitoring, a constant temperature of $37 \pm 0.3^\circ\text{C}$ is kept using an infrared heat lamp and moist sponges of warm saline, covering the exposed outer surface [104, 107].

To understand the relationship between P_tO_2 and bowel ischaemia, several onsets resulting in hypoxia were introduced under operative conditions. Piasecki [105] applied graded ischaemia by reducing the blood flow; where the reduction of serosal P_tO_2 was observed with the polarographic oxygen electrode. As bowel ischaemia can occur during a cardiopulmonary bypass, Haisjackl et al. [107] assess mucosal P_tO_2 during these surgeries. On the onset of the bypass, decrease in the mucosal P_tO_2 was observed with the probable cause of redistribution of blood flow to areas of low oxygen delivery.

Sheridan et al. [111] assessed serosal P_tO_2 on 50 patients undergoing bowel resections. With the aim to measure and relate colonic mucosal P_tO_2 with anastomotic healing, polarographic oxygen electrodes were placed 1 cm either side of the intended location of the anastomosis. P_tO_2 measurements were obtained before and after the procedure and validated with arterial blood gas samples. The study concluded P_tO_2 were closely related to P_aO_2 , indicating P_tO_2 could be used as an indirect measurement of P_aO_2 . For patients identified with anastomotic leaks via radiology, significantly lower P_tO_2 post-resection were found compared to those whose anastomosis were healing successfully. Based on the observations presented by Sheridan et al. [111], the P_tO_2 of post-resection patients were less than half of the pre-resection P_tO_2 and were associated with 100% leakage incidences.

Limitations Reviews with successful outcomes concluded to have found polarographic oxygen electrodes a repeatable, quantitative technique [105, 103]. However, the technique has not proceeded to routine clinical use because of the limitations with the principle and the sensing design.

Regarding the principle of operation, the surface area of the transcutaneous electrodes used is confined to a limited area, which poses doubts of detecting hidden hypoxic

areas [112]. To overcome the area restriction, electrode arrays could be developed to increase the assessment area [112, 36].

Being a diffusion technique, an accurate measurement is obtained only when oxygen equilibrates between the two chambers, which is time consuming. Due to the equilibrium period, measurements are considered non-continuous, as readings are taken at intermittent times. Advancements on the technology has been seen, where needle polarographic electrodes are being used, allowing continuous P_tO_2 assessments, though requiring calibration prior to each measurement with a solution or gas of known oxygen tension [113, 99, 38].

There are contradictory results for the relationship of P_tO_2 with anastomotic complications. Jacobi et al. [114] obtained contradictory results where no changes in P_tO_2 were observed in patients with anastomotic perfusion deficiency after oesophageal resections. Thorén et al. [115] main findings during human cardiopulmonary bypass indicated an increase in jejunal mucosal P_tO_2 . Postoperative measurements cannot be obtained, as the technique requires direct contact on the tissue surface, which may require additional incision and a constant clinician presence. The limitations, performance incapability and the lack of large samples of data prevents the method to be used as a routine clinical use.

3.2.2 Gastric tonometry

The bowel mucosa is known to be the primary layer affected by blood flow redistribution due to shock, trauma and sepsis [36]. Gastric tonometry, commonly used within the stomach, measures the partial pressure of carbon dioxide (PCO_2) diffused from the gastric mucosal [116]. The technique could be utilised within the intestine aiding in monitoring bowel viability [36]. The increase in bowel PCO_2 could represent the anaerobic production of lactate and the release of dissolved CO_2 from bicarbonate, implying mucosal dysoxia (low oxygen concentration) [117]. Additionally, the increase in bowel PCO_2 may represent blood flow stagnation and the inability of removing CO_2 which is the by-product of oxidative phosphorylation, referring to the formation of ATP for aerobic metabolism.

Principle of operation To measure PCO_2 , a sample of fluid that has been in contact with the intra-mucosal wall for a certain time, must be obtained and analysed for its gas content [118]. As shown in Figure 3.10, the desired samples can be obtained using a tonometer catheter via naso-gastric or rectal insertion, depending on the region

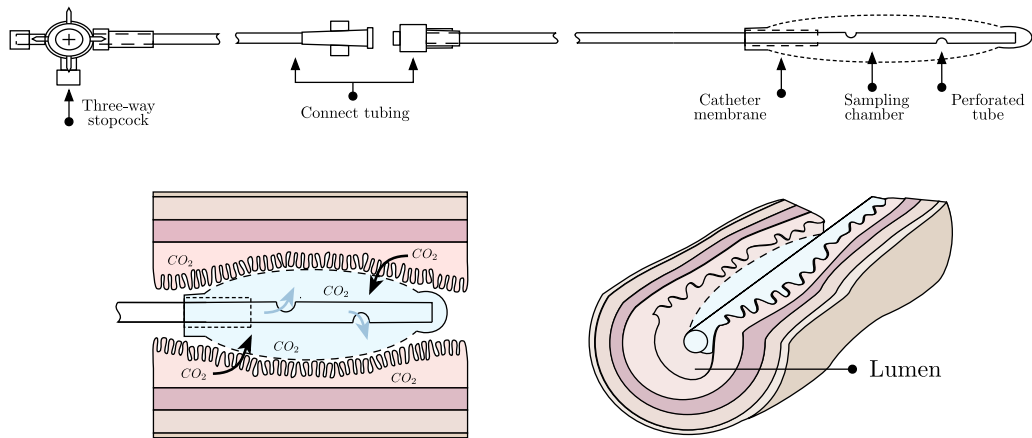


Figure 3.10 Principle of gastric tonometry. A gastric tonometer catheter allowing intraluminal measurements of partial pressure of carbon dioxide (CO_2) within the lumen of the bowel. The catheter membrane allows the diffusion of CO_2 from the intramucosal lining into the sampling chamber. Image redrawn from Fiddian-Green [118].

of interest. The tonometer catheter composes of a sampling chamber (distal) and a complimentary fitting to allow attachments of additional connective tube.

Whilst placing the tonometer catheter in direct contact with the intra-mucosa, the sensing chamber is filled with a medium such as saline to cause the catheter membrane to distend [30, 36]. The membrane, commonly manufactured from silicone, allows the diffusion of CO_2 from the intra-mucosal lining into the sampling chamber [117]. After reaching equilibrium, the saline sample is assumed to be proportional to the intestinal mucosal PCO_2 , therefore withdrawn and measured using a blood gas analyser [116].

Once quantifying the PCO_2 , an indirect measurement commonly reported is the gastric mucosal pH (pHi), which can be calculated using the modified Henderson-Hasselbach as shown in Equation 3.3 [119, 30, 120],

$$pHi = 6.1 \log \left[\frac{HCO_3^-}{0.03 \times PCO_{2(m)}} \right] \quad (3.3)$$

where HCO_3^- is the concentration of bicarbonate ions and $PCO_{2(m)}$ is the partial pressure of carbon dioxide within the mucosa. The pHi index is a good indication of mucosal oxygenation, where the normal value for pHi is 7.35 and a lower pHi implies mucosal hypoperfusion and the development of acidosis [30, 116]. The method assumes that the concentration of bicarbonate ions (HCO_3^-) delivered to the gastrointestinal

tract is the same as the concentration of HCO_3^- obtained via arterial blood gas analysis [121, 116].

Use of technique for monitoring bowel viability Gastric tonometry has been reported as a research tool for monitoring bowel viability conducted on animal and human participants [122–124]. Animal studies were mainly researched on small samples of anaesthetised pigs [32]. Rémi et al. [117] and Frøjse et al. [125] demonstrated the possibility of measuring mucosal PCO_2 within the ileum and jejunal, respectively. Through antimesenteric enterotomy, the tonometry catheter was positioned within the lumen and sutured in place. For consistent monitoring, the tonometry balloon was injected with room-temperature saline, with 30 minute interval measurements.

To understand the relationship between PCO_2 and bowel ischaemia, adjustable clamps were placed on the superior mesenteric artery for gradual ischaemia. By altering the blood flow, observations were made on the pHi, where reduction of blood flow correlated to the reduction in pHi [125]. Furthermore, Rémi et al. [117] induced hypoxic hypoxia by reducing the oxygen fraction in the inspired air, where an increase in the small intestine PCO_2 was observed.

Less invasive methods were performed by inserting the tonometry catheter intraluminal via the rectum [126, 121]. During aortic surgery, Björck and Hedberg [127] positioned the tonometry catheter in the lumen of the sigmoid colon attempting to detect intestinal ischaemia early. Sigmoid acidosis, a pHi below 7.10, served as an early identification of bowel ischaemia, whereas a pHi below 6.86 would allow endoscopic detection of ischaemia by visual inspection. As stated, a lower pHi is believed to suggest bowel ischaemia, however, Vahl [128] observed individuals with a pHi less than 6.86 who did not develop ischaemia but encountered postoperative complications such as sepsis and heart failure.

Limitations Despite various research studies utilising gastric tonometry for the assessment of bowel viability, the technique has not been adopted as a routine clinical tool due to its technical difficulties and methodologies [116]. Gastric tonometry is known to be a laborious technique obtaining intermittent measurements. The technique consists of several steps such as the insertion of the catheter, infusion of the liquid sample and withdrawal, increasing the risk of error and therefore, reducing the reproducible results [129, 119]. The technique depends on calibrating the system, where the sensor requires this process at the beginning of each experiment and every 4 hours [125].

Saline tonometry has been replaced with air tonometry, allowing measurements to be obtained every 10 minutes [130, 23, 99, 131]. This is achieved with an automated close-system using an external pump inflating and deflating the balloon [129, 132]. The use of gas, such as helium, would allow rapid diffusion of CO_2 , resulting in shorter equilibrium periods [133, 132].

To determine the pHi, Equation (3.3) is used based on the assumption that the arterial HCO_3^- concentration is equal to the mucosal HCO_3^- concentration. However, as Groeneveld and Kolkman [120] noticed, further evaluation is required to verify the assumption. These uncertainties were viable, as studies reported the use of arterial HCO_3^- caused pHi over-estimations during severe regional ischaemia [125, 134].

3.2.3 Microdialysis

Microdialysis is a validated bedside technique extensively used in various surgeries such as neurosurgery and plastic surgery [135]. For several years, the technique has been explored within bowel resections [123]. Microdialysis monitors intermittently metabolites such as glucose, lactate and pyruvate, which provide biochemical information on the metabolic events occurring at an intra-cellular level of the tissue [136–138]. Rising lactate to pyruvate ratio (L/P ratio) or falling glucose concentration indicate anaerobic metabolism or arterial compromise [137]. During postoperative periods of bowel surgery, monitoring L/P ratio could provide complementary information regarding the intestinal metabolic state and hence, aid in identifying bowel ischaemia [136, 29, 135].

Principle of operation A catheter incorporating microdialysis is placed in contact with the tissue region of interest, under direct vision, to assess the extra-cellular fluid [139, 137]. The microdialysis catheter, as seen in Figure 3.11, is a thin double lumen with parallel inlet and outlet tubes, lined with a semi-permeable membrane at the distal end [139, 140].

The catheter is irrigated with isotonic perfusate entering the inlet of the catheter with the use of an external pump which controls the flow rate [137, 139, 34]. The semi-permeable membrane allows the movement of metabolites between the tissue's extra-cellular fluid and the perfusate [139]. Subsequently, once the perfusate equilibrates with the extra-cellular fluid, samples of the fluid, the microdialysate or dialysate, is withdrawn through the outlet and analysed for the metabolite compounds of interest [139, 26].

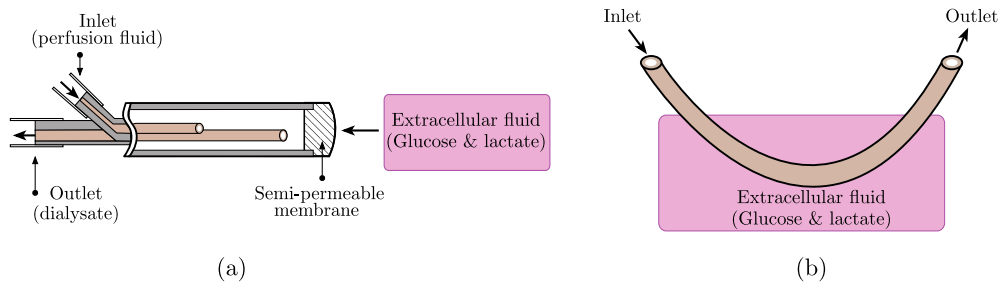


Figure 3.11 Principle and geometries of microdialysis. Perfusion fluid enters the probe through an inlet to take up substances from the surrounding tissue through the semi-permeable membrane. The perfusion fluid becomes a dialysate which is extracted from the outlet for analysis. There are two types of microdialysis geometries, where (a) is a surface probe or, (b) an intraluminal geometry which can be placed within a cavity. Image redrawn from Johansson [139], Hochmuth and Mischler [140].

Use of technique for monitoring bowel viability Microdialysis has been reported as a research tool for monitoring bowel viability on animal and human participants, where changes in the metabolites have shown correlation with bowel ischaemia [29]. The microdialysis catheter has been sutured in various areas within the bowel, as illustrated in Figure 3.11(b), including intra-luminal [141], extraluminal surface [142] or free-floating within the intraperitoneal cavity [143, 26]. The results of the principal studies using this technique for bowel viability are described below.

To understand the relationship between the changes in metabolite levels and bowel ischaemia, arterial occlusion was induced [144, 145]. By compromising the arterial blood flow, Birke-Sorensen and Andersen [146] found an increase in lactate concentration and L/P ratio within ischaemic segments of 12 pigs' small intestine. Pronounced changes in the L/P ratios were reported after one and a half hours of occlusion, where the L/P ratio increased 9 times and was significantly different to values obtained with non-ischaemic segments.

Jansson et al. [143] determined normal L/P ratio values with 33 non-complicated, postoperative patients. The microdialysis catheter was placed free-floating in the intraperitoneal cavity, where the catheter was sutured to the skin to avoid movement and measurements were obtained every second hour. An hour post-operation, the normal mean L/P ratio was found to be 15, reducing to 11 after 45 hours. The high L/P ratio is due to early metabolic changes due to patients undergoing major gastrointestinal surgery.

Pedersen et al. [147] conducted a study on postoperative rectosigmoid cancer patients, where measurements were analysed every 4 hours, in an attempt to determine

Current state of the art for assessing intestinal viability

anastomotic complications before visual clinical symptoms. Patients who developed late anastomotic leaks, more than 10 days postoperative, were found to have a significant increase in the lactate concentration and L/P ratio several days before visual symptoms. However, patients with earlier complications displayed clinical symptoms together with the increase in L/P ratio. The mean L/P ratio of cases of non-complication and complication were 18.3 (ranging from 0 – 36.6) and 44.7 (0 – 120.3) respectively. Notice the ranges of values obtained show a sizeable variability.

Limitations Despite its features, several limitations can be observed from microdialysis as a technique for bowel viability assessment. Such limitations include (i) the difficulty to operate the catheter due to its reduced size, (ii) high variability between instances it has been used and (iii) interpreting the data.

As the catheter is approximately 1 mm thick, the technique is fragile by nature, requiring excessive care during insertion and withdrawal from the tissue [139, 34]. Daams et al. [135] reported approximately 37.5 % of patients incurred technical failure due to iatrogenic damage to the catheter or trapped air bubbles within the catheter due to physician mishandling. Microdialysis is based on the principle of diffusion, therefore, the time required for equilibrium of metabolites between the perfusate and bowel results in single readings obtained periodically every 30 minutes [137, 139, 142] or every several hours [135, 29].

Studies that have been performed all show an increase in lactate concentration and L/P ratio, however values differ considerably between cases [139]. The location of the catheter varies, which could suggest the variability in the results. A study on 12 patients undergoing right-sided hemi-colectomy surgery was performed to investigate potential differences in lactate concentration and L/P ratio depending on the catheter location [139]. Microdialysis catheters were placed in multiple intraperitoneal locations. The study concluded the L/P ratios were significantly different between the locations, therefore confirming the measurements is dependent on the catheter location [139].

Due to the large variability of results and the lack of clinical data, larger samples of data and studies have been requested to understand the usefulness of the technique [148]. Additionally, interpreting the metabolic data is unclear when associated with anastomotic healing, therefore requiring further investigation before considering the method as a routine clinical method [82].

3.3 Imaging modalities

Imaging modalities refer to techniques where the area of interest is excited with some form of energy, such as visible light or infrared light. The energy interacts with the tissue, producing a single image or an image sequence (video). The techniques described within this section differ from each other by the energy used, and include (i) near infrared fluorescence, (ii) multi-photon microscopy, (iii) sidestream dark-field imaging and (iv) colonoscopy.

3.3.1 Near-infrared fluorescence

Fluorescent angiography (FA) is a technique increasingly used within other surgical fields such as reconstructive flaps following breast cancer [149]. The imaging technique provides enhanced visualisation of blood vessels and provides relevant information on the tissue viability [150]. Within the body, cells surrounded by tissue fluid allow to receive and deposit nutrients and waste. To constantly replace the tissue area with more nutrients and removing the waste, the capillaries' function is to pass blood through the vessel. If obstructed, the blood flow within the capillary reduces, limiting the transfer of nutrients from the capillaries wall into the tissue. A fluorescent dye is injected into the bloodstream, which should reach the capillaries under normal functioning conditions. This procedure allows a direct assessment of nutritive blood flow due to the accumulation of the dye, causing illumination of the region of interest after exciting the area with an external light source [70, 151].

Principle of operation To undergo FA, a fluorophore, which is a compound emitting light when excited, is required. Over 30 years, a commonly used fluorophore is indocyanine green (ICG) which is a sterile, water soluble compound [149]. A single bolus of ICG is injected via a peripheral intravenous catheter which rapidly binds to plasma proteins, especially high-density lipoproteins [152, 153].

For ICG to fluoresce, light within the near infrared (NIR) region, specifically 806 nm, provides enough energy for an ICG electron to absorb and move to an excitation state of a higher energy level, represented as S1 in Figure 3.12. To return to ground state, the electron emits energy in the form of a photon which has less energy than the absorbed photon; thus, having a longer wavelength relative to the excitation photon which can be visualised using a camera [155, 156]. In addition to ICG attaching to plasma proteins, referring to the major optical absorbers, haemoglobin and water,

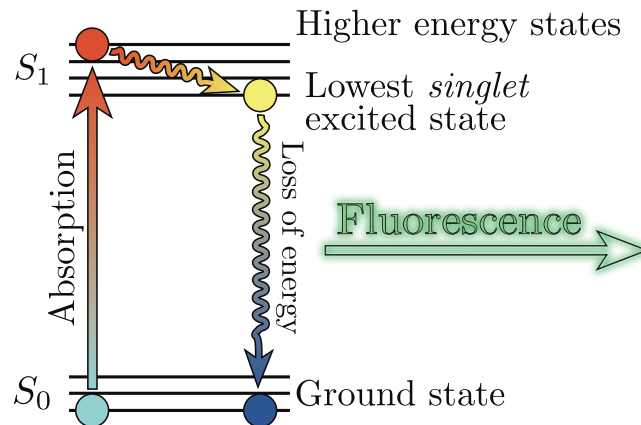


Figure 3.12 Principle of fluorescence. For Indocyanine green to fluoresce, the electron requires enough energy from an infrared wavelength to move to an excitation state of a higher energy level, S_1 . The electron returns to the ground state (S_0) by emitting energy in the form of a photon of lower energy compared to the energy of the absorbed initially. Image adapted from Solís-Iemus [154].

the optical properties of ICG are advantageous since haemoglobin and water are low absorbers within the ICG optical window. Additionally, the energy range is capable of penetrating into the intestine without causing thermal damage [29]. With a half-life of 3 – 5 minutes, the ICG dye is removed from the blood by the liver and excreted via the bile within 15 minutes [149].

Use of technique for monitoring bowel viability ICG-FA has been reported as a research tool for monitoring intestinal viability, where the majority of studies have been conducted on human participants [157, 7, 158, 151]. For visualisations of the outer surface of the intestine, sections of the intestine were isolated and exposed via surgical incisions. With an ICG dose ranging from 0.2 – 0.5 mg/kg injected intravenously, a hand-held NIR camera system is utilised to capture a video and displayed on a monitor [150, 159].

Given the intestine has adequate blood flow, the ICG should reach the vessels within the section of intestine under investigation. Using the NIR camera system, the intestine section would emit a vivid green-gold fluorescence. In contrast, inadequate blood flow would result in a dark blue–black image indicating the absence of the ICG dye within the region of interest, as illustrated in Figure 3.13.

An advancement was reported by Sherwinter [160], describing the first feasibility study and development of an NIR ICG-FA system to evaluate the colorectal mucosa

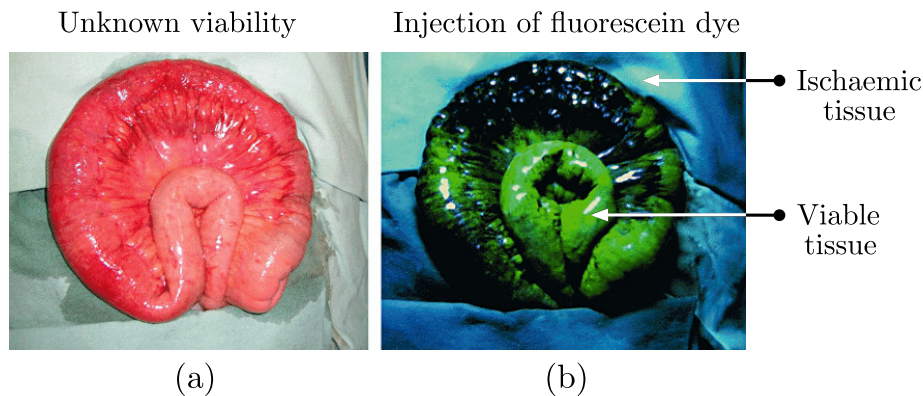


Figure 3.13 Visibility of fluorescein dye in intestine. (a) A section of the intestine with unknown viability. (b) After an injection of fluorescein dye, the bowel is illuminated under ultraviolet light, where emission of green-gold indicates viability, compared to the dark areas indicating ischaemia. Image adapted from Paral et al. [155].

viability. Mucosal viability was accomplished with the introduction of a custom-built trocar and disposable sigmoidoscope. A trocar is a needle-like surgical instrument, typically used in laparoscopic surgery, functioning as a portal for the placement of instruments or a drain collection of fluid.

The development called the PINPOINT system is the current imaging system available within the market designed for laparoscopic use, consisting of an endoscopic camera and light source with the ability to acquire white light and NIR images.

Following successful, high definition mucosal images of the entire bowel circumference [160], PINPOINT was trialled on 147 patients undergoing left-sided colectomy, where the fluorescence intensity was determined by a scoring system similar to the clinical assessment scoring [70]. With the additional visual aid, the use of PINPOINT altered 11 surgical plans resulting anastomotic success. However, no significant difference was found with the death rate, where 17% died due to postoperative complications.

Several additional studies were conducted with the use of PINPOINT for intra-operative assessment of the mucosal lining [158, 7, 157]. Jafari et al. [7] reported a success rate of 99% for the technique on 139 patients undergoing laparoscopic left-sided resection. ICG-FA provided indications for 8% changes of surgical plans, resulting in successful recoveries. Overall, the study concluded with anastomotic leaks and morbidity rates of 1.4% and 17%, respectively.

To understand the effectiveness of ICG-FA on postoperative complications, Boni et al. [161] performed ICG-FA evaluations on 42 patients undergoing laparoscopic surgery and compared to a control group of 38 patients assessed solely on visual

inspection. The control group were of previous surgeries, operated by the same surgeon to reduce the bias relation of surgical technique and experience. ICG-FA lead to 4.7% of surgical alterations and no events of anastomotic leaks, in comparison to the control group, where postoperative anastomotic complications occurred for two patients. As the study was conducted on a limited number of patients, no significant difference was found between the use of ICG-FA and postoperative complications.

Blanco-Colino and Espin-Basany [162] published a current systematic review highlighting the efficiency of ICG-FA to reduce anastomotic leaks. The review included 5 non-randomised trials where 1302 patients participated in the study comparing ICG-FA to clinical evaluation. Considering a large summation of data, there is a low level of evidence of ICG reducing the risk of anastomotic leaks. Additionally, where 555 patients were assessed with ICG-FA, no significant difference could be found with or without the use of the imaging technique.

Limitations The use of fluorescence is an advancement from the uses of radioactive molecules, where fluorophores have been reported to be as accurate as radioactive molecules [163]. ICG-FA shows positive impact in assessing intestine viability, where the technique extends operating time by an average of 5.1 minutes due to the almost immediate fluorescence visibility of up to 45 seconds [149, 161].

Although ICG-FA aids surgeons as an additional visualiser, the technique relies on a subjective evaluation of the fluorescence intensity and interpreting the cut-off between sufficient and insufficient intestinal viability. With the scoring system based on visual inspections, abnormal ICA-FA's were overlooked, leading to postoperative complications [160, 162]. Quantitative analysis of fluorescence imaging is the most desirable, however not currently available [149, 42]. To minimise observational variability, studies have been conducted to quantify the fluorescence intensity and identify threshold values [7].

Wada et al. [164] attempted to predict postoperative complication by measuring certain parameters from a time curve of fluorescence intensity. To obtain the time curve, a commercial analysis software was used, where the region-of-interest was positioned to assess the colon's serosal surface by evaluating the ICG pixel intensity. Specific parameters such as the time taken for the fluorescence or the intensity difference between the maximum and baseline were investigated as shown in Figure 3.14. The time taken for the ICG to be visible after injection was shown to be significantly delayed compared to non-ischaemic segments [165, 164].

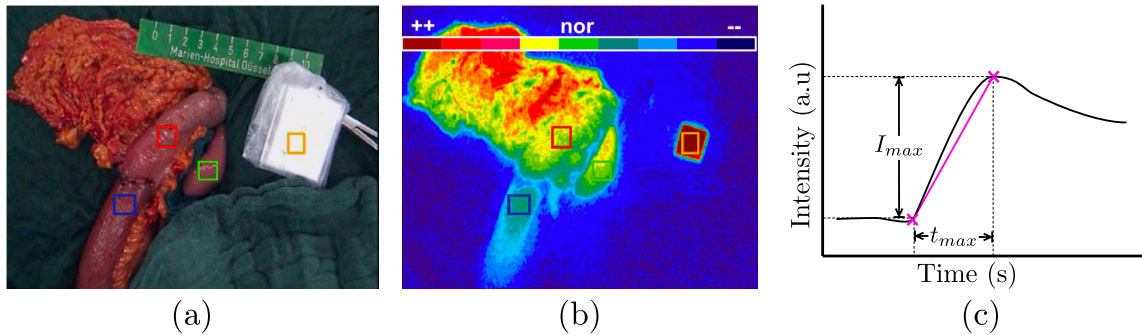


Figure 3.14 Quantifying fluorescence imaging. A right bowel resection undergoes fluorescence imaging to assess the perfusion state. Regions of interest shown in (a-b) as coloured squares can be chosen, where the blue square focuses on the preanastomotic bowel; the red square focuses on the postanastomotic bowel; the green square focuses on an unaffected region as the internal standard, and the yellow square focuses on an external standard with constant fluorescence. The change in pixel intensity of the fluorescence image (b) at each region of interest can be displayed onto a graph (c) to calculate the rate of change of intensity. The rate of change of intensity could provide a quantifiable measurement. Image adapted from Kudszus et al. [166].

Drawbacks using the fluorescence intensity have been found as the light source position is inversely related to the intensity of the tissue of interest [150]. Measurements of strong intensity in an area of inadequate blood flow can be obtained if the camera is placed close to the tissue. Additionally, the intensity of fluorescence is dependent on the surrounding light condition, therefore requiring the operating theatre to be darkened during measurements [36, 149].

As there is low evidence of ICG-FA reducing the risk of anastomotic leaks, the technique warrants further study in a larger group [70, 149, 162]. To conclusively determine ICG-FA as a reliable clinical assessment capable of being used routinely, a study with over 600 patients would be required to participate in the ICG-FA and control group [32].

3.3.2 Multi-photon microscopy

Multiphoton microscopy (MPM) is a type of intravital microscopy (IVM) technique, which is a powerful imaging tool allowing biological processes to be visualised *in-vivo* [167, 168]. An IVM study attempting to describe the anatomy and physiology of the alveoli is the earliest report known [169], resulting to be a gold standard technique for lung immunology of small animals [170] and for micro-circulatory research [30, 171]. Assessing the micro-vasculature has brought significant advancement in the

understanding of the white blood cells (WBC); as *in-vitro* techniques were failing due to the short life span of the cells [169].

The micro-vasculature consists of three types of small vessels, arterioles, capillaries and venules, which form a network to conduct blood-tissue exchange [172, 173]. Arterioles are of great interest when determining regional blood flow [172]. Similarly to the lung and heart vasculature, bowel capillaries are made of continuous layers of endothelial cells, allowing molecules less than 3nm radii to pass passively [172]. As IVM can visualise changes at capillary level, imaging the bowel micro-vasculature could provide sensitive insights to viability and bowel complications [99]. More specifically, visualising the vasculature closest to the mucosa would be beneficial, as the layer is highly susceptible to changes in the blood and oxygen supply [171].

Principle of operation There are various light microscopy techniques utilised for IVM, however, MPM is the most performed technique [168], using fluorescently-labelled plasma or red blood cells (RBC) [30]. Unlike FA, as seen in Section 3.3.1, which requires a single excitation photon, MPM requires two or more excitation photons to move a fluorophore electron to a higher energy state [168, 174].

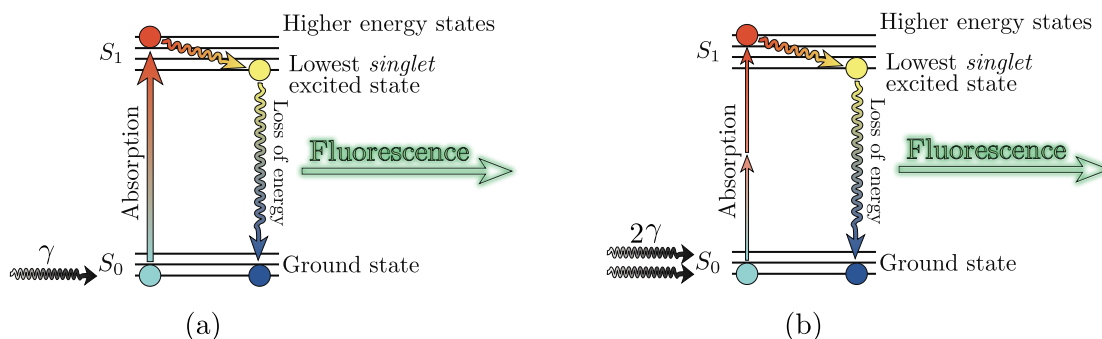


Figure 3.15 Difference between single photon (a) and multiphoton excitation (b). A multiphoton excitation undergoes the process with several photons. As illustrated, two photons are absorbed by the fluorophore for excitation to a higher energy state. The fluorophore simultaneously absorbs two photons, which are half the energy of a single photon absorption. For both types of excitation, the fluorophore emits energy in the form of a photon, to return to the ground state. Image adapted from Solís-lemus [154].

Referring to Figure 3.15, two photons, with half the original excitation energy, are simultaneously absorbed by the fluorophore, causing the fluorophore to be excited at the same higher energy state as a single excited fluorophore. This advantageous principle allows the use of lower energy and longer wavelengths, resulting in high

resolution images due to less scattering [168, 167]. This eliminates out-of-focus light, as multi-photon excitation is highly probable in the central region of the spot source [156]. By emitting short laser pulses of low energy to the tissue sample, the excitation photons are less absorbed by unlabelled biological tissues and allowing deeper penetration [156].

Due to its high quality, MPM is considered as a common choice of imaging if the tissue depth is up to 1 mm [167]. As for the small imaging depth, the technique requires direct contact with the tissue, therefore a rigid glass window could be attached to hold the tissue in place [170].

Use of technique for monitoring bowel viability MPM at cellular level has only been performed on animals [174, 175] and has not been introduced to human participants [30]. Whilst undergoing the process of obtaining images, the body temperature of small animals is maintained using electrical warmers or heat pads, as the imaging process is lengthy [176]. In preparation for MPM, the animals are placed on a microscope stage and the section of the bowel to be studied is exteriorised via surgical incisions and held in place to minimise disturbance of the blood supply [169, 177]. To ensure there is a flat field view and direct contact for the MPM, cover slips are directly applied onto the tissue surface [175, 177], in some cases with saline-soaked gauze to keep the tissue moist [169]. Prior to imaging blood vessels, cells are labelled with fluorescence via intravenous injections [177, 178].

MPM has shown promising abilities in imaging bowel structures, for example, the presence or absence of blood circulation [177], RBCs [99] and neurons in addition to nerve fibres [176]. To understand further mucosal micro-circulation, Farquhar et al. [179] performed MPM on 12 rats during cecum occlusion. By recording images consisting of six villi per animal, sepsis induced by ligation lead to a reduction in the number of perfused capillaries. A common finding was observed, where the reduction of perfused capillaries changed the micro-regional blood flow, correlating to the structural and functional alterations in the mucosal layer [179, 178].

Closely related to anastomotic surgeries, Diller et al. [178] performed MPM on sixty mice immediately after a colonic resection, imaging the functional capillary density, which is the number and length of perfused capillaries. A comparison was made between a control and a septic-induced group. A reduction in the functional capillary density was found in septic mice, compared to the control. Such findings contribute to a reduction in bowel viability. Furthermore, within the septic mice, the number of

perfused capillaries were found to be approximately double in regions further away from the anastomotic site [178].

Limitations MPM is an example where techniques, *i.e.* optical and imaging, begin to merge, resulting in powerful tools; suggesting a more reliable monitoring requires a combination of techniques to provide valuable information. Despite being presented as a powerful tool, some drawbacks can be outlined. The main challenge, as seen by researchers, were blurry and non-interpretative images, caused by (i) motion artefacts related to bowel motility and (ii) the presence of debris and mucosal secretion [176, 179, 177, 168]. Fixturing of the organ via the use of suction windows or glue have been performed, however the imaging remains to be unreliable [177].

The major limitation of MPM is its extreme invasiveness, where the method requires subjects to be re-anaesthetised and reopening of the incised abdomen to place the tissue region of interest onto the microscopic stage [179]. Exteriorising and fixating the bowel may provoke micro-circulation dysfunction if the bowel physiology has not been maintained [177, 168]. In addition to time constraints during human surgeries [30], MPM undoubtedly is not a technique for human participation, hence unfound results of the technique.

MPM remains as a research technique aiding in understanding immune cell functions [169] and potentially a main tool for studying cell biology [168]. With the attempt to use MPM for assessing bowel viability, the technique furthers the notion that the micro-vascular dysfunction surrounding an anastomosis is an early indicator of healing impairment; as a reduction in oxygen availability may lead to an increase rate of cell death postoperatively. Therefore, measurements such as oxygen saturation may be possible to detect the onset of unsuccessful healing [178].

3.3.3 Sidestream dark-field imaging

Sidestream dark-field (SDF) imaging is another intravital microscopic technique advancing from the use of fluorescent dyes, allowing quantitative micro-circulatory measurements [180]. By imaging the micro-vasculature, clinicians could diagnose the condition of an organ [173].

Principle of operation SDF is an imaging technique comprising of a handheld device at direct contact to the tissue area of interest to illuminate and utilise the scattering properties of the tissue [181, 173]. The green light source is obtained

3.3 Imaging modalities

from concentrically mounted light emitting diodes (LEDs); where a wavelength of approximately 530 nm [182] is typically used, as this corresponds to the isobestic point of a haemoglobin absorption spectrum [181]. As haemoglobin absorbs green light, RBCs, also known as erythrocytes, appear dark in images, compared to leucocytes which are seen as refringent bodies [181]. Referring to Figure 3.16, the centre of the device holds the light guide core consisting of a magnifying lens, which is used to project the back-scattered light into a video camera. To minimise tissue surface reflections from entering the light guide, the LEDs are optically isolated from the core [181], producing high resolution images of micro-circulation. By collecting sequential frames (videos) and utilising image processing techniques, measurements such as blood flow can be assessed by identifying individual RBCs from multiple frames, vessel density and dimension [38].

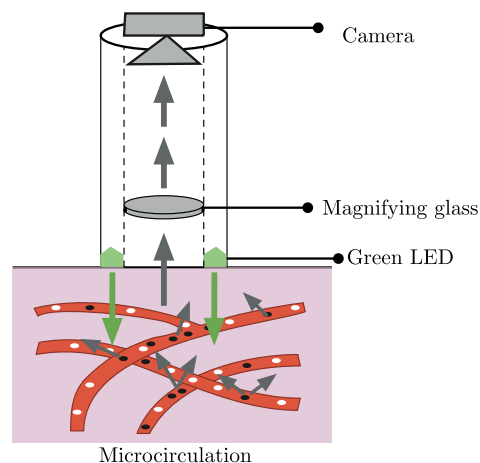


Figure 3.16 Principle of sidestream dark-field imaging. Green light is emitted from an outer ring of light emitting diodes. Red blood cells containing the pigment haemoglobin, absorbs the light penetrating through the tissue, where dark moving cells are observed. Images are obtained by the core, collecting the scattered light and passing through a magnifying lens, projecting the image onto a camera. To produce high resolution images, tissue surface reflections are minimised by optically isolating the light source from the detector. Image redrawn from Turek et al. [183].

Use of technique for monitoring bowel viability SDF has been reported as a research tool for monitoring bowel viability, where studies have been conducted on animals [183, 180] such as sheep [184] and horses [185], and human participants [182, 181]. Before images are obtained, the bowel section of interest is isolated and exposed via surgical incisions, allowing the SDF imaging device to be placed on the bowel

surface. Subsequently, blood and secretions found on the surface are removed and cleaned with sterilised saline [181]. For additional sterility and prevention of artefacts which could hinder the image, the SDF hand-held device is covered with a disposable sterile endoscopic camera cover, heated to body temperature prior use [181].

Given the micro-circulation in the intestine is adequate with a rich supply of RBCs containing haemoglobin, dark structures representing the RBCs can be observed, as shown in Figure 3.16(b). For both participating categories, common micro-circulation quantification are extracted from the image, such as, perfused vessel density (PVD), total vessel density (TVD) and most importantly, micro-vascular flow index (MFI), proportion of perfused villi (PPV).

MFI is a categorical flow score, ranging from 0 to 3, indicating the type of flow which corresponds to no flow (0) and continuous flow (3) respectively [181, 186, 187]. The approach in calculating the MFI is to sum the scores given within an image, divided by the number of visible villi [186]. PPV is obtained with the number of villi having normal flow, which is a flow score greater than 1, divided by the total number of villi within the image [186].

Where SDF imaging on animal studies dominate, there are limited findings on human gastrointestinal micro-circulation. de Bruin and Kornmann [181] reported a feasibility study of SDF imaging with human participants, where serosal micro-vasculature of 17 participants during laparoscopic colorectal surgery were observed. de Bruin and Kornmann [181] demonstrated the ability to obtain images of the serosal micro-vasculature alongside sublingual SDF imaging. Clear visuals of the bowel microcirculation allowed its quantification, where the bowel PPV and TVD were significantly lower than the sublingual micro-vasculature. Comparing measurements from both tissue sites, the acquisition time to obtain a clear image on the bowel was significantly higher; taking 108 seconds compared to 46 seconds.

Boerma et al. [187] showed evidence of SDF being applied less invasive by acquiring images from intestinal stomas. To understand the relationship between micro-circulatory changes between regions of stomas and sublingual, Boerma et al. [187] evaluated 23 patients with newly constructed stomas and experiencing abdominal sepsis in comparison to 10 non-septic participants with stomas. The results support the hypothesis where micro-circulation abnormalities are main indicative factors of sepsis compared to systemic haemodynamic, such as heart rate, mean arterial pressure and cardiac index. Additionally, comparisons between the tissue regions highlight the importance of regional monitoring.

Limitations SDF is a beneficial technique in comparison to visual techniques such as FA, as it is the only technique providing information such as, the number of vessels perfused, the quality of flow and determining areas of occlusion [181]. However, most studies encounter image stabilisation difficulties, due to bowel peristalsis and arterial pulsation within the intestinal region, therefore affecting the image quality [181]. NIR-ICG, described in Section 3.3.1, would be a preferred imaging technique compared to SDF, as the fluorescence technique has monitoring abilities without the need of direct contact to the tissue region [181].

A relevant conclusion from analysing SDF is the highlighted importance of regional monitoring. In studies where comparisons between tissue regions of stoma and sublingual in septic participants, sepsis could not be predicted with sublingual SDF images; as the MFI on postoperative day 1 were not correlated between the two regions [187].

3.3.4 Colonoscopy

Colonoscopy is an imaging technique increasingly used by clinicians to examine the lumen of the colon. First introduced in 1966 [188], colonoscopy has become a gold standard technique allowing visualisation and diagnosis of pre-cancerous lesions within the intestine cavity [189]. The first layer of the colon to be affected by ischaemia is the mucosa and was identified due the ability of gaining access with such technique to otherwise inaccessible regions [43, 22]. Long duration of colonic ischaemia, deprives the colon from oxygen and nutrients; resulting in hypoxia [54]. Progressively, hypoxic damage progresses from the lumen outwards to the serosa [54]. Recalling intraoperative visual inspections of the bowel colour (Section 3.1.1), ischaemia could be identified from the serosa, which is the last layer affected by ischaemia. Intraoperative colonoscopy provides direct visualisation of the mucosal lining and anastomosis, allowing surgeons to revisit their resection minimising postoperative complications.

Principle of operation A colonoscope, Figure 3.17, is a small, flexible and minimally invasive instrument which enters through the rectum and advances to the section of the colon requiring examination. The modern colonoscope is a state-of-the-art imaging technology which uses optical fibres for illumination. Enclosed in a water-tight, biocompatible, plastic tubing of approximately 2000 mm and 13 mm in length and diameter respectively [190, 191], the colonoscope holds the optical fibres, angulation cables and various channels such as suction, air inflation and water [190]. Thorough design considerations have been taken, where the insertion tube has been made durable

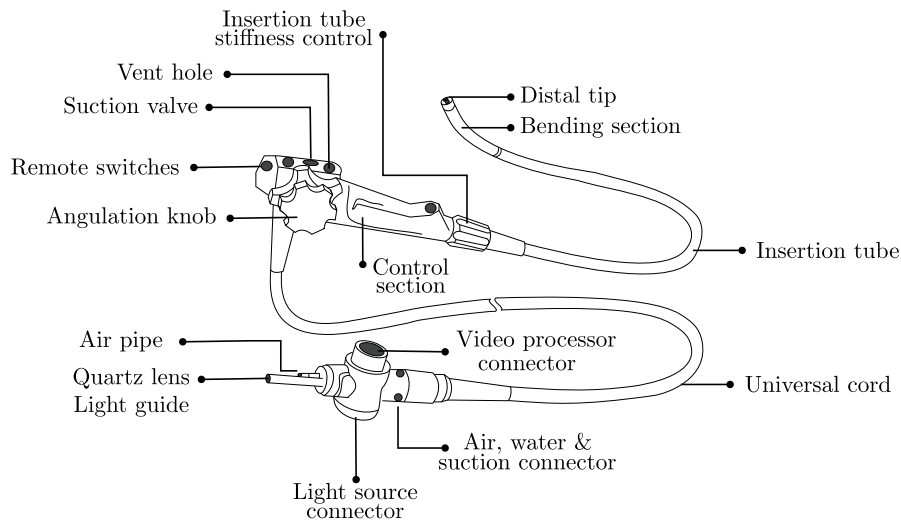


Figure 3.17 Parts and accessories of a colonoscope. A colonoscope is a minimally invasive instrument, where the insertion tube enters the rectum and advances to the section of the colon requiring examination. The colonoscope allows image and video capturing, with a control section allowing the clinician to manoeuvre the distal tip and provide suction or air to the region. The universal cord aids in the transmission of sources such as light, air, water and suction. Image redrawn from Wayne et al. [190].

to withstand force when inserting the instrument through the colon. Additionally, flexibility has been accomplished to allow sharp bends of the instrument within the bowel and to return to its normal straight shape when withdrawn from the patient.

The colonoscope consists of a control section which branches into two connector tubes known as the universal cord and the insertion tube [190]. The universal cord aids in the transmission of xenon light from the light source to the distal tip of the insertion tube and receives information from the distal tip which can be fed into a video monitor. The insertion tube, as the name refers, intubates the colon, consisting of hollow channels commonly used for suction or biopsy, air or water for lens cleansing and insufflation, and a forward directed water channel [191]. The distal end of the insertion tube has a bending section of approximately 100 mm, controlled by the technician-operated switches. The control section consists of various switches and valves that control many colonoscope functions. The imaging capability is due to the camera located behind the objective lens; capturing the image and transmitting to the video processor through the universal cord [190].

Use of technique for monitoring bowel viability Colonoscopy is utilised intraoperatively in various ways to identify ischaemia or intestinal viability [192, 193, 76, 194].

With the colonoscope, surgeons are able to perform mechanical patency assessments, as mentioned in Section 3.1, by observing changes in the mucosal lining in a less invasive manner. Although bowel cleansing prior colonic surgery is debatable, full cleansing of the bowel is essential for a safe and effective intraoperative colonoscopy [195]. To capture a video within the lumen of the intestine and to be able to manoeuvre the instrument for optimal viewing, extreme care is taken to insufflate the section due to risks of perforation and further reduction in intestinal perfusion due to high intraluminal pressures [192, 54].

Mucosal changes in colour during ischaemia have been observed, where changes of the lining may reflect the severity of ischaemia [192, 22, 196]. Early indications of mucosal changes have been observed by Washington and Carmichael [22], where the mucosa appears pale with areas of petechial haemorrhage (bleeding from broken capillaries) and signs of oedema. Exceeding 48 hours, the mucosa appears grey-green or black, indicating severe ischaemia [22]. Similar attempts of grading viability have been performed, assessing the appearance of the anastomosis circumference by colour [197]. Sujatha-Bhaskar and Jafari [197] suggested immediate intraoperative revision of the anastomosis when patients were graded with ischaemia or congestion involving over 30 % of the region on both sides of the staple line. Although identifying the need for revisions and re-grading to normal appearing anastomoses, 12.2 % of the entire cohort encountered anastomotic leaks. Furthermore, with an accumulated result based on similar studies [198, 196, 199, 200, 76, 32], no statistically significant reduction in postoperative leak rates whilst using a colonoscope were found.

Air or fluid leak tests are also performed during intraoperative colonoscopy, by insufflating CO₂ into the lumen of the bowel. The method is performed as described in Section 3.1.4, where the anastomosis is submerged under saline, however the use of colonoscope provides advantages to visually locate areas of the anastomosis requiring revision [195, 201]. Leak tests intraoperatively are not routinely used, however it was hypothesised by Simianu et al. [202] that routine intraoperatively leak testing would increase after an anastomotic leak based on the recency effect.

Limitations Colonoscopy is an attractive technique for monitoring intestinal viability due to its flexible and minimally invasive design. Whilst remaining small, colonoscopy can incorporate several additional channels to introduce medical instruments, therefore increasing the preference to use within the gastrointestinal department [192, 195]. There are several evidences that intraoperative colonoscopy could reduce rates of leakage and

bleeding [71, 196, 197], followed by diagnosis of postoperative complications within 48 hours [54]. Unfortunately, no benefit of the technique has been established [197], as studies performing colonoscopy for anastomotic integrity showed to be inconclusive [196]. Where intraoperative visualisation of the anastomosis and mucosal lining deemed successful, postoperative complications are still occurring [196].

Performing colonoscopy bears the risk of weakening or damaging the anastomosis, therefore careful training is required [196, 191]. Continuous training is required for colonoscopists to ensure they are made proficient in the fast-evolving imaging technique [203].

The technique undoubtedly is an improvement from extraluminal assessments, as surgeons are able to evaluate and obtain real-time feedback once resections are made to ensure technical excellence is achieved [195, 190]. The subjectivity remains as the decision-making is based on visual inspection; with the possibility of overlooking mucosal abnormalities [188]. To address the subjectivity of the technique, additional information such as quantitative measurements of the micro-circulation could make colonoscopy a desirable technique for assessing intestinal viability.

3.4 Optical

Optical techniques utilise light as the main principle to acquire and extract physiological measurements. The techniques described in this section are (i) biochemical inflammatory response, (ii) laser Doppler flowmetry, (iii) flow cytometry, (iv) visible light spectroscopy and (v) pulse oximetry.

3.4.1 Biochemical inflammatory response

Biochemical inflammatory response is a technique assessing indicators within the body relating to the severity or presence of inflammation, known as biomarkers [26]. The most common biomarker for inflammation is C-reactive protein (CRP), which is regarded as a useful indicator to monitor treatment response and an inflammatory disease diagnosis [55, 204]. Signs and symptoms of infection such as sepsis takes several days to be observed, however, CRP response is the earliest observation which can be made within hours following an onset of infection or injury [205].

CRP has a normal range of less than 3.0 mg/L in healthy individuals [26]; with the detection of inflammation, infection or tissue damage causing CRP levels to

increase within 2 – 6 hours, peaking approximately at 48 hours [206, 26]. Detection of inflammation or tissue damage causes CRP production mainly in the liver, otherwise produced locally by neighbouring tissues [26].

In the context of an anastomosis, with reference to Figure 3.18, the protein binds to the cell surface of pathogens, dying or dead cells to promote phagocytosis. Upon resolving the inflammation or tissue damage, CRP levels rapidly decline, else suggesting the presence of infection or likelihood of an anastomotic leak [29, 206, 207]. Therefore, monitoring the release of CRP found in the systemic bloodstream or locally within the surgical site provides a rapid indication of the protein aiming to restore the body and remove the cause of disturbance [55, 26].

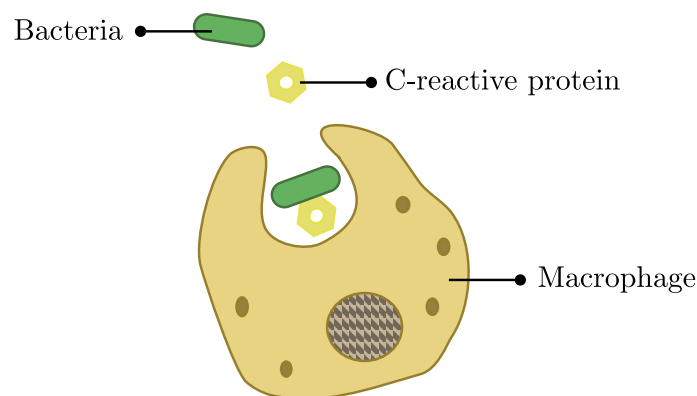


Figure 3.18 Process of C-reactive protein (CRP) binding to bacteria for the promotion of phagocytosis. An increase in CRP levels are the earliest observations that can be made; being at its highest level at 48 hours. The production of CRP occurs within the liver where they go onto binding with the bacteria or dead cells, to promote phagocytosis, where a macrophage (white blood cell) engulfs the pathogen.

Principle of operation Measuring CRP levels requires a sample of blood to be extracted from a vein and centrifuged to obtain serum. Until late 1970, CRP was measured using a qualitative or semi-quantitative laboratory technique known as latex agglutination [208]. The technique begins with the formation of antigen-antibody clumping of latex beads, coated with CRP antibodies and bound to CRPs in a patients' serum sample [207]. Results are obtained qualitatively by observing for visible agglutination under artificial light or quantitatively by comparing the result to known dilutions of CPR containing serum and saline buffer [207].

Currently, accurate and rapid quantitative measures of CRP are obtained using optical techniques known as laser nephelometry and turbidimetry [209, 208]. Advancing

from visual observations of the formed clumps, the concentration of CRP is determined by the amount of cloudiness, or turbidity, in a serum sample through measurements of scattered light.

Turbidimetry and nephelometry are techniques based on measuring light passing through a medium. Like photometry, when a beam of light passes through a sample, the intensity of light is reduced by scattering, which is dependent on the concentration and size of the particles. Similar to spectrophotometry, turbidimetry measurements are obtained when the incident beam is detected at a light detector placed at 180 degrees (Figure 3.19). Nephelometry measurements are obtained when the incident beam is detected at light detectors placed approximately between 10 – 90° [204]. Accurate measurements are obtained within 30 minutes and a sensitivity of approximately 0.04 mg/L with the use of a calibration curve based on known CRP concentrations in a saline buffer solution [207].

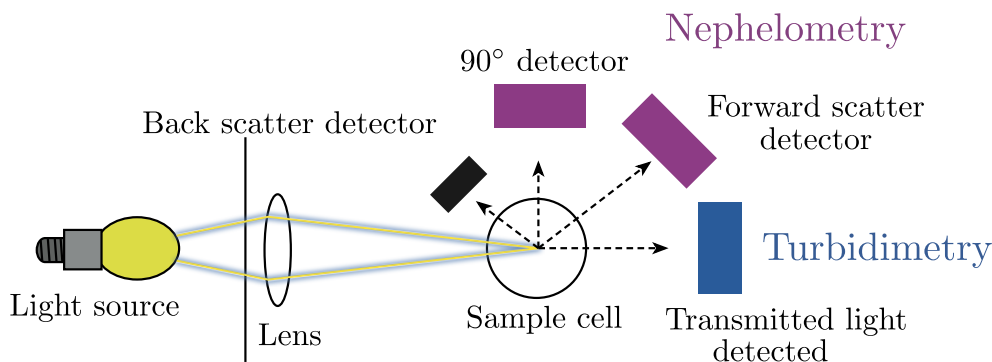


Figure 3.19 Set-up for nephelometry and turbidimetry. Each technique detects light passing through a medium to measure the concentration of suspended particulates within a liquid. Turbidimetry is similar to spectrophotometry, where light is detected at 180°. Scattered light detected at angles between 10 – 90°.

Use of technique for monitoring bowel viability Quantifying CRP has led to increased application from cardiovascular disease to postoperative indications of anastomotic leaks and sepsis due to the improved methods [207]. CRP levels are measurable postoperatively by obtaining venous blood samples intermittently or in the peritoneal drain fluid [29]. Several studies indicate significant elevation of CRP levels prior to an anastomotic leak, compared to patients with successful healing and reduction in levels by postoperative day 3 [29, 206, 135, 210].

Studies attempted to choose a cut-off value for CRP levels indicating postoperative complications, ranging from 124 mg/L to 172 mg/L between the third and fifth day after surgery [210, 205, 211]. As the level of CRP is affected by the degree of surgical trauma and operating time, Facy et al. [212] suggested levels below 100 mg/L on postoperative day 4 strongly correlate to the absence of postoperative complications, allowing patients to be discharged.

Limitations Given the promising results, monitoring CRP levels could allow the prediction of anastomotic complications, aiding surgeons in decision making with regards to early patient discharge or requiring additional stay for further observation [205]. However, measurements of CRP are not specific as an increase could mimic less severe infections including urinary and wound infections [26]. Additionally, patients with a successful anastomosis may exhibit a severe or prolonged systemic inflammatory response due to surgical trauma, blood loss and operating time, thus producing a false positive [213, 82, 211].

As daily CRP levels range considerably between studies, isolating daily CRP levels as a predictive value for determining complications may not be accurate, therefore Smith et al. [213] suggested to determine the rate of change of CRP combined with future predictions of the rate with the use of linear regression. The prediction approach achieved an area under the receiver operating characteristic (ROC) curve to be 0.961, where values above 0.90 are considered as trustworthy information to support a clinical decision [213]. Regrettably, the high achieving predictive model has a potential for spurious results due to results based on 197 patients, were only 11 (5.6%) encountered anastomotic complications.

The predictive values are limited and unclear as the concluding cut-off values vary considerably. With the lack of clinical data, interpreting a specific predictive value to associate with anastomotic complication remains difficult [82, 206]. Routine measurements of CRP are beneficial for identifying cases of major ineffective complications at an early stage, however the technique is unable to correlate specifically to a type of complication [205, 55, 214].

3.4.2 Laser Doppler flowmetry

Laser Doppler Flowmetry (LDF) is known to be a feasible and reliable technique in cardiology, for the estimation of blood flow in the micro-circulation [85]. Following the first LDF blood flow measurements reported by Riva et al. [215], the non-invasive

technique has been adopted in many areas including the skin, dental and the intestine [37, 85, 216–218]. Regarding the technique's name, LDF is an optical technique utilising a laser light to interact with RBC for blood flow estimations and average velocity [85]. Blood supply at the suture line of the anastomosis is crucial [219], thus qualitative estimation of the blood flow and velocity within the bowel would be a good indicator of viability.

Principle of operation The principle originates from the Doppler effect, described in Section 3.1.5, which relies on laser light reflected from moving RBC and measuring the frequency shifts [219, 220]. A continuous light source transmits through an optical fibre to the tissue of interest, where different types of probes can be used to collect the information [217, 219, 218, 221].

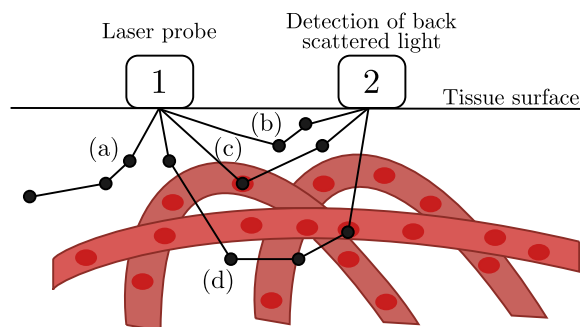


Figure 3.20 Schematic diagram of Laser Doppler flowmetry. Illuminating the tissue by a laser source (1), majority of light is either absorbed or scattered by static structures (a, b). Only 3 – 7% of photons are reflected by moving red blood cells (c, d), returning to the second optical fibre (2). Image redrawn from Lima and Bakker [98].

Depending on the intended use of LDF, there are different types of probes for needle and endoscopic assessments [217], which require direct contact between the probe and tissue [222]. Referring to Figure 3.20, when light photons transmit through the tissue with a penetrating volume of approximately 1 mm^3 [85], 93 – 97 % of photons undergo absorption or scattering after interacting with static structures [218, 98]. The remaining 3 – 7 % of light is reflected by the moving RBCs [98], resulting in a shift in frequency between the emitted and detected light, known as the Doppler shift. This back-scatter is collected by a second optical fibre, connected to a monitor for further analysis. Analysis of the backscatter results in an arbitrary term known as flux, which is directly proportional to the product of both the RBC concentration and average

velocity within a sample volume, as shown,

$$Flux = k \times v \times V, \quad (3.4)$$

where k is the proportionality constant, v is the mean speed of the RBCs, which is proportional to the mean change of frequency, and V is the concentration of moving RBCs. The difference between flow and flux should be noted. Flow is the rate of change in a sample volume, whereas flux is the number of RBCs passing through a sample volume in a given time [85]. Equation (3.4) produces a unit-less value, as all tissues have different properties, the LDF instruments are not calibrated to provide absolute blood flow measurements [38].

Use of technique for monitoring bowel viability LDF has been reported as a research tool for monitoring intestinal viability on animal and human participants [223]. Animal studies have been performed on small samples of anaesthetised cats [224], rats [179], pigs [145] and dogs [225–227]. For blood flow monitoring, sections of the bowel were isolated and exposed via surgical incisions. This allowed the LDF probe to be placed on the surface of the intestine to obtain blood flow measurements from the serosa [145, 226, 227, 224, 228]. Direct measurements of mucosal blood flow are uncommon, however Thorén et al. [229] demonstrated the possibility of measuring jejunal mucosal blood flow within the small intestine during a cardiopulmonary bypass. Through the nasogastric route, a catheter consisting of the LDF probe was guided with a fluoroscope. Close contact of the probe with the mucosal lining was assumed due to the jejunum being collapsed whilst the patient was anaesthetised.

To understand the relationship between blood flow and intestinal ischaemia with the use of LDF, reduction of blood flow was induced by occluding the mesenteric artery with a clamp under operative conditions. Before the onset of an occlusion, LDF measurements require baseline measurements to be obtained. Several studies such as Seike et al. [223], demonstrated LDF measurements decreasing significantly from the baseline after clamping the mesenteric artery [145, 55, 225].

Vignali et al. [230] attempted to predict the occurrence of anastomotic leaks in 55 colorectal cancer patients by obtaining intraoperative LDF measurements. Comparing micro-vascular blood flow measurements of patients with uncomplicated recovery and those who developed anastomotic leaks, a decrease of 6.2% and 16% respectively was observed. Similar observations were found, where a decrease of more than

50 % [223] or 30 % blood flow [226, 227], suggested a risk of anastomotic ischaemia and complications [231].

Limitations Although the majority of studies demonstrate the value of LDF measurements as an indication of non-viability [232], the technique presents major limitations. LDF measurements are susceptible to artefacts. For instance, Abdollahi et al. [8] found insignificant differences between blood flow measurements before and after clamping. The same has been observed by most LDF users, where motion artefacts are introduced by tissue motion or the operators' stability [30, 216]. To overcome this limitation, methods of isolating the tissue region of interest have been considered in addition to the use of a fixed and constant probe position [216, 217].

Results from LDF cannot be easily reproduced. Wide individual variations have been observed by researchers suggesting no correlation between the measurements and blood flow [225, 145]. Similar to Doppler ultrasound (Section 3.1), the technique is considered subjective due to the use of arbitrary units [98], causing an incapability of discriminating between positive or negative frequency shifts [30, 233].

Scanning LDF, a technique which produces a colour image representing changes in colonic viability, has been presented to overcome the limitations previously described of single point LDF, which obtains spot measurements of 1 mm^3 [219]. Scanning LDF requires the technology to be positioned approximately 32 cm above the patient and requiring full exposure of the tissue of interest [219]. Although this proves to be advantageous as direct contact is not required, which neglects the chances of the probe pressure from impairing the local blood flow [219], scanning LDF takes several minutes for an image to be produced and suffers image quality degradation due to motion artefacts [30].

LDF is not appropriate as a technique for colorectal viability measurement. Several undesirable characteristics and limitations have been found in LDF, through the description of various studies. Thus, the assessment of blood flow using the LDF technique fails to be embraced in the clinical setting.

3.4.3 Flow cytometry

White blood cells (WBC), also known as leukocytes, are important cells within the immune system, circulating throughout the bloodstream [234]. WBCs main function is to protect the body from infections by attacking foreign substances [234, 20]. Like

CRP, WBCs are regarded as useful indicators for inflammatory complications such as tissue damage, ischaemia and necrosis [235].

For healthy individuals, the normal WBC count ranges between 3500 μL to 10 500 μL of blood [20, 235]. As an inflammatory response, the number of WBCs increases to eliminate inflammation by congregating at sites of infection via cell migration [119]. A high WBC count called leucocytosis, could provide an indication of unseen infections [234]. Therefore, monitoring the number of WBCs could provide an early detection of infectious complications postoperatively; allowing clinicians to intervene with a suitable treatment to resolve the issue [236].

Principle of operation Counting the number of WBC has advanced from manual viewing under the microscope to an automated, precise analyser [237]. Flow cytometry is an optical clinical laboratory technique which sorts, counts and measures multiple characteristics of cells or particles in extracted blood from a vein, a heterogeneous fluid mixture [238]. The cells, suspended in the liquid, are passed through a laser light beam in a single file, where the scattering of light at different angles distinguish cell characteristics such as size via forward angle light scatter [238].

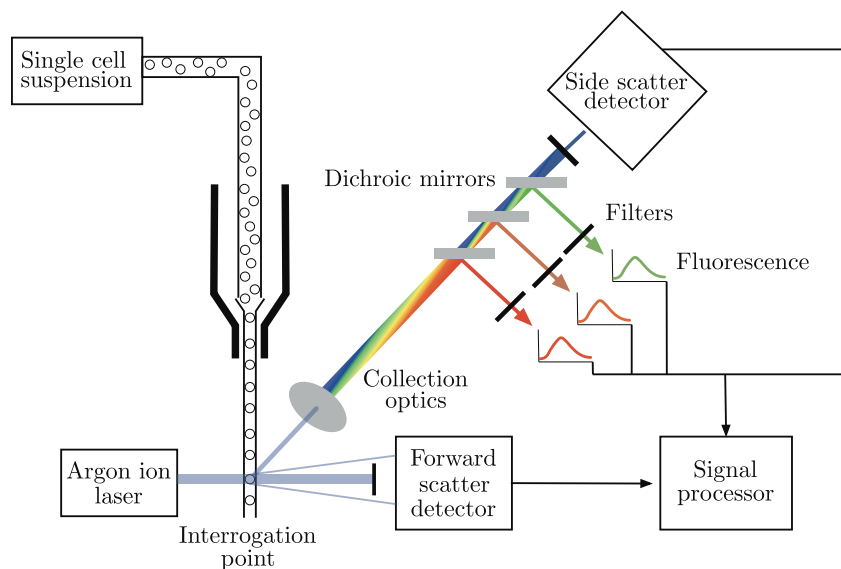


Figure 3.21 Principle of flow cytometry. Single cell suspension surrounded by sheath fluid to allow laser beam interception. Signals from forward angle light scatter and side scatter are detected by photodetectors and several fluorescence emission detectors. Detected light is digitally converted for computational analysis and represented as quantitative data. Image redrawn from Brown and Wittwer [238].

Current state of the art for assessing intestinal viability

For cells suspended in the blood sample to be drawn into a single file, laminar flow, the sample is surrounded by an isotonic buffer, known as a sheath fluid. Referring to Figure 3.21, the cells are passed individually through an interrogation point, also known as the laser intercept, where a laser light interacts with a single cell and measurements of forward angle scatter and side angle scatter are obtained by photodetectors. Additionally, fluorescent dyes may be incorporated in the sample to label cells; where fluorescence emission occurs when the laser beam excited fluorophores within the cells. By passing the light through a series of filters and dichroic mirrors, wavelengths of light are isolated and digitised for computational analysis, producing results in the form of histograms and scattered graphs.

Use of technique for monitoring bowel viability Flow cytometry has become a powerful tool due to its simultaneous multi-parametric analysis of thousands of cells and particles per second [237]. Several studies have shown WBC count as a predictive factor of postoperative complications [235].

Automated WBC counts have become a powerful tool due to its simultaneous multi-parametric analysis of thousands of cells or particles per second [237]. This has led to increased applications where WBC counts are seen as a predictive factor of postoperative complications such as sepsis and anastomotic leaks [235]. WBCs are measurable postoperatively by obtaining venous blood samples intermittently and compared to pre-operative values [213]. Several studies following colorectal resection monitored WBCs preoperatively and postoperatively to evaluate the parameter to patients who encountered anastomotic leaks and to those who healed successfully [239, 210, 240]. A common finding showed an increase in the WBC count by postoperative day 5 [236, 210], however postoperative WBC values had a insignificant rise between the two groups [210, 240], in addition to elevations seen for patients prior a leak diagnosis [239].

Limitations When comparing the two inflammatory biomarkers, CRP and WBC, WBCs were significantly lower, resulting in no substantial contribution in distinguishing patients with inflammatory complications [236]. An increase in WBC values were delayed resultants of a postoperative complication, similar to assessing vital signs of a patient, such as their temperature and heart rate [205, 239]. It must also be noted that the increase in these inflammatory biomarkers are non-specific, where an increase

in values during the postoperative period is a common response [235] and could mimic less severe infections, such as urinary tract infections or wound infections [26, 82].

Advancing from manual to electronic counting allowed closed tube sampling, minimising sample contamination and preventing direct exposure to the clinicians [237]. Additional advantages such as the techniques simplicity, availability and low costs, has allowed WBC counts to be monitored extensively postoperatively [235, 237]. However, evidence in their diagnostic value in predicting inflammatory complications and the optimal time to measure the number of WBCs postoperative to colorectal surgeries remains unknown [236]. Rather than the technique, the use of biomarkers has failed to demonstrate its usefulness in identifying bowel viability due to the small group studies, therefore inadequate for routine clinical practice [192].

3.4.4 Visible light spectroscopy

Visible light spectroscopy (VLS), also known as reflectance light spectroscopy (RLS) or white light spectroscopy (WLS), is an optical technique commonly used to measure the concentration of compounds within a mixture [241]. Blood is a mixture of compounds, with special interest in the chromophores oxygenated haemoglobin (HbO_2) and deoxygenated haemoglobin (HHb), where the molecules absorb wavelengths of light differently. By analysing the chromophores absorption, oxygen saturation within a tissue can be estimated [36, 242].

WLS has been employed to assess regional tissue oxygenation within the bowel [99]. As the mucosal layer consists of a complex network of capillaries, majority of haemoglobin molecules can be examined to measure tissue capillary oxygenation as an indicator of bowel ischaemia [242].

Principle of operation WLS utilises white light which is a mixture of wavelengths spanning from the visible to near-infrared region of approximately 400 nm to 700 nm [241]. The typical setup of a WLS consists of a lamp source and fibre optics to deliver the light from the source to tissue and a secondary fibre to collect the reflected light from the tissue [241, 36, 242]. The reflected light is analysed by a processing instrumentation which splits the white light into their corresponding wavelengths to produce a reflectance spectrum [36, 243, 242].

As HbO_2 and HHb absorb different wavelengths of light, the concentration of these chromophores can be extracted from the reflectance spectra. This is performed by mathematical comparisons between the measured reflected spectra and a reference

spectrum for each chromophore [241]. Once estimating the concentrations, the tissue haemoglobin oxygenation saturation (S_tO_2) can be calculated using the following equation,

$$S_tO_2 = \frac{oxy}{totalHb}, \quad (3.5)$$

where the *totalHb* is the summation of oxygenated and deoxygenated haemoglobin [30].

Use of technique for monitoring bowel viability WLS has been reported as a research tool for monitoring bowel viability on animal such as pigs [107, 244] and rats [33, 245], and human participants [246, 247, 6, 248].

For intestinal S_tO_2 measurements, the small and large intestine has been examined with the use of a handheld probe, where the bowel requires isolation and exposure via surgical incisions [6]. For direct measurements of mucosal S_tO_2 , Haisjackl et al. [107] conducted the study by exposing the mucosal tissue via the antimesenteric enterotomy, however, an endoscopic probe is commonly used [248]. Lee et al. [6], demonstrated mucosal S_tO_2 measurements by introducing the WLS probe through the rectum and held in place, close to the bowel mucosal lining. When assessing mucosal S_tO_2 , light transmits approximately 2mm through the mucosa undergo scattering and a fraction of reflected light which is directed to the collecting fibre optic [242, 30].

To understand the relationship between S_tO_2 and intestinal ischaemia, several onsets of hypoxia were introduced under operative conditions. S_tO_2 measurements required baseline measurements before the onset of an occlusion. Several studies such as Haisjackl et al. [107], Karliczek et al. [33] and Lee et al. [6] observed the reduction of S_tO_2 , where a continuously low S_tO_2 within a six-minutes, suggests the likeliness of colon ischaemia and infarction. During aortic reconstructions, Lee et al. [6] found a significant decrease in S_tO_2 measurements, where 12% were unable to return to their baseline, resulting in postoperative colon ischaemia.

Similar observations were made when the occurrence of anastomotic leaks and colonic mucosa S_tO_2 measurements were evaluated [32]. Based on 77 patients, Karliczek et al. [247] obtained reproducible and stable S_tO_2 measurements. After anastomotic constructions, a significant rise in S_tO_2 measurements were observed in patients without postoperative leaks. The increase in regional oxygen saturation is a compensatory mechanism when undergoing anastomotic healing; where patients with a leak fail to respond.

Limitations WLS demonstrates the capability of providing continuous, quantitative tissue oxygen saturation from the mucosal lining via rectum insertion, however, the measurements are sensitive to several affecting factors. For accurate and consistent measurements, the probe requires to be perpendicular to the area of interest, to ensure the region of interest is solely assessed [30, 242]. Although incorporating WLS with endoscopy is less invasive, light from the endoscope affects the performance, resulting in inaccurate estimations of S_tO_2 ; where the presence of ambient light produces a higher reflectance spectra [245, 242, 249]. Another contributing factor is the presence of bile or faeces within the bowel, which interferes with the transmission of light due to their high absorbency within the visible light wavelengths [30, 242, 36].

Thus far, techniques for assessing bowel viability fall short due to the inability of directly assessing the mucosal lining. In addition to the factors effecting the measurement accuracy, the technique is unable to provide bowel assessments, where low anastomotic resections within 5 cm of the anus, cannot be obtained due to the narrowing of the pelvis [247]. Confidence in utilising WLS requires additional studies to be carried out to determine an average threshold to aid in the assessment of the bowel integrity [30].

3.4.5 Pulse oximetry

Pulse oximeters (PO) are commercially available monitoring devices, commonly found in areas such as operating theatres, critical care units and ambulances. This non-invasive device provides continuous measurements of the amount of haemoglobin carrying oxygen through the arterial vessel; also known as the arterial oxygen saturation. Pulse oximeters are commonly known to be placed on the extremities such as the finger to detect hypoxaemia earlier than visual inspections of cyanosis [85], where a low concentration of oxygen in the blood causes a blue discolouration of the extremities or mucous membranes.

Pulse oximeters has also been proven to work as effective in other locations such as the earlobe [250], fontanelle [251] and body cavities such as the oesophagus [252]. Understanding the level of oxygen reaching the large intestine could allow the identification of bowel ischaemia [228], where there is a restriction of blood supply, resulting in the shortage of oxygen delivery to the tissues. As seen in previous techniques, the intestine could be visually identified as clinically dead which may in fact have a viable blood supply; therefore, a technique which could measure objectively the level of oxygen, would be ideal [42].

Principle of operation Red blood cells contain a compound known as haemoglobin, which allows the transport of oxygen to various organs. When transporting oxygen, the haemoglobin is referred to as oxyhaemoglobin (HbO_2), in contrast, a haemoglobin without oxygen is known as a deoxyhaemoglobin (Hb). As an optical technique, POs use light to measure the arterial oxygen saturation (S_pO_2), which refers to the percentage of the available haemoglobin that carries oxygen within the artery. Therefore, illustrated in Figure 3.22, the higher the number of HbO_2 , the higher the percentage.

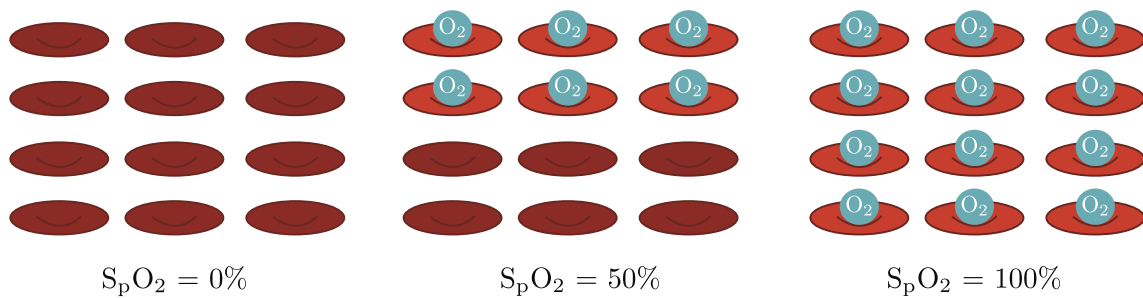


Figure 3.22 Understanding the measurement of oxygen saturation. Haemoglobin carrying oxygen (O_2) are known as oxyhaemoglobin, whilst a haemoglobin without oxygen is known as deoxyhaemoglobin. The measurement of arterial oxygen saturation is the percentage of oxyhaemoglobin within the artery. Thus, as the number of oxyhaemoglobin increases, the percentage of oxygen saturation increases.

Light sources, typically light emitting diodes (LEDs), illuminates the tissue and reaches the light detector. Depending on the placement of the light source and detector, there are two types of pulse oximeter probes as shown in Figure 3.23; a transmission or reflectance probe, where the reflectance probe can be placed on any surface of the body.

Pulse oximetry works on the basis where the attenuation of light relates to the medium properties; known as Beer-Lambert law, which will be discussed in further details in Chapter 4. Light of two different wavelengths, usually red and infrared, illuminate the tissue bed to measure the transmitted or reflected light to estimate the oxygen saturation within the artery. The reasoning for the use of two different wavelengths is due to pulse oximetry utilising the property where HbO_2 and Hb absorb different wavelengths of light.

As the arterial blood has a pulsatile behaviour, the vessel diameter causes a change in absorbance, resulting in the change in light detection as seen in Figure 3.24. During the systolic phase of the cardiac cycle, the absorbance of light in the tissue increases, therefore less detection of light. The detected light from either wavelength results in a

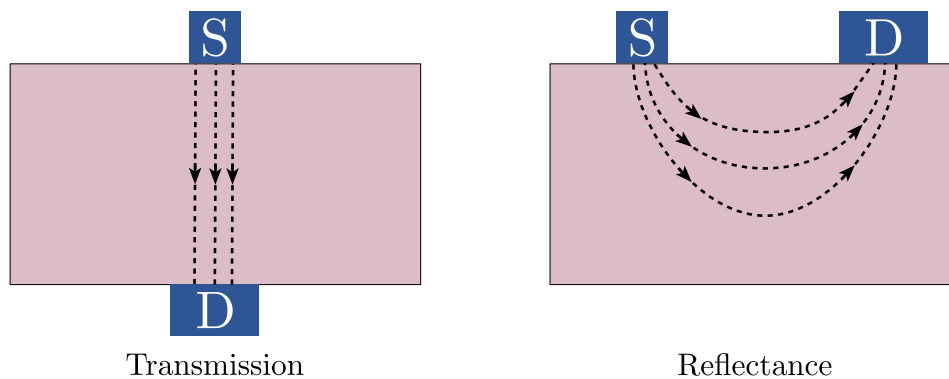


Figure 3.23 Types of photoplethysmography configurations. There are two types of photoplethysmography modes, (a) transmission and (b) reflectance. In transmittance mode, the optical source (S) and detector (D) are placed in the opposite sides of the tissue, whereas the reflectance mode position the S and D on the same side of the tissue. The black dotted lines represent the direction of the light propagating through the tissue.

pulsatile, time-varying waveform known as a photoplethysmography signal shown in Figure 3.24, corresponding to changes in the light absorbance, allowing the monitoring of changes in blood volume and S_pO_2 .

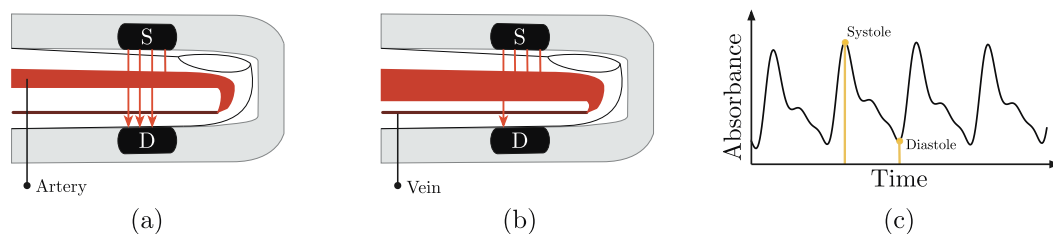


Figure 3.24 Pulsatile signal arising from the change in the artery vessel diameter. (a-b) illustrates the change in artery vessel diameter during diastole and systole, respectively. As the vessel diameter increases, light absorbance within the artery increases. Due to these fluctuations, a pulsatile, time-varying waveform (c) known as photoplethysmography signal corresponds to the changes in the light absorbance.

Image redrawn from Kyriacou et al. [241].

Use of technique for monitoring bowel viability Pulse oximetry has been reported as a research tool for monitoring intestinal viability on animal and human participants [136, 97, 252, 253, 128]. Animal studies, mainly researched on small samples of anaesthetised dogs, pigs and rats, have been reported [254–256, 225, 86, 228, 126].

Most studies report serosal S_pO_2 measurements by utilising a PO probe on the serosal surface of the intestine [255, 97, 257]. Direct measurements of mucosal oxygen

Current state of the art for assessing intestinal viability

saturation (S_mO_2) are uncommon, however studies such as Gardner et al. [228], Koga et al. [126] and Vahl [128] demonstrated the possibility of measuring S_mO_2 with the use of commercial pulse oximeters utilising two wavelengths within the red and infrared region of the electromagnetic radiation spectrum [257, 228, 126]. This has been achieved with the insertion of a PO which was attached to an inflating balloon of a Foley catheter [228, 126, 128], as shown in Figure 3.25. Once inserting the PO through the rectum, the balloon was inflated until contact between the sensor and mucosa was achieved to acquire PPG signals [228, 126].

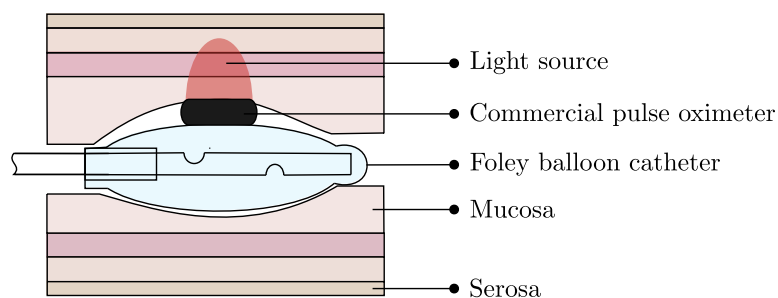


Figure 3.25 Transanal pulse oximeter. An illustration of the pulse oximeter probe used by Gardner et al. [228] to obtain mucosal oxygen saturation. Direct contact with the inner wall of the intestine is achieved placing the commercial pulse oximeter probe on a Foley balloon catheter.

To understand the relationship between S_pO_2 and bowel ischaemia, clamps were placed on the mesenteric artery to introduce gradual colonic ischaemia [257, 128]. Unimpeded blood flow resulted in colonic S_pO_2 measurements ranging between 90 % to 100 % [257, 228, 126, 252, 253], where no statistical differences were found between PPG signals from common measurand sites such as the finger [97, 253]. Utilising a commercial ear probe, clipped to the colon, Ouriel et al. [257] demonstrated the development of colonic ischaemia highly correlating to the absence of arterial pulsatile flow during abdominal aortic reconstructions, which is a common finding for alternative serosal S_pO_2 studies impeding colonic blood flow [97, 136, 254, 126, 258, 225, 128]. Colonic visual inspection was performed on all 30 patients, where two findings presented grossly viable colons, however postoperative colonoscopy revealed changes in the mucosal lining such as ischaemic damage and oedema [257].

La Hei and Shun [42] also demonstrated the importance and usefulness of obtaining quantitative measurements such as S_pO_2 during a laparotomy. During a second-look laparotomy of an infant, the appearance of an ischaemic bowel marginally altered, where some arterial pulsations were observed. Based on the gold standard visual

inspections, there were clinical uncertainty if the bowel was viable. With the use of a commercial PO, spot measurements were taken at different distances of the ischaemic region. Serosal S_pO_2 measurements ranged between 86 % to 95 %, where the absence of colonic saturation resulted in removed sections. With the use of a PO, approximately one-half of the ischaemic bowel was preserved.

As the mucosal is the initial lining to respond to bowel ischaemia, mucosal saturation should be of interest. The objective for Vahl [128], Gardner et al. [228] and Koga et al. [126] was to determine the capabilities of monitoring S_mO_2 using a commercial reflectance PO probe, commonly used for transcutaneous forehead measurements [228]. With the pulse oximeter applied to a balloon catheter, the catheter was introduced through the rectum of pigs and advanced to an approximate distance of 20 cm, with reference to the anus. A linear decrease in the S_mO_2 occurred when the mesenteric artery flow decreased, where S_mO_2 at 20 % of the baseline blood flow was recorded to have an average of $54 \% \pm 4.1 \%$ [228].

Limitations The use of PO within research studies do not attempt to quantify bowel viability [228], however, the changes and damage in the intestinal mucosal when the intestinal blood flow decreases have been identified [86, 228] by the PPG signal and oxygen saturation readings [228]. Pulse oximetry shows potential in providing qualitative measurements for the assessment of bowel viability, however, Koga et al. [126] disagrees due to unanswered questions and doubt regarding the technique. When inserting the pulse oximeter via the rectum, the sensor was anticipated to always face the posterior mucosa wall, however, Koga et al. [126] could not confirm. Additionally, unaware of the direction of the sensor, the tissue evaluated was questioned.

The majority of pulse oximeters assessing bowel viability utilised either a transmission or reflectance probe as a clip-on or embedded in a catheter, respectively. With such methods, both require an amount of pressure to ensure direct contact between the tissue and sensor [136]. This introduces a drawback, as the minimal pressure applied to the bowel is unknown, which could compromise the bowel by reducing the blood flow, oxygenation [257] and likelihood of perforation. To avoid clip-on probes, the sensor could be held by a clinician during measurements [97], however movement artefacts could reduce the quality of the signal.

The major drawback with PO based on the performed studies is the evaluation of the serosal lining. Due to accessibility intraoperatively, placing the sensor on the outer surface of the bowel deems appropriate, however, measurements from the serosa

may suggest viability when the mucosal lining may be identified as total ischaemia histologically [42]. As it is known that early identification of ischaemia appears on the mucosal lining, qualitative measurements such as PO should assess the mucosa to prevent irreversible tissue damage [136].

3.5 Summary

Several techniques have been critically reviewed to highlight their capabilities in assessing bowel tissue viability. There are seventeen (17) techniques mentioned in this chapter, indicating the difficulty surgeons are facing to assess bowel viability reliably and confidently. Majority of the techniques share the same limitations, which is the inability to provide continuous, reproducible, quantitative measurements, thus failing to reach clinical use. Furthermore, postoperative monitoring is crucial for monitoring surgical complication. However, the available techniques are unable to transfer their intraoperative measurements postoperatively, due to their limitation of requiring to be on the outer surface of the intestine.

The gold standard for assessing bowel viability remains to be the assessment of the mechanical patency through visual inspection. This technique is an unreliable and subjective method, therefore requiring a technique ideally providing real time, qualitative monitoring, in both intraoperative and postoperative settings. After a discussion with the colorectal team at the Royal London Hospital, a sensor incorporating pulse oximetry was of interest. As seen this chapter, pulse oximetry is a well known technique providing continuous, reproducible and quantitative measurements relating to blood volume changes in a tissue. Therefore, the following chapter (Chapter 4) will discuss further the principle of pulse oximetry.

Chapter 4

Photoplethysmography and pulse oximetry

Photoplethysmography (PPG) was previously presented in Section 3.4, as an optical technique applied to pulse oximetry (PO). PPG is an optical technique, where a light source illuminates a biological tissue, undergo interactions and returns small variations of light to a photodetector. PO devices are widely used as a standard of care for anaesthesiology and critical care medicine for the monitoring of haemoglobin oxygen saturation of arterial blood (S_pO_2) [38]. Utilising PPG and PO has provided the ability to identify early indications of hypoxemia with a user-friendly device, which has been adopted in many clinical settings.

Motivation To explain the interactions that undergo with light and tissue, it is necessary to have a basic understanding of the behaviour and properties of light. Light has a dual nature, behaving as a wave whilst moving through space, or behaving as a discrete particle with a discrete amount of energy that can be absorbed or emitted. Within a vacuum, light travels at a universal constant speed expressed as $c = 2.99 \times 10^8 \text{ ms}^{-1}$, however, light propagating through a medium changes its behaviour whilst conserving energy. This chapter explains the principles of light interaction within a medium such as tissue, which aids in the understanding of the underlying science of PPG and PO.

4.1 Principles of light-tissue interaction

When light travels through any medium, including biological tissue, an interaction takes place within a single medium or several different media. For the application of PPG and PO, there are three interactions that can occur: (1) Reflection and refraction, (2) Absorption and, (3) Scattering [85, 259, 260].

4.1.1 Reflection and refraction of light

When an incident light strikes a boundary between two different media, a change in the light direction can occur. As a result, a fraction of light could stay within the same medium, known as reflection, or transmit through to the next medium whilst altering the light speed, known as refraction [174].

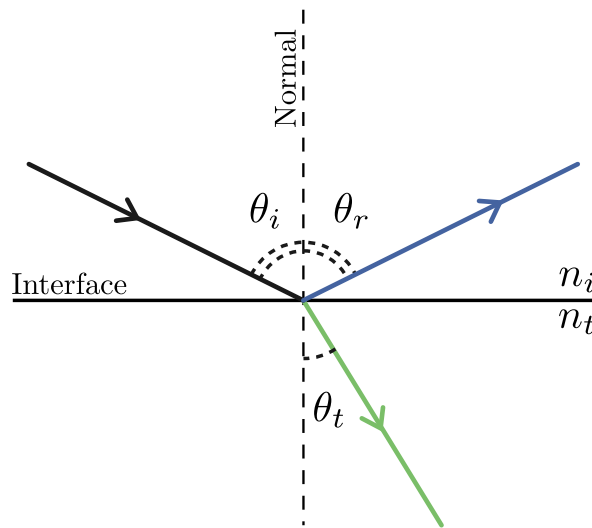


Figure 4.1 Illustration of reflection and refraction. The incident, reflected and refracted light rays are represented with black, blue and green lines, respectively. Where there are different media, there are two refractive indices to be considered, n_i and n_t . The angles θ_i, θ_r and θ_t , corresponds to the angle of incidence, reflection and refraction with respect to the normal.

As illustrated in Figure 4.1, there are two different media having different refraction indices (n_i and n_t) due to the media varying in densities. Assuming an incident of light is at the interface of a boundary with an incoming angle θ_i , light can be partially reflected with an angle θ_r , where the law of reflection is obeyed ($\theta_i = \theta_r$). The remainder of the incident light is refracted or transmitted to the other medium with an angle θ_t ,

4.1 Principles of light-tissue interaction

determined by Snell's law,

$$n_i \sin \theta_i = n_t \sin \theta_t. \quad (4.1)$$

The intensity of reflected light, also known as reflectance (R), can be determined by the Fresnel equation which is expressed as,

$$R = \frac{1}{2} \left(\frac{\sin^2(\theta_i - \theta_t)}{\sin^2(\theta_i + \theta_t)} + \frac{\tan^2(\theta_i - \theta_t)}{\tan^2(\theta_i + \theta_t)} \right). \quad (4.2)$$

For instances where the light is of normal incidence, the reflected light would also be along the normal to the surface ($\theta_i = \theta_r = 0$), where Equation (4.2) simplifies to

$$R = \left(\frac{n_i - n_t}{n_i + n_t} \right)^2. \quad (4.3)$$

Referring to the law of conservation of energy which states energy cannot be created or destroyed in an isolated system, the sum of reflectance (reflected intensity, R) and transmittance (transmitted intensity, T) would always be equal to the intensity of the incident light, where,

$$R + T = 1, \quad (4.4)$$

assuming the intensity of the incident light is 1 and the interaction occurs within a non-absorbing media [174].

4.1.2 Absorption of light

Absorption is a transfer of light energy from the electromagnetic wave to the atoms or molecules of the medium. This energy transfer results in electron excitation, molecule vibrations or molecule rotations. The light spectrum exiting the medium would have certain wavelengths removed due to absorption [85].

Light absorption through a medium containing absorbers can be understood with the Beer-Lambert law, also known as Beer's law. Beer's law describes the attenuation of light travelling through a uniform medium containing absorbing substance. When a monochromatic beam of light with an intensity of I_0 enters, light is partially transmitted through the medium, whilst the remaining is absorbed. The intensity of transmitted light (I) travelling through the medium decreases exponentially with distance and can be expressed as,

$$I = I_0 e^{-\epsilon(\lambda)cd}, \quad (4.5)$$

where $\epsilon(\lambda)$ is the extinction coefficient relating to the absorbing strength of the absorbing substance ($Lmmol^{-1}cm^{-1}$), c is the concentration of the absorbing substance ($mmolL^{-1}$) and d being the geometrical optical path length (cm) [102].

The ratio of the transmitted light to the incident light is known as the transmittance (T) corresponding to the amount of unabsorbed light. This is directly related to the absorbance (A) which corresponds to the amount of absorbed light in a medium. The relationship is as follows,

$$A = -\ln(T) = \epsilon cd, \quad \text{where} \quad (4.6)$$

$$T = \frac{I}{I_0} = e^{-\epsilon cd}. \quad (4.7)$$

Referring to Equation (4.7), it should be noted that the absorbance of a medium can vary as the concentration or the optical path length varies [102]. With ϵ referred as the absorption coefficient per unit of molar concentration, an absorption coefficient (μ_a) for a single absorbing substance is $\mu_a = \epsilon c$.

For a medium containing more than one absorbing substance, Beer's law can be applied, where the total absorbance of the medium is expressed as,

$$A(\lambda) = (\epsilon_{1(\lambda)}c_1 + \epsilon_{2(\lambda)}c_2 + \dots + \epsilon_{n(\lambda)}c_n) d, \quad (4.8)$$

which is a linear sum of all contributing absorbing substances (n) for a given wavelength (λ) in a medium [260]. As seen in Equation (4.8), there can be n unknown concentrations, therefore n linear equations at different wavelengths and their respective extinction coefficients can be used to determine the unknown [36, 102].

4.1.3 Scattering of light

Scattering of light differs to reflection and refraction, where scattering causes the incident light to be deflected in all directions when encountered by a scattering particle. There are two types of scattering, (i) elastic and (ii) inelastic scattering, where elastic scattering redirects the light path whilst the light energy does not change, resulting in the scattered light to have the same wavelength as the incident light.

For research purpose, elastic scattering will be taken into consideration, which can be further categorised depending on the size of the scattering particles with respect to the wavelength of the incident wavelength [260]. Rayleigh scattering, being the first type of elastic scattering, occurs when the radius of the scattering particles is smaller

4.1 Principles of light-tissue interaction

than the wavelength of the incident light. In comparison, the second type of elastic scattering is Mie scattering which occurs when the radius of the scattering particles is greater or equal to the wavelength of the incident light. For a medium containing multiple scattering particles, a scattering coefficient (μ_s) is defined as the product of the cross-section of a single scattering particle and the density [260].

Considering biological tissue as the medium, incident light does not only split into absorbed and transmitted light; reflection and scattering must also be included. Referring to Equation (4.5), Beer's law does not account for the reflection of light at the surface of the medium or scattering. Therefore, to consider all light interactions, specifically the effect of scattering, the law is altered and known as the modified Beer-Lambert law. The modified Beer's law is expressed as,

$$A_{(\lambda)} = (\epsilon_{1(\lambda)}c_1 + \epsilon_{2(\lambda)}c_2 + \dots + \epsilon_{n(\lambda)}c_n) l_{(\lambda)} + G, \quad \text{where} \quad (4.9)$$

$$l_{(\lambda)} = d \times DPF_{(\lambda)}. \quad (4.10)$$

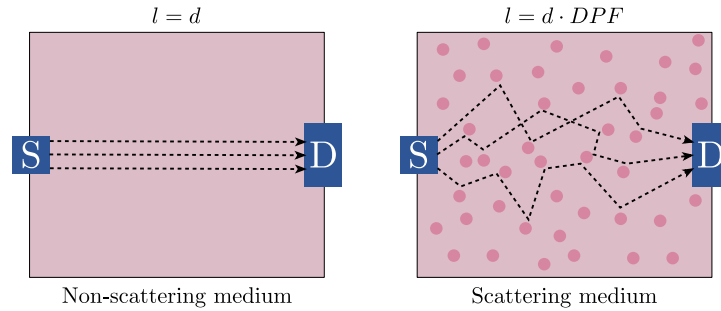


Figure 4.2 Optical path through a scattering and non-scattering medium. Illustration of the optical path (l) between the source (S) and detector (D) through a medium. The photon path is represented by the black dotted lines. Within a non-scattering medium (a), the optical path is the same as the source-detector separation. Within a scattering medium (b), the photon travels randomly, resulting in the optical path to be higher than the source-detector separation due to the differential pathlength factor (DPF).

Image redrawn from Budidha [261].

The differential pathlength factor (DPF) is a unit-less, wavelength dependent coefficient. For an absorbing and scattering medium, the optical pathlength (l) is greater than the geometrical optical path (d). Referring to Figure 4.2, for a non-scattering medium, the DPF value is 1, thus, Equation (4.10) reduces to Equation (4.5), where the medium is solely absorbing and the optical path length corresponds to the

source-detector separation. For biological tissues, the DPF is greater than 1 resulting in random optical paths, thus the optical path length is DPF-times higher than the source-detector separation. Values of DPF varies for all individuals, however DPF of different tissues and age groups can be found in public domains [261]. The additional term G , which is the scattering factor corresponds to the nature and geometry of the tissue associated to the experimental setting.

4.2 Principles of photoplethysmography

PPG represents volumetric changes in the micro-vascular bed of tissue by analysing the change in volume of blood. Light sources are used to illuminate the tissue and a photodetector senses the reflected or transmitted light from the tissue, which is dependant on the optical configuration. As illustrated in Figure 3.23, there are two types of PPG configurations, (i) transmission mode and (ii) reflectance mode, both depending on the geometry arrangement of the light source and detector [262].

Transmission mode The light source and detector are geometrically configured to allow a tissue sample to be placed between the two electronic components. By applying a small pressure to the tissue sample to hold the sensor in place, the photodetector detects light transmitted through the tissue thus measurement sites are limited to extremities such as the finger, earlobes and toes [241].

Reflectance mode The light source and detector are geometrically arranged side by side to allow the PPG sensor to be placed on a tissue surface such as the forehead and oesophagus. Due to the scattering of light within a tissue, the back-scattered or reflected light follows a banana shape path, where the photodetector receives this light. It is possible for the photodetector to be illuminated by the light source without propagating through the tissue; known as the penumbra effect or optical shunting. To avoid such effect, an opaque shield is positioned between the electronic components. Additionally, good contact is required between the sensor and tissue to minimise motion artefact and ambient light interference. In comparison to the transmission mode, the PPG waveform through reflectance is smaller.

The light intensity received by the photodetector results in small variations in the photodetector current which relates to the change in the blood volume within the sensing region [262]. To interpret the detected light, the photodetector current

is electrically converted into a voltage signal known as the photoplethysmographic waveform. The waveform typically referred as PPG will be explained further in Section 4.2.2. The change in blood volume arises from the cardiac cycle, where there are two cardiac phases, systole and diastole phase. Systole is the contraction period when the blood is ejected by the left ventricle of the heart, causing the arteries to distend. Distension occurs due to the high pressure exerted onto the arteries by the arterial blood. Pressure exerted on the arteries increase until reaching a maximum and begin to decrease prior the onset of the second cardiac phase. During the diastole phase, where ventricular relaxation occurs, the pressure decreases to a minimum corresponding to minimal distension of the arteries.

4.2.1 Incorporating the modified Beer-Lambert law

As PPG works on the basis of illuminating a tissue to measure small variations in the light intensity associated with changes in blood volume, PPG is best described using the modified Beer-Lambert law (Section 4.1.3). Recalling the systolic phase of the cardiac cycle, there is an increase in arterial blood resulting in a decrease of light intensity received by the photodetector due to greater absorption within the sensing region. Alternatively, during the diastolic phase of the cardiac cycle, there is a decrease in blood volume and absorbers which corresponds to an increase in light intensity received by the photodetector.

Figure 4.3(a) and (b) illustrates the relationship between the absorbance and detected light intensity. As seen in Figure 4.3(b), the resultant waveform produced by the photodetector is known as the PPG waveform. It is noticeable that the PPG waveform has an inverse relationship with the absorbed light within the tissue. By reversing the order of the elements in the PPG waveform, the PPG resembles the arterial blood pressure waveform, where the increase in the waveform corresponds to the increase in blood volume. Further explanation, including the components of the PPG waveform will be discussed in the next section (Section 4.2.2).

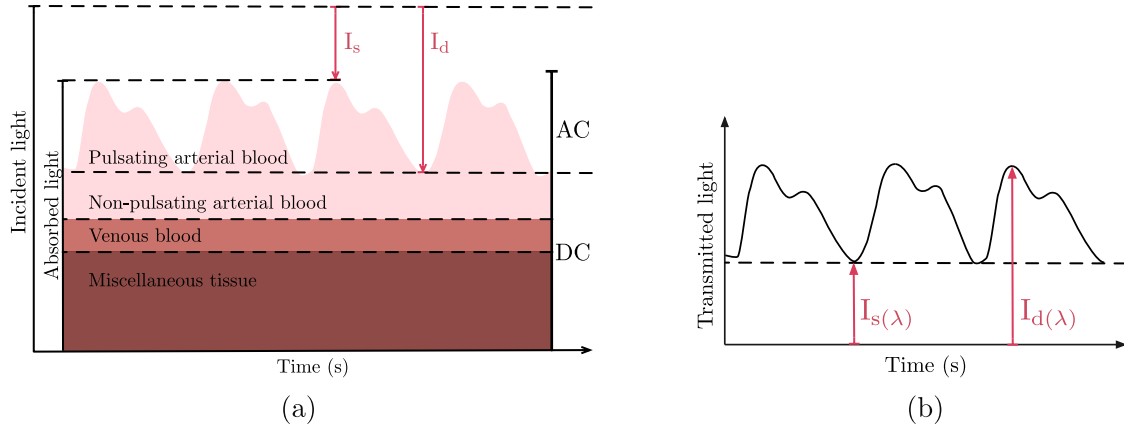


Figure 4.3 Absorbed and transmitted light in biological tissue. (a) illustrates the amount of absorbed light correlating to the pulsation of arterial blood, where the constant absorbed light is due to the non-pulsatile components such as the venous blood and other tissues. (b) $I_s(\lambda)$ and $I_d(\lambda)$ are the transmitted light intensity in the arteries during systole and diastole, respectively. As the blood volume is greater during systole compared to diastole, more light is absorbed. The transmitted light is equivalent to the detected light intensities at a photodetector for a given wavelength, λ .

Recalling and combining Equation (4.7) and Equation (4.10), the absorbance (A) of light propagating through a tissue during the systolic and diastolic phase can be expressed as,

$$A_s(\lambda) = \ln\left(\frac{I_0}{I_s}\right) = \epsilon c_s l_s + G, \quad (4.11)$$

$$A_d(\lambda) = \ln\left(\frac{I_0}{I_d}\right) = \epsilon c_d l_d + G, \quad (4.12)$$

where s and d correspond to the systolic and diastolic phases of the cardiac cycle respectively. As mentioned previously, there is an increase in arterial blood during systole, resulting in greater absorption compared to absorption during diastole ($A_s > A_d$). Furthermore, due to the inverse relationship between the absorbance of light and light intensity, the light intensity received by the photodetector during systole is lower compared to the light intensity received during diastole ($I_s < I_d$).

4.2 Principles of photoplethysmography

With the assumption that the optical pathlength within the cardiac cycle are approximately equal ($l_s \approx l_d = l$), the change in absorbance between the two cardiac phases can be expressed as,

$$\Delta A(\lambda) = A_s(\lambda) - A_d(\lambda) = \epsilon \Delta c l, \quad (4.13)$$

where Δc is the change in the concentration of the absorbers within blood. Thus, the change in absorbance in PPG in relation to the cardiac cycle is,

$$\Delta A(\lambda) = \epsilon \Delta c l \quad (4.14)$$

$$\Delta A(\lambda) = \ln \left(\frac{I_0(\lambda)}{I_s(\lambda)} \right) - \ln \left(\frac{I_0(\lambda)}{I_d(\lambda)} \right) \quad (4.15)$$

$$\Delta A(\lambda) = \ln \left(\frac{I_d(\lambda)}{I_s(\lambda)} \right) \quad (4.16)$$

4.2.2 Components of a photoplethysmographic waveform

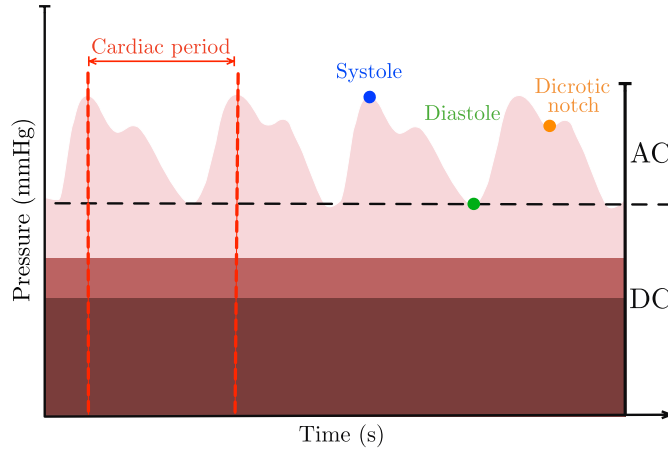


Figure 4.4 Components of a photoplethysmographic (PPG) waveform, where one complete cycle is equivalent to the cardiac period. The alternating signal of PPG waveform (AC), corresponds to the changes in blood volume, where the peak and trough relates to the systole and diastole phases of the cardiac cycle. The dicrotic notch relates to the vascular resistance of the peripheral vessel.

When observing a PPG waveform, similar to Figure 4.4, two distinctive components can be identified, an alternating component (ac) and a relative constant component (dc) [262]. The two components can be extracted from a PPG waveform with the use of electronic filters. The separation technique is discussed further in Appendix A.

ac component The ac component of the PPG waveform (ac PPG) can be identified as a high frequency, pulsatile signal. synchronous with the cardiac cycle. The ac PPG represents 1 – 2% of the total light absorption corresponding to the pulsating arterial blood [241]. As seen in Figure 4.4, the ac PPG can be separated further to two phases corresponding to the cardiac cycle; systole and diastole phases. With reference to light intensity, ac PPG corresponds to the change in light intensity between the two phases ($\Delta I = I_d - I_s$). When invasive measurements of the arterial pressure within the aorta are acquired, a notch known as the incisura intercepts the two waveform and represents the small increase in pressure due to the closure of the aortic valve. As PPG's are acquired peripherally, the incisura diminishes and is replaced by what is known as the dicrotic notch, which vaguely relates to the behaviour of the aortic valve closure but rather relates to the vascular resistance of the peripheral vessel.

With the ac PPG synchronised with the cardiac cycle, the pulsatile behaviour of the waveform is used for the estimation of heart rate or for the assessment of arrhythmia. By accessing the ac PPG amplitude, information such as vasoconstriction and vasodilation of arteries can be obtained, where the ac PPG either decreases or increases respectively.

dc component The dc component of the PPG waveform (dc PPG) can be identified as a low frequency, non-pulsatile signal. As seen in Figure 4.4, with reference to the light intensities received by the photodetector, dc PPG corresponds to the light intensity during systole (I_s). The remaining 98 – 99% of the total light absorption corresponds to the dc PPG which includes the absorption of non-pulsatile components such as the venous blood and the tissues within the sensing region [241]. Small changes of dc PPG can be observed due to respiration, vasomotor activity, vasoconstrictor waves and thermoregulation.

As the dc PPG represents the total blood volume within the sensing region, the component can be used to provide information on blood pooling. A common use of dc PPG is within pulse oximetry, which is a measuring technique applying PPG which will be discussed in the next section (Section 4.3).

4.3 Principles of pulse oximetry

Pulse oximetry (PO) has been introduced in Chapter 3 as a non-invasive optical technique that is widely used to estimate the arterial blood oxygen saturation (S_aO_2). By applying the principles of PPG on peripheral locations such as the fingers and toes, the estimation of S_aO_2 from PO provides the peripheral blood oxygen saturation (S_pO_2). In red blood cells, haemoglobin function as the transporters of oxygen from the lungs to the tissue (oxygenated haemoglobin, HbO_2) and collecting waste products (deoxygenated haemoglobin, HHb), thus being the main absorbers of interest. To determine the percentage of oxygen being delivered to the tissue, the following equation can be used to calculate the arterial oxygen saturation,

$$S_aO_2 = \frac{c_{HbO_2}}{c_{HbO_2} + c_{HHb}} \times 100 \quad (4.17)$$

As seen in the principles of PPG (Section 4.2), the acquisition of PPG relies on the determination of the optical properties of the tissue within the sensing area [262]. As the absorbers of interest are HbO_2 and HHb , there are two unknown concentrations, therefore requiring two wavelengths, as mentioned in Section 4.1.2. Typically, PO operates at wavelengths within red (R, 600 – 700nm) and infrared (IR, 800 – 1000nm). Figure 4.5 illustrates the absorption spectra of HbO_2 and HHb , where it is noticeable that HbO_2 absorbs less R whilst absorbing more light in the IR. Within the typical operating wavelengths of PO (600 nm to 1000 nm), the absorption spectra of HbO_2 and HHb differ significantly except specific wavelengths such as 590 nm and 805 nm, known as the isobestic wavelengths [263]. At the isobestic wavelength, HbO_2 and HHb absorb light equally, resulting in signals largely unaffected by changes in S_aO_2 . When choosing the wavelengths for the development of PPG sensors and PO, the ideal wavelength should be located where maximum differences in absorption between HbO_2 and HHb occurs [85].

4.3.1 Deriving arterial oxygen saturation

The modified Beer's law (Section 4.1.3) can be incorporated in PPG to explain the derivation of S_aO_2 . Continuing from Equation (4.16), which is the expression for the change in absorbance in PPG in relation to the cardiac cycle, and taking into consideration the change in intensity between systole and diastole ($\Delta I = I_d - I_s$), ΔA

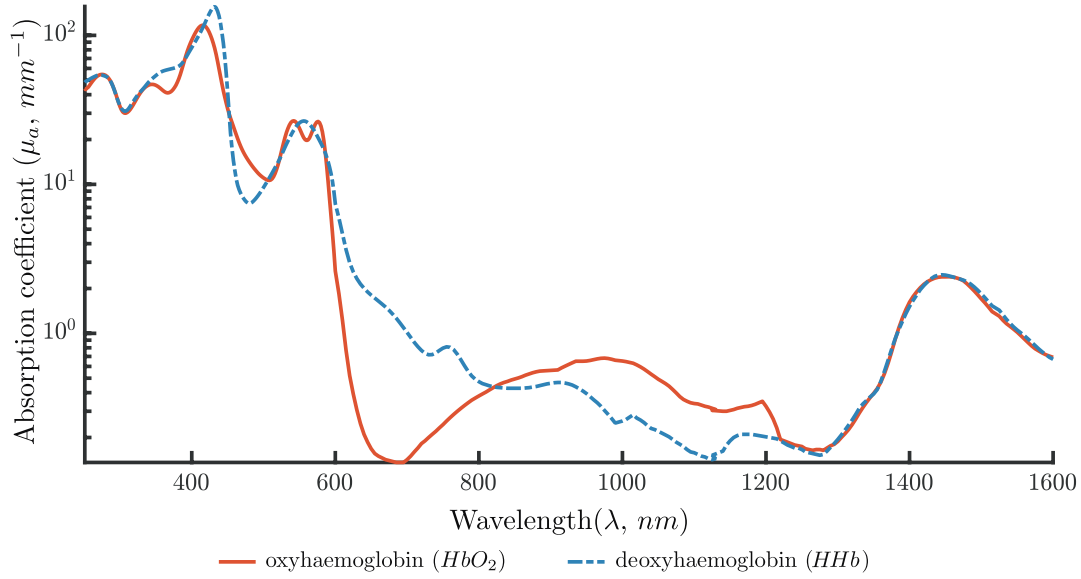


Figure 4.5 Absorption coefficient spectra for oxyhaemoglobin (HbO_2 , —, red) and deoxyhaemoglobin (HHb , -., blue) across a spectrum from 300 nm to 1600 nm. Figure re-plotted from Budidha [261].

can be reexpressed as,

$$\Delta A_{(\lambda)} = \ln \left(\frac{I_s + \Delta I}{I_s} \right)_{(\lambda)} = \ln \left(1 + \frac{\Delta I}{I_s} \right)_{(\lambda)} \approx \left(\frac{\Delta I}{I_s} \right)_{(\lambda)} \equiv \left(\frac{AC}{DC} \right)_{(\lambda)} \quad (4.18)$$

To express the relationship between the absorption of two wavelengths (λ_1 and λ_2) corresponding to red (R) and infrared (IR) respectively, the ratio of ratios (R_{OS}) can be determined as shown below,

$$R_{OS} = \frac{\Delta A_{(R)}}{\Delta A_{(IR)}} \equiv \left(\frac{AC}{DC} \right)_{(R)} / \left(\frac{AC}{DC} \right)_{(IR)} \quad (4.19)$$

Recalling in Equation (4.8), to calculate n unknown concentrations, n linear equations of different wavelengths would be used. As R and IR are the two wavelengths used to distinguish the difference in absorption between HbO_2 and HHb , the total absorbance for a given wavelength can be re-expressed as the following:

$$\Delta A_{(\lambda)} = \left(\epsilon_{HbO_2(\lambda)} c_{HbO_2} + \epsilon_{HHb(\lambda)} c_{HHb} \right) l_{(\lambda)}, \quad (4.20)$$

where ϵ_{HbO_2} and ϵ_{HHb} are the extinction coefficients and c_{HbO_2} and c_{HHb} are the concentrations for oxyhaemoglobin and deoxyhaemoglobin respectively.

By rearranging Equation (4.17) making either c_{HbO_2} or c_{HHb} the subject, the concentration terms (c) in Equation (4.20) can be expressed as,

$$c_{HbO_2} = S_a O_2 (c_{HbO_2} + c_{HHb}) \quad (4.21)$$

$$c_{HHb} = (1 - S_a O_2) (c_{HbO_2} + c_{HHb}), \quad (4.22)$$

where the concentrations can be replaced to relate to ΔA with $S_a O_2$ as shown below,

$$\Delta A_{(\lambda)} = (\epsilon_{HbO_2(\lambda)} S_a O_2 + \epsilon_{HHb(\lambda)} (1 - S_a O_2)) (c_{HbO_2} + c_{HHb}) l_{(\lambda)}. \quad (4.23)$$

Once knowing the relationship between ΔA with $S_a O_2$, Equation (4.20) can now be expressed where R_{OS} is related to $S_a O_2$ as the following,

$$R_{OS} = \frac{(\epsilon_{HbO_2(R)} S_a O_2 + \epsilon_{HHb(R)} (1 - S_a O_2)) l_{(R)}}{(\epsilon_{HbO_2(IR)} S_a O_2 + \epsilon_{HHb(IR)} (1 - S_a O_2)) l_{(IR)}}. \quad (4.24)$$

Furthermore, by rearranging Equation (4.24) to make $S_a O_2$ the subject, the following equation expresses the derivation of $S_a O_2$ in relation to the R_{OS} ,

$$S_p O_2 = \frac{R_{OS} \cdot \epsilon_{HHb(IR)} l_{(IR)} - \epsilon_{HHb(R)} l_{(R)}}{R_{OS} (\epsilon_{HHb(IR)} - \epsilon_{HbO_2(IR)}) l_{(IR)} + (\epsilon_{HbO_2(R)} - \epsilon_{HHb(R)}) l_{(R)}} \times 100\%. \quad (4.25)$$

Recalling in Section 4.2.1, the optical pathlength at each wavelength are considered approximately equal ($I_s \approx I_d \approx l$). Therefore, $S_p O_2$, which corresponds to the estimation of the arterial oxygen saturation measured by a PO is expressed as,

$$S_p O_2 = \frac{R_{OS} \cdot \epsilon_{HHb(IR)} - \epsilon_{HHb(R)}}{R_{OS} (\epsilon_{HHb(IR)} - \epsilon_{HbO_2(IR)}) + (\epsilon_{HbO_2(R)} - \epsilon_{HHb(R)})} \times 100\%. \quad (4.26)$$

4.3.2 Calibration of pulse oximeters

With the chosen wavelengths, $S_p O_2$ can be directly calculated from Equation (4.26), where R_{OS} is obtained by the PPG waveform (referring to Equation (4.19)), whilst the extinction coefficients (ϵ) is determined from the absorption spectra. However, in practice, $S_p O_2$ is determined empirically with a linear function approximation globally recognised as,

$$S_p O_2 = 110 - 25 R_{OS}. \quad (4.27)$$

Commercial PO manufacturers have their own calibration curves rather than relying on the available empirically determined formula (Equation (4.27)) [261]. To obtain an empirically calibrated curve, manufacturers use *in-vitro* data, such as the S_aO_2 obtained from CO-oximeters. The data would be deduced by asking subjects to breathe hypoxic gaseous mixture and obtaining optical measurements at different steady-state oxygenation levels [85]. Patient desaturation occurs to a certain percentage, which is 80 %, therefore the accuracy of the PO decreases when S_aO_2 drops below 80 %. The calibration method for PO is a limitation due to the inability of obtaining data below 80 %, as there are ethical implications due to the risk of hypoxic brain damage [261].

4.4 Summary

The basic principles of light-tissue interaction has been explained, where such interactions aids in the understanding of PPG and PO. For the assessment of bowel tissue viability, PO has been previously attempted, however with most reporting on the acquisition of S_pO_2 from the outer surface of the intestine. PPG and PO remains as a questionable technique for assessing colon ischaemia due to the lack of information regarding the behaviour of light within the colorectum. To investigate the nature of light propagating through the inner walls of the colorectum, a computation model simulating the tissue with an intraluminal optical sensor will be presented in Chapter 5.

Chapter 5

Assessing light-tissue interactions within the colon using Monte Carlo simulations

Photoplethysmography (PPG) and pulse oximetry (PO) is the proposed method to monitor bowel viability due to its large clinical and research applications. As seen in Chapter 4, the behaviour of light with biological tissue is well understood. This is achievable with theoretical models, such as Monte Carlo, where physical systems which are complicated or poorly understood could be modelled for a better understanding.

Motivation The monitoring technique aims to be minimally invasive, by positioning an optical sensor within the lumen of the colon. As seen in Chapter 3, there is a lack of understanding and confidence with PPG and PO, where researchers question the tissue volume being interrogated by the sensor, such as the depth or path the light travels within the colon. There is also a desire to develop the sensor without the use of a balloon design, which aids in maintaining contact between the sensor and inner walls of the colon. However, with this design concept, the effects of the sensor-tissue separation with the light propagation are unknown. Therefore, this chapter details computational models to evaluate the behaviour of light within the colon whilst simulating an intraluminal reflectance-mode optical sensor based on Monte Carlo simulations. The aim of this chapter is to gain more knowledge of the path taken by photons to obtain a better understanding of the relevant light interactions, such as the effect of light scattering and the depths at which the light propagates. Additionally, it is necessary to understand the acquisition of information from the tissue via contact and non-contact situations.

5.1 Principles of Monte Carlo modelling for light-tissue interactions

A Monte Carlo (MC) simulation is a computational algorithm utilising random sampling of variables from probability distribution functions to compute a prediction. MC simulations are often used for complex systems by undergoing a large number of repeated calculations based on random input variables, where the prediction accuracy increases with the number of repetitions [264]. This section explains the MC simulation applied to light-tissue interaction, where the position of each photon is modelled from an optical source to a detector. Furthermore, the general requirements for a MC simulation is explained in this section.

5.1.1 Geometric representation and co-ordinate system

The MC model is designed to allow photon propagation in a three-dimensional tissue structure as shown in Figure 5.1. There are two co-ordinate systems used in the MC model at the same time; (i) the Cartesian system to define the position of the photons within the tissue and, (ii) the polar system to describe the movement of the photon [260].

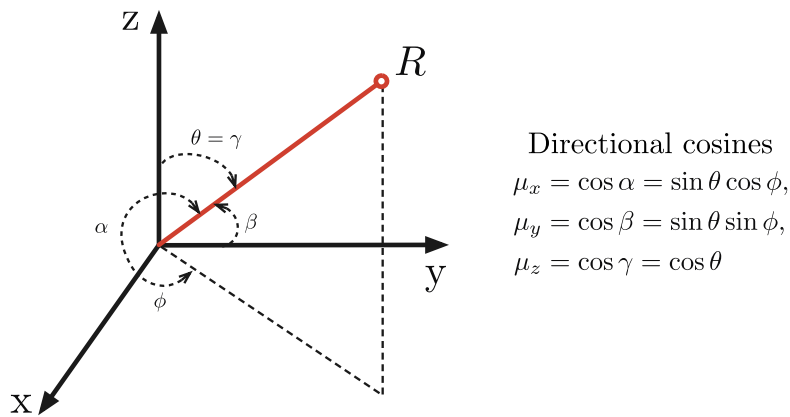


Figure 5.1 Relationship between the Cartesian and polar co-ordinate systems. Assuming the movement of a photon at a given instant is represented as a vector (R), the photon moves with a scattering angle (θ) and an azimuthal angle (ϕ) within the polar co-ordinates. The angles, α , β and γ correspond to angles within the Cartesian system. The polar system can be translated into the Cartesian co-ordinates using the directional cosines, which refers to the cosine angles made by the position vector with the unit vectors (μ_x, μ_y, μ_z).

5.1 Principles of Monte Carlo modelling for light-tissue interactions

By utilising the Cartesian co-ordinate system (x, y, z) , the origin of the co-ordinate system corresponds to the photon incident point on the tissue surface from an optical source. The positive z-axis corresponds to the depth within the tissue, and the xy-axis corresponds to the tissue surface. A polar co-ordinate system (θ, ϕ) is required to describe each photon movement, where the z-axis is always aligned with the direction of the photon propagation [260].

As a result of scattering, the photon changes direction, which is represented in the polar system and translated into Cartesian co-ordinates using the directional cosines (μ_x, μ_y, μ_z) as shown below:

$$\mu_x = \sin \theta \cos \phi, \quad \mu_y = \sin \theta \sin \phi, \quad \mu_z = \cos \theta, \quad (5.1)$$

where the scatter angle (θ) and azimuthal angle (ϕ) are randomly generated within the MC model.

5.1.2 Optical properties in the Monte Carlo model

To model the light-tissue interaction within a given location, the model must include the design of the light source and the multi-layered biological tissue. Each layer is assumed to be infinitely wide and is defined by several parameters which have been introduced briefly in Chapter 4. The parameters per layer of tissue include: (i) the absorption coefficient, (ii) the scattering coefficient, and (iii) the anisotropic factor. This section will address each parameter further in relation to the MC model.

Absorption coefficient Recalling Beer's law equation using Equation (4.5), μ_a is the absorption coefficient and d is the optical path length through a medium. The absorption coefficient is defined as the probability of a photon being absorbed whilst travelling a unit distance through a medium.

Scattering coefficient Scattering, which is not accounted in Beer's law, occurs when light interacts with a medium consisting of non-absorbing objects. The scattering coefficient (μ_s) is defined as the number of scattering events per unit distance travelled by a photon. Within the medium, photons travel in a straight line until elastic scattering occurs, where the wavelength and energy are conserved. From the initial direction, the photon deviation caused by scattering is referred as the scatter angle (θ) .

An additional angle known as the azimuthal scatter angle (ϕ) affects the new position of the photon as shown as Figure 5.2.

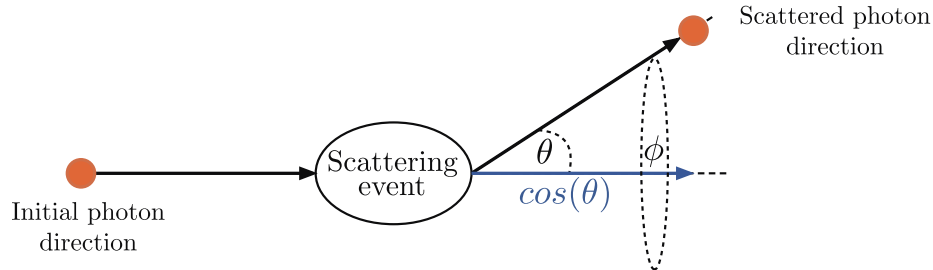


Figure 5.2 Illustration of a photon undergoing a scattering event. A scattering event causes the photon to change direction by altering the scattering angle (θ) and azimuthal angle (ϕ).

Calculating the angle of scatter is important in order to simulate photon deflections each time a photon undergoes a scattering event. The Henyey-Greenstein (HG) phase function has been successfully implemented for explaining the scattering of light in tissue. The HG function is described as the probability of $\cos(\theta)$ given by,

$$p_{HG}(\cos \theta) = \frac{1 - g^2}{2(1 - 2g \cos(\theta) + g^2)^{3/2}}, \quad (5.2)$$

where g is known as the anisotropic factor.

Anisotropic factor The dimensionless unit, $g \in [0, 1]$, corresponds to a measurement of the amount of forward direction that a photon has kept after a single scattering event. The anisotropic factor is equal to the average cosine of θ caused by a large number of scattering events. When $g = 0$, photons undergo total isotropic scattering, where a photon scatter occurs at any angle. Alternatively, when $g = 1$, the scatter angle is zero, resulting in the direction of the photon to be unaffected (forward scattering). Typically, a tissue medium g is close to 1, implying forward scattering dominates [260].

5.1.3 Sampling of random variables

The MC simulation utilises random sampling of variables from probability distribution functions in order to compute a prediction [259]. In the case of this model, probability distribution functions are required to describe the behaviour of the photons interacting with the biological tissue. The four cases where a random variable is used to describe

5.1 Principles of Monte Carlo modelling for light-tissue interactions

a physical property are: (i) the initial position of the photon (source), (ii) the path length taken by a photon (step size), (iii) the photon scattering angle and (iv) the interactions occurring at a given tissue boundary (reflectance or transmittance).

Considering a general case, let X be the random variable needed in the simulation. The probability density function, $p(X)$, can be defined as:

$$\int_a^b p(X)dX = 1, \quad (5.3)$$

where X can take values within an interval (a, b) . To choose a random value for X given its distribution, consider ξ to be a sample from a uniformly distributed variable $E \sim U(0, 1)$. The value ξ can be generated in a computer simulation. Notice how the cumulative distribution function of E , is such that $CDF_E(\xi) = \xi$ when $0 \leq \xi \leq 1$. Furthermore, any cumulative distribution function will have its range between 0 and 1, including $CDF_X(x)$. Assuming a mapping between X and ξ , then a sample x of X could be obtained from a given sample ξ of E by solving for x in the equation $CDF_X(x) = \xi$, explicitly stated as:

$$\int_a^x p(X)dX = \xi. \quad (5.4)$$

The generic method of sampling a random variable is illustrated in Figure 5.3.

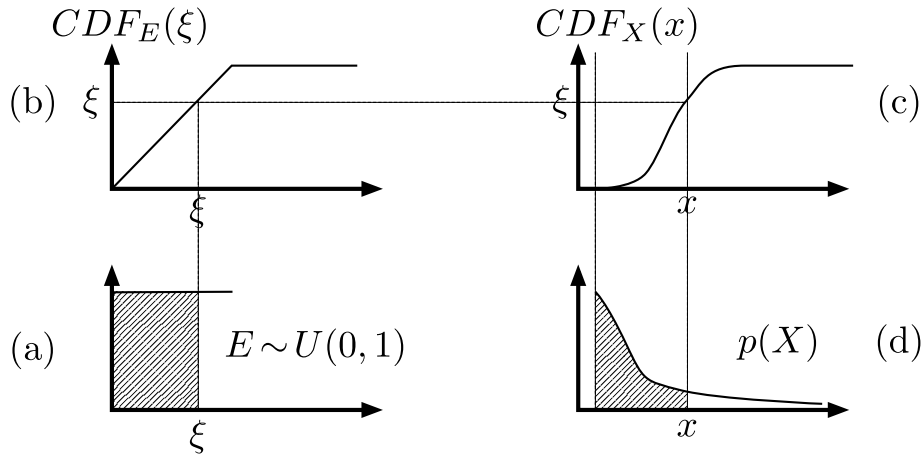


Figure 5.3 The steps of sampling a random variable X , given an assumed link to a uniformly distributed variable E . (a) From a uniform distribution E , generate a random value, ξ between 0 and 1. (b) Because $E \sim U(0, 1)$, then the cumulative distribution function for E (CDF_E) is such that $CDF_E(\xi) = \xi$. (c) Assuming the mapping between X and E , find x such that $CDF_X(x) = \xi$, which (d) will correspond to the sample value x in the probability density function $p(X)$ in Equation (5.4). Illustration redrawn from Wang and Jacques [265].

(i) Optical source Photons can be injected into the tissue through several types of sources. However, for this research, there are two types of optical sources which will be considered; (i) a point source and, (ii) a Gaussian beam. Both will be explained; however, the Gaussian beam is the only optical source requiring a definition involving random sampling.

Point source With the photon initialised to $(0, 0, 0)$, the photons were launched orthogonal to the tissue, where $\theta = 0$. Thus the directional cosines of the incident photon were set to $(0, 0, 1)$ for μ_x , μ_y and μ_z respectively.

Gaussian beam To simulate a light emitting diode as close as possible, a Gaussian beam could be considered. With the use of a Gaussian beam, the photons are considered to launch from a ring-shaped source, where the launch position is described by a radius r and an angle ψ . The Gaussian beam has a probability distribution function expressed as,

$$p(r) = \frac{e^{-\frac{r^2}{b^2}} 2\pi r}{\pi b^2}, \quad (5.5)$$

where b is the radius where the intensity values fall to $1/e^2$ of its axial values. Given Equation (5.4), the radial position will be found by solving for r , in the following equation,

$$\int_0^r p(R) dR = \xi \quad \therefore \quad r = b\sqrt{-\ln(\xi)}. \quad (5.6)$$

With the radial position (r) generated randomly, the radial angle (ψ) is randomly generated between 0 and 2π using the expression below:

$$\psi = 2\pi\xi. \quad (5.7)$$

Using Equation (5.6) and Equation (5.7), the initial photon position are determined with the following,

$$x = r \cos \psi, \quad y = r \sin \psi, \quad z = 0, \quad (5.8)$$

where r can be determined by the user and the directional cosines are fixed to $(0, 0, 1)$, similar to the point source directional cosines.

5.1 Principles of Monte Carlo modelling for light-tissue interactions

(ii) Photon step size Whilst a photon travels without interacting with the medium, the mean free path length, or step size (S) is described by,

$$S = \frac{1}{\mu_t} = \frac{1}{\mu_a + \mu_s}, \quad (5.9)$$

where the total attenuation coefficient (μ_t) is defined as the sum of the attenuation coefficients due to absorption (μ_a) and scattering (μ_s).

As the photon takes a random path within the tissue, the step size is calculated by the random sampling of the probability of a photon path through tissue. As seen in Chapter 4, Beer's law states that light travelling through a medium is attenuated exponentially, therefore, the probability density function that describes the distribution of S is also exponential with rate μ_t and expressed as,

$$p(S) = \mu_t e^{-\mu_t S}. \quad (5.10)$$

Given Equation (5.4), the step size will be found by solving for s , in the following equation,

$$\int_0^s p(S) dS = \xi \quad \therefore \quad s = \frac{-\ln(\xi)}{\mu_t}. \quad (5.11)$$

(iii) Photon scattering angle Photon scattering occurs by deviating the photon direction by the deflection angle ($0 \leq \theta < \pi$) and rotation through the azimuthal angle ($0 \leq \phi < 2\pi$). The scattering angle is calculated with the use of the HG phase function, Equation (5.2). By applying the random sampling methodology (Equation (5.4)), $\cos(\theta)$ can be expressed as a function of the random number ξ as,

$$\cos \theta = \begin{cases} \frac{1}{2g} \left[1 + g^2 - \left(\frac{1-g^2}{1-g+2g\xi} \right) \right] & \text{if } g \neq 0 \\ 2\xi - 1 & \text{if } g = 0. \end{cases} \quad (5.12)$$

Furthermore, the azimuthal angle (ϕ) is uniformly distributed between 0 and 2π , thus sampled using,

$$\phi = 2\pi\xi. \quad (5.13)$$

(iv) Boundary interactions Photons approaching a boundary could either be transmitted into the next layer or reflected back within the current layer; where this will be discussed further in Section 5.2.3. Although boundary interactions do not

require the random sampling methodology, it will be included in this section, as it requires a form of randomness.

To determine whether the photon is internally reflected, a random number (ξ) is generated and compared to the calculated internal reflectance ($R(\theta_i)$). For internal reflection to occur, $\xi \leq R(\theta_i)$. The photon packet stays on the tissue boundary it is closest to, with the directional cosines updating, where the z component is reversed. Alternatively, for the photon to escape the tissue and to be transmitted to the next layer, $\xi > R(\theta_i)$. Once transmitted, the photon direction is updated and the layer is updated, ready for the next run of the simulation.

5.2 Development of multi-layer colon model

The MC modelling developed is based on those described by Wang et al. [259] and Chatterjee [260] in MATLAB[®] (*Version 2017*). The MC model includes the design of an intraluminal reflectance mode optical sensor, where a narrow beam of photons propagate into a multi-layered colon tissue, with reference to Chapter 2. This section explains the processes based on the principles described in Section 5.1 to develop a multi-layer model of the intestine.

5.2.1 Geometric representation and co-ordinate system

The MC model required the tissue and proposed intraluminal optical sensor parameters to represent the geometric tissue structure. As shown in Figure 5.4(a), the origin on the Cartesian co-ordinates system $(0, 0, 0)$ was set to correspond to the photon incident point on the tissue surface from an optical source (S). Whilst the photons propagate through the tissue along the positive z-axis, a photon is detected by a detector (D). As the intraluminal optical sensor has been chosen to be a reflectance mode sensor, the detector was placed on the top surface with a fixed x-distance of 5 mm away from the origin $(5, 0, 0)$. The source-detector separation was chosen to be within an acceptable range of 4 mm to 6 mm [36], where large, good quality, pulsatile signals are achievable. Illustrated in Figure 5.4(b), the multi-layered intestine model consists of four (4) layers, where the mucosa is the inner most layer of the intestine which progresses towards the outer surface known as the serosa. For the tissue volume, each layer was defined to be infinitely wide, where each layer was represented with a finite thickness reported

5.2 Development of multi-layer colon model

in Chapter 2. It should be noted that the standard unit of length throughout the simulation is in mm for consistency.

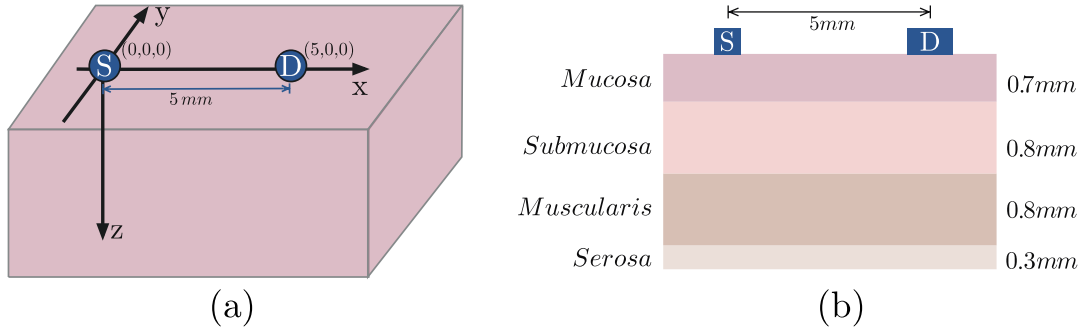


Figure 5.4 Illustration of the geometry and tissue structure of the colorectum. (a) Illustration of single layer tissue within a three-dimensional Cartesian co-ordinate system. The origin of the co-ordinate system $(0,0,0)$ corresponds to the centre of the optical source (S). Based on a reflectance mode optical sensor, the detector (D) is placed at a distance of 5 mm, thus the co-ordinates of $(5,0,0)$. The positive z-axis corresponds to the depth within the tissue. (b) illustrates the multi-layered tissue layers of the colorectum and the corresponding thickness.

5.2.2 Optical properties of the Monte Carlo model

The primary aim of the model was to gain an understanding of the behaviour of light illuminating the colon. For the development of a dual-wavelength PPG sensor, two wavelengths, (660 nm) and (880 nm), were chosen; corresponding to red (R) and infrared (IR) respectively. The choice of wavelengths were based on the regions where the absorption coefficient (μ_a) of oxygenated (HbO_2) and deoxygenated (Hb) haemoglobin, as shown in Figure 5.5, are relatively flat and significantly different. Additionally, the choice of wavelengths aid in the estimation of the oxygen saturation (S_pO_2), described in Chapter 4. The multi-layer tissue consisted of four (4) layers of tissue with different optical parameters, where parameters were based on published experimental results for the chosen operating wavelengths, as shown in Table 5.1 [266–268, 173]. It should be noted that the standard unit for the attenuation coefficients throughout the simulation is mm^{-1} for consistency.

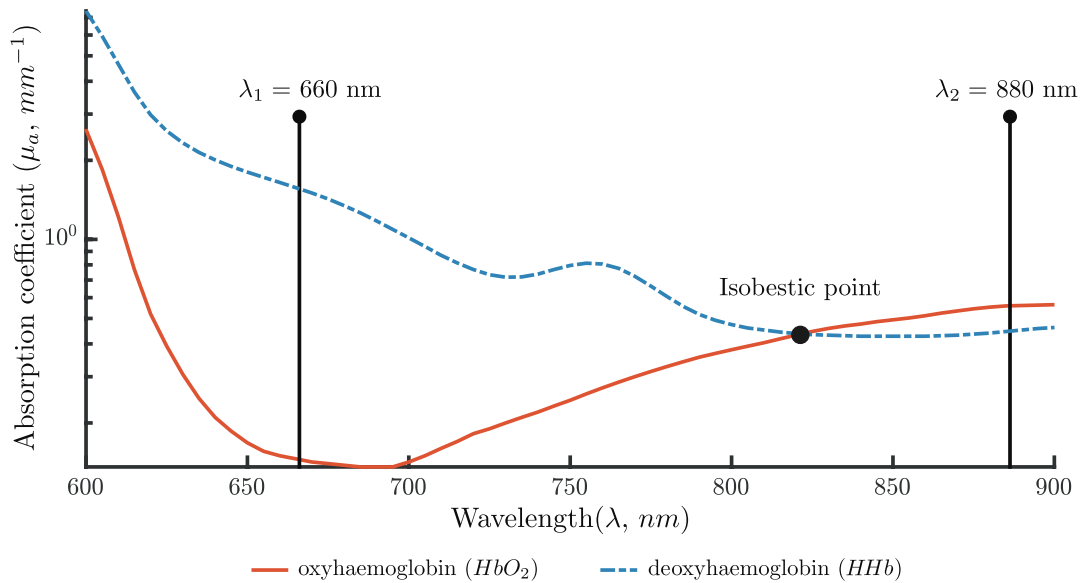


Figure 5.5 Wavelength selection for the dual-wavelength intraluminal optical sensor. Two wavelengths were chosen, 660 nm and 880 nm, corresponding to red and infrared light. Selected wavelengths are based on the absorption coefficients of oxyhaemoglobin and deoxyhaemoglobin, where both are relatively flat and significantly different. This allows easier differentiation between the two components to aid in the estimation of the oxygen saturation. The isobestic point corresponds to approximately 805 nm, where HbO_2 and HHb absorb light equally. Figure re-plotted from Budidha [261].

Table 5.1 Colon optical properties, where each sub-layer consists of different optical properties for different emitter wavelengths. The table presents values specifically for the two emitter wavelengths chosen; red (R, 660 nm) and infrared (IR, 880 nm).

Tissue	$\mu_a(mm^{-1})$	$\mu_s(mm^{-1})$	g	r_i
	R/IR	R/IR	R/IR	
Mucosa	0.050	26.33	0.934	0.948
[266, 269, 267]	0.050	22.05	0.956	
Submucosa	0.039	9.170	0.939	1.360
[266, 269, 267]	0.050	8.249	0.956	
Muscularis	0.025	9.476	0.914	1.357
[268, 267]	1.740	9.848	0.928	
Serosa	0	0	0.9	1.350
[173]				

5.2.3 Monte Carlo algorithm

Algorithm 1 presents the MC algorithm developed in MATLAB[®] to simulate photons propagating through multi-layered tissue. The main functions within the algorithm will be described further in this section. The algorithm runs for a single wavelength (λ) and iterates until a specific number of detected photons (N_p). The output provides the photon trajectories of the detected photons as well physical quantities of each photon. The algorithm consists of nested loops where the outer one launches the photons and the internal one iterates a single photon until it is terminated.

Initialisation Knowing the number of tissue layers, the tissue order (\mathbf{t}_o) and the depth of the layers to set the boundaries (\mathbf{b}), the tissue geometry was created. With the wavelength (λ) chosen, the optical properties for the tissues were assigned. The target number of photons (N_p) is provided, where the algorithm continues until the number of photons reaches N_p . Prior to the launch of a photon packet, each packet was assigned to have a unity weight and injected into the tissue with the choice of two sources; (i) a point source or, (ii) a Gaussian beam with a radius of 0.5 mm.

Photon launch Upon launch, the photon is automatically assigned to the first layer, as the initial position of the photon is at the origin of the Cartesian co-ordinates. Once the layer is selected, the photon is ready to make its first movement.

Photon movement Whilst a photon travels without interacting with the medium, the mean free path length, or step size (Δs) must be calculated. The step size is determined by Equation 5.11, allowing the photon to move to a new position, which is updated with the following expressions,

$$x \leftarrow x + \mu_x \Delta s, \quad y \leftarrow y + \mu_y \Delta s, \quad z \leftarrow z + \mu_z \Delta s,$$

where the arrow indicates the replacement of new co-ordinate values on the left-hand side, whilst the right-hand side holds the old value.

Layer selection To ensure an indefinite number of layers could be modelled, a layer selector was implemented. The position of the photon at a given time also determines the two adjacent layers (above and below). This would allow the parameters and boundary positions of the two adjacent tissues to be known continuously.

Algorithm 1: PROCESSING PIPELINE PER PHOTON

Input: Photon goal: N_p , Separation: s , Wavelength: λ , Boundaries: \mathbf{b} , tissue order: t_o , Optional: S_tO_2, Vb

Output: Photon trajectories: (X, Y, Z) , Output per photon: D_M, W, OP, W_A

```

1  % Initialisation
2  SetTissueBoundaries( $t_o, \mathbf{b}, \lambda$ );
3  AdjustTissueParameters( $S_tO_2, Vb$ );
4   $n \leftarrow 0$ ;
5   $\mu \leftarrow (0, 0, 1)^T$ ;
6  while Photon goal not reached:  $n \leq N_p$  do
7      % Photon launch
8      PhotonLaunch();
9      layer  $\leftarrow 1$ ;
10     IsPhotonMoving  $\leftarrow$  true;
11     % Photon movement
12     while IsPhotonMoving do
13         LayerSelection(layer);
14          $(x, y, z)^T \leftarrow$  PhotonStep( $\mu$ );
15         if  $z \leq 0$  then
16             % Photon is within detection region
17             if  $(x - s)^2 + y \leq \tau$  then
18                 StorePhotonTrack;
19                  $n \leftarrow n + 1$ ;
20             else
21                 KillPhoton;
22             end if
23             IsPhotonMoving  $\leftarrow$  false;
24         else
25             if Photon is: Tired, bored or out of bounds then
26                 KillPhoton;
27                 IsPhotonMoving  $\leftarrow$  false;
28             else
29                 % Photon boundary distance
30                  $[b_d] \leftarrow$  DistanceToBoundary( $\mu$ );
31                 if Photon within tissue then
32                     % Tissue absorption or scattering
33                      $\leftarrow$  ScatterPhoton();
34                      $\leftarrow$  Absorption();
35                 else
36                     % Boundary reflection or transmission
37                     ReflectTransmission();
38                 end if
39             end if
40         end if
41     end while
42     layer  $\leftarrow$  UpdateLayer();
43 end while

```

5.2 Development of multi-layer colon model

Photon boundary distance A similar approach to Wang et al. [259] was taken to compute the distance the photon was away from the boundary. Once the photon has taken a step, the distance between the current photon location (x, y, z) and the boundary of the current layer in the direction of the photon is computed with the following formulas,

$$b_d = \begin{cases} \frac{(z_0 - z)}{\mu_z} & \text{if } \mu_z < 0 \\ \infty & \text{if } \mu_z = 0 \\ \frac{(z_1 - z)}{\mu_z} & \text{if } \mu_z > 0 \end{cases} \quad (5.14)$$

where z_0 and z_1 are the z co-ordinates of the upper and lower boundaries of the current layer.

Tissue absorption or scattering Once the photon has taken a step and remains within a tissue, an attenuation of the photon weight due to scattering or absorption would occur. The absorbed fraction of photon weight (w) is expressed as, $\Delta w = w \cdot \frac{\mu_a}{\mu_t}$, where the unabsorbed photon weight ($w = w - \Delta w$) is recorded and subjected to scattering.

With the deflection and azimuthal angles calculated, the new direction of the photon can be updated using the following relationships [259],

$$\mu'_x = \frac{\sin \theta (\mu_x \mu_z \cos(\phi) - \mu_y \sin(\phi))}{\sqrt{1 - \mu_z^2}} + \mu_x \cos(\theta), \quad (5.15a)$$

$$\mu'_y = \frac{\sin \theta (\mu_y \mu_z \cos(\phi) + \mu_x \sin(\phi))}{\sqrt{1 - \mu_z^2}} + \mu_y \cos(\theta), \quad (5.15b)$$

$$\mu'_z = -\sin(\theta) \cos(\phi) \sqrt{1 - \mu_z^2} + \mu_z \cos(\theta). \quad (5.15c)$$

If the angle of the photon is close to the z -axis, which corresponds to the normal of the tissue surface ($|\mu_z| > 0.99$), then the following formulas should be used,

$$\mu'_x = \sin(\theta) \cos(\phi), \quad \mu'_y = \sin(\theta) \sin(\phi), \quad \mu'_z = SIGN(\mu_z) \cos(\theta), \quad (5.16)$$

where $SIGN(\mu_z)$ returns 1 when μ_z is positive and -1 when a negative. Finally, the current photon direction is updated where $\mu_x \leftarrow \mu'_x$, $\mu_y \leftarrow \mu'_y$ and $\mu_z \leftarrow \mu'_z$.

Boundary reflection or transmission During a photon step, the photon may encounter a boundary depending on its position. An all-or-none approach was employed, where photons at a boundary, could either experience transmission, where the photon packet passes through to the next layer, or alternatively, the photon internally reflects.

The photons being internally reflected depends on the angle of incidence (θ_i), where the angle is calculated by,

$$\theta_i = \cos^{-1}(|\mu_z|), \quad (5.17)$$

thus, $\alpha_i = 0$ corresponds to an orthogonal incidence. Recalling from Chapter 4, there are three methods in calculating reflectance: (i) Equation 4.2 if $\theta_i \simeq 0$, (ii) Equation 4.3 if $0 < \theta_i < \theta_c$, or (iii) reflectance equal to 1 if $\theta_c \leq \theta_i < \pi/2$.

Photon termination Once a photon packet is launched, the photon has two ways in which it could be terminated, (i) photon detection or, (ii) photon death.

Photon detection The photons were detected if their position and directional co-ordinates were within the area of the modelled detector, which had a known radius of 0.66 mm^2 and placed on the top tissue surface. Once the photon was detected, the propagation process through the tissue was terminated. The detected weight (W) is also referred as the reflectance as the detector was placed on the same side of the tissue, adjacent to the source. Once detected, variables are updated and stored, such as the weight detected (W), weight absorbed (W_A), optical pathlength (OP), photon positions (X, Y, Z) and the penetration depth.

Photon death There are two conditions where a photon can be terminated: (i) "Tired" due to the photon weight attenuating and (ii) "Bored" due to the photon continuously scattering without detection. With every interaction the photon encounters, the photon weight attenuates. Thus, after each interaction, the weight is compared to a threshold weight (w_{th}) of 10^{-4} . Additionally, the photon can be terminated if it has scattered too many times as it no longer carries valuable information from the tissue region of interest. Thus, the number of scattering is compared to a threshold scattering number ($N_{scatter} = 10^3$). These certain thresholds were chosen as it is commonly used for simulating photons migrating through biological tissues [260].

Once the photon was terminated, all variables would be reinitialised, except for the detected photons, to allow a new photon to be launched. The programme continues its loops until the desired number of photons are detected.

5.2.4 Methods for validating the multi-layer model

The Monte Carlo model required validation prior to modelling the colon. Therefore, the validating process was to obtain results from the model and to compare with already established analytical solutions. For the purpose of validation, a mono-layer tissue volume was simulated. With the model described in Section 5.2, a mono-layer tissue was chosen to validate the developed MC. Validations were performed for two case models with pre-validated results.

Case I The developed MC model was validated by creating a finite tissue layer of 0.2 mm thickness having an anisotropic scattering property and a matched refractive index boundary. The optical parameters used for the simulation are presented in Table 5.2. Let the total reflectance R_T be the total amount of light which exits the top surface of the tissue and the total transmittance T_T be the total amount of light transmitted from the bottom of the tissue. Both parameters were computed through ten MC simulations of 5×10^4 photons.

Case II The developed MC model was validated by creating a single tissue layer having an isotropic scattering property and a mismatched refractive index boundary. The optical parameters used for the simulation are presented in Table 5.2. The R_T was computed through ten MC simulations of 5×10^4 photons, identical to the parameters used by Wang et al. [259].

Table 5.2 Optical parameters for model validation, where case I corresponds to a finite tissue slab of having an anisotropic scattering property and a matched refractive index boundary. Case II corresponds to an isotropic slab of infinite thickness with a mismatched refractive index boundary.

Case	μ_a (mm ⁻¹)	μ_s (mm ⁻¹)	g	t (mm)	RI
I	1	9	0.75	0.2	1
II	1	9	0	∞	1.5

5.2.5 Computational analysis

For both cases, the ten simulations are presented in Table 5.3, with the mean values presented in bold. For each case, the mean results were compared with results by Prahl [270], Wang et al. [259], [271] and Chatterjee [272], as shown in Table 5.4.

Assessing light-tissue interactions using Monte Carlo simulations

Table 5.3 Total reflectance R_T and total transmittance T_T values obtained from ten simulations of 5×10^4 photons in two cases. Case I models a mono-layer with an anisotropic scattering property and a matched refractive index boundary. Case II models a mono-layer with a isotropic scattering property and a mismatched refractive index boundary. The mean of both cases are presented in bold.

Run	Case				
	1			2	
	R_T	T_T	Time (s)	R_T	Time (s)
1	0.0986	0.6611	26	0.2515	4
2	0.0983	0.6592	26	0.2525	4
3	0.0962	0.6622	26	0.2518	4
4	0.0980	0.6601	28	0.2553	4
5	0.0964	0.6623	26	0.2499	4
6	0.0985	0.6607	27	0.2515	4
7	0.0972	0.6598	27	0.2583	4
8	0.0980	0.6610	27	0.2537	4
9	0.0971	0.6600	19	0.2529	4
10	0.0950	0.6638	24	0.2492	4
Mean	0.09733	0.66100	25.6	0.2566	4

It can be seen that the values of reflectance and transmittance obtained from the present MC simulation in fair agreement with the pre-validated data.

In addition, the law of energy conservation was also verified to check the accuracy of the model. The law of energy conservation states that the total weight of the photon should be the same. Therefore, the sum of the absorbed weight (W_A), reflected weight (R_T) and transmittance weight (T_T) should always equal to the initial weight of the photon, being 1. In Case I, the summation $W_A = 0.24167$, $R_T = 0.09733$ and $T_T = 0.66100$, resulted in the original photon weight of 1. Similarly in Case II, with no transmittance recorded, the summation of $W_A = 0.7434$ and $R_T = 0.2566$ resulted in the original photon weight of 1. Thus, the energy in both cases of the MC simulation was conserved.

With the developed MC model validated with values of previous accepted work, it was concluded that the necessary modifications to the model could be made to replicate the colon to understand further the interaction between light and the colonic tissue.

5.3 Modelling the effects of colonic perfusion states and light propagation

Table 5.4 Comparison of experimental results, in bold, to the accepted validation results from several authors. The validation results include the reflected weight (R_T) and the transmittance weight (T_T).

Source	Case		
	1	2	
	R_T	T_T	R_T
Prahl	0.09711	0.66159	0.26079
Wang-Jaques	0.09734	0.66096	0.25907
Jurovata	0.09734	0.66100	0.25803
Chatterjee	0.09732	0.66142	0.26052
Present work	0.09733	0.66100	0.25660

5.3 Modelling the effects of colonic perfusion states and light propagation

The current research is focusing in the ability to monitor intestinal viability by applying the principles of PPG and PO. As seen in Chapter 4, the change in perfusion, such as the change in blood volume, is an important factor for PPG and PO [260]. With the change in the perfusion, the light path through tissue is likely to deviate. Currently, no information regarding the light-tissue interaction within the colon tissue at different states of tissue perfusion is available in the literature. Therefore, this section describes the MC modelling to investigate the effects of colonic perfusion states and the light path. The light path can be quantified by parameters such as the optical path (OP) and penetration depth (PD), which are invaluable for predicting and optimising the performance of an optical sensor for monitoring intestinal viability. Furthermore, the following section is reproduced verbatim from Patel et al. [273].

5.3.1 Materials and methods

The algorithm in Section 5.2 developed to model a multi-layered tissue was utilised to model the colon and its four layers, along with the colonic optical properties found in Table 5.1. Additional parameters were required for the investigation, which will be described further.

Optical properties and tissue parameters To allow the model to simulate the volumetric changes in blood within a tissue, additional input parameters indicating the physiological state of the tissue were included. The additional parameters included

the blood oxygen saturation (S_tO_2) and blood volume (V). A homogeneous mixture of mucosa and blood was assumed to model a perfused colonic tissue, where the blood volume was characterised by the combination of absorption (μ_a) and scattering (μ_s) coefficients of oxyhaemoglobin (HbO_2) and deoxyhaemoglobin (Hb). The total μ_a of the mucosa perfused with V and S_tO_2 was written as the sum of the individual absorption coefficients of the components:

$$\mu_a = (1 - V)\mu_{a_{MB}} + V[S_tO_2\mu_{a_{HbO}} + (1 - S_tO_2)\mu_{a_{Hb}}], \quad (5.18)$$

where μ_{a_M} is the absorption coefficient of the mucosa, $\mu_{a_{HbO_2}}$ and $\mu_{a_{Hb}}$ are the absorption coefficient of oxyhemoglobin and deoxyhemoglobin, respectively. Furthermore, as the mean S_tO_2 has been reported as 70 %, the S_tO_2 was kept constant [242, 269]. Equation (5.18) defines the effective optical properties for the mucosa, which is the cumulative effect of the optical and physiological properties of the tissue. With the optical wavelengths chosen to be 660 nm (red, R) and 880 nm (infrared, IR), the optical properties for blood having a haematocrit (Hct, proportion of RBC in total blood volume) of 45 % were collected from published literature [274] and presented in Table 5.5.

Table 5.5 Optical properties for blood (mm^{-1}) for each emitter wavelength (λ), red (660 nm) and infrared (880 nm). Optical properties for blood having 45 % hemotocrit (Hct) were collected from Bosschaart et al. [274].

λ (nm)	$\mu_{a_{HbO}}$		$\mu_{a_{Hb}}$	
	Hct = 0.45		Hct = 0.45	
	μ_a	μ_s	μ_a	μ_s
660	0.15	92.29	1.64	81.50
880	0.56	54.76	0.44	62.50

Monte Carlo modelling The developed algorithm in Section 5.2 was used, where a reflectance mode intraluminal optical sensor was also modelled. With a fixed source-detector separation of 5 mm, the source was chosen to be a point source and a detector defined to have an active area of 0.66 mm^2 for 10^3 photons for each wavelength to be simulated. Referring to Equation (5.18) the range of V within the mucosa was chosen to be between 2 – 10%, as seen in Hidović-Rowe and Claridge [269].

For each simulation, quantities from the detected photons such as the total OP, the remaining weight, absorbance and reflectance were recorded. Referring to Section 5.1

5.3 Modelling the effects of colonic perfusion states and light propagation

and Figure 5.6, the sum of the step size for a single photon (s_i) is defined as the total optical path (OP) for a photon. Thus, for the total detected number of photons (N_p), the mean optical path (MOP) was calculated as the average of the sum of all total optical paths for N_p . Additionally, the mean penetration depth (PD) of the detected photons was calculated as the mean of the depths of each photon, which corresponds to the maximum distance covered along the positive z-axis.

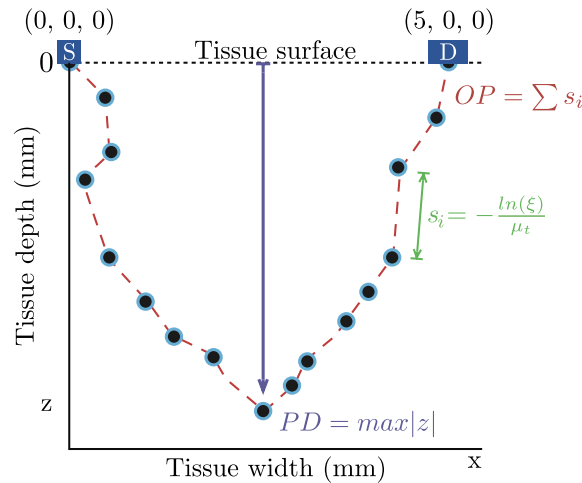


Figure 5.6 2D illustration of an optical path in a reflectance geometry using the x-z plane of a 3D model. The source (S) is placed on the origin of the Cartesian co-ordinates (x, y, z) and detector (D) has a separation distance of 5 mm from the source, in respect to the tissue surface ($z = 0$). The blue dots (\bullet) represent the position of the photon. The red dotted line (--) represents the optical pathlength (OP), where the distance between two photon positions is equivalent to the photon's step size (s). Image redrawn from Chatterjee [260].

5.3.2 Computational analysis

The photon scattering distribution within the multi-layered colon where the mucosa contains a V of 7% and a S_tO_2 of 70% at each wavelength is presented as a two-dimensional image as shown in Figure 5.7. It should be noted that only the detected photons are presented in the image. As expected for both wavelengths, the photons followed a "banana" shaped distribution from the source and detector. To interpret the scattering distribution image, the colour bar represents the number of scattering events in a specific region, where the minimum and maximum number of scattering events corresponds to black and white respectively. With the source modelled as a point source, the number of photons are highest at the source and detector, and decreased at deeper penetration depths. Furthermore, a clear boundary can be observed between

the mucosa-submucosa layer, which is a result of very different scattering coefficients between the two layers. With a fixed source-detector separation of 5 mm, the photons did not travel through the entire tissue volume (2.6 mm) and lost most of the photon energy within the muscularis layer, where the muscularis is at a tissue depth between 1.5 mm and 2.3 mm.

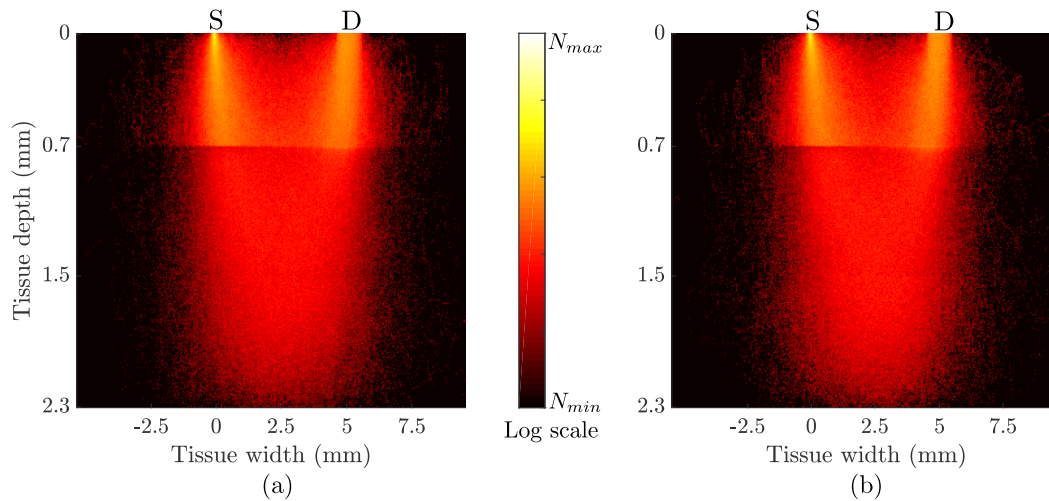


Figure 5.7 Light image in multi-layer colon model. Image of scattering distribution in the multi-layer model of the colon, between the source (S) and detector (D), when the mucosa contains a blood volume of 7% at a saturation of 70%. The scattering distribution is shown for the wavelengths of (a) red and (b) infrared. The colour bar represents the number of scattering events where black and white represents the minimum (N_{min}) and maximum number (N_{max}) of scattering events respectively. For better representation, the logarithm of the data points have been taken. Notice a clear boundary at 0.7 mm corresponding to the mucosa-submucosa layer.

For each wavelength, the mean PD and OP are presented in Table 5.6 as the V varied. Observing the PD at each wavelength, the R photons were found to penetrate deeper compared to the IR photons. The R photons tend to be confined within a penetration depth of 1.73 mm to 1.75 mm, whilst the IR are confined within the depths of 1.67 mm to 1.68 mm. At both wavelengths, the photons penetrated through similar tissue depths, corresponding to the muscularis layer. Observing the mean OP, both quantities do not vary considerably with the increase of V . This is due to V only affecting the photon absorbance within the mucosal layer. Similarly to the PD, the R photons encountered a higher mean OP than IR photons. Although the changes in the path length and the PD are not high, an abrupt change in the blood volume may result in a sudden change in the tissue-volume interrogated by the optical sensor.

5.3 Modelling the effects of colonic perfusion states and light propagation

Table 5.6 Mean penetration depth (PD) and optical path (OP) of photons propagating through the colon tissue layers at red (R) and infrared (IR) wavelengths, as the blood volume (V) increases from 2% to 10%.

V (%)	R		IR	
	Mean PD (mm)	Mean OP	Mean PD (mm)	Mean OP
2	1.75	11.60	1.68	9.98
3	1.74	11.49	1.66	9.90
4	1.74	11.50	1.68	9.96
5	1.74	11.63	1.68	9.92
6	1.74	11.48	1.67	9.92
7	1.74	11.46	1.67	9.90
8	1.74	11.48	1.67	9.96
9	1.74	11.50	1.67	9.90
10	1.73	11.41	1.67	9.88

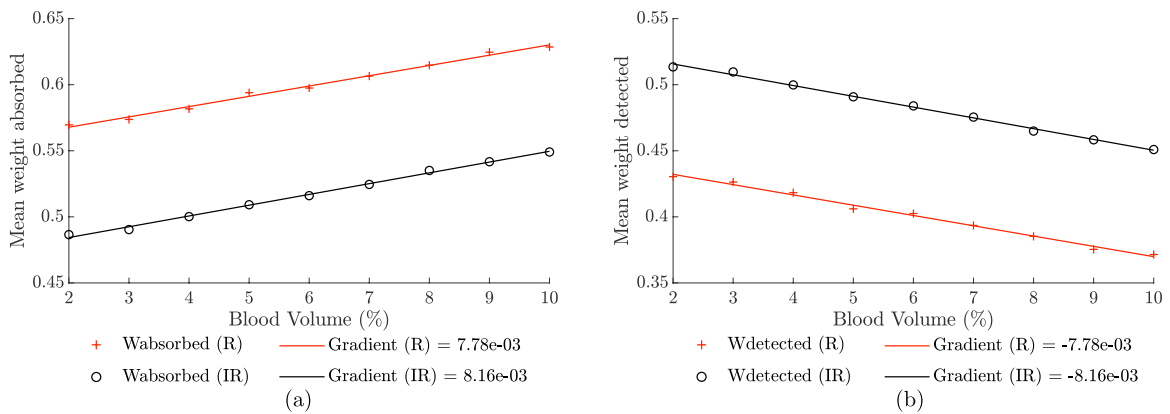


Figure 5.8 Mean absorbance (a) and mean weight (b) for the 10^3 photons detected when the blood volume varies between 2 – 10%. Data points for each wavelength are shown as red (+) and infrared (o). In addition, a linear fit has been created for easier data analysis.

Figure 5.8 presents the mean absorbance and mean weight of the detected photons whilst varying the blood volume. Whilst the V increased, Figure 5.8(a) presents that the mean weight absorbed by the detected photons linearly increases for both wavelengths. Furthermore, the R photons experienced higher absorbance than the IR. As the absorbance corresponds to the number of interactions, the result of lower remaining weight of R photons at the detector was reasoned, as shown in Fig 5.8(b). Overall, the increase in blood volume, resulted in the mean weight detected to decay consistently at both wavelengths.

5.4 Modelling the effects of sensor-tissue distance and light propagation

With the aim to develop an intraluminal optical sensor for an endocavity environment such as the colon without the use of a Foley catheter (inflatable balloon catheter), introduces uncertainty. The uncertainty arises as the sensor after insertion within the colon through the back passage would not be visible to the operator, therefore creating doubts of the positioning of the sensor. Using a PO requires direct contact between the sensor and the tissue. An imaging modality such as the colonoscope which is a camera guided tool (Section 3.3.4) could aid in visualising the sensor during the monitoring period, however this results in the intraluminal sensor technology to be more complicated and increasing the operator dependency. A simulation is required to understand the sensor dependence on the sensor-tissue separation. Therefore, this section describes the MC modelling to investigate the effects of the sensor-tissue separation and the light path.

5.4.1 Materials and methods

The multi-layered tissue model presented in Section 5.2 was used to model the colon, along with modelling an intraluminal optical sensor source.

Optical properties and tissue parameters The colon was modelled with its four layers using the optical properties found in Table 5.1. The simulation required the introduction of an optical sensor and tissue separation between the sensor and the mucosa layer. An air gap was used to simulate the sensor-tissue separation, thus the

5.4 Modelling the effects of sensor-tissue distance and light propagation

optical properties for air was an additional parameter required. For both wavelengths, the μ_a and μ_s were negligible and g and refractive index were set to 1.

Monte Carlo modelling For the sensor-tissue separation, a corresponding thickness of air layer was modelled, where Figure 5.9 is a simplified illustration of the MC modelling methodology. For each wavelength, 9 sensor-tissue separations were simulated, which were 0 mm, 1 mm, 2 mm, 3 mm, 4 mm, 5 mm, 6 mm, 8 mm and 10 mm.

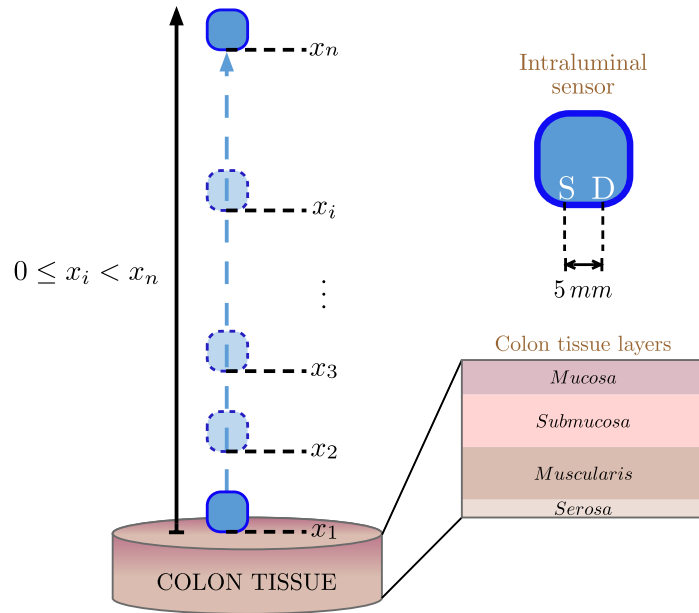


Figure 5.9 Simplified representation of the source-tissue separation method. The intraluminal sensor (blue) with a fixed source-detector of 5 mm emits light photons into the colon tissue at several distances, x_i , from the colon mucosa layer. Let x_1 be 0 mm from the colon mucosa. Initial simulations would be acquired at x_1 , before increasing the sensor-tissue distance to x_2 , x_3 till x_n by introducing a layer of air equivalent to the distance simulated.

The additional layer was easily implemented to the developed algorithm described in Section 5.2. An intraluminal optical sensor was also modelled, with a fixed source-detector separation of 5 mm. A Gaussian beam source with a beam diameter of 1 mm was simulated to emit photons with a wavelength of 660 nm (red, R) and 880 nm (infrared, IR), where a detailed explanation of the source type can be found in Section 5.1. The detector was defined to have an active area of 0.66 mm^2 to detect 10^4 photons for each wavelength. For each simulation, quantities from the detected photons such as the total OP, the remaining weight, absorbance, reflectance and PD were recorded.

5.4.2 Computational analysis

The photon scattering distribution within the multi-layered colon whilst a sensor-tissue separation was introduced, is presented in Figure 5.10. It should be noted that the detected photons are presented in the image. Both wavelengths are presented in the figure, where the first and second column presents simulations from R and IR respectively. To interpret the scattering distribution image, the colour bar represents the number of scattering events in a specific region, where the minimum and maximum number of scattering events corresponds to black and white respectively. Whilst increasing the sensor-tissue separation, which corresponds to the thickness of the air layer, a clear band with high number of scattering events can be observed. This band for all cases corresponds to the mucosa layer.

As the increase in sensor-tissue separation becomes greater than the total thickness of the multi-layered colon (2.6 mm), it is difficult to observe the scattering distribution within the tissue. Therefore, Figure 5.11 solely presents the scattering distribution within the tissue, whilst excluding the layer of air. For each separation, a boundary can be seen at 0.7 mm, corresponding to the mucosa-submucosa layer. This boundary can be explained by the very different scattering coefficients the two layers. To interpret the presented results in Figure 5.11, in a single x-z plane image, there are two axis present on the z-axis, both corresponding to the tissue depth in respect to either the sensor-tissue separation or the tissue layers. The left hand side axis corresponds to the tissue depth including the thickness of the air layer and the right hand side corresponds to the tissue depth of the colon with 0 mm corresponding to the beginning of the mucosa layer.

Figure 5.12(a-b) presents the mean absorbance and mean weight of the detected photons whilst altering the sensor-tissue separation. Referring to Section 5.1, the sum of the weight absorbed and the weight detected is equivalent to the initial unity weight of the photon, hence the opposite trends can be seen. The mean detected weight decays exponentially as the sensor-tissue increases. This is expected as the increase in distance from the sensor to the tissue causes photons to experience greater number of scattering and absorbing effects. For each wavelength, the affects of the mean OP due to the variation of the sensor-tissue separation was assessed and presented in Figure 5.12(c). Whilst the sensor-tissue separation increased, the mean OP linearly increased for both wavelengths. Whilst observing the effects of the sensor-tissue separation and PD, as shown in Figure 5.12(d), photons did not travel through the entire volume and lost

5.4 Modelling the effects of sensor-tissue distance and light propagation

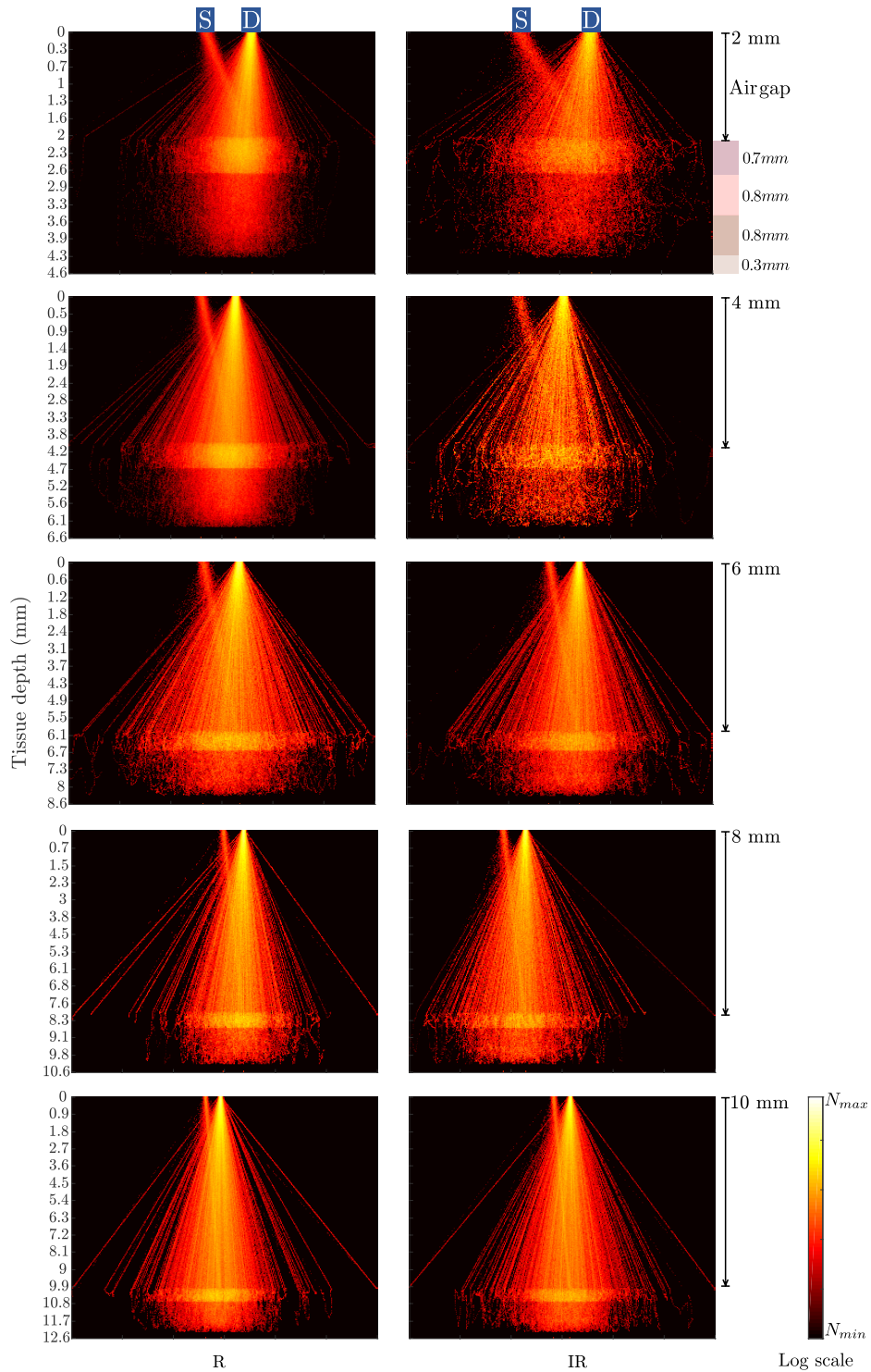


Figure 5.10 Light image whilst varying the sensor-tissue separation. The scattering distribution within the colon whilst increasing the air gap and keeping the source (S) and distance (D) constant at 5 mm. The two columns represent both wavelengths, where the first is red (R) and second infrared (IR). The colour bar represents the number of scattering events, where black is the minimum (N_{min}) and white is the maximum (N_{max}). For better representation, the logarithm of the data points have been taken and the tissue depth for each row are equal.

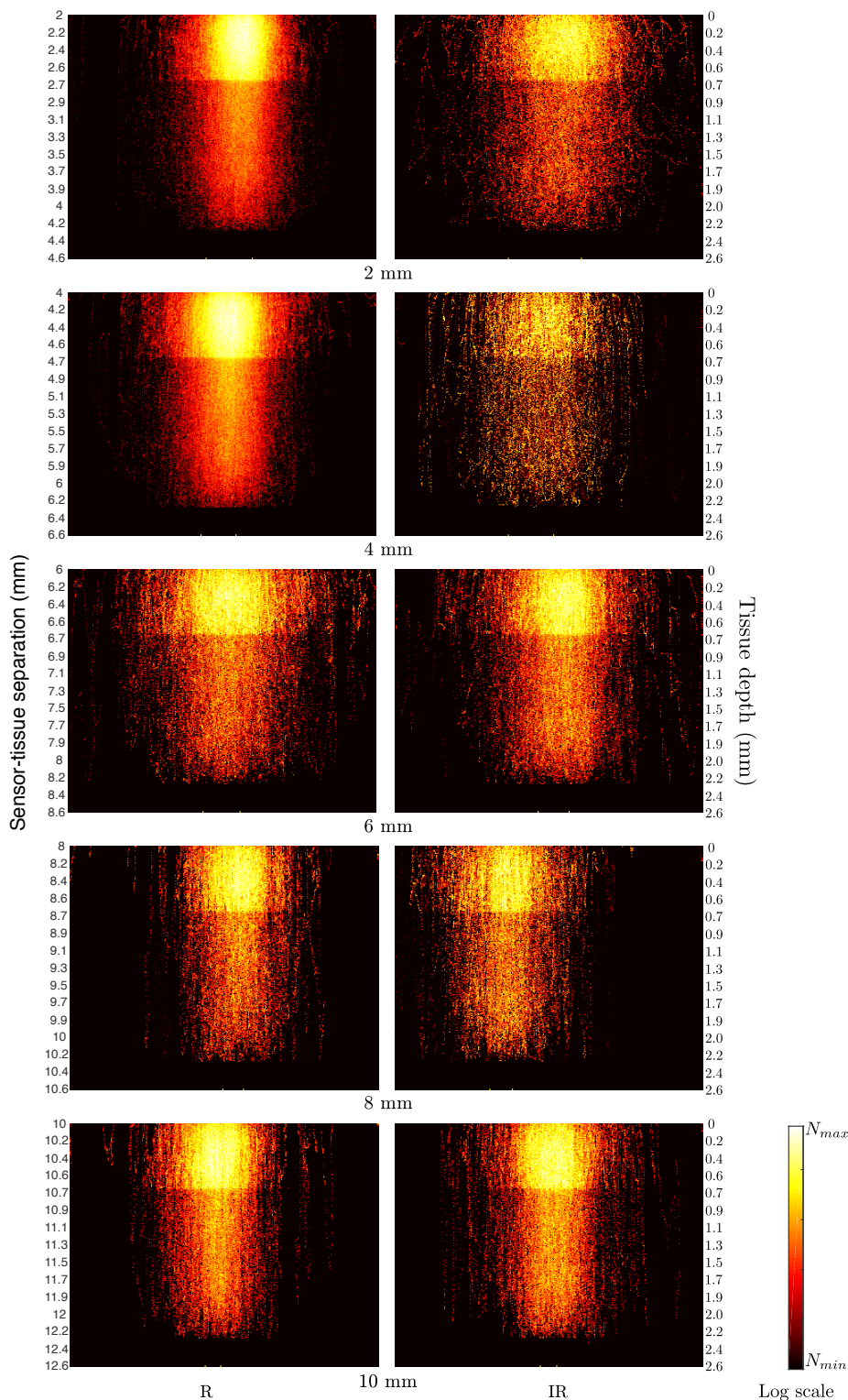


Figure 5.11 Light image in tissue when varying the sensor-tissue separation. The scattering distribution within the colon, excluding the air gap is presented. The first column and second column present red (R) and infrared (IR) respectively. The colour bar represents the number of scattering events, where black is the minimum (N_{min}) and white is the maximum (N_{max}). For better representation, the logarithm of the data points have been taken.

most energy within the submucosa layer, where the submucosa is at a tissue depth between 0.7 mm and 1.5 mm.

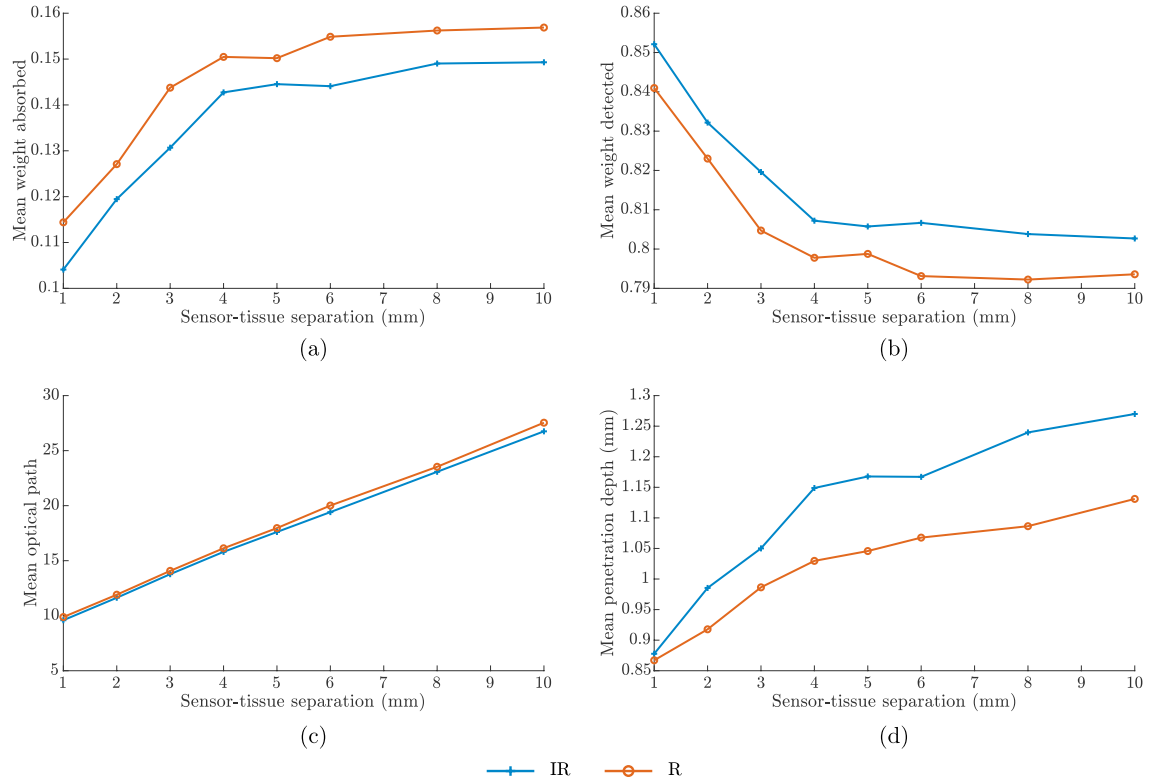


Figure 5.12 Mean optical quantities within the colon, where (a) weight absorbed; (b) weight detected, (c) optical pathlength (OP), and (d) penetration depth (PD) for 10^3 detected photons whilst the sensor-tissue separation varies between 1 – 10 mm. Data points for each wavelength are shown as red (o) and infrared (+).

5.5 Summary

To evaluate the behaviour of light within the colon with an intraluminal reflectance optical sensor, a computational model based on Monte Carlo was developed in MATLAB[®] by the author. This chapter detailed the principle and development of the model created for multi-layer tissues such as the colon, with the methodology following the principles of light-tissue interactions, discussed in Chapter 4. The model was known to be implemented successfully, through validation processes, where similar results were obtained to those accepted within the computational Monte Carlo modelling community.

The MC algorithm has been carefully optimised by using the optical and anatomical parameters available in the literature to replicate the human colon as close as possible, during normal conditions. human colon as close as possible. The effect of the changes in perfusion states and light propagation within the mucosa has been demonstrated. By increasing the blood volume, the investigation showed a consistent decay in the detected light intensity, together with small yet persistent changes in the optical path length and penetration depth.

The modelling of light-tissue interaction in the colorectum whilst introducing a sensor-tissue separation has been attempted for the first time and presented in this chapter. For the acquisition of PPGs, it is common practice to place the optical sensor in direct contact with the tissue of interest, to obtain large amplitudes and high-quality signals. As there is a desire to design an intraluminal optical sensor without a balloon, to hold the sensor in contact with the mucosa, it was necessary to investigate the influence of direct contact versus no contact PPG measurements. During non-contact cases of up to 5 mm separation, light photons continue to enter the tissue, where most energy were lost within the submucosa.

The volume of information gathered from the computational studies has played a crucial role in designing the intraluminal reflectance PPG sensor for monitoring bowel tissue viability. The following chapter (Chapter 6) will describe the development and manufacturing of the intraluminal optical sensor and the PPG processing system.

Chapter 6

Design and development of the intraluminal PPG sensor and processing system

By understanding the principle of photoplethysmography (PPG) and pulse oximetry (PO), as seen in Chapter 4, simulations of light photons were modelled through the colorectum (CR). Based on the simulation results, custom-made optical sensors for signal acquisition within the colorectum and on the finger can be developed. Simultaneously, the two custom-made sensors require a processing system to operate the dual-wavelength light sources and digitise the analogue PPG signals for storage. Furthermore, an offline signal analyser is required to calculate the blood oxygen saturation (S_pO_2) and perform statistical analysis for the comparison of S_pO_2 of different locations. Thus, this chapter presents the design, development and manufacturing process of the custom-made optical sensors and processing system, where the main contribution for the processing system relates to an offline signal analyser. The offline signal analyser is required to calculate the blood oxygen saturation (S_pO_2) and perform statistical analysis for the comparison of S_pO_2 of different locations.

Motivation Utilising the principles of PPG, the research explores the capability of providing valuable information relating to the bowel viability. The assessment within the inner walls of the CR requires a custom-made PPG sensor for the acquisition of PPG signals within the CR. With reference to Figure 6.1, the objective of this chapter is to justify the design considerations to develop the intraluminal PPG sensor and the manufacturing process. The chapter continues to describe relevant functionalities of the PPG processing system where contributions have been made. Although no

contributions have been made with the instrumentation unit, as this has been designed by the Research Centre of Biomedical Engineering (RCBE) with the intention of providing a common research tool for PPG acquisitions, the functionality description can be found in Appendix A. The main contributions in this chapter are the two remaining modules, which will be presented in further details.

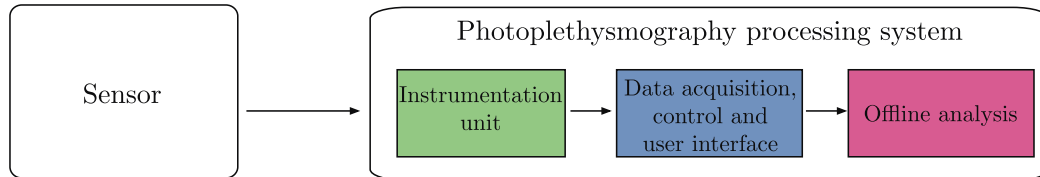


Figure 6.1 Overall block diagram for the development of the photoplethysmography sensors and processing system. A top-down approach has been taken where initial steps would be taken to develop the sensors, followed by the processing system. Within the processing system, there are three modules required for a functioning intraluminal optical system, where main contributions are seen within the last two modules.

6.1 Specifications of the intraluminal PPG sensor

PPG and PO are optical techniques requiring light sources to shine into the tissue region of interest. As the PPG sensor will be inserted within the CR, as shown in Figure 6.2, a reflectance mode sensor was chosen, where the light backscatters from the mucosal layer and acquired with the use of a photodetector. The PPG sensor developed was a dual-wavelength sensor, comprising of red (R) and infrared light (IR) emitters and a single photodetector (PD) to detect the back-scattered light. This section presents the properties of the chosen light emitters and PD. Subsequently the sections describe the electrical and mechanical development of the intraluminal sensor.

6.1.1 Light emitting diodes

For the development of a dual-wavelength PPG sensor, two surface-mounted light sources corresponding to the wavelengths modelled in Chapter 5 were chosen. The R wavelength light source selected for the intraluminal PPG sensor was a surface-mount light emitting diode (LED) of 660 nm (*KP-2012SRC-PRV*, *Kingbright, Taiwan*), measuring $2.0\text{ mm} \times 1.25\text{ mm} \times 1.1\text{ mm}$ ($l \times w \times h$). The IR wavelength light emitter was also a surface-mount LED of 880 nm (*KP-2012 SF4C*, *Kingbright, Taiwan*), measuring

6.1 Specifications of the intraluminal PPG sensor

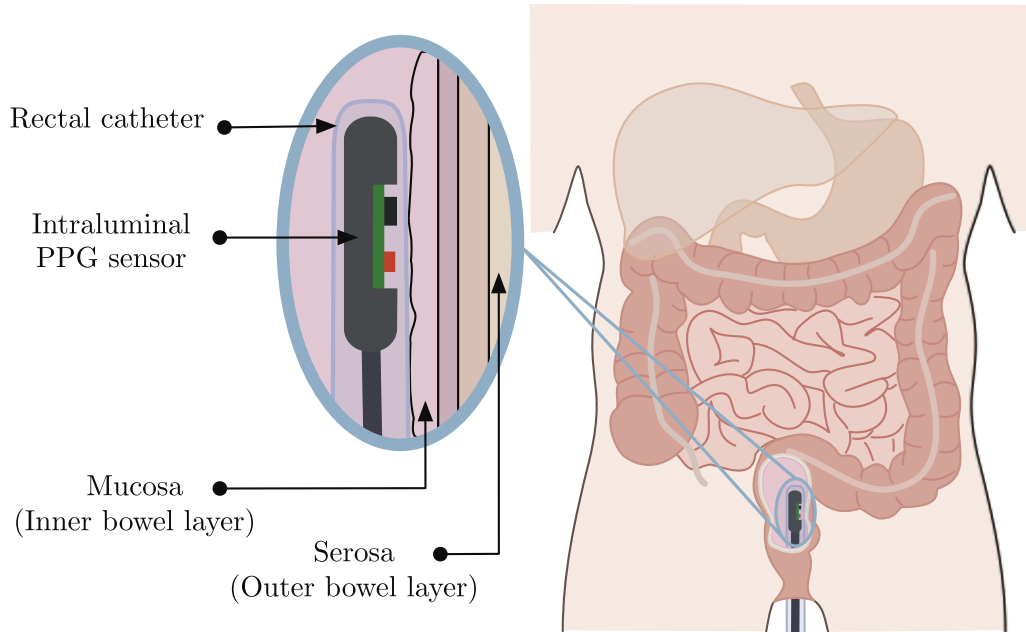


Figure 6.2 Illustration of the intraluminal sensor design. The photoplethysmography (PPG) sensor would be inserted into a rectal catheter and inserted into the colorectum through the anal verge. The sensor would be in contact with the inner walls of the colorectum, corresponding to the mucosa for the continuous monitoring of oxygen saturation.

2.0 mm × 1.25 mm × 1.1 mm ($l \times w \times h$). The optical and electrical characteristics of the chosen LED components are shown in Table 6.1.

6.1.2 Photodetector

To detect the back-scattered light from the tissue, a surface-mount, flat top PD measuring 2.00 mm × 1.25 mm × 1.20 mm ($l \times w \times h$), was used. The PD has the capability of detecting both chosen wavelengths, with an active area of 0.66 mm². Additional optical and electrical characteristics of the PD are shown in Table 6.2.

Design and development of the intraluminal PPG system

Table 6.1 Light source specifications for the intraluminal sensor. Specific light emitting diodes (LEDs) corresponding to red and infrared have been chosen. The table presents their optical and electrical specifications.

Characteristics	Red (R)	Infrared (IR)
Manufacturer	Kingbright	
Model	KP-2012SRC-PRV	KP-2012SF4C
Peak emission wavelength (λ)[nm]	660	880
Forward voltage at 20 mA [V]	1.85	1.3
Power dissipation [mW]	75	80
Dimensions ($l \times w \times h$) [mm]	2.00 x 1.25 x 1.1	
Operating temperature [°C]	-40 to +85	
Soldering temperature [°C]	245	
Light emitting angle [°]	120	
Reverse leakage current [μ]	10	
Peak forward current at 10 μ s [mA]	155	
Minimum reverse voltage [V]	5	

Table 6.2 Light detector specifications for the intraluminal sensor. A specific photodetector has been chosen, where the table presents its optical and electrical specifications.

Characteristics	Photodetector
Model	SR10BP-B-H
Manufacturer	CERLED
Peak wavelength sensitivity (λ_{max})[nm]	900
Radiation sensitive area [mm^2]	0.66
Switching time [ns]	10
Junction capacitance [pF]	10
Open circuit voltage [mV]	440
Reverse dark current [nA]	10
Reverse breakdown voltage [V]	170
Operating temperature [°C]	-25 – +80
Soldering temperature [°C]	240

6.2 Electrical design of the intraluminal sensor

The main components of the intraluminal PPG sensor are the LEDs and the PD, whilst the PPG processing system, provides the current supply to operate the LEDs and process the detected signals from the PD. This section describes the electrical design of the intraluminal PPG sensor.

To provide a form of structure to the optical sensor and electrical connection between the sensor and the PPG processing system, a Printed Circuit Board (PCB) technology was used. A PCB is a circuit board consisting of electrically conductive tracks and pads connecting various connectors and components together. To create a PCB, an electronic design software, Altium Designer (*Altium Ltd, Australia*) was used.

The double-layer PCB was designed to be rectangular with the dimensions of $10.4\text{ mm} \times 5.2\text{ mm} \times 0.4\text{ mm}$ ($l \times w \times h$), to be able to fit into a rectangular recess found in the sensor casing which will be described later in Section 6.3. Figure 6.3 shows the PCB schematic for the intraluminal PPG sensor, where the pads were designed to allow the placement of the two surface-mount LEDs and PD. The tracks were designed to have a width of 4 mm, and where necessary, angled greater than 90°C . Angles less than equal to 90°C are undesirable, as the tracks would act as antennas at high frequencies, therefore introducing noise and changing the behaviour of any frequency dependent components on the board.

Bearing in mind that the sensor is a reflectance PPG sensor, the PD was chosen to be placed 5 mm away from the LEDs, referencing the separation distance from the centre of the LEDs and PD as seen in Figure 6.3(c). This separation distance was chosen as the acceptable range for detecting large, good-quality, pulsatile signals without exceeding the LEDs driving current of 50 mA is known to be between 4 mm to 6 mm [275]. Additionally, from the computation modelling of the colon in Chapter 5, the separation of the source and detector at 5 mm presented as a suitable distance. This is because the optical path propagated through the muscularis or submucosa, depending on cases of contact or non-contact respectively. The LEDs were placed in an anti-parallel configuration, where the anode of the R LED connected to the cathode of the IR. This configuration allows intermittent switching of the LEDs when connected to the processing system, explained in Appendix A [56].

6.3 Intraluminal PPG sensor casing

Solely manufacturing the PCB and its ability to connect to the PPG processing unit was insufficient and unsuitable for a clinically acceptable tool. As the sensor will be inserted into the CR, the electrical design required to be isolated, protected and unarmful to the inner layer of the intestine. This section describes the development of the sensor casing which was designed to protect the optical components and suitable for the entry of the sensor into the body.

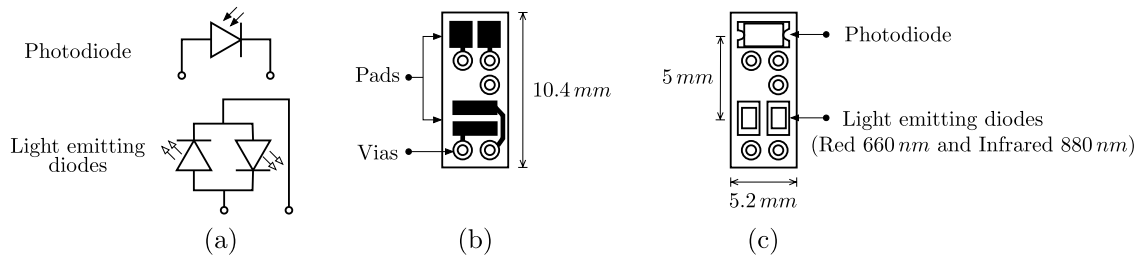


Figure 6.3 Intraluminal reflectance sensor circuit board design, where (a) presents the schematic diagram of the photodetector and light emitting diodes. Both circuits are independent and are open ended to be connected to the processing system. (b) presents the pads and routing to allow the placement of the electrical components as seen in (c). The vias allows the connection of wires to provide the connection to the processing unit.

6.3.1 Design of the sensor casing

As the measurement site of interest is the colorectal region of the bowel, more specifically the rectum, the anatomical features were taken into consideration. The CR is a tubular shaped structure with an approximate lumen dimension and wall thickness of 50 mm and 3 mm respectively [9].

The overall design of the sensor casing was chosen to be a pill-shaped capsule. Having a pill-shaped capsule would provide a smooth casing with the ends of the capsule rounded, to ensure the sensor does not have sharp edges which could pierce or damage the wall of the bowel. As the PCB and the wired connection are seen as two parts, the design required a smooth transition between them. The design aim of the sensor casing was to minimise the number of parts to reduce the chances of ingress of bowel contents. Any ingress during the use of the sensor into the electrical components could potentially cause an electrical short.

The sensor casing was designed using SolidWorks 2016 (*Dassault Systems, Vlizy-Villacoublay, FR*). The capsular design had the diameter and length of 5.5 mm \times 20 mm, respectively with a rectangular recess, allowing the placement of the PCB within the capsular casing. In order to have a smooth transition between the PCB and wire, a hollow bore with a radius of 2.5 mm and depth of 15 mm was created which extends from the distal end of the case to the opposite end. The bore dimension was chosen to be the same dimension as the multi-core screened wire, ensuring the bore provides a tight, secure fit for the wire.

Once the sensor casing and the PCB were designed separately, the fit was assessed by generating a 3D model assembly, as shown in Figure 6.4(a). This allowed the verification of dimensions of all components without the need of printing.

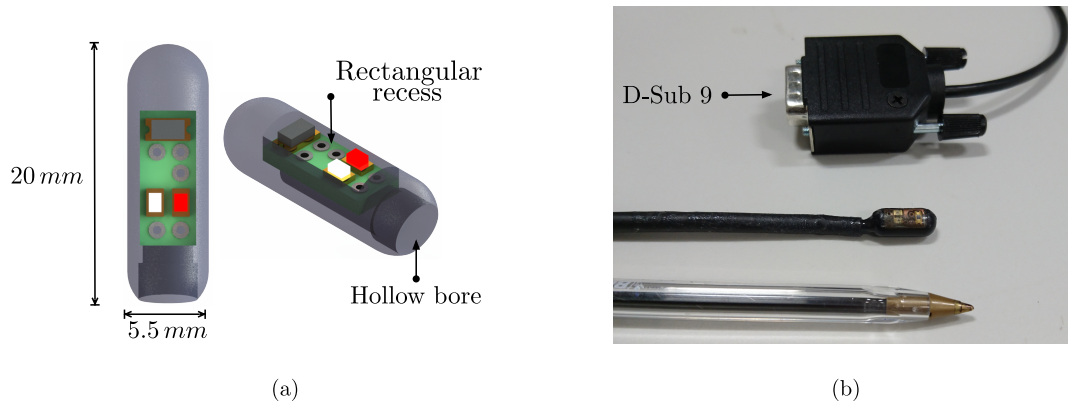


Figure 6.4 Development of the intraluminal optical sensor. A 3D model (a) visualises the assembly of the sensor casing and the circuit board prior to manufacturing for the verification of all components and sizing. The rectangular recess allows the circuit board to fit within the sensor casing and the hollow bore to allow the insertion of a multi-wire. The manufactured intraluminal sensor (b) has a multi-wire allowing a link between the optical sensor and processing system through a D-sub 9 connector.

6.3.2 Manufacturing of the sensor casing

After designing the sensor casing, a 3D printing technology, Objet30 3D printer (*Stratasys Ltd, Minnesota, US*) was used due its capability of printing thin layers with great accuracy ($28 \mu\text{m} \pm 0.1 \text{mm}$). The 3D printer works similar to an ink-jet printer, where layers of liquid photopolymer jets onto a building tray and cures instantaneously with ultraviolet light. This process continues, resulting in a model built layer by layer with a bottom-up method. To manufacture the sensing casing, stereolithography (STL) files were generated, allowing the 3D printing technology to print the design with the print-path files.

The sensor casing was manufactured black, to minimise the reflection of light during use. Once the sensor casing was successfully manufactured, the PCB with the multi-core cable was drawn into the case. The optical components were covered by applying a layer of clear medical epoxy (*Dymax 141-M, Dymax Cororation, Torrington, CT, US*). The unconnected side of the cable was drawn through the sensor casing before soldering a male D-Sub 9 connector to allow the detected signals to connet with the PPG processing unit. The reader is referred to Figure A.5 for the D-Sub 9 pin configuration.

6.3.3 Modifications to the intraluminal PPG sensor

The capsular prototype described in Section 6.3 having a diameter and length of 5.5 mm and 10.2 mm respectively, was deemed unsuitable for the intraluminal insertion into the human CR. This was due to strain being introduced at the boundary between the sensor casing and wiring; causing sensor defects whilst a pressure was being applied. This section describes the modifications made to the intraluminal sensor further miniaturisation and minimise the potential strain caused on the sensor during the insertion process within the bowel.

Printed circuit board modifications The optical components and orientation of the components remained the same, however the double-sided circuit board was replaced to a single-sided copper board. This single-sided layer copper sheet had a thickness of 0.2 mm, which was sufficient for manufacturing a smaller intraluminal sensor. The overall dimensions of the sensor PCB was 22 mm \times 4.2 mm \times 2.51 mm ($l \times w \times h$).

Sensor casing modifications A similar approach was taken when redesigning the sensor casing, where a capsular design was developed using the 3D designing and printing technology. The casing was designed to provide smooth and even surfaces with round edges to minimise any intestinal damage during the placement of the sensor. The modified sensor casing, shown in Figure 6.5, has a diameter of 6 mm and length of 36 mm, with a rectangular recess, allowing the placement of the PCB within the capsular casing. Elongating the sensor without compromising the internal environment of the intestine and a wire stopper was introduced. This was decided as the insertion technique which requires the clinician to push the sensor through the rectum creates potential strain on the initial prototype, resulting in sensor defects.

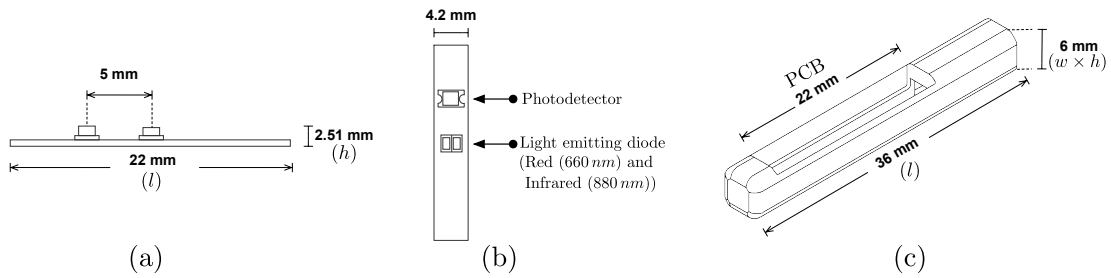


Figure 6.5 Mechanical drawing with dimensions of the components required to develop the modified intraluminal photoplethysmography (PPG) sensor. Drawings illustrate: (a) reflectance PPG sensor (side view), where the emitter-detector separation distance and the length and total height are annotated; (b) reflectance PPG sensor (top view), indicating the width and location of the components, such as the light emitting diodes and the photodetector. (c) sensor casing dimensions, where the rectangular recess is of the same length of the reflectance PPG sensor, allowing the placement of the reflectance PPG sensor.

Once the sensor casing and the PCB were designed separately, the modelled assemblies were generated to illustrate the concept. This allowed the verification of dimensions of all components without the need of printing. After verifying the sensor casing design, the casing was printed with the same methods mentioned in Section 6.3.2.

With the PCB securely fixed within the sensor casing, a black absorbing material was used to surround the optical components to reduce the effect of optical shunting, also known as the penumbra effect (light reaching the PD without passing through the tissue). Similarly to the previous prototype, an optically clear medical epoxy (*Dymax 141-M*, *Dymax Cororation, Torrington, CT, US*), was used to seal the PCB within the casing to provide electrical isolation. Figure 6.6 presents the modified intraluminal PPG sensor.

6.4 Reflectance finger PPG sensor

When using a pulse oximeter, the gold standard measurement location is the finger. In order to compare the PPG signals acquired from the CR, a reflectance finger PPG sensor was also developed. For comparisons to be made, the reflectance finger PPG sensor required to be optically and electrically identical to the CR PPG sensor. A PCB consisting of the identical optical components of the intraluminal PPG sensor was manufactured in a rectangular shape. This was to allow the finger PCB to be placed inside a modified commercial pulse oximeter finger clip. After reassembling the finger PPG PCB in the finger clip, the optical components were surrounded by the

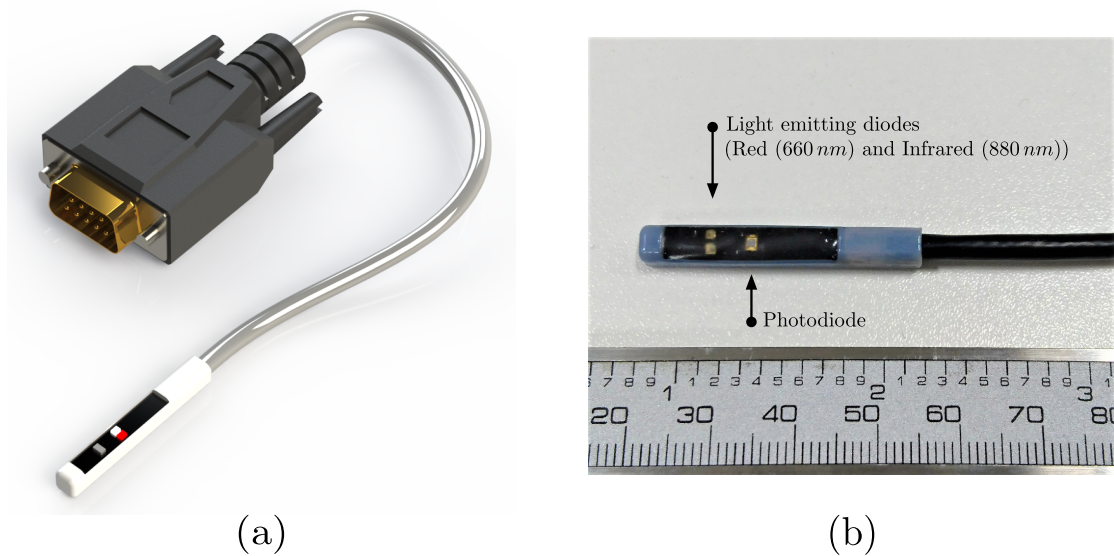


Figure 6.6 The intraluminal photoplethysmography (PPG) sensor for the assessment of intestinal viability. (a) 3D visualisation of the intraluminal PPG sensor; (b) image of the developed intraluminal sensor. A black absorbing material surrounds the optics, acting as an optical barrier before being sealed with a medical epoxy. The sensor includes a D-Sub 9 connector allowing connection capabilities with the PPG processing system.

black absorbing material, followed by sealing with the optically clear medical epoxy (*Dymax 141-M, Dymax Cororation, Torrington, CT, US*). The other end of the sensors wire was soldered onto a D-Sub 9 connector, for the connection to the PPG processing system.

6.5 Specifications of the processing system

To provide context of the processing system, this section briefly describes the different subsystems observed in Figure 6.1, and the required flow of information. The PPG sensors consist of two light emitting diodes (LEDs) which require an instrumentation unit to provide a supply of current. Additionally, to obtain signals from each LED independently, the dual LEDs require a modulator to alternatively vary the operating time of each LED. The detected light from the photodetector which gathers information from both LEDs requires separation and a voltage conversion. All acquired physiological signals require conditioning, including filtering and amplification, to minimise unwanted interference prior to digitisation. The instrumentation unit which will be introduced in Section 6.6, is a standardised research tool developed by researchers within RCBE, where minor adjustments were implemented for the current research application.

To digitise PPG signals, the exchange of information between the hardware from the instrumentation unit and software from a laptop has to be established. To display signals acquired in real-time and store the signals for offline analysis, a virtual instrument (VI) would be developed using a graphical programming language, LabVIEW (*Version 2016*). Appendix A.2 will discuss further the capability of allowing user control for varying the LED light intensities and enabling real-time calculation of blood oxygen saturation (S_pO_2). Furthermore, an event logger function is required to allow the user to synchronise observations or experimental adjustments with the acquired signals as a digital copy.

Offline analysis can be performed with the stored data. Data extraction, processing and statistical analysis would be possible with the use of MATLAB[®] (*Version 2017*). The development of a semi-automated data processing program will be discussed in Section 6.8.

6.6 Instrumentation unit

An instrumentation unit, also known as ZenPPG [241], has been previously designed by other RCBE researchers with the purpose of providing a standardised research tool for all PPG research applications. ZenPPG is a modular, customised unit, allowing the operation of custom-built or commercially available pulse oximeters (PO). Compared to commercial devices, ZenPPG permits the acquisition of raw, dual-wavelength PPG signals for offline signal analysis, rather than solely providing S_pO_2 values on a display. Minor modifications were implemented in ZenPPG, where the transimpedance amplifier was set to a gain of 330. The acquisition of PPG signals within the human colorectum is novel, therefore no literature was found suggesting the values of amplification required for adequate signals. With the understanding that the colorectum has an extensive network of collateral blood supply and signals have been acquired previously from the outer surface of the intestine [21], the gain of 330k was chosen. Thus the resultant PPG signals exiting the instrumentation unit had a total amplification of 59400. As ZenPPG was utilised within this research and no contributions were made, the key features can be found in Appendix A.

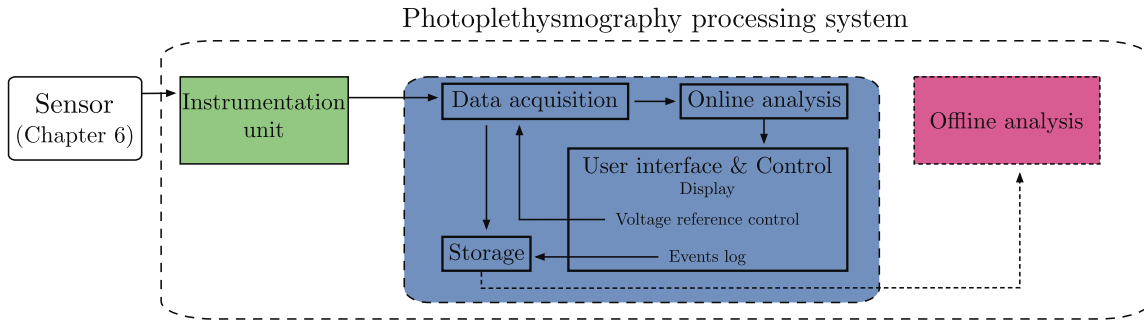


Figure 6.7 Detailed block diagram of the data acquisition, control and user interface within the processing system. This module allows the conversion of the signal from analogue to digital. The module features an online analysis through a virtual instrument, allowing users control of the light intensity of one developed sensor and the ability to store signals with events.

6.7 Data acquisition, control and user interface

This section describes the development of a virtual instrument (VI) to allow digital acquisition of signals obtained from the instrumentation unit and PPG sensors. Referring to Figure 6.7, the analogue signals from the instrumentation unit require digitisation by a data acquisition device in order to store signals for offline analysis. As mentioned in Appendix A.1, the user has the ability to control the light intensity of each LED of Channel 1 by adjusting digital voltage references through a VI. Additionally, without risking the subject under investigation, the user interface (ui) provides a safe method of viewing the acquired signals to calculate physiological parameters such as S_pO_2 in real-time and store the signals for offline analysis. In order to have such capabilities, a VI was developed using LabVIEW, which is an environment with a graphical programming language. It should be noted that some functionalities of the VI existed when the instrumentation unit was developed. The VI functionality was extended for the in-vivo studies performed within this research, highlighted in Figure 6.7.

Analogue-to-digital conversion The resultant analogue signals from the instrumentation unit were digitised with a National Instrument (NI) digital acquisition card (DAQ, *NI-PcIe 6321 DAQ, National Instruments, USA*). Further details of the set-up procedure can be found in Appendix A.

Voltage reference user control Acquiring PPG signals through LabVIEW is advantageous due to its capability in allowing user control of certain parameters.

This is achieved by designing a ui on LabVIEW, which is visible to the user on the front panel window. As mentioned in Appendix A.1, the instrumentation unit was designed to allow user control of the light intensities of the LEDs for Channel 1. The choice of operating the intraluminal PPG sensor digitally was to ensure no harm was inflicted to the subject under investigation. In an event of device failure, the laptop would terminate the operation of the entire channel. The DAQ was configured to simultaneously obtain signals acquired from the sensors, whilst allowing the user to have the ability to change the light intensity of the intraluminal PPG sensor LEDs. A more detailed explanation can be found in Appendix A.

Online analysis and display Another advantage of using LabVIEW is for allowing acquired physiological measurements to be analysed and displayed continuously in real-time. Prior to signal analysis, including continuous estimations of blood oxygen saturation (S_pO_2), the incoming digitised signals from both PPG channels require filtering. Detailed explanation of the filters and estimation of S_pO_2 can be found in Appendix A.

The most important aspect of the ui is the display, allowing the user to observe continuous real-time signals and measurements, as well as the ability to adjust necessary parameters. For each channel, the filtered ac components of the PPG were displayed on a graphical chart on the front panel. As seen in Figure 6.8, two graphical charts represent each channel, where both R and IR PPG signals can be observed simultaneously. This allowed the user to visually assess the morphology and size of the acquired signals which could aid in the decision of adjusting intensities of the LEDs via the digital voltage reference control or the on-board reference voltage found on ZenPPG. If necessary, a tabulated control was implemented to allow the user to choose the type of PPG signals viewed, such as the filtered PPG signals (ac and dc), unfiltered ac PPGs and filtered ac PPGs. For both channels, the dc and S_pO_2 values were displayed on the front panel as numerical indicators. The dc values were closely monitored, as the value indicates whether the saturation rail of the trans-impedance amplifier has been reached, thus allowing the user to adjust the LED intensities. Additional indicators were added to the front panel, as shown in Figure 6.8, where the user could continuously monitor the operation of the PPG sensors used and the electrical parameters of the instrumentation unit. The ui was solely developed for the research, therefore the displayed data during *in-vivo* investigations and clinical studies were not accessible to clinicians, which could alter their decision making in treatment or intervention.

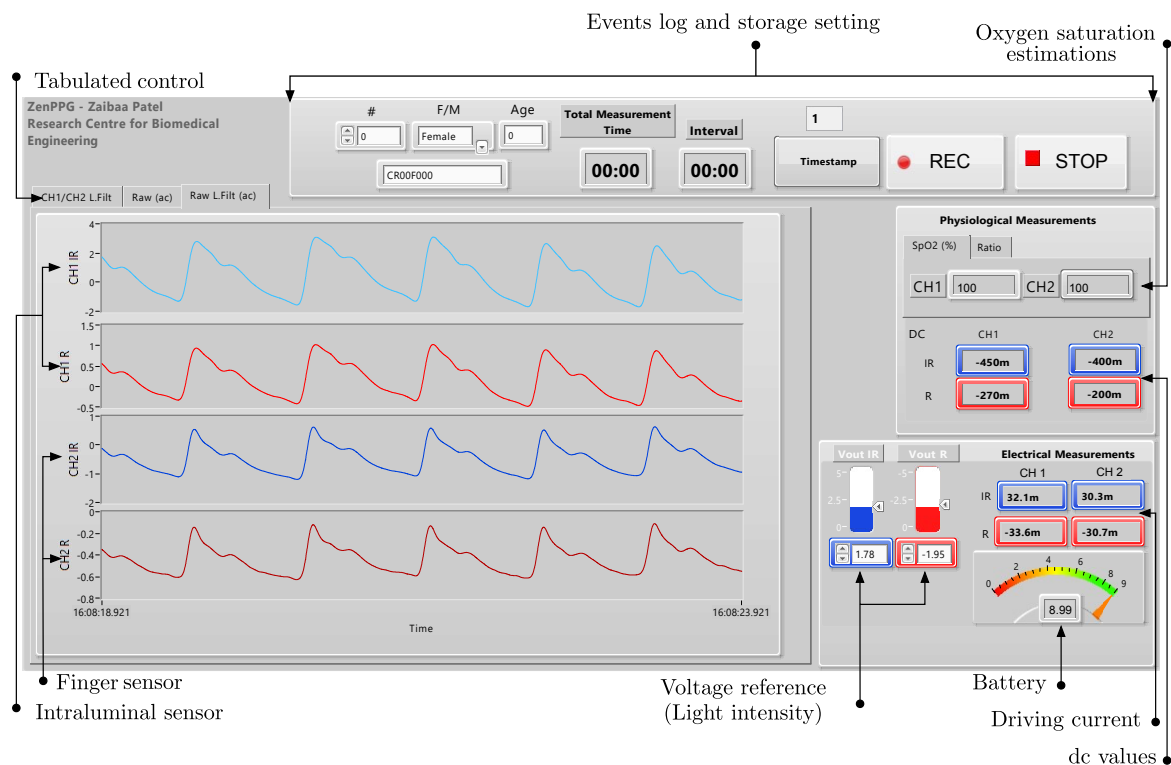


Figure 6.8 Front panel of the virtual instrument showing the continuous display of photoplethysmography (PPG) signals from the two channels. The top two graphs presents PPG signals from the intraluminal sensor where the infrared (sky blue) and red (red) ac PPG signals are displayed separately. The bottom two graphs presents PPG signals from the optically identical finger sensor, where the infrared (blue) and red (dark red) ac PPG signals are displayed separately. The user has the ability to input details of the patient, which corresponds to the file name, and events logging corresponding to a timestamp. The user can adjust the voltage reference which is passed to the instrumentation unit, to alter the light intensity through the adjustment of the driving currents of the light emitting diodes. Oxygen saturation (S_pO_2) are estimated continuously during the monitoring period and displayed solely for the user. Additional indicators are also present, monitoring the electrical parameters of the instrumentation unit and the sensors.

6.7 Data acquisition, control and user interface

Events log An additional user input was integrated within the VI to log events to allow the user to synchronise observations or comments noted during each investigation to the raw data file being stored. With the events log initialised to 1 and corresponding to the start time of the recorded data, the user can click on the "Timestamp" button to log an event. Each event logged would increase the timestamp incrementally by 1 and saved as an additional column with the raw signals.

Storage To ensure data was anonymised and saved in a consistent manner, the VI was modified to include a naming scheme. As several *in-vivo* investigations would be carried out within the research, a naming scheme shown in Figure 6.9 was adopted, which indicates the location of the PPG sensor, the study number, gender, age and where necessary a distance with the unit fixed to milli-metre (mm). All analogue signals digitised by the DAQ were immediately stored to a file for offline analysis. It should be noted that the raw signals prior to the online analysis in LabVIEW are stored to preserve as much information as possible from the acquired measurements. The VI was designed to store data as a text-based measurement file (.lvm) continuously with a tabulator delimiter format. As shown in Figure 6.10, each column in the text file corresponds to the assigned physical channels. The data storage format was most important to ensure easy access of the stored data within the offline, data processing analysis which will be discussed in the next section (Section 6.8).



Figure 6.9 Naming scheme for the data storage. The file name has a specific naming strategy based on the location, gender, age and distance, if applicable for the study. The naming scheme was adopted to allow easy access of the stored data when used within the offline module.

Design and development of the intraluminal PPG system

Time (s)	Channel 1 $IR(V)$ $R(V)$	Channel 2 $IR(V)$ $R(V)$	Channel 1 $IRac(V)$ $Rac(V)$	Channel 2 $IRac(V)$ $Rac(V)$	ISENSE $CH1(A)$ $CH2(A)$	PSVMON (V)	Events

Figure 6.10 Format of stored data within a file. The data is saved as a text based measurement file with a tabulator delimiter format for easy access of the stored data when used within the offline module.

6.8 Data processing

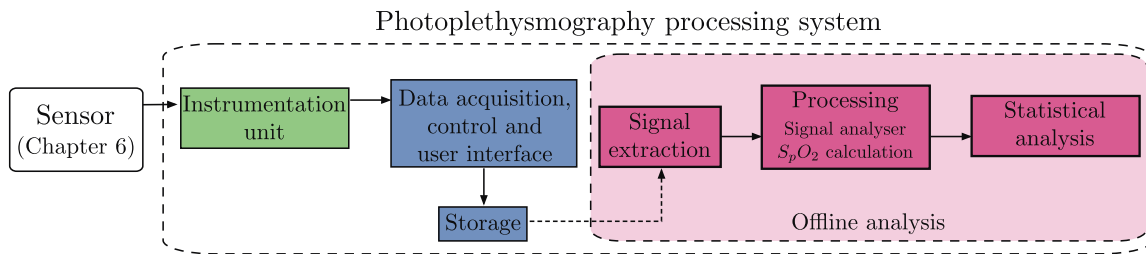


Figure 6.11 Detailed block diagram of the offline analysis module within the processing system. The module, highlighted in pink, analyses the stored data by extracting and processing the signal to provide calculations such as the oxygen saturation (S_pO_2) and amplitude analysis. The processed data is also analysed statistically for comparisons to commercial standard devices.

Physiological measurements from the experiments were acquired by analysing the stored signals. The stored data was processed and analysed through MATLAB[®] (*Version 2016*), where three major modules were developed to create a semi-automated PPG analyser, capable of producing robust and reproducible measurements from the signals. The objective of the data processing routine is to assess the capability of obtaining information on intestinal viability through the estimations of S_pO_2 . As observed from Figure 6.11, this section presents the modules that allow the (i) processing of raw PPG signals, (ii) computing valuable physiological information and (iii) provide the different types of statistical analysis for the results obtained. The modules will be described using synthetic data developed by Charlton et al. [276], to outline idealised signals modulated by a baseline wander respiratory modulation.

6.8.1 Signal extraction

The acquired PPG signals from the PPG sensors can be found in text files, created through the VI described in the previous section (Section 6.7). In this module of the offline analyser, the raw information within the files are organised and processed.

Each investigation performed within the research contains a number of studies, n , depending on the number of volunteers recruited. For each study, the stored data is imported into a matrix of size $(D \times 13)$, where, $D = 1000d$, when d is the time of the recorded data in seconds (s). Recalling Figure 6.10 (Section 6.7), there are thirteen (13) variables stored within a text file. For the purpose of signal extraction, there are ten (10) variables of interest, where the excluded variables are shaded in Figure 6.12.

Time (s)	Channel 1		Channel 2		Channel 1		Channel 2		ISENSE		PSVMON	Events
	$IR(V)$	$R(V)$	$IR(V)$	$R(V)$	$IRac(V)$	$Rac(V)$	$IRac(V)$	$Rac(V)$	$CH1(A)$	$CH2(A)$	(V)	

Figure 6.12 Data columns required for offline signal analysis. There are ten variables of interest, where the remaining, which are shaded, are excluded from the offline analysis. The excluded variables include the monitoring parameters such as the driving current of the light emitting diodes (ISENSE) and the supply voltage of the battery (PSVMON).

To minimise noise from the recorded data, digital band-pass filters similar to the filters implemented within the VI (Appendix A.2) were needed. A default setting of a band-pass filter was set to have a pass-band between 0.45 Hz to 5 Hz. For clinical setting investigations, parameters of the band-pass require adjustments for each study due to inter-subject variability such as the introduction of interference including ventilators, movement and the bed warming devices. Therefore, to assess each study and determine the filter parameters, short-time Fourier transforms (STFT, or spectrograms) were inspected of the pairs of signals (IR , R and IR_{zac} , R_{zac}).

As seen in Figure 6.13, STFT is a visual representation of the frequency spectrum in respect to time, where the columns represent time and the rows represent frequencies. The signal strength at a specific frequency is represented by a black jet colour map, where black and red are the two extremes corresponding to low and high signal strength respectively. The variables IR_{zac} and R_{zac} were included in the inspection to allow the user to determine whether ac PPGs from the raw signals or the ac PPGs acquired directly from the instrumentation unit should be used for further analysis. The method

results in the band-pass cut-off frequencies being $0.45 \text{ Hz} - f_L \text{ Hz}$, where f_L is set to 5 Hz by default, but could change to a user-selected input.

Whilst acquiring signals for each study, events were logged by the investigator, corresponding to specific events within the time of acquisition (Section 6.7). For instances where non-contact geometries were introduced between the intraluminal sensor and biological tissue (see Chapter 8), the investigator would be able to create an event to correspond to the separation between sensor and tissue. The logging of events is a beneficial addition as it also allows data to be automatically extracted and stored.

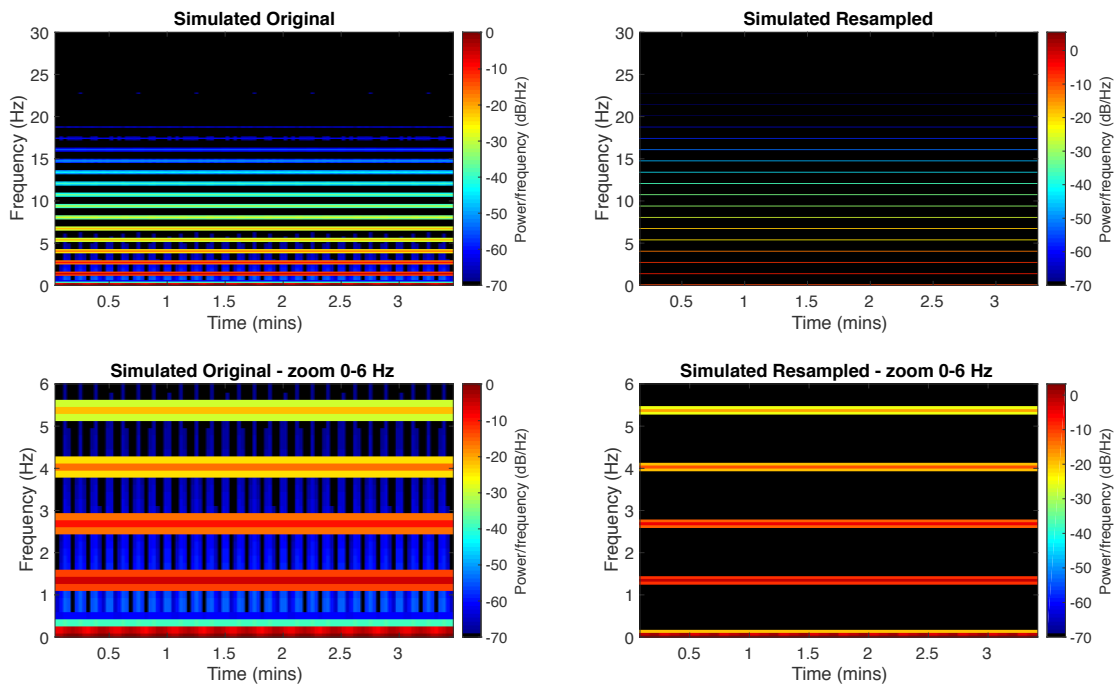


Figure 6.13 Short-time Fourier transforms on simulated photoplethysmography (PPG) signals. A visual representation of the frequency spectrum in respect to time can be observed where the columns represent time and the rows represent frequencies. The signal strength at a specific frequency is represented by a black jet colour map. A simulated PPG was used, where (a) is the original frequency spectrum, (b) is zoomed into the PPG frequency, where the dominant band between $1 \text{ Hz} - 2 \text{ Hz}$ corresponds to the heart rate. (c) and (d) are the same frequency spectrum after resampling the signals to 100 Hz .

The output of the signal extract module corresponds to the raw signals separated by distance and filter parameters. The signal extraction module is a semi-automated process, only requiring the user input when assessing the cut-off frequencies of the band pass filters. Figure 6.14 illustrates how a single raw PPG is separated for the next process, the signal analyser.

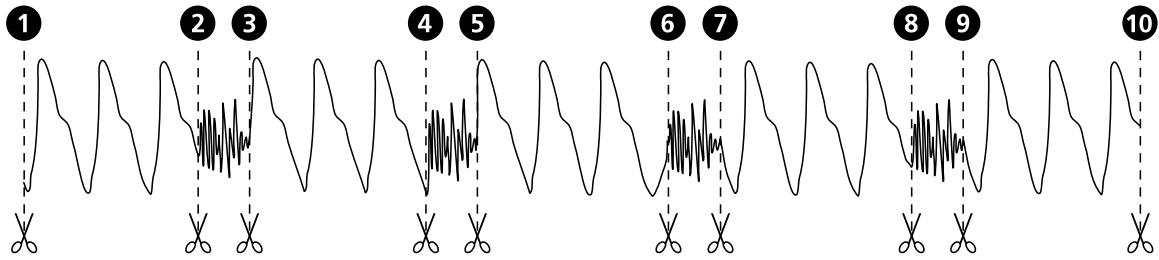


Figure 6.14 Signal extraction of raw photoplethysmography (PPG) signals. Extraction of PPG signals are performed with the use of the events logged, corresponding to specific events within the time of acquisition. The separated raw PPGs can be saved as individual files, ready for the signal analyser.

6.8.2 Signal analyser

The processing stage is a semi-automatic set of routines developed for extracting relevant sections of the signals and producing S_pO_2 calculations for any study, n , and where applicable, at any distance x (see Chapter 8). Twenty seconds (20s) were extracted per signal for comparison purposes. Recalling from the extraction of the signal, each study could be separated into different sections, corresponding to different distances. The naming conventions allow to select easily all studies at a specific distance. Furthermore, each study was assigned different cut-off frequencies for the low band of the filtering stage, f_L , also loaded with the subject's data. Algorithm 2, shows the full processing block for a single subject at a specific distance.

Let S be the subject represented by their information in the naming conventions, and x be the distance of the sensor; the context of it varying depending on the experiment. Algorithm 2 shows the flow of information and three main processes needed to obtain three information tables per subject.

Most function names in the pseudo-code are self-explanatory. It is worth noting, however, that the routine "crop(\cdot, \cdot)" selects the relevant interval \mathcal{I} from the filtered signal $dataFilt$ and stores it into a table structure with four columns corresponding to $ac_{IR}, ac_R, dc_{IR}, dc_R$ per patient S . The **preprocessing**, **interval acquisition** and S_pO_2 **calculation** are thoroughly explained next.

Preprocessing From the stored data, all data were down-sampled from the acquired sampling rate of 1 kHz to 100 Hz to remove high frequency noise. The re-sampling of the data was performed using "resample(\cdot, \cdot)" before further filtering and signal analysis could be undertaken.

Design and development of the intraluminal PPG system

Algorithm 2: PROCESSING PIPELINE PER SUBJECT / DISTANCE

```
Input: Subject:  $S$ , Distance:  $x$ 
Output: Tables:  $\text{table}(acdc)$ ,  $\text{norm}(acdc)$ ,  $\text{table}(S_pO_2)$ 
1  $dataIn \leftarrow$  Load file for subject  $S$  at distance  $x$ 
2  $f_L \leftarrow$  Load pre-selected cut-off frequency for subject  $S$  at distance  $x$ 
3 % Preprocessing
4  $dataRe \leftarrow$   $\text{resample}(dataIn, 100)$ 
5  $dataFilt \leftarrow$   $\text{filter}(dataRe, f_L)$ 
6 % Interval acquisition
7  $\mathcal{I} \leftarrow (dataFilt)$ 
8  $\text{table}(acdc) \leftarrow$   $\text{crop}(dataFilt, \mathcal{I})$ 
9 %  $S_pO_2$  Calculation
10  $[\text{table}(S_pO_2), \text{norm}(acdc)] \leftarrow S_pO_2\text{calc}(\text{table}(acdc))$ 
```

The raw mixed signals, IR and R , containing the changes in absorbance of the arterial blood (ac component), can be identified from the non-pulsatile venous blood and other tissue (dc component). An additional digital filter, similar to the filters within the VI (see Appendix A), was required to separate the two components. Signals from a single recording were separated using a band-pass Finite Impulse Response (FIR) filter with a passband of 0.45 Hz - f_L Hz and 60 dB attenuation in the stop-band was designed. The cut-off frequency f_L , is the assigned low pass filter parameter assigned during the signal extraction (Section 6.8.1), where 5 Hz is the default value of the filter. The designed filter was performed utilising the MATLAB[®] function `filtfilt` to perform zero-phasing filtering of all signals to preserve the PPG features, where the features of the filtered waveform corresponds to the features present in the original unfiltered waveform.

Interval acquisition For the analysis of the signals, time intervals for each study were selected at each light intensity. A graphical ui was developed to dynamically visualise the acquired ac PPG signals from the two channels of the instrumentation unit. Furthermore, the user has the ability to change certain parameters such as the size of the interval to extract.

As shown in Figure 6.15, there are three displays where ac signals from the two wavelengths, R and IR , overlap: (i) the entire length of the recorded data from both channels, (ii) PPGs from Channel 1 corresponding to signals acquired from the intraluminal sensor, and (iii) PPGs from Channel 2 corresponding to signals acquired from the identical finger sensor. For the interval selection, a default time of twenty seconds (20s) was chosen. Alternatively, the user can adjust the preferred time interval,

in addition to moving the displayed window across the entire length of recorded signal. The user is able to save and proceed to the subsequent analysis by pressing the "Get interval" button.

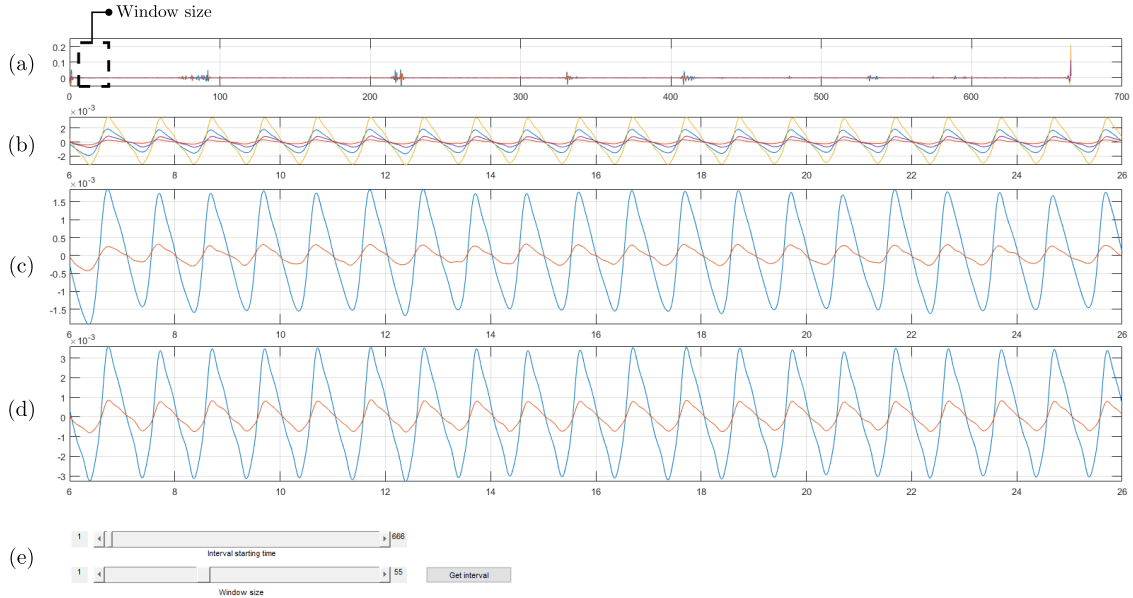


Figure 6.15 Graphical user interface of interval acquisition. (a) Entire recording time of both wavelengths for both Channel 1 and 2; (b) Within the window size, both wavelengths for both Channel 1 and 2 are shown. Within the window size, each channel is separated for easier visualisation of their corresponding wavelengths, where (c) contains both wavelengths for Channel 1 and (d) contains both wavelengths for Channel 2. The user is able to adjust parameters such as the window size and time to store the wanted interval by pressing the 'Get interval' button.

Oxygen saturation calculations For the estimation of the arterial oxygen saturation, S_pO_2 , the estimation follows two steps: (i) calculating the ratio of the components (i.e. ratio of ratios, R_{OS}) at two wavelengths, as derived in Equation (4.19), and (ii) correlating the ratio of ratios to S_pO_2 , Equation (4.27) [277].

With the selected interval, for each channel and wavelength, a two second (2s) rolling window was used to obtain parameters such as the ac amplitudes and the relatively constant values of the dc signals. To obtain the ac amplitudes for each wavelength, the peak-to-peak amplitude was calculated using `max` and `min` with the rolling window over the selected interval. Figure 6.16 illustrates this.

The R_{OS} at two wavelengths is calculated using Equation (4.19), where all PPG signals from a specific wavelength are divided by their respective dc component for

Design and development of the intraluminal PPG system

normalisation. The process of normalising is necessary as the acquired signals at each wavelength are of different light intensities due to light absorption characteristics varying for each subject [102].

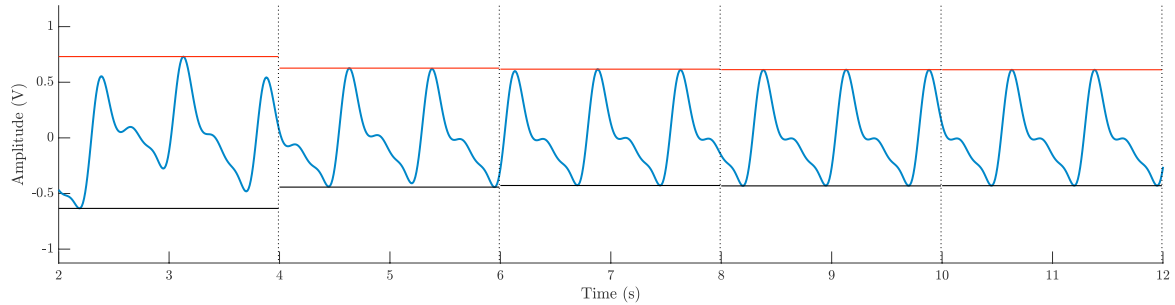


Figure 6.16 Process for amplitude measurements from a photoplethysmography (PPG) recording. Utilising a simulated PPG recording of 10 s, a rolling window of 2 s is used to calculate the peak-to-peak amplitude by identifying the maximum (peak) and minimum (trough) of the signal.

Correlating the R_{OS} to S_pO_2 , Equation (4.27) was used to provide the estimation of S_pO_2 . To provide accurate readings similar to a manufacturers medical PO, precise calibrations would require human hypoxic studies alongside blood gas analysis measurements to provide accurate S_pO_2 readings. S_pO_2 estimations were calculated within the rolling window over the selected interval, where S_pO_2 values were rounded to two significant figures.

Signal-to-noise ratio The quality of the acquired ac PPG signals was assessed by measuring the signal-to-noise ratio (SNR). The SNR was estimated by using measurements of the signal against background noise in the time domain with the usage of MATLAB[®]'s `snr` function, which takes the clean signal and the noise as separate input arguments. For each channel and each wavelength, the noiseless signals were estimated using MATLAB[®]'s implementation of a robust quadratic regression over a window of 18 data points. The noise was then calculated by subtracting each clean signal from the raw signal. The diagram in Figure 6.17 shows the described process using the synthetic data with the addition of random noise.

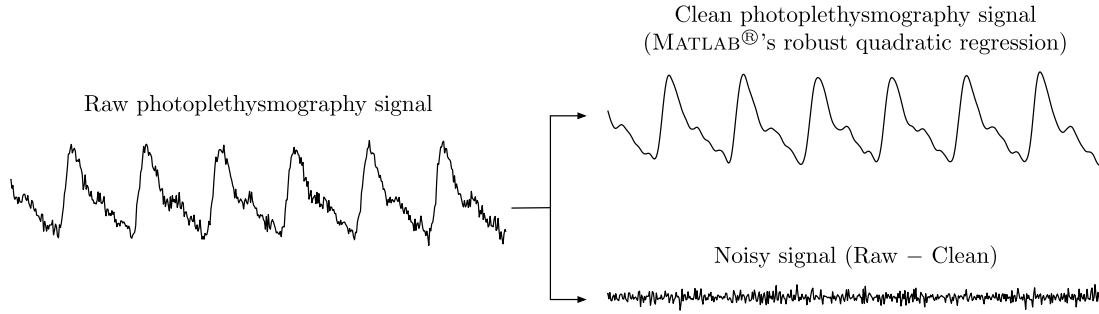


Figure 6.17 Signal-to-noise ratio method for photoplethysmography (PPG) signals. For illustration purposes, the raw data is represented by the synthetic data with the addition of random noise. A clean PPG signal is estimated using MATLAB®'s implementation of a robust quadratic regression, whilst the noisy signal is calculated by subtracting the clean signal from the raw.

6.8.3 Statistical analysis

Subsequent to obtaining the ac amplitudes, dc values, the estimations of S_pO_2 and SNR, various statistical analysis and tests were performed to ensure appropriate comparisons could be made. Specific objectives require different approaches and methodologies. Four categories can be identified from all the methods implemented: (i) Definition of statistics, (ii) tests for validation of verification, (iii) tests for comparisons of results and, (iv) measurements for the agreement between variables.

Definitions of statistics Let the term ‘overall mean and standard deviation’ ($\overline{M}_q \pm \overline{SD}_q$) be the mean of the means of the signal parameter of interest (q) from all subjects. Therefore, for a signal parameter (q), first the mean per subject are obtained; followed by an average of all the subjects’ mean (\overline{M}_q) and standard deviation ($\pm \overline{SD}_q$). Examples of several types of overall mean and standard deviation are shown in Table 6.3.

Table 6.3 Definitions of statistical variables within the offline analysis module, \overline{M} refers to the overall mean of a signal parameter and \overline{SD} refers to the overall standard deviation.

$(\overline{M}_{ac} \pm \overline{SD}_{ac})$	ac amplitudes
$(\overline{M}_{SNR} \pm \overline{SD}_{SNR})$	signal-to-noise ratio
$(\overline{M}_{S_pO_2} \pm \overline{SD}_{S_pO_2})$	oxygen saturation estimations

Verification tests Prior to any statistical analysis, the Kolmogorov-Smirnov (KS) test [278], was used to validate normality of the signal parameter of interest between the two channels. For the KS test, the null hypothesis was defined as q coming from a study in which its values come from a standard normal distribution, thus the values tested will correspond specifically to the standardised values $Z_q = \frac{q-M}{SD}$. The alternative hypothesis indicates that q does not come from a normal distribution. The hypothesis test can be described mathematically as:

$$H_0 : Z_q \sim \mathcal{N}(0, 1), \quad H_1 : Z_q \text{ does not come from } \sim \mathcal{N}(0, 1).$$

The KS test produces a decision of 1 if the test rejected the null hypothesis at the significance level of 5 % or 0 if the null hypothesis cannot be rejected. It is important to notice that a decision of 0 would not guarantee the normality of the values, only that these cannot be rejected.

Comparison tests A paired t-test was used to determine a significant difference between the means of two groups with relatable features. For the t-test, the null hypothesis was defined as q coming from a normal distribution with the mean equal to zero, whereas the alternative hypothesis is where q does not have a mean equal to zero. The t-test produces a decision of 1 if the test rejected the null hypothesis at a significance level of 5 %.

When multiple comparisons were necessary, the one-way analysis of variance (ANOVA) [279] was applied, to test for statistical significance between two \overline{M}_q amongst several groups. ANOVA tests the null hypothesis,

$$H_0 : \mu_1 = \mu_2 = \mu_3 = \dots = \mu_g, \tag{6.1}$$

where μ is the overall mean of a signal parameter and g is the number of groups. If significant difference were found, a post-hoc correction method, Bonferroni, was used to determine the specific groups which differed [280]. P-values less than 0.05 were considered to be statistically significant.

Variable agreement tests To determine the relationship between two quantitative, continuous variables, the Pearson product-moment correlation coefficient (r) was used.

An agreement analysis between two techniques was performed using the Bland-Altman (BA) statistical analysis. For this research, the BA was used to evaluate the

level of agreement of q between two PPG sensors; the intraluminal sensor and the routinely used clinical PO. BA suggests the best representation of the analysis is to plot the difference between the two methods (m_1 and m_2) as shown in Figure 6.18. The x-axis represents the mean of the two methods ($m_1 + m_2/2$) and the y axis represents the difference of the two methods ($m_2 - m_1$).

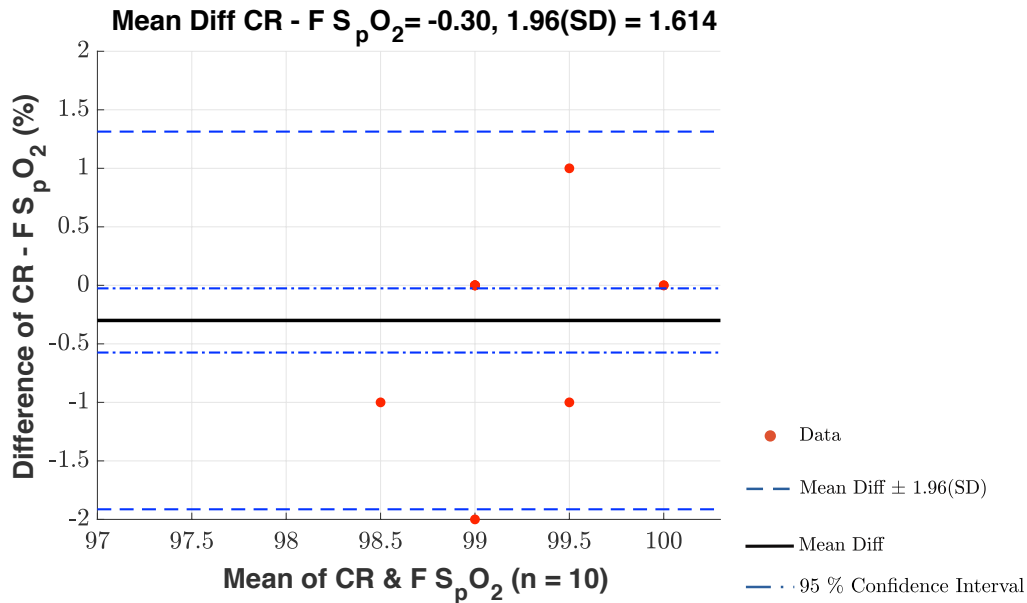


Figure 6.18 Example of a Bland-Altman representation. The level of agreement between the oxygen saturation (S_pO_2) from two photoplethysmography (PPG) sensors can be evaluated. CR represents PPG signals within the colorectum using the intraluminal PPG sensor, whilst F represents PPG signals from a finger using a commercially available pulse oximeter.

If there are no obvious relations between the mean and difference or a lack of agreement, a bias can be calculated using the mean difference (d) and the standard deviation of the difference (s). It is assumed that the difference between two methods will be at most two standard deviations from the mean ($d \pm 2s$), known as the limits of agreement (LoA). Providing the LoA are narrow, the two measurement methods could be used interchangeably.

6.9 Summary

This chapter described the design and development of the intraluminal PPG sensor and processing system. Two custom-made sensors were manufactured to acquire signals within the CR and on the finger, respectively. In addition, the chapter presented the relevant modules for a PPG processing system, which is capable of acquiring and analysing the raw PPG signals from both custom-made dual-wavelength PPG sensors simultaneously. The PPG processing system consisted of an instrumentation unit (ZenPPG) which is an available RCBE research tool, a virtual instrumentation (VI), developed in LabVIEW, and an offline signal analyser, developed in MATLAB®.

The gain amplification was modified within the ZenPPG, for the research application. A VI was created for the signals to be digitised and stored for offline analysis. Additionally, the VI was created to allow the user control of the light intensity and to display continuous estimations of S_pO_2 whilst a measurement is being performed. It should be noted that the VI was developed solely for the investigator, thus the displayed data during *in-vivo* investigations were not accessible to clinicians which could alter their decision. A semi-automated offline signal analyser was developed, allowing users to manually extract signal segments from lengthy recorded data and calculate parameters such as the PPG amplitude, SNR and the S_pO_2 .

The methods of signal and statistical analysis within the PPG processing unit will be used for each investigation addressed in the following chapters. Appropriate referral to this chapter will be included for readers to revisit the methods performed.

Chapter 7

Evaluation of the reflectance photoplethysmography system

Before attempting any *in-vivo* investigations, the intraluminal optical system, which includes the custom-made sensors and the photoplethysmography (PPG) processing system, required thorough testing. This chapter describes *in-vitro* evaluations performed on the complete system such as thermal testing. Once safety checks were performed, *in-vivo* quantitative analysis of the system was performed, to compare the acquired S_pO_2 's from the developed system, compared to a commercially available pulse oximeter (PO) device.

Motivation Assessing the functionality of the system is required to reassure the developer the systems safety and proceed into gaining approval prior to the clinical trial (Chapter 9). Prior to *in-vivo* studies, the thermal effect on tissue, similar to the colorectum tissue, from the intraluminal optical sensor system are required. The conduction of heat from the electrical components of the sensor to the tissue must be minimal to prevent the risk of thermal damage to the tissue. Furthermore, it is necessary to ensure that both custom-made sensors are optically similar, if signals from each were to be compared.

7.1 Hardware and software integration

Once developing the intraluminal PPG sensor and modifying sub-units of the PPG processing system, the integration of the two required testing. The communication between the hardware and software through the data acquisition card (DAQ) was tested as the VI presented in Chapter 6.7 allows the user to control the light intensity of the LEDs of Channel 1.

7.1.1 Materials and methods

Measurement set-up Mentioned in Appendix A.1, altering the voltage reference (V_{ref}) proportionally alters the driving current of the LEDs, resulting in the change of the light intensity. To verify emitter control of both channels, commercial PO's were connected to the instrumentation system to obtain measurements from the left index finger. For each channel, the V_{ref} for each LED wavelength was independently adjusted. Adjustment of the V_{ref} of Channel 1 was adjusted through the VI whilst Channel 2 was manually adjusted by altering the attenuating gains of the variable resistors found on the instrumentation unit (Appendix A). Table 7.1 presents the four tests carried out, where the V_{ref} 's were adjusted for each channel to obtain the corresponding driving currents for each LED.

Table 7.1 Voltage adjustments and the corresponding driving current for the dual light emitters corresponding to red (R) and infrared (IR). Four evaluations are presented, where the voltage reference V_{ref} for each wavelength of the commercial pulse oximeter are adjusted. The V_{ref} corresponds to the driving current for each light emitter in mA.

Voltage reference (Vref, V)		Driving current (mA)	
IR	R	IR	R
0	0	0	0
1	0	20	0
0	1	0	20
1	1	20	20

Signals from the commercial PO's were digitised using LabVIEW through the DAQ, described in Appendix A.2. The VI was used to observe the final output once the V_{ref} 's were adjusted according to the test carried out. Additional functions created in the VI, such as the ability to view the raw and filtered signals continuously were assessed.

Volunteer and investigation set-up Following institutional research ethics approval, one healthy 24 year old female volunteer was recruited. The *in-vivo* study was carried out within the RCBE physiological measurement room, where the volunteer sat comfortably on a chair. The room was kept at a temperature of $20 \pm 2^\circ\text{C}$, with the overhead lights switched off throughout the investigation to eliminate additional light interference. Two commercial PO's were utilised concurrently for measurements from the left, first and third digit. Whilst the four tests of altered V_{ref} 's, the resultant signals were observed on the user interface (ui) of the VI for one minute.

7.1.2 Data analysis

Online analysis of the signals of each channel and wavelength were observed on the ui in LabVIEW. Four tests were performed to determine the ability of adjusting the V_{ref} 's of each channel. By adjusting the voltage references for both light emitters, the transmission of light through the finger altered. Figure 7.1 presents the expected result when the V_{ref} of each LED were set to 0 V; where neither wavelengths produced a PPG output. This was expected as a driving current of zero supplied to the LEDs causes the optical component to behave switched off, therefore no transmission of light through the tissue. By adjusting a single wavelength to operate at a driving current of 20 mV, the presence of a PPG signal can be observed for the corresponding wavelength as shown in Figure 7.1.

Whilst both LEDs were supplied with a driving current of 20 mV, successful acquisition of PPG signals were observed as shown in Figure 7.1. The operation of additional functions within the ui was verified such as observing the estimation of S_pO_2 's, which were within the expected values for a healthy individual.

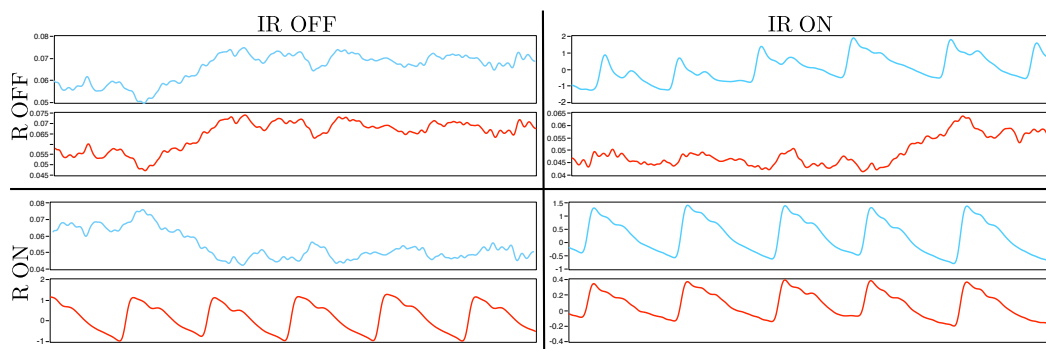


Figure 7.1 Results from altering the light emitter driving current, where red (R, red) and infrared (IR, blue) are switched on at a driving current of 20 mA or switched off. When switched off, there is an absence of a photoplethysmography (PPG) waveform.

7.2 *In-vitro* and *in-vivo* thermal testing

Prior to *in-vivo* evaluations of the intraluminal PPG sensor, it was imperative to evaluate the thermal contribution of the sensor to ensure no thermal injury to biological tissues could be caused when the sensor is in full operation. Two sets of thermal evaluations were conducted, (i) an *in-vitro* set-up using a section of a pig's intestine, and (ii) an *in-vivo* set-up using the mucosal lining of the inner cheek (buccal mucosa) of a healthy human volunteer. The reason for both set-ups was to investigate the temperature in a simulated environment and secondly, on living tissue.

7.2.1 Materials and methods

Measurement set-up The intraluminal PPG sensor presented in Chapter 6 was used along with the PPG processing system for the two thermal evaluations. A temperature monitoring system was developed to evaluate the intraluminal photoplethysmography sensors temperature, with the use of K-type thermocouples. The set-up for one thermocouple will be described, however, for the thermal testing, two thermocouples were used to measure the temperature of the sensor (T_{sensor}) and surrounding tissue (T_{tissue}). To be able to use the second thermocouple, the set-up described below was replicated.

A K-type thermocouple was connected to a thermocouple amplifier (*AD595, Analog Devices Inc., US*). The AD595 is a pre-calibrated instrumentation amplifier with reference to an ice point, producing a linear output of 10 mV/°C from a thermocouple signal. The AD595 was supplied with a voltage of 5 V and the output from the thermocouple amplifiers were connected to a DAQ, allowing continuous monitoring and saving of the temperature variations using a VI developed in LabVIEW.

Volunteer and investigation set-up The *in-vitro* thermal evaluation was set-up by attaching a thermocouple to the surface of the intraluminal sensor, immediately adjacent to both LEDs for T_{sensor} measurements. The intraluminal sensor was then placed in a plastic rectal sheath, which was then placed within a section of a pig's intestine. The sensor was kept in contact with the mucosa and held in position with a clamp. A second thermocouple was held in position with a second clamp on the outer surface of the intestine, the serosa, to provide T_{tissue} measurements. Following the positioning of the thermocouples and intraluminal sensor, the intestine was immersed in a static water bath set to 36 °C. A water bath replicated the human core temperature

7.2 *In-vitro* and *in-vivo* thermal testing

and is known to have similar thermal properties to those of soft tissue [277]. Figure 7.2 illustrates the set-up of the *in-vitro* thermal evaluation.

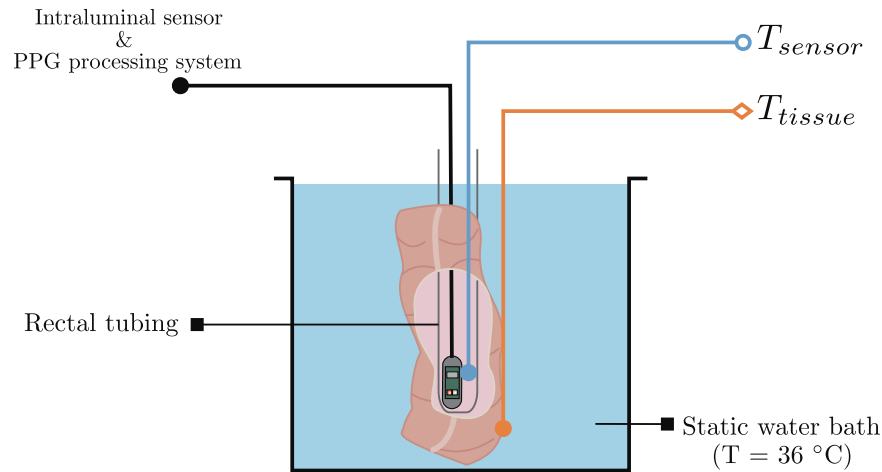


Figure 7.2 *In-vitro* thermal evaluation set-up using a pig's intestine. Illustration of the intraluminal photoplethysmography sensor covered with a plastic rectal sheath, placed within a pig's intestine. Immersed in a fixed temperature water bath, the temperature rise during the operation of the light emitters was measured with thermocouples attached to the sensor (T_{sensor}) and serosa (T_{tissue}).

The *in-vivo* thermal evaluation was set-up similarly as the *in-vitro* set-up, where a thermocouple remained on the surface of the intraluminal sensor for T_{sensor} measurements. Following institutional research ethics approval, one healthy 24 year old female volunteer was recruited. The intraluminal sensor was placed in a sterile rectal tubing (*Pennine Healthcare, Derby, UK*) and placed in contact with the buccal mucosa of a volunteer. The second thermocouple was placed approximately 1 cm away from the intraluminal sensor and in contact with the buccal mucosa to measure the surrounding temperature of the tissue (T_{tissue}). The *in-vivo* thermal evaluation was carried out within the RCBE physiological measurement room, where the volunteer sat comfortably on a chair. The room was kept at a temperature of $21 \pm 2\text{ }^{\circ}\text{C}$.

The rise of temperature was recorded for both thermal evaluations by driving the LEDs simultaneously with a driving current of 20 mA and 40 mA. Before switching on the LEDs, a baseline measurement was achieved. Once turning on the LEDs with the chosen driving current, the temperature was recorded until a steady state condition had been achieved. The same method was repeated in order to obtain the temperatures

whilst the LEDs were switched off, and to observe if the temperature would return to the baseline value.

7.2.2 Data analysis

Referring to Figure 7.3, after ten minutes of baseline measurements, the LEDs were switched on for twenty-five minutes. At a driving current of 20 mA, Figure 7.3(a) shows that the rise in temperature at the intraluminal sensor (T_{sensor}) was no more than 0.32°C. In addition, the temperature rise at the serosa (T_{tissue}) was no more than 0.23°C. At a driving current of 40 mA, Figure 7.3(b) shows that the rise in temperature at the intraluminal sensor (T_{sensor}) was no more than 1.02°C. In addition, the temperature rise at the serosa (T_{tissue}) was no more than 0.74°C.

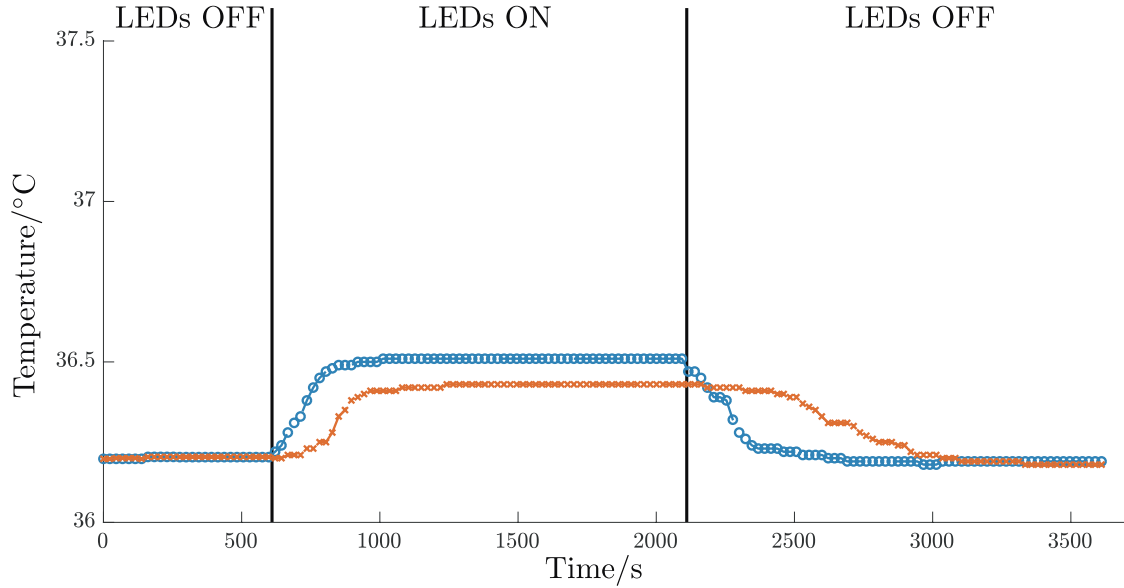
Referring to Figure 7.4(a), at a driving current of 20 mA, the rise in temperature at the intraluminal sensor (T_{sensor}) was no more than 0.29°C. In addition, the temperature rise at the serosa (T_{tissue}) was no more than 0.22°C. At a driving current of 40 mA, Figure 7.3(b) shows that the rise in temperature at the intraluminal sensor (T_{sensor}) was no more than 0.91°C. In addition, the temperature rise at the serosa (T_{tissue}) was no more than 0.72°C.

Concluding from the two thermal evaluations, the rise in temperature was minimal. This can be explained due to the encapsulation of the sensor with the clear medical epoxy which behaves as a thermal insulator [251]. As the temperatures did not exceed 38°C, it was concluded that the risk of thermal injury to any biological tissue would be negligible when using the intraluminal PPG sensor.

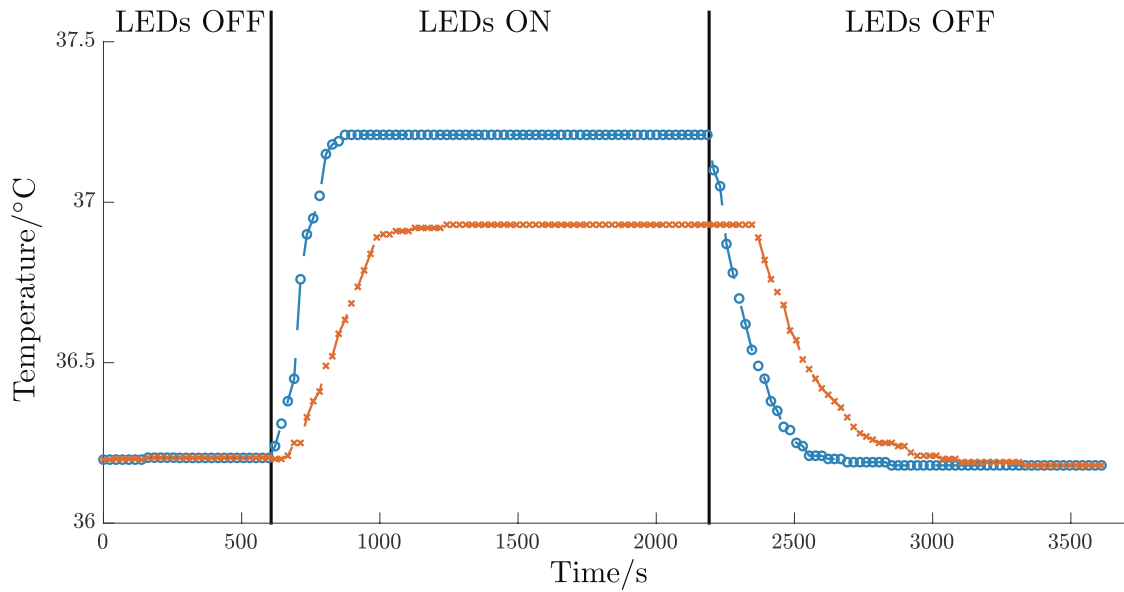
7.3 Validation of acquiring photoplethysmography signals

The reflectance PPG system which includes the sensors and PPG processing system was evaluated prior to its evaluation within the human colorectum. The system was evaluated in an *in-vivo* pilot study from the inner lining of the human oral cheek, given the tissue similarity to the intestinal mucosa and its easy accessibility.

7.3 Validation of acquiring photoplethysmography signals

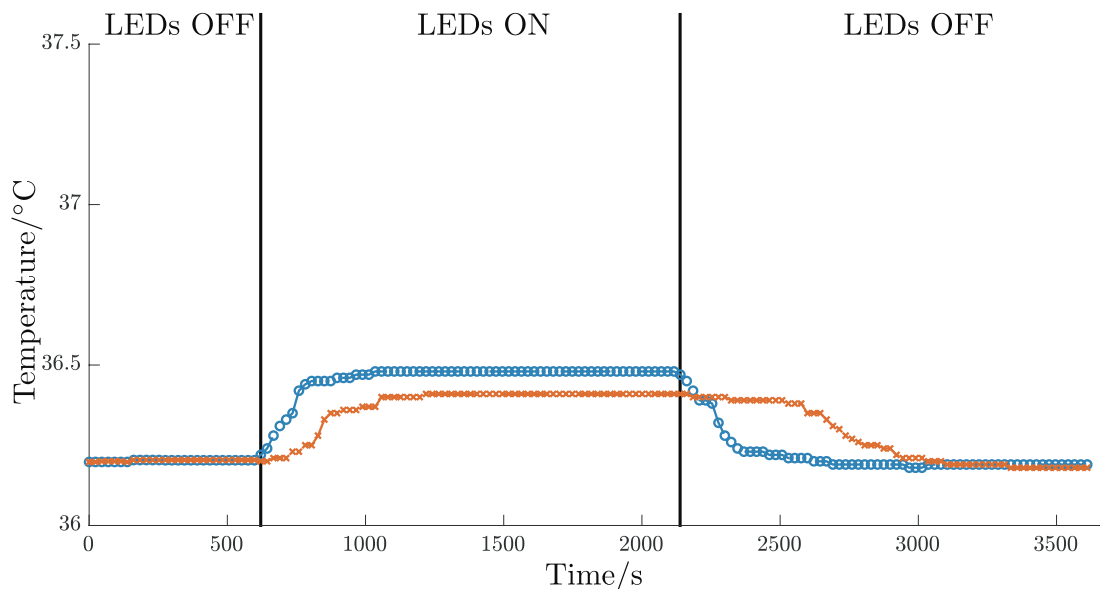


(a) LED driving current: 20 mA

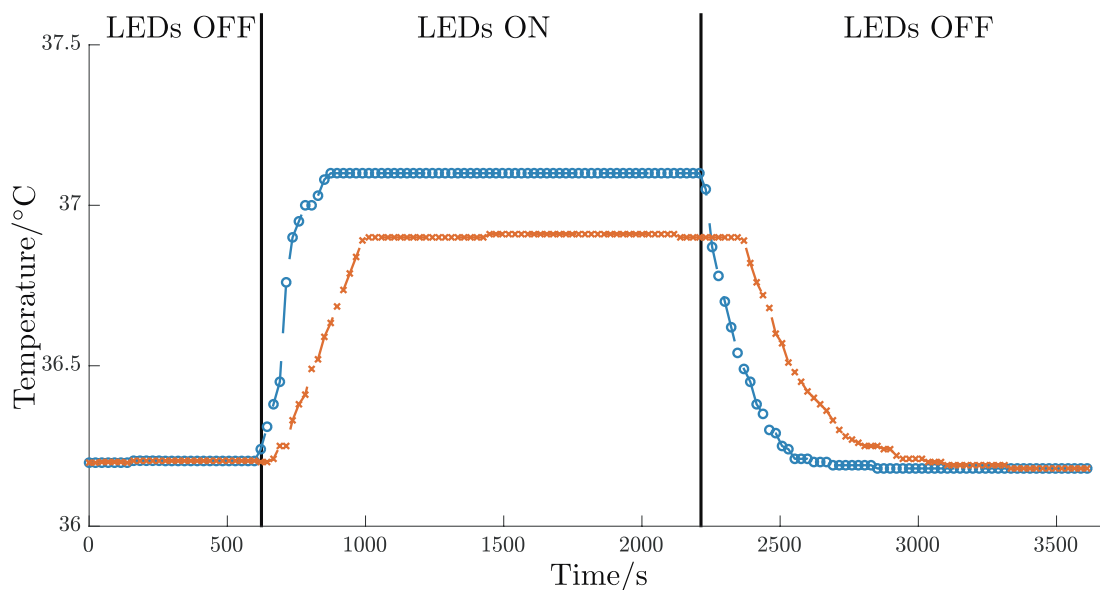


(b) LED driving current: 40 mA

Figure 7.3 *In-vitro* thermal evaluation using a section of a pig's intestine. The rise of temperatures were recorded on the intraluminal sensor, adjacent to the light emitting diodes (LEDs) (T_{sensor} , blue -o-) and the surrounding tissue (T_{tissue} , orange -x-). Thermal evaluations were performed at two LED driving currents, (a) 20 mA and (b) 40 mA.



(a) LED driving current: 20 mA



(b) LED driving current: 40 mA

Figure 7.4 *In-vivo* thermal evaluation on the buccal mucosa of a healthy volunteer. The rise of temperatures were recorded on the intraluminal sensor, adjacent to the light emitting diodes (LEDs) (T_{sensor} , blue $- \circ -$) and the surrounding tissue (T_{tissue} , orange $- \times -$). Thermal evaluations were performed at two LED driving currents, (a) 20 mA and (b) 40 mA.

7.3.1 Materials and methods

Measurement set-up The initial intraluminal PPG sensor presented in Chapter 6, prior to modifications, was used to obtain measurements from the inner lining of the human oral cheek. Additionally, the developed finger PPG sensor along with a commercial PO as a reference for S_pO_2 were adopted. The PPG processing unit (ZenPPG) and the developed PPG sensors were used to acquire PPG signals.

The intraluminal PPG sensor was covered in a sterile, transparent plastic sheath, which was inserted into the mouth and positioned in the maxillary vestibule, directing the emitted light into the inner cheek buccal mucosa lining. PPG signals were obtained concurrently from the left index finger, using the identical reflectance finger PPG sensor. Signals from the developed sensors were digitised using LabVIEW through the DAQ, described in Appendix A. The VI described in Chapter 6 was used to observe the signals during the measurement period and save the data for offline analysis.

Volunteer and investigation set-up Following institutional research ethics approval, twelve (12) healthy volunteers were recruited based on the completion of a patient questionnaire regarding current and past medical conditions. The healthy volunteers were equally distributed between male and females, with ages ranging from 23 to 38 (mean age [$\pm SD$] : 28 [± 4] years). Following full explanation of the study objective, written consent was obtained from all subjects prior to the commencement of the study. Volunteers with a history of cardiovascular abnormalities were excluded from the study. The *in-vivo* study was carried out within the RCBE physiological measurement room, where volunteers rested comfortably in a semi-Fowlers position, which is the supine position with the head of the bed at an upright angle between 30 – 40° [281]. This position aided in swallowing, aided by gravitational pull and facilitating overall relaxation to avoid movement or electromyogram (EMG) artefacts impeding the PPG signals. The room was kept at a constant temperature of $22 \pm 2^\circ\text{C}$, with the overhead lights switched off throughout the entire investigation to eliminate additional light interference.

The intraluminal PPG sensor, the identical finger PPG sensor and a commercial PO was utilised concurrently for measurements within the buccal mucosa and finger respectively. For mucosal measurements, the intraluminal sensor was covered in a sterile plastic sheath. The covered sensor was inserted into the mouth and positioned in the maxillary vestibule, directing towards the left cheek buccal mucosa. The identical PPG sensor and commercial PO was clipped onto the first and third digit of the left

Evaluation of the reflectance PPG system

hand, respectively. All raw measurements were acquired at a driving current of 20 mA. Ten minutes of recorded data was saved and displayed in a laptop running LabVIEW.

7.3.2 Data analysis and statistics

Offline analysis of the recorded PPG signals was performed on twelve (12) healthy volunteers using MATLAB[®]. PPG signals were recorded ($n = 12$), from both wavelengths at the two locations; (i) the buccal mucosa lining, and (ii) the finger. The pre-processing procedures described in Section 6.8 were used, where Figure 7.5 presents the functioning of the data processing steps which takes the raw PPGs to resample and filter the signals for the extraction of relevant components of the signal.

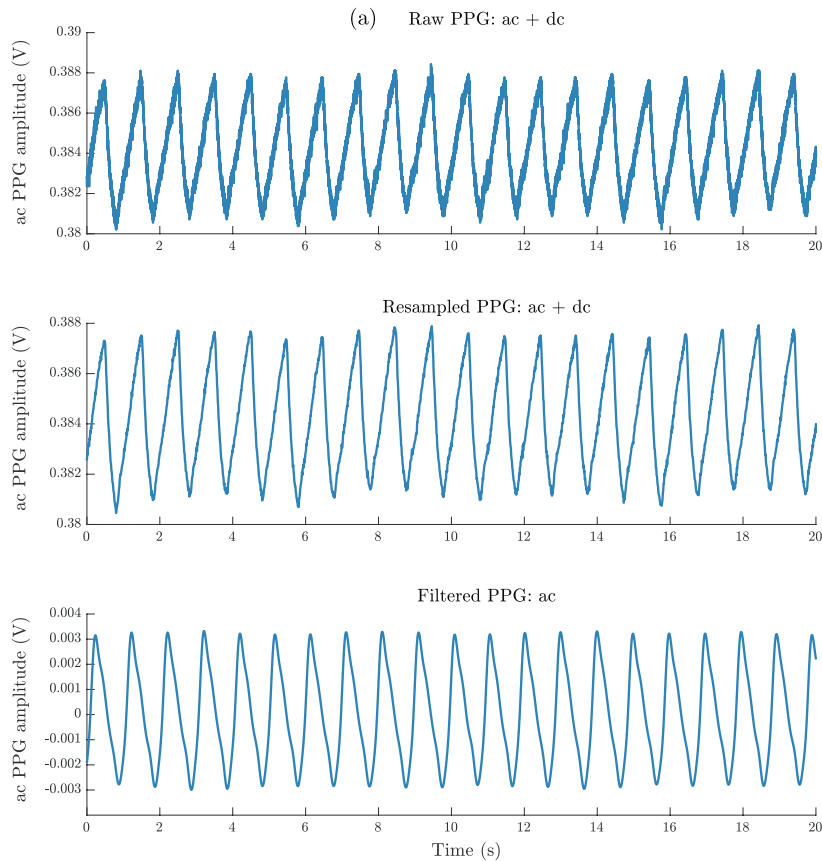


Figure 7.5 Photoplethysmography (PPG) pre-processing procedure is presented. The raw PPG signals acquired from the developed optical sensor is presented in the top graph, where the raw PPG waveform consists of both components of a PPG signal; the alternating waveform (ac) and the static waveform (dc). The raw PPG signal is down-sampled from 1 kHz to 100 Hz, as shown in the middle graph. The raw, re-sampled PPG signal is finally filtered to separate the PPG components, where the ac is presented in the bottom graph.

7.3 Validation of acquiring photoplethysmography signals

With ten second intervals selected for each subject, Figure 7.6(a) depicts typical infrared ac PPG traces from the buccal mucosa and finger. Figure 7.6(b) depicts typical red ac PPG traces from the buccal mucosa and finger. It can be seen that the R and IR ac PPG signals detected from each location were of good quality with large amplitudes to enable clear identification of the PPG morphology.

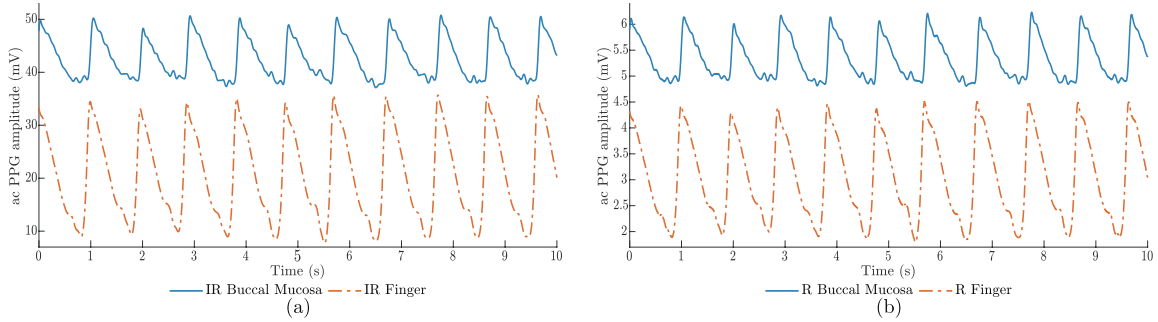


Figure 7.6 Typical ac photoplethysmography (PPG) signals from the buccal mucosa and finger. The results present signals from the buccal mucosa (—, blue) and left index finger (-.-, orange) from a healthy volunteer using wavelengths of (a) infrared and, (b) red, respectively.

Comparison of the ac PPG amplitudes for each volunteer were made to obtain the overall mean and standard deviation ($\overline{M}_{ac} \pm \overline{SD}_{ac}$). Table 7.2 presents the $\overline{M}_{ac} \pm \overline{SD}_{ac}$ for the buccal mucosa and finger at both wavelengths.

Table 7.2 Overall mean peak-to-peak amplitude and standard deviation (\pm SD) of the ac components of the red (R_{ac}) and infrared (IR_{ac}) photoplethysmography signals acquired from the buccal mucosa and the left index finger.

	$IR_{ac} \pm SD$ (mV)	$R_{ac} \pm SD$ (mV)
Buccal	82.6 ± 1.41	54.4 ± 6.1
Finger	86.0 ± 3.67	46.0 ± 1.5

To quantify the quality of the PPG signals obtained from each wavelength, the signal-to-noise ratio (SNR) was calculated using the signal against the background noise as described in Section 6.8. The overall mean of the SNR for ac PPGs and standard deviation ($\overline{M}_{ac} \pm \overline{SD}_{ac}$) were obtained for both wavelengths at each location. The SNR for signals obtained from the buccal mucosa was found to be 25.6 dB and 23.4 dB for infrared and red respectively. The SNR for signals obtained from the finger using the identical finger PPG sensor was found to be 25.1 dB and 24.6 dB for infrared and red respectively.

Preliminary estimation of blood oxygen saturation for each volunteer was acquired from the buccal mucosa and the index finger using the developed PPG sensors. Referring

Evaluation of the reflectance PPG system

to Table 7.3 the S_pO_2 results were found to be within the expected range of 97% to 100% for healthy volunteers. A statistical comparison between the S_pO_2 values at two sites, the buccal mucosa and index finger were made using the Pearson's correlation, where the coefficient (r^2) was found to be 0.80 with a confidence level of 95%. Furthermore, a comparison between the S_pO_2 values from the finger using the developed finger sensor and the commercial PO were made, where the r^2 was found to be 0.82 with a confidence level of 95%.

Table 7.3 Comparison of blood oxygen saturation S_pO_2 calculated from the acquired photoplethysmography signals from the intraluminal sensor and the identical finger sensor, measuring at the site of the buccal mucosa and the left index finger respectively. In addition, a commercial pulse oximeter (PO) was placed on the finger as reference.

Subject #	Buccal Mucosa (S_pO_2 , %)	Index Finger (S_pO_2 , %)	Commercial PO (S_pO_2 , %)
1	98	99	100
2	98	98	99
3	99	99	100
4	100	100	100
5	100	99	100
6	98	99	100
7	98	99	100
8	98	98	99
9	100	100	100
10	98	99	100
11	97	98	99
12	100	100	100
Mean \pm SD	98.67 \pm 1.07	99.00 \pm 0.74	99.75 \pm 0.43

7.4 Summary

In this chapter, evaluations of the intraluminal optical system were demonstrated through *in-vitro* and *in-vivo* studies. Thermal tests were carried out in both *in-vitro* and *in-vivo* setups, where thermal effects from the electrical components of the sensors were minimal, concluding the risk of thermal injury would be negligible. After successful technical evaluations, an *in-vivo* investigation was carried out to confirm the capability of acquiring raw PPG signals with large amplitudes and high SNR, from the intraluminal optical system. In comparison to a commercial PO, the developed system showed a strong correlation through a statistical analysis ($r^2 = 0.82$ with a confidence level of 95%). Furthermore, strong correlation between the two custom-made sensors were found, thus confidently allowing comparisons of PPGs acquired from different locations.

Although computational modelling, as seen in Chapter 5, simulates the light-tissue interaction within the colon in cases of contact versus non-contact, an experimental investigation is required. This is to ensure the simulated results match an actual experimental investigation. Through an *in-vivo* investigation, the optical path and penetration depth would not be obtained, however, the investigation would demonstrate the capability of acquiring PPG signals in contact and non-contact cases. Therefore, Chapter 8 investigates the influence of direct contact versus non-contact PPG measurements.

Chapter 8

Investigation of the effects of optical sensor-tissue separation

The intraluminal photoplethysmography (PPG) sensor was developed with the long-term aim of dynamically assessing bowel tissue viability during colorectum cancer surgeries. Maintaining direct contact between the sensor and the inner intestinal wall or an endocavitary organ, can be difficult in an intraluminal geometry. Recalling from the principles of PPGs (Section 4.2), the conventional method of acquiring good quality PPG signals and the accuracy of blood oxygen saturation (S_pO_2), depends on a reliable contact between the optical sensor and the tissue surface [262, 263, 282]. As addressed in Section 5.4, the sensor-tissue surface contact is uncertain within the colorectum. This chapter entails the investigation on the effect of direct contact versus variable separation between the sensor and a tissue. Furthermore, the following chapter is reproduced verbatim from Patel et al. [283].

Motivation As an extension to the computational modelling of the colon and the effects of the sensor-tissue separation (Section 5.4), an *in-vivo* investigation will be performed. The measurement sites are chosen to be the finger and the oral cavity, where the inner wall of the buccal has similar tissue properties to that of the colorectum mucosa [284].

8.1 Materials and methods

Measurement set-up The modified intraluminal reflectance PPG sensor presented in Section 6.3.3 was used to obtain measurements from the inner lining of the human oral cheek, given the location’s tissue similarity and its easy accessibility. The research PPG processing unit (ZenPPG) presented in and the developed PPG sensors presented in Chapter 6 were used to acquire PPG signals.

As the investigation required the introduction of an optical sensor and tissue separation between the sensor and the buccal mucosa, an adjustable distance apparatus was developed. The development of such apparatus, as shown in Figure 8.1, allowed five optical sensor-tissue separations in a controlled and repeatable manner.

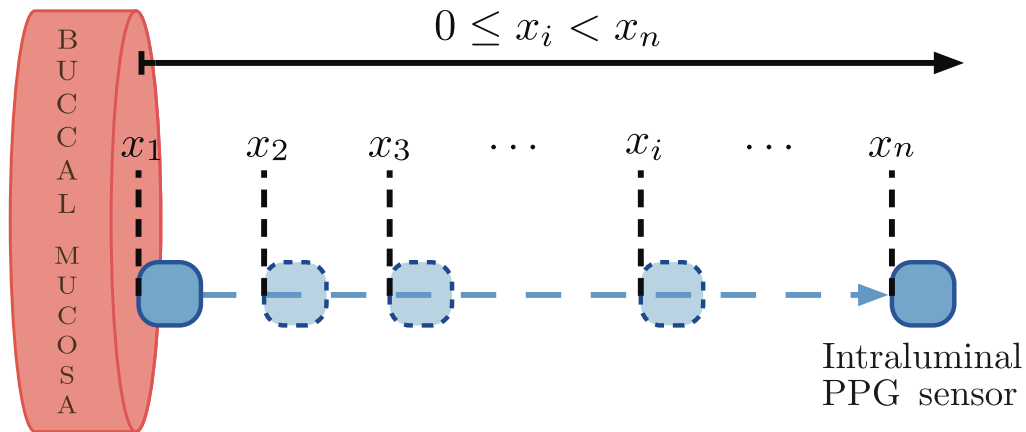


Figure 8.1 Simplified representation of the signal acquisition method. The intraluminal PPG sensor (blue) records photoplethysmography signals at several distances, x_i , from the buccal mucosa. Let x_1 be 0mm from the buccal mucosa. Initial photoplethysmography signals would be acquired at x_1 for a chosen measurement period, before increasing the sensor-buccal distance to x_2, x_3 till x_n .

Measurements at the optical sensor-tissue distance of 0mm (contact) required the sensor to be covered in a clean plastic sheath. Measurements with the use of the plastic sheath was considered as direct contact between the intraluminal PPG sensor and the buccal mucosal lining, with the assumption of the sheath being of negligible thickness. The remaining measurements utilised customised clean, clear rectal catheters (*Pennine Healthcare, Derby, UK*), with inner dimensions of 13.2mm and the length of 40mm . The purpose of the catheters was to obtain optical sensor-tissue distances. The first non-contact separation was 2.3mm , which corresponds to the wall thickness of the catheter.

In order to adjust the distances within the catheter, catheter caps were designed using SolidWorks 2016 (*Dassault Systems, Vélizy- Villacoublay, FR*). Each catheter cap was designed to ensure the sensor was accurately positioned at the needed distance. The portion of the cap that resides within the catheter (inner catheter cap) was designed to have the same dimension as the inner dimensions of the catheter. Figure 8.2(a) illustrates the recess position changing depending on the distance required. To guarantee the intraluminal PPG sensor directed towards the buccal mucosal lining at all times, a flat indent to the catheter cap was created indicating the direction required for the sensor, as shown in Figure 8.2(a-b). The further the sensor moves away from the flat indent, the optical sensor-tissue distance increases. A recess within the catheter cap was designed to have the same dimensions of the intraluminal PPG sensor, ensuring the sensor would fit precisely, preventing movement or rotation within the catheter. Additional to the extruded catheter caps, sealed catheter caps were developed to avoid liquid ingress, as shown in Figure 8.2(c).

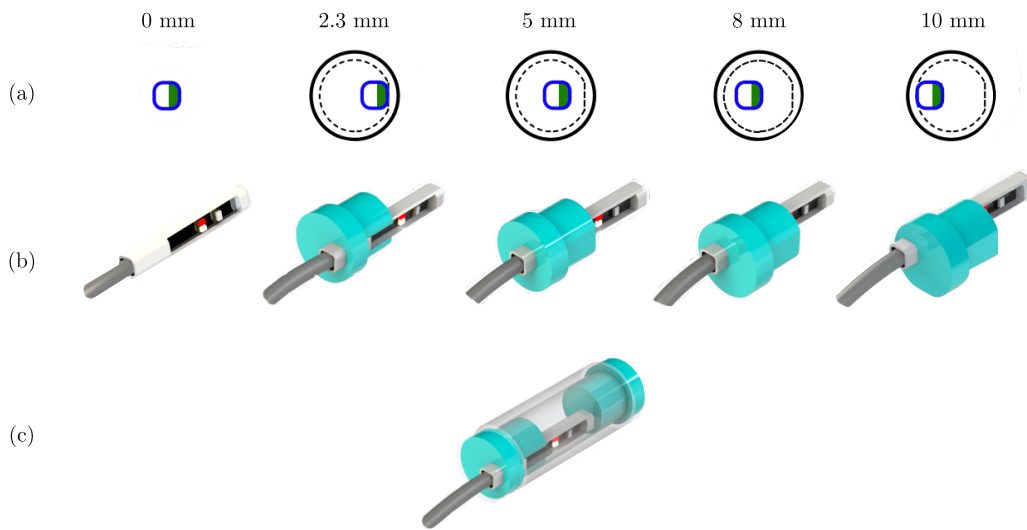


Figure 8.2 Adjustable distance apparatus achieving five separation distances between the intraluminal PPG sensor and the buccal mucosa. (a) Mechanical drawing of the apparatus, where all measurements, except at 0 mm, requires the use of catheters and catheter caps. The inner cap (\cdots) corresponds to the measurement distance of 2.3 mm. (b) 3D visualisation of the intraluminal PPG sensor fitting into the extruded catheter caps, where the flat indent indicates the sensor direction. (c) Example of the full assembly for measurements at 2.3 mm, where the intraluminal PPG sensor is inserted within the customised catheter and both catheter caps, extruded and sealed, placed on either ends of the catheter.

The effects of optical sensor-tissue separation

The effect of optical sensor-tissue separation was also investigated on the second digit of the left hand using an identical opto-electrical finger PPG sensor and the adjustable distance apparatus. A commercial pulse oximeter was adopted to continuously measure S_pO_2 from the first digit of the left hand as an ‘in contact’ (0 mm) measurement.

Signals from the developed sensors were digitised using LabVIEW through the data acquisition card, which can be found in Appendix A.2. The VI was used to observe the signals during the measurement period and save the data for offline analysis.

Volunteer and investigation set-up Following institutional research ethics approval, twenty (20) healthy volunteers were recruited. The healthy volunteers were equally distributed between male and females, with ages ranging from 18 to 38 (mean age [$\pm SD$] : 28 [± 4]) years. Following full explanation of the study objective, informed consent was obtained from all subjects prior to the commencement of the study.

The *in-vivo* study was carried out within the RCBE physiological measurement room, where volunteers were resting comfortably in a semi-Fowler position. For similar reasons explained in Chapter 7, this position aided in swallowing, aided by gravitational pull and facilitating overall relaxation to avoid movement or electromyogram (EMG) artefacts impeding the PPG signals. The room was kept at a constant temperature of $20 \pm 2^\circ\text{C}$, with the overhead lights switched off throughout the entire investigation to eliminate additional light interference.

The intraluminal PPG sensor and the identical finger PPG sensor were used concurrently for measurements within the buccal mucosa and finger respectively. Measurements from both locations were obtained at five sensor-tissue separations, 0 mm, 2.3 mm, 5 mm, 8 mm and 10 mm. For mucosal measurements to commence at 0 mm, the intraluminal PPG sensor was covered in a plastic sheath. The covered sensor was inserted into the mouth and positioned in the maxillary vestibule, directing towards the left cheek buccal mucosa. Subsequently, the separation distance between the sensor and the mucosal lining was achieved with the use of the adjustable distance apparatus (Figure 8.2). After positioning the sensor correctly in the maxillary vestibule, volunteers were asked to close their mouth.

All raw measurements were acquired at two light intensities, by driving the LEDs simultaneously with currents of 20 mA and 40 mA, respectively. Two minutes of recorded data at each distance was saved and displayed on a laptop running LabVIEW. The overall study duration lasted for up to 45 minutes, where short breaks were provided between changes of the sensor-tissue separations and the driving currents of the LEDs.

All reusable material materials were disinfected using a sterilising fluid (*Milton, UK*) and volunteers were offered to rinse their mouth with dental mouthwash, before and after the study.

8.2 Data analysis and statistics

Offline analysis of the recorded PPG signals was performed on 19 of the 20 volunteers using MATLAB[®]. In one volunteer, the recorded signals were particularly hindered due to electromyogram interference from the cheek and overall motion artefact. Identifying fundamental characteristics of the PPG waveform was challenging, therefore this data set was excluded from further analysis.

PPG signals were recorded ($n = 19$), from both wavelengths and all separations of the PPG sensors at the two locations; (i) the buccal mucosa lining, and (ii) the finger. The pre-processing procedures described in Section 6.8 were used, where 20 second intervals of PPG signals for each subject were selected from the recorded signals from the buccal mucosa and finger at the five sensor-tissue separations at each light intensity.

Figure 8.3 depicts typical infrared ac PPG traces from the buccal mucosal at each sensor-tissue distance, at two light intensities, utilising LED driving currents of 20 mA and 40 mA, respectively. Figure 8.4 depicts typical red ac PPG traces from the buccal mucosal at each sensor-tissue distance, at two light intensities, utilising LED driving currents of 20 mA and 40 mA, respectively. Figure 8.5 depicts typical infrared ac PPG traces from the finger at each sensor-tissue distance, at two light intensities, utilising LED driving currents of 20 mA and 40 mA, respectively. Figure 8.6 depicts typical red ac PPG traces from the finger at each sensor-tissue distance, at two light intensities, utilising LED driving currents of 20 mA and 40 mA, respectively. For illustration purposes, Figure 8.7 depicts an example of noisy PPG signals obtained at a sensor-buccal distance of 10 mm, when the LEDs driving currents were set to 20 mA.

Comparison of the ac PPG amplitude changes against the sensor-tissue separation were made, where the overall mean and standard deviation ($\overline{M}_{ac} \pm \overline{SD}_{ac}$) was calculated for each of the five separations, when the LEDs were driven with currents of 20 mA and 40 mA, respectively. Illustrated in Figure 8.8, the $\overline{M}_{ac} \pm \overline{SD}_{ac}$ from the buccal mucosa for different sensor-tissue distance at each light intensity are shown. Similarly, Figure 8.9 presents the $\overline{M}_{ac} \pm \overline{SD}_{ac}$ from the finger for different sensor-tissue distance at each light intensity.

The effects of optical sensor-tissue separation

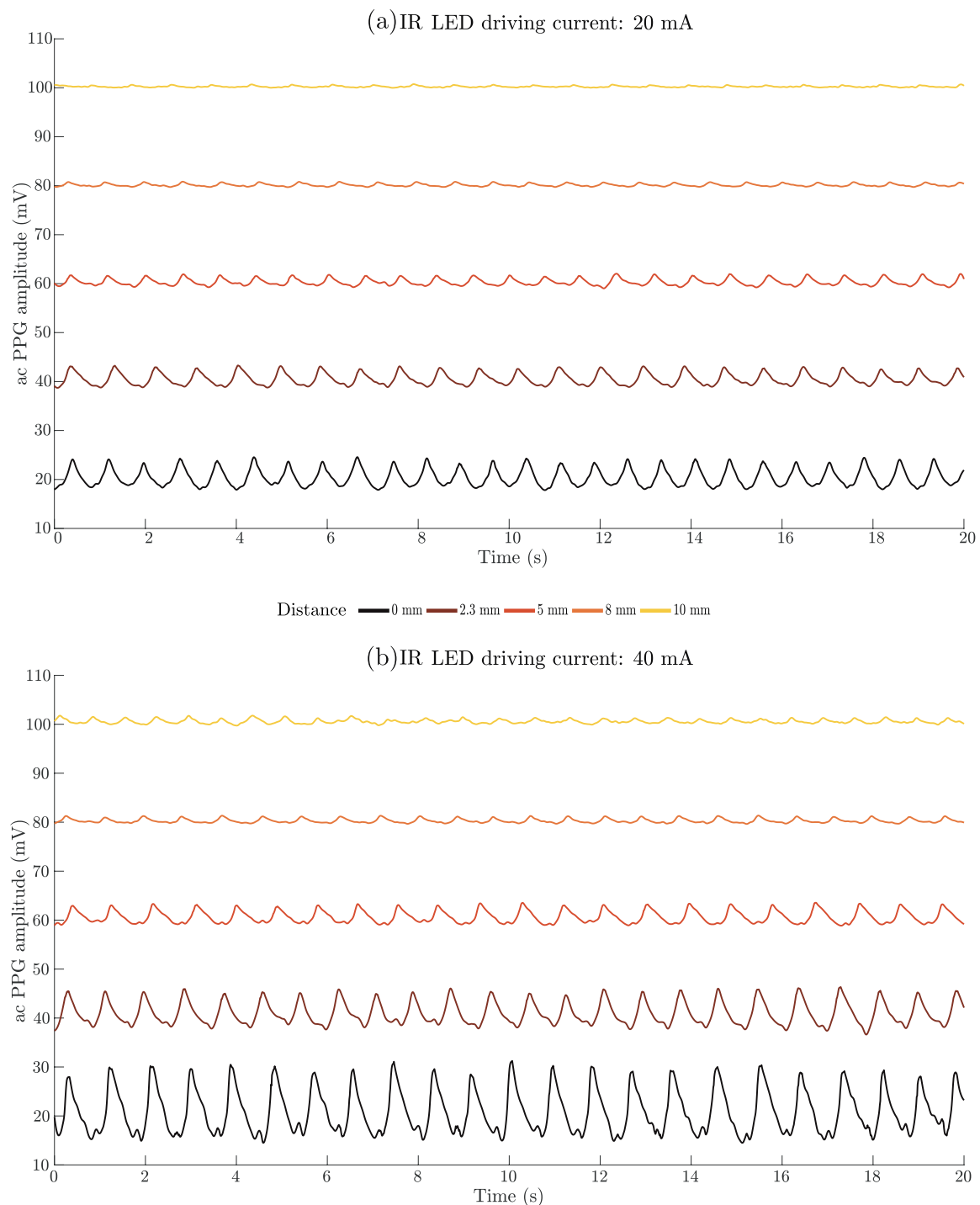


Figure 8.3 Twenty seconds of typical infrared ac PPG traces from a healthy volunteer at different sensor distances from the buccal mucosa. For visualisation purposes, five signals are equally spaced with a 20 mV offset; as the offset increases, the separation increases. PPG measurements were obtained at two light intensities by driving the LEDs with currents of (a) 20 mA and (b) 40 mA.

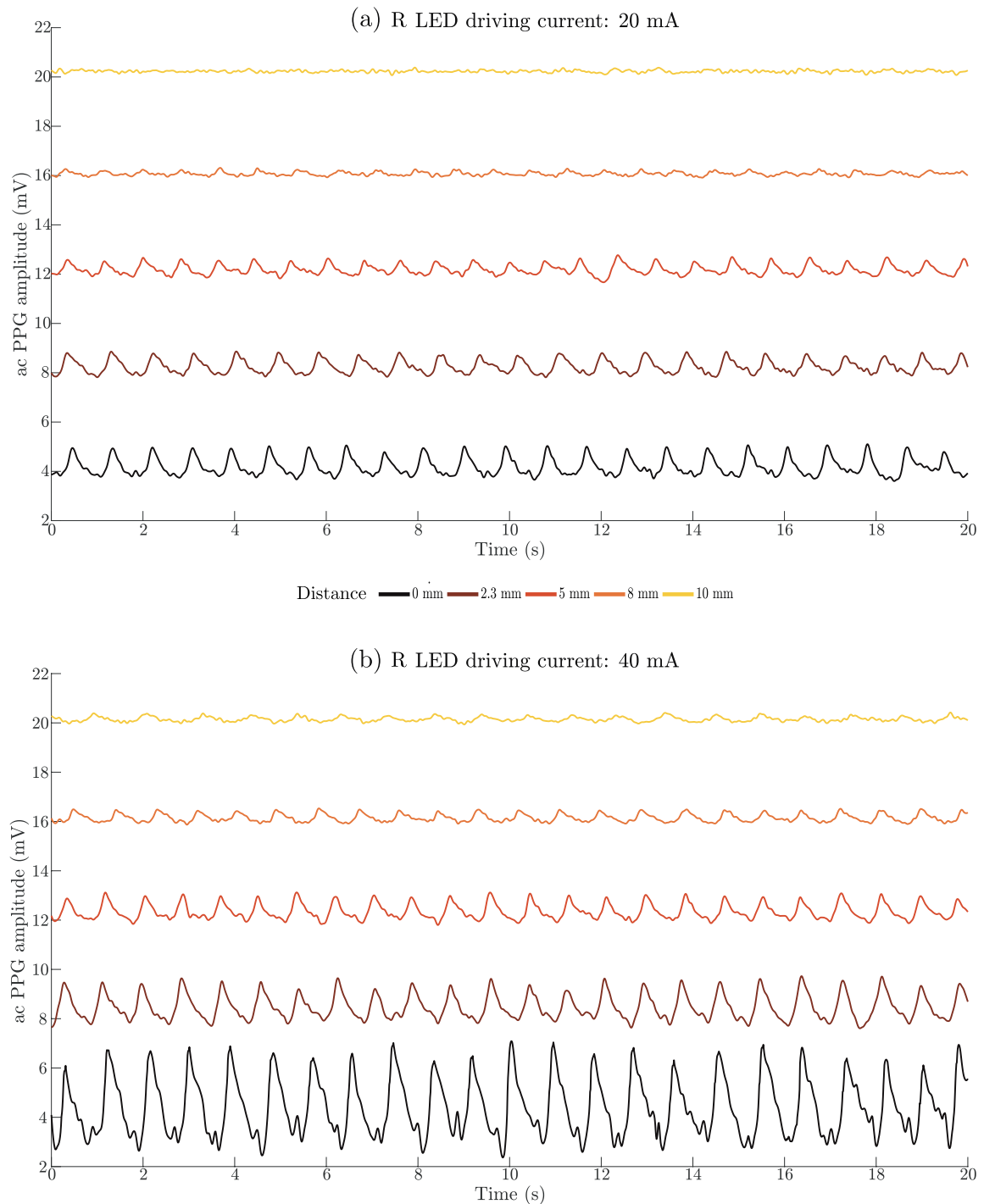


Figure 8.4 Twenty seconds of typical red ac PPG traces from a healthy volunteer at different sensor distances from the buccal mucosa. For visualisation purposes, five signals are equally spaced with a 4 mV offset; as the offset increases, the separation increases. PPG measurements were obtained at two light intensities by driving the LEDs with currents of (a) 20 mA and (b) 40 mA.

The effects of optical sensor-tissue separation

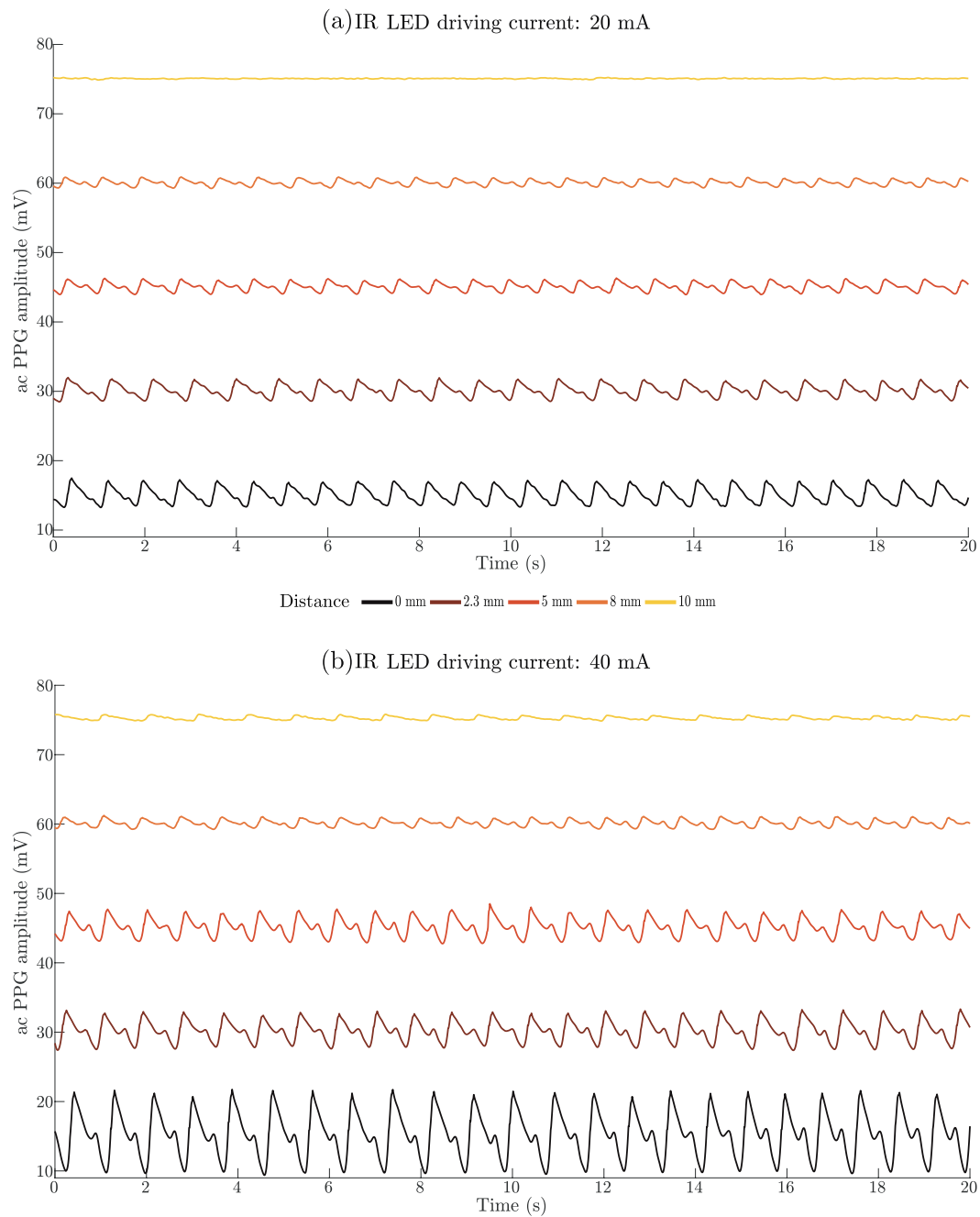


Figure 8.5 Twenty seconds of typical infrared ac PPG traces from a healthy volunteer at different sensor distances from the finger. For visualisation purposes, five signals are equally spaced with a 40 mV offset; as the offset increases, the separation increases. PPG measurements were obtained at two light intensities by driving the LEDs with currents of (a) 20 mA and (b) 40 mA.

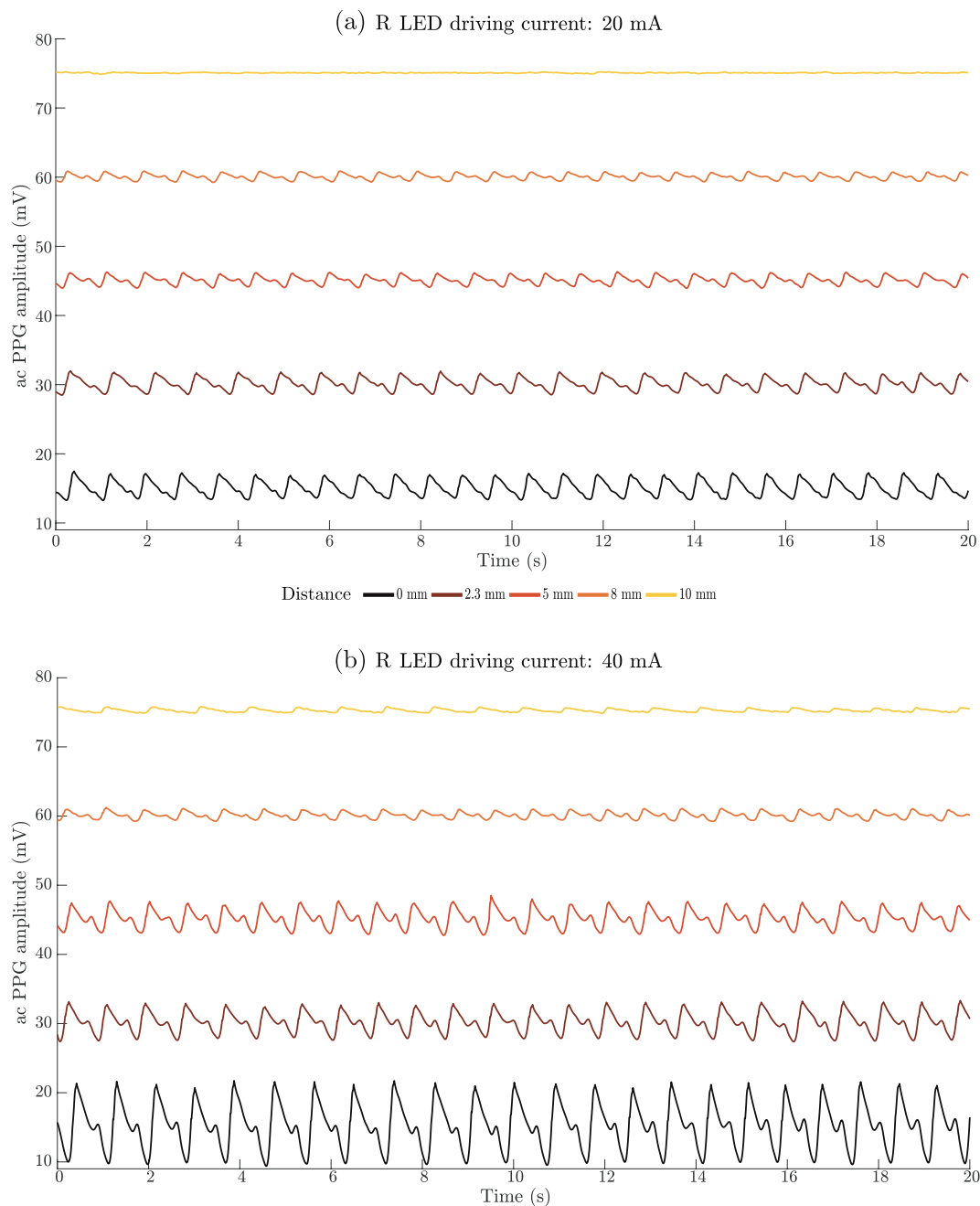


Figure 8.6 Twenty seconds of typical red ac PPG traces from a healthy volunteer at different sensor distances from the finger. For visualisation purposes, five signals are equally spaced with a 15 mV offset; as the offset increases, the separation increases. PPG measurements were obtained at two light intensities by driving the LEDs with currents of (a) 20 mA and (b) 40 mA.

The effects of optical sensor-tissue separation

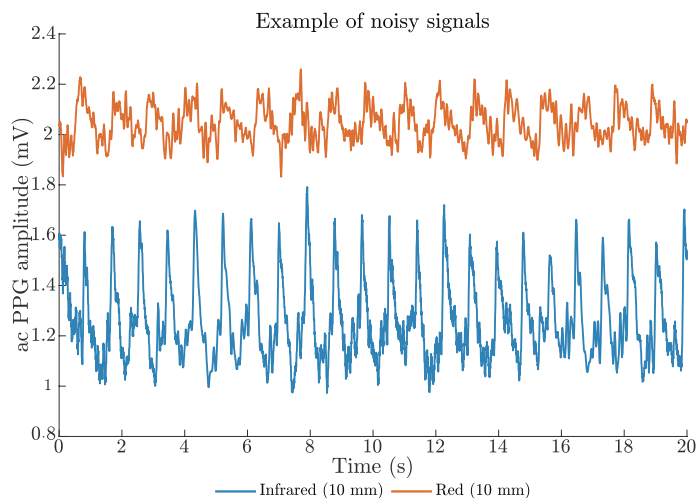


Figure 8.7 Example of noisy signals from both wavelengths, red (top, orange) and infrared (bottom, blue). These were obtained at a separation of 10 mm, where the LEDs driving current was 20 mA. The two signals are equally spaced with a 1 mV offset.

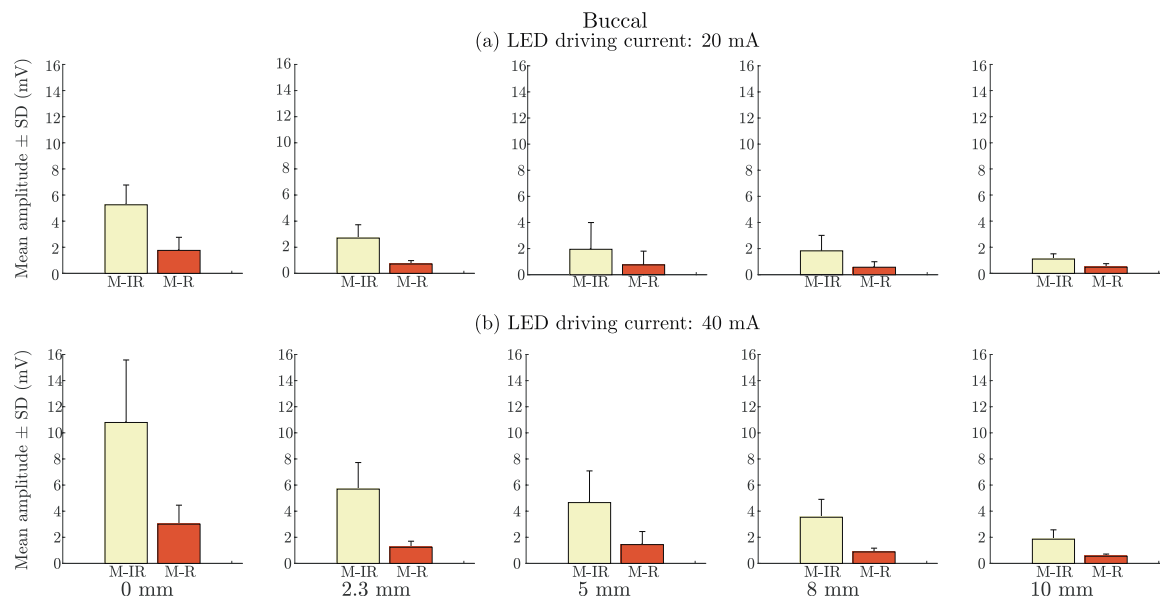


Figure 8.8 Overall mean and standard deviation of the ac PPG amplitudes ($\overline{M}_{ac} \pm \overline{SD}_{ac}$) at different sensor-buccal distances. The results present the overall mean and standard deviation from the buccal mucosa using red (M-R, red) and infrared (M-IR, yellow) wavelengths at two light intensities by driving the LEDs with currents of (a) 20 mA and (b) 40 mA.

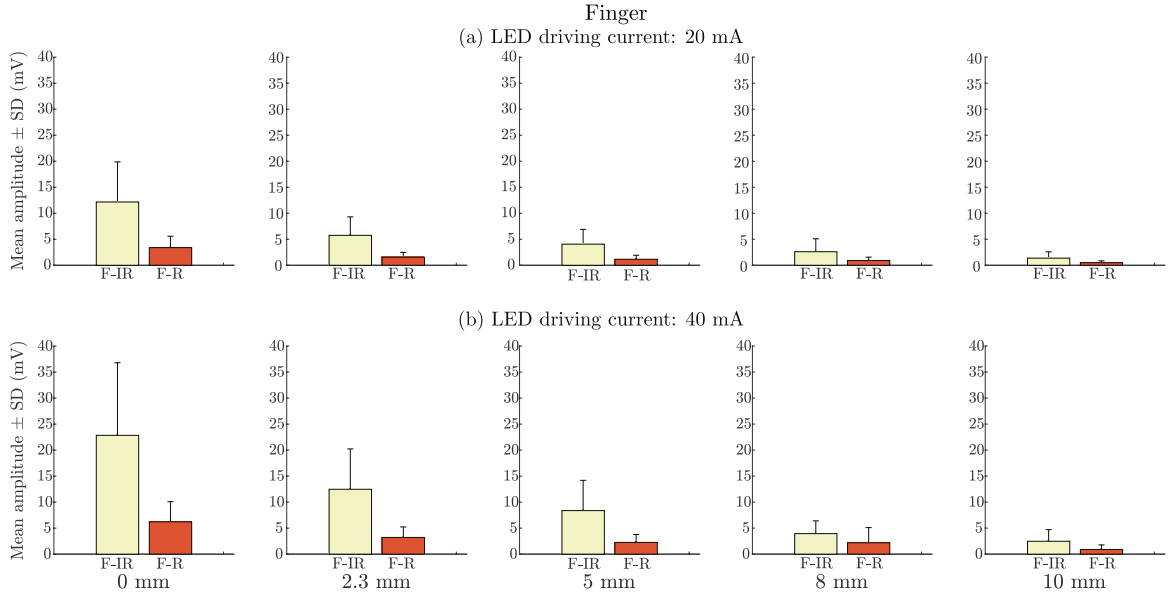


Figure 8.9 Overall mean and standard deviation of the ac PPG amplitudes ($\overline{M}_{ac} \pm \overline{SD}_{ac}$) at different sensor-finger distances. The results present the overall mean and standard deviation from the finger using red (F-R, red) and infrared (F-IR, yellow) wavelengths at two light intensities by driving the LEDs with currents of (a) 20 mA and (b) 40 mA.

In addition, to quantify the quality of the PPG signals obtained from each wavelength, the signal-to-noise ratio (SNR) was calculated using the signal against the background noise as described in Section 6.8. For comparisons, the overall mean of the SNR of the ac PPG signals (\overline{M}_{SNR}) were obtained for each of the five separations and the two LED driving currents. Figure 8.10 presents the $\overline{M}_{SNR} \pm \overline{SD}_{SNR}$ for red and infrared ac PPGs from the buccal mucosa and finger at each sensor-buccal separation with driving currents of 20 mA and 40 mA.

For the estimation of the blood oxygen saturation (S_pO_2), the methods described in Section 10 were performed. Similarly, the comparisons of S_pO_2 against the sensor-tissue separation were obtained by calculating the overall mean and standard deviation ($\overline{M}_{S_pO_2} \pm \overline{SD}_{S_pO_2}$) for each of the five separations and the two LED driving currents. The KS test described in Section 6.8.3 was used to validate normality of the $\overline{M}_{S_pO_2}$ values presented in Table 8.1. With the values found to have a normal distribution at each separation, a t-test was used to determine the significant differences between the $\overline{M}_{S_pO_2}$ from the buccal mucosa and finger per sensor-tissue distance. At each sensor-tissue separation, no significance were found, where all p-values were below 0.05.

Referring to the \overline{M}_{ac} from the buccal mucosa (Figure 8.8), the values were of a normal distribution using the KS test and hence, the ANOVA, described in Section 6.8.3,

The effects of optical sensor-tissue separation

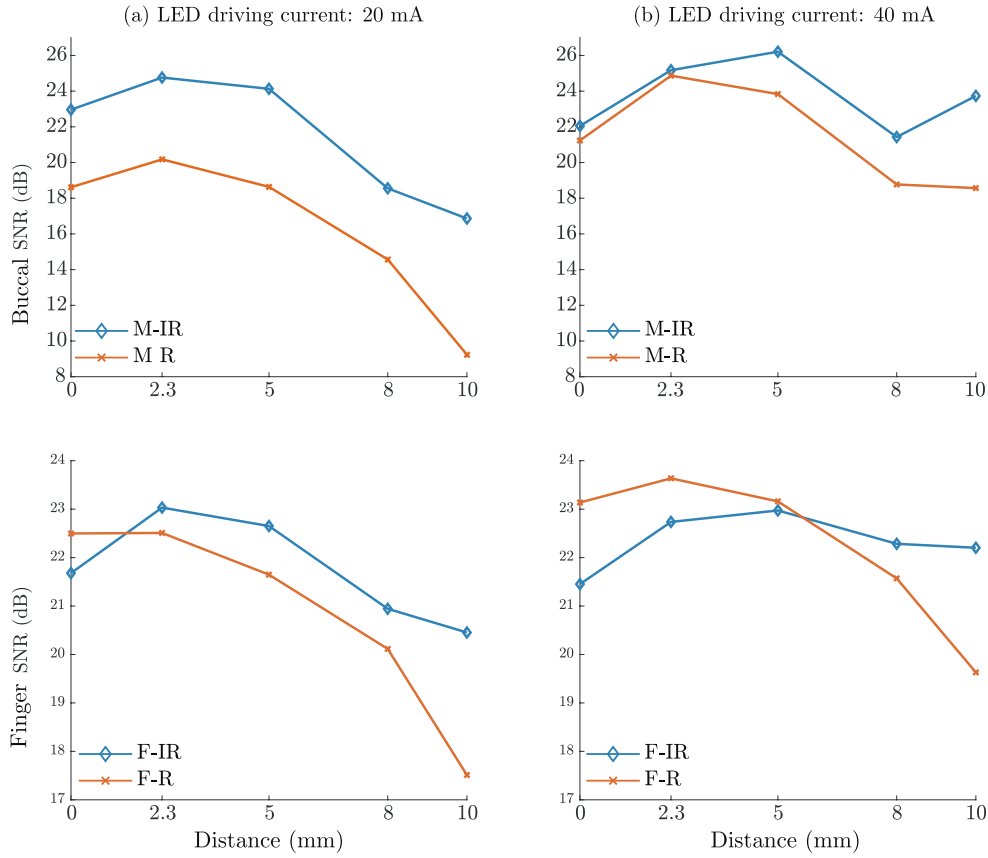


Figure 8.10 Overall mean of the signal-to-noise ratio (\overline{M}_{SNR}) for red (R, orange $- \times -$) and infrared (IR, blue $- \diamond -$) at different sensor-tissue separations. The SNR was obtained within the mouth, on the buccal mucosa (M) and on the finger (F). The SNR was calculated for each LED driving current, where the first column (a) presents SNR at a driving current of 20 mA and the second column (b) presents SNR at a driving current of 40 mA.

Table 8.1 Overall mean and standard deviation of blood oxygen saturation ($\overline{M}_{S_pO_2} \pm \overline{SD}_{S_pO_2}$) estimated at each sensor-tissue separation. The results present the overall mean and standard deviation of blood oxygen saturation from the buccal mucosa and left middle finger; each obtained at the five distances.

Distance (mm)	$\overline{M}_{S_pO_2} \pm \overline{SD}_{S_pO_2}(\%)$	
	Buccal	Finger
0	96 ± 3	97 ± 1
2.3	98 ± 1	96 ± 2
5	97 ± 2	96 ± 2
8	96 ± 4	94 ± 4
10	95 ± 3	94 ± 5

8.2 Data analysis and statistics

tested for the statistical significance between the \overline{M}_{ac} from the buccal mucosa from two related sensor-buccal distance, for example, 8 mm versus 10 mm sensor-tissue distance. As significant differences were found, a post-hoc Bonferroni correction was used. Table 8.2 is a multiple comparisons table presenting the p-values from the Bonferroni correction of the paired tests on each sensor-buccal distance pair. The Bonferroni correction was tested at the two light intensities, by driving the LEDs with currents of 20 mA and 40 mA. Tests that were unable to reject the null hypothesis are highlighted in red.

Table 8.2 One-way analysis of variance (ANOVA) tested for statistical significance between the overall mean ac photoplethysmography signals (\overline{M}_{ac}) from two related sensor-buccal distance. A post-hoc comparison test, Bonferroni, was used to determine where statistical significance were found. The table presents the p-values of the paired test on each pair (first and second column). Bonferroni correction was tested at two light intensities by driving the LEDs with currents of 20 mA and 40 mA. Tests where the null hypothesis could not be rejected are highlighted in red.

Distance (mm)		p-values			
		20 mA		40 mA	
		Infrared	Red	Infrared	Red
0 vs.	2.3	0.001	0.001	0.001	0.001
	5	0.001	0.002	0.001	0.001
	8	0.001	0.001	0.001	0.001
	10	0.001	0.001	0.001	0.002
2.3 vs.	5	> 0.05	> 0.05	> 0.05	> 0.05
	8	> 0.05	> 0.05	0.001	> 0.05
	10	0.001	> 0.05	0.001	0.002
5 vs.	8	> 0.05	> 0.05	> 0.05	> 0.05
	10	> 0.05	> 0.05	0.020	0.018
8 vs.	10	> 0.05	> 0.05	> 0.05	> 0.05

Observation from the investigation PPGs were obtained at two light intensities driven with currents of 20 mA and 40 mA from the buccal mucosa and finger at various sensor-tissue separations. At the two wavelengths, IR and R, Figure 8.3 and Figure 8.4 corresponds to PPG signals obtained from the buccal mucosa, whilst Figure 8.5 and Figure 8.6 respectively. At both tissue locations, the PPG amplitude and morphology differed with the changes in the separation between the PPG sensor and tissue. The overall trend displayed a decrease in signal amplitude as the sensor-tissue separation increased. With an increase in the driving current from 20 mA to 40 mA, a visual observation can be made, where there is an enhancement in the signal amplitude and

The effects of optical sensor-tissue separation

morphology. Referring to Figure 8.5(a-b), with an increase in the driving current, signals at a separation of 8 mm and 10 mm are more apparent.

Similar trends were observed when comparing the \overline{M}_{ac} between the infrared and red PPG signals obtained from the buccal mucosa, as shown in Figure 8.8. For the infrared LED with a driving current of 20 mA, the ANOVA test indicated statistical significance within the five \overline{M}_{ac} obtained at each distance [$F = 41.025, p = 0.001 (< 0.05)$]. Results from the Bonferroni correction presented in Table 8.2 showed the multiple comparison of sensor-buccal distance of 0 mm against the remaining distances, having significant differences at 5% level between the \overline{M}_{ac} of infrared ac PPG amplitudes from the buccal mucosa at 0 mm ($\overline{M}_{ac} = 5.25$ mV) compared to the \overline{M}_{ac} of infrared ac PPG amplitudes at 2.3 mm, 5 mm, 8 mm and 10 mm ($\overline{M}_{ac} = 2.70$ mV, 1.95 mV, 1.83 mV, and 1.09 mV respectively).

At both locations, the detected R ac amplitudes were smaller than the IR ac amplitudes. This is a common finding due to the differences in the light absorption of HbO_2 and HHb at these two wavelengths [285, 102]. For the R LED with a driving current of 20 mA, the ANOVA test indicated statistical significance within the five \overline{M}_{ac} obtained at each distance [$F = 16.516, p = 0.001 (< 0.05)$]. The Bonferroni correction showed there were significant differences between the buccal distance of 0 mm against the remaining distances at a 5% level between the \overline{M}_{ac} of red ac PPG amplitudes from the buccal mucosa at 0 mm ($\overline{M}_{ac} = 1.76$ mV) compared to the \overline{M}_{ac} of red ac PPG amplitudes at 2.3 mm, 5 mm, 8 mm and 10 mm ($\overline{M}_{ac} = 0.75$ mV, 0.72 mV, 0.57 mV, and 0.47 mV respectively). The \overline{M}_{ac} of red ac PPG amplitudes were found to have no statistical difference between the sensor-buccal distance of 2.3 mm and all distances up to 10 mm at a 5% level.

At a driving current of 40 mA, observations from Table 8.2 suggests more pairs of different distances showing a significant difference between the \overline{M}_{ac} 's. By increasing the LED driving currents from 20 mA to 40 mA, the light intensity increases by two folds, resulting in the \overline{M}_{ac} for both wavelengths to approximately double. For instance, at 0 mm (contact), the \overline{M}_{ac} for infrared was found to be 5.25 mV and 10.79 mV, respectively. The increase in amplitude is due to the increase in the number of photons emitted in order to penetrate the tissue; similarly increasing the number of returning photons to the photodetector, therefore resulting in a larger PPG amplitude.

Referring to Figure 8.10, high SNRs from the buccal mucosa were observed up to distances of 5 mm. Exceeding 5 mm led to a substantial reduction in the R SNR, from approximately 18 dB to 8.5 dB. As the sensor-buccal separation increased, the

PPG signals detected at both LED driving currents became of poor quality, which are identifiable due to the erratic and slight resemblance of the conventional signals, as shown in Figure 8.7. As the sensor-tissue separation increases, the photons' reaching the mucosal lining diminishes, resulting in the reduction of photons penetrating the tissue. The number of photons returning to the photodiode could also be compromised by the physical distance of the optics and the buccal mucosa. As the number of photons returning to the photodiode is significant to the quality of PPG signals, the use of 40 mA within the intestine would be chosen. Referring to Figure 8.10, with the increase of emitted photons, the overall SNR for both wavelengths were seen to increase and approximately halve the SNR range.

Preliminary S_pO_2 estimations were conducted as an indication whether the system had the capability of calculating reliable S_pO_2 values when a sensor-tissue separation was present. Considering the finger S_pO_2 at 0 mm (contact) as the reference value, Table 8.1 shows an agreement between the estimated saturation obtained from the buccal mucosa and finger. The t-test suggests no significant differences between the $\overline{M}_{S_pO_2}$ buccal mucosa and finger at each distance, where p-values below 0.05 were found. As an observation, when the optical sensor is at a farther distance, there are slight reductions in the estimated $\overline{M}_{S_pO_2}$ values and an increase in the $\overline{SD}_{S_pO_2}$. This is due to the inaccurate determination of the ratio of ratios (Equation 4.27), which relates to the diminishing SNR.

Finally, discrepancies in the results for the separation distance of 0 mm (contact) was due to a challenge encountered by the stabilisation of the intraluminal sensor within the mouth. As measurements during contact were obtained with a plastic sheath, each individual handled the sensor differently. Furthermore, assumptions were made for the SNR to decrease proportionally as the separation distance increased. However, due to participants swallowing and the resultant electromyogram interference from the cheek, recorded signals were hindered.

8.3 Summary

This chapter demonstrated the feasibility of acquiring non-contact endocavitary PPGs using the human buccal mucosa as a surrogate of the colorectum mucosa. Non-contact PPGs within the buccal cavity has been presented for the first time. As an extension to the computational modelling of the effects of non-contact measurements with the light-tissue behaviour, similar results were obtained with the *in-vivo* study. The overall trend displayed a decrease in signal amplitude as the sensor-tissue separation increased. Consequently, the S_pO_2 reduced in accuracy, which was purely due to the reduction in amplitude and SNR. The study provides confidence and reassurance that the sensor would obtain good quality PPG signals from an endocavity with a sensor-tissue separation of up to 5 mm. Following discussions with the colorectal team at the Royal London Hospital and with medical reference to the intestine anatomy [9], it is known for the intestine to be in a collapsed state once a patient has been anaesthetised, which supports the assumption of the sensor not exceeding a separation of 5 mm. Consequently, a higher light intensity such as 40 mA, would enhance the capability of acquiring reliable PPG signals and S_pO_2 estimations to aid in the dynamic monitoring of bowel tissue viability via an intraluminal route.

Chapter 9

Clinical evaluation on healthy tissue regions within the colorectum

A clinical protocol was written and approved by the local ethics committee (*National Research Ethics Service, Research Ethics Committee London: City & East*) to evaluate the intraluminal sensor as a tool for assessing large bowel viability at The Royal London Hospital (RLH, *Barts London, National Health Service (NHS) Trust, UK*) (Appendix E). The clinical pilot study was specifically aimed to investigate the feasibility of reliably obtaining raw photoplethysmography (PPG) signals and estimate S_pO_2 values within the human colorectum (CR). As part of the ethical approval process, electrical safety tests of the complete system were performed and approved by RLH's clinical engineering department (Appendix C). This chapter presents the clinical pilot study led by the author, along with the data analysis obtained by patients prior to an elective bowel resection within the department of colorectal surgery.

Motivation The first acquisition of colorectum PPG signals with the use of the custom-made intraluminal PPG system will be presented. The aim of this chapter is to demonstrate the systems capability of obtaining raw PPG signals and continuously estimating the S_pO_2 in an *in-vivo* clinical setting.

9.1 Materials and methods

Measurement set-up The modified intraluminal PPG sensor presented in Section 6.3.3 was used to obtain measurements from the lumen of the CR. The identical finger PPG sensor presented in Chapter 6, along with a routinely used PO by RLH as a reference for S_pO_2 were adopted. To acquire all PPG signals from the developed sensors, the research PPG processing unit (ZenPPG) was used. The study and the measurement set-up did not interfere with the routine monitoring procedures and the developed technology was not used as a replacement for the routinely used devices.

As the pilot study requires the introduction of the intraluminal PPG sensor via the transanal route of the patient, a conventional rectal catheter was required. The intraluminal PPG sensor was designed to fit into a 26 French Gauge (FG) disposable and transparent rectal catheter. At the distal end of a rectal catheter, the eyelets were blocked using a silicone bung prior to use, as shown in Figure 9.1. Blocking the distal end of the rectal catheter isolated the sensor from body fluids, thus allowing the sensor to be reused with a new sterile catheter without the risk of cross contamination between each study. As a further precaution, the sensor itself was decontaminated in a sterilising solution between each study. To determine the depth at which the sensor was inserted into the CR, the sensor was labelled using medical tape at 3 cm intervals.

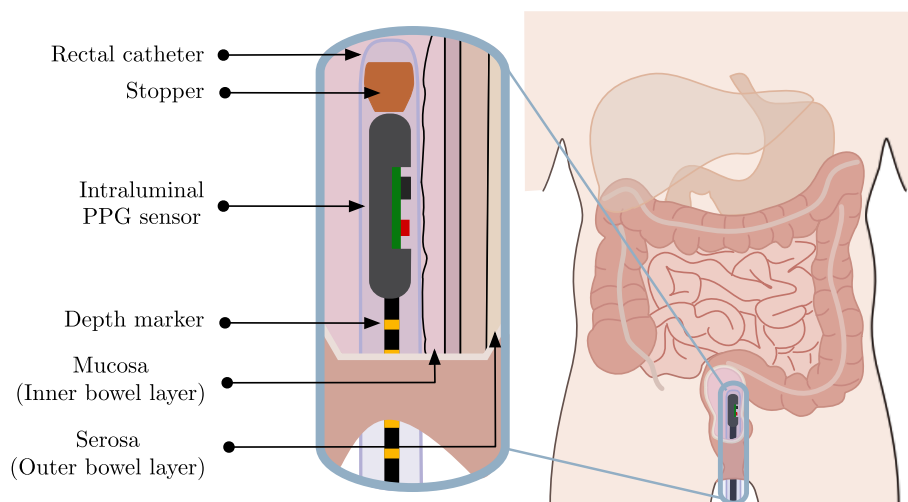


Figure 9.1 Illustration of measurement setup of the clinical pilot study. The intraluminal optical sensor is placed in a rectal catheter, with a silicone stopper blocking the distal end of the catheter. The optical sensor records photoplethysmography signals at several depths within the CR with reference to the opening of the back passage. The sensor is placed to a maximum depth of 15 cm and withdrawn by 3 cm. The sensor is labelled using medical tape at 3 cm intervals.

9.1 Materials and methods

To insert the sensor into the CR, a rigid proctoscope and a sterile lubricating gel (*optiLube*) was used for each patient. The developed finger PPG sensor was placed on an available digit, ideally where the chosen hand was free from an arterial line and blood pressure cuff. Figure 9.2 presents all materials required for a single study.

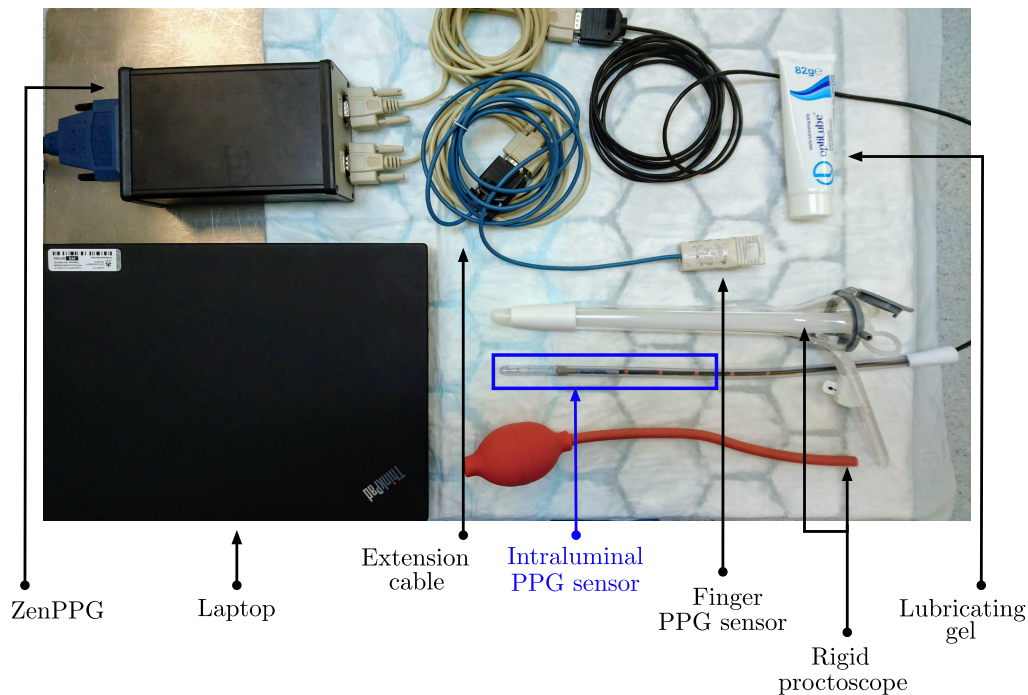


Figure 9.2 Clinical trolley set-up. All materials required for a single study is presented. The developed intraluminal optical sensor and optically identical finger sensor are connected to the instrumentation unit (ZenPPG). A rigid proctoscope and lubricating gel is used for the insertion of the intraluminal sensor. Photoplethysmography signals are acquired from the colorectum and finger which are digitised and recorded onto the laptop. Note, all material materials were placed on a single trolley for image purposes. In the theatre, the laptop and ZenPPG are isolated on a sterile trolley at approximately 1.2 m away from the surgical radius.

Volunteer and investigation set-up Following approval from the ethics committee, patients were recruited from RLH surgical lists prior to their surgical procedures by the lead clinician. As the intraluminal sensor was needing to be evaluated within healthy regions within the CR, the clinical study allowed patients undergoing either right or left sided bowel resection, with the absence of rectal pathology or previous providing rectal diseases or previous colorectal surgeries. All patients recruited were categorised within ASA I - IV (*American Society of Anaesthesiologists*), which estimates the patients postoperative mortality. An extensive list of the inclusion and exclusion criteria can be found within the protocol (Appendix E).

Clinical evaluation on healthy tissue regions within the colorectum

Following full explanation of the study, informed consent was obtained from all patients prior to the commencement of the study. Twenty (20) patients were recruited (10 female (F), 10 male (M)) with a mean age of 65 years ($\pm SD$: 13 years) and mean weight of 67 kg ($\pm SD$: 12 kg) and 81 kg ($\pm SD$: 21 kg) for female and male volunteers respectively, as shown in Table 9.1. General anaesthesia was performed as planned, where the delivery technique of either total intravenous anaesthesia (TIVA) or the traditional anaesthetic delivery of Sevoflurane or Desflurane were used. The *in-vivo* study was performed within the operating theatre room, where the patient under general anaesthetic was placed in a lithotomy position, where the patient has their legs separated and supported in raised stirrups [9]. Bowel preparation prior to the surgery was noted, where patients were either provided a laxative (*Picolax*) 24 hours before the scheduled surgery or flushed with saline immediately before the surgery commenced.

After performing the surgical "time out", the study was performed prior to the start of the operation. To ensure the study was minimally interfering the routine surgery set-up, the ZenPPG was isolated on a sterile trolley at approximately 1.2m away from the surgical radius. An additional sterile trolley was used to place the intraluminal PPG sensor, rigid proctoscope and lubricating gel.

Measurements within the CR and finger were obtained, where measurements at five depths were taken within the CR. For the CR measurements to commence, the catheter mounted intraluminal PPG sensor was inserted gently via the transanal route by the surgeon, over a proctoscope and use of lubricating gel. Initial measurements were recorded at a depth of 15 cm, followed by the sensor being withdrawn by 3 cm; thus, obtaining measurements at depths of 12 cm, 9 cm, 6 cm and 3 cm, with respect to the back passage. The identical finger PPG sensor was placed on a finger preferably without an arterial line and pressure cuff to ensure continuous PPG acquisition.

Signals acquired from both locations were displayed on a laptop running LabVIEW. Once signals were stabilised, at least one-minute of recorded data at each depth was saved. When the depth of the sensor was adjusted, a time-stamp was recorded on the data file. The overall study duration lasted no longer than 30 minutes, where all reusable materials were disinfected between studies. A case report form (CRF) was prepared for each patient, where detailed patient information and measurement observations were documented. Measurement observations included data readily available from the routinely used devices, such as the S_pO_2 , heart rate, blood pressure, ventilation and anaesthetic parameters.

Table 9.1 Recruited patient statistics. The type of surgery has been abbreviated, where each corresponds to the following: open (\oplus), right hemicolectomy (\triangleright) which could be extended (E.) or performed as a robotic surgery (R.). Surgeries including liver resection (LR), total pelvic exenteration (TPE) and anterior resection (AR) were recruited. Bowel preparation prior to the surgery was noted, where patients were either flushed with saline (W), provided a laxative (P) or neither (N). Additionally, after the study, the catheter was assessed and categorised based on cleanliness upon removal, where each category corresponds to the following: clean (1), covered with watery stool with sensor visible (2) and completely covered with stool and sensor cannot be seen (3).

Study	Gender (F/M)	Age (yrs)	Weight (kg)	ASA (I-IV)	Surgery	Bowel prep (N/P/W)	Catheter (1-3)
1	M	83	87	III	R. \triangleright & LR	P	2
2	M	57	79	II	$\triangleright \pm \oplus$	P	-
3	M	86	70	III	$\triangleright \pm \oplus$	W	1
4	M	67	100	II	$\triangleright \pm \oplus$	P	2
5	F	73	80	III	\triangleright	P	2
6	M	61	108	III	R. \triangleright & LR	N	3
7	F	66	67	II	\triangleright	P	2
8	F	32	58	II	R. $\triangleright \pm \oplus$	P	3
9	M	70	89	III	E. \triangleright	W	2
10	F	66	76	II	\triangleright	W	2
11	F	48	74	III	E. $\triangleright \pm \oplus$	P	2
12	F	59	78	II	$\triangleright \pm \oplus$	W	1
13	F	75	83	III	\triangleright	N	-
14	M	75	35	III	$\triangleright \pm \oplus$	P	1
15	M	62	68	III	-	-	-
16	F	60	67	II	\triangleright	N	1
17	M	56	95	II	E. \triangleright	N	1
18	F	52	47	II	TPE	P	2
19	M	64	76	III	AR	N	3
20	F	85	57	III	$\oplus \triangleright$	P	1

9.2 Data analysis and statistics

Offline analysis of the recorded PPG signals was performed on seventeen (17) volunteers using MATLAB[®], where three volunteers were excluded due to clinical difficulties. PPG signals were recorded ($n = 17$) from both wavelengths and at two locations; (i) the CR at all five depths, and (ii) the finger. The preprocessing procedures described in Section 6.8 were used, where the recorded data were re-sampled and digital filter parameters were determined by inspecting each patients spectrogram (Section 6.8.1). For the analysis of the signals, intervals for each study were selected at each light intensity, where a default window size of 20s was chosen.

9.2.1 Data exclusion

Whilst analysing each study, it was apparent that more studies required exclusion from further analysis, as they failed to yield adequate PPGs for the study. The signals were particularly hindered due to severe motion artefact whilst the patient was being prepared for surgery and artefacts from the core temperature management system.

For comparison purposes, Figure 9.3 presents the comparison between a typical spectrogram retrieved from a study and an example of one of the hindered studies. As seen in the Figure 9.3(a), there are distinctive bands, highlighted with red blocks, where a range of frequencies were present at a given time. These bands correspond to the times where the sensor has moved due to the surgeon withdrawing the sensor to the next depth or due to other types of movements. By comparing the two cases, there is a difficulty in observing the fundamental PPG frequency at approximately 1 Hz - 1.5Hz, which corresponds to a pulse rate between 60 bpm and 90 bpm. Rather than an immediate exclusion, the interval selection window size was reduced to 10s, as a reliable signal could be obtained within a shorter time-frame. Figure 9.4(a) summarises the studies excluded prior to main data analysis and the studies which were selected to have a window size reduction of 10s.

After reducing the window size, an indirect analysis on the quality of signals was performed, by assessing the S_pO_2 values for each study. The difference between the S_pO_2 values from the finger and CR were calculated, where differences between channels greater than three to five percent were noted. Referring to Figure 9.4(b), specific studies had recurring large differences between the channels, such as studies 1, 5, 6, 18 and 19. As a result, there was an immediate exclusion of study 6 and 19, where the reduction in window size did not improve the signal quality.

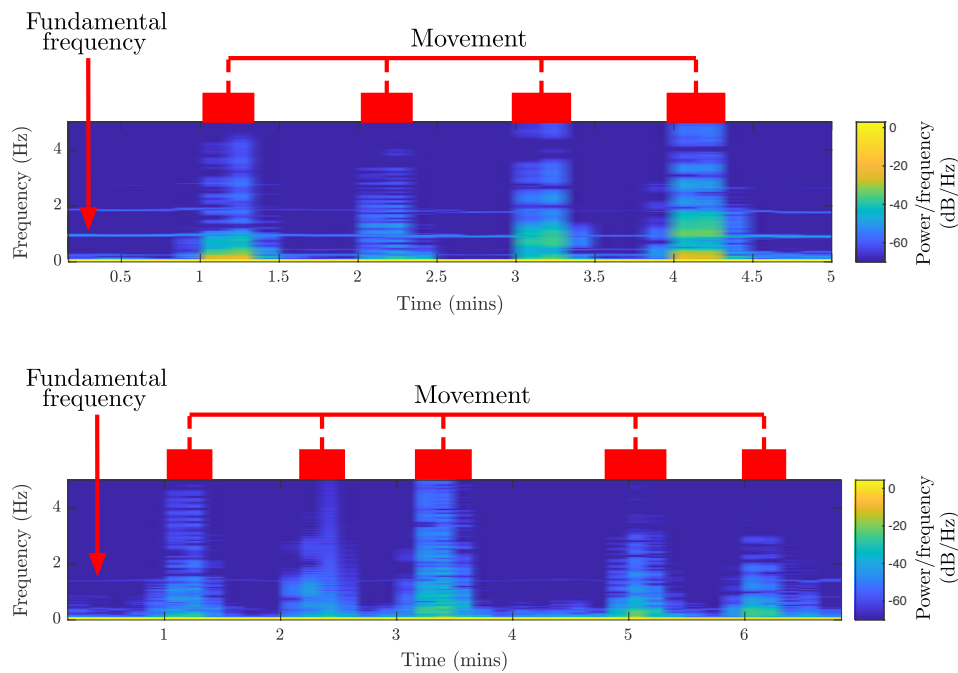


Figure 9.3 Comparison of spectrograms of two studies. The top spectrogram is a typical response where a constant fundamental frequency is visible, which corresponds to the heart rate of an individual and an indication of profound photoplethysmography (PPG) signals. The bands of multiple frequencies indicates the time when the sensor was moved to a different depth within the colorectum. The bottom spectrogram is an example of an excluded participant, where there is a faint presence of the fundamental frequency, indicating the difficulty in acquiring PPG signals.

Clinical evaluation on healthy tissue regions within the colorectum

Depth (cm)	Study																			
	1	2	3	4	5	6	7	8	9	10	11	12	13	14	15	16	17	18	19	20
3		×				◇					◇		×		×					◇
6		×				◇					◇		×		×					◇
9		×				◇					◇		×		×					◇
12		×				◇					◇		×		×					◇
15		×				◇					◇		×		×					◇

(a)

Depth (cm)	Study																			
	1	3	4	5	6 [◇]	7	8	9	10	11 [◇]	12	14	16	17	18	19 [◇]	20			
3	***			***	***										*	***	*			
6	***			***										*	**	***				
9	***			*	***		***							*	**	***				
12	***			**	***								*			***				
15	**	***		***	***					**				**	*	***				
	◇			◇	×										◇	×				

◇ Window size 10 s × Excluded data % Difference between channels: * > 3 ** > 4 *** > 5

(b)

Figure 9.4 Overview of all consented and exclusion studies. (a) presents all twenty consented participants, and (b) presented the second correction of data selection. The × refers to the excluded studies and ◇ are studies which were analysed with a signal window size of 10s rather than 20s. The stars (★) represent the S_pO_2 percentage difference between the developed intraluminal and finger sensors.

9.2 Data analysis and statistics

The remaining studies (Study 1, 5 and 18) which were selected to have a reduced window size of 10s were reanalysed with the remaining studies. Figure 9.5 presents the distribution of the S_pO_2 values at each stage of analysis. Referring to Figure 9.5(a), the variability of values in Channel 1 (CH1) appeared too large compared to Channel 2 (CH2) and the reference, being the commercial PO (REF). Small under estimations of S_pO_2 can be overlooked, however the spread in the S_pO_2 in CH1 were great, suggesting calculations may have not been as accurate. By assessing individual studies, the erroneous data, which may have been altered by unanticipated external factors, would be removed from further analysis. The reduction in distribution of S_pO_2 between Figure 9.5(a-b) suggests the benefits of reducing the signal window size to 10s. Furthermore, the outliers become apparent, where the most recurring outlier at each depth corresponds to Study 1, where the data for this study diverges greatly from the overall values within the set. By excluding Study 1, Figure 9.5(c) illustrates the greater reduction in variability of values which visually is in agreement with CH2 and REF. The outliers present in Figure 9.5(c) correspond to Study 5 and 18, however these were chosen to remain within the analysis as they were within 90% to 100%. Note, Table 9.2 presents the SNR for the excluded patients which will be discussed further in Chapter 10. The remaining analysis in this chapter will be based on a sample size of fourteen ($n = 14$) from the original twenty ($n = 20$).

Table 9.2 Overall mean of the signal-to-noise (\overline{M}_{SNR}) of patients whom were excluded from the analysis. The \overline{M}_{SNR} consists of three exclusions due to poor signal quality.

Depth (cm)	\overline{M}_{SNR} (dB)			
	Colon		Finger	
	IR	R	IR	R
3	21.8	19.6	25.1	25.2
6	19.6	18.4	26.1	20.5
9	21.3	18.5	26.2	23.8
12	22.4	20.8	26.5	25.6
15	21.2	18.9	26.3	22.3

Clinical evaluation on healthy tissue regions within the colorectum

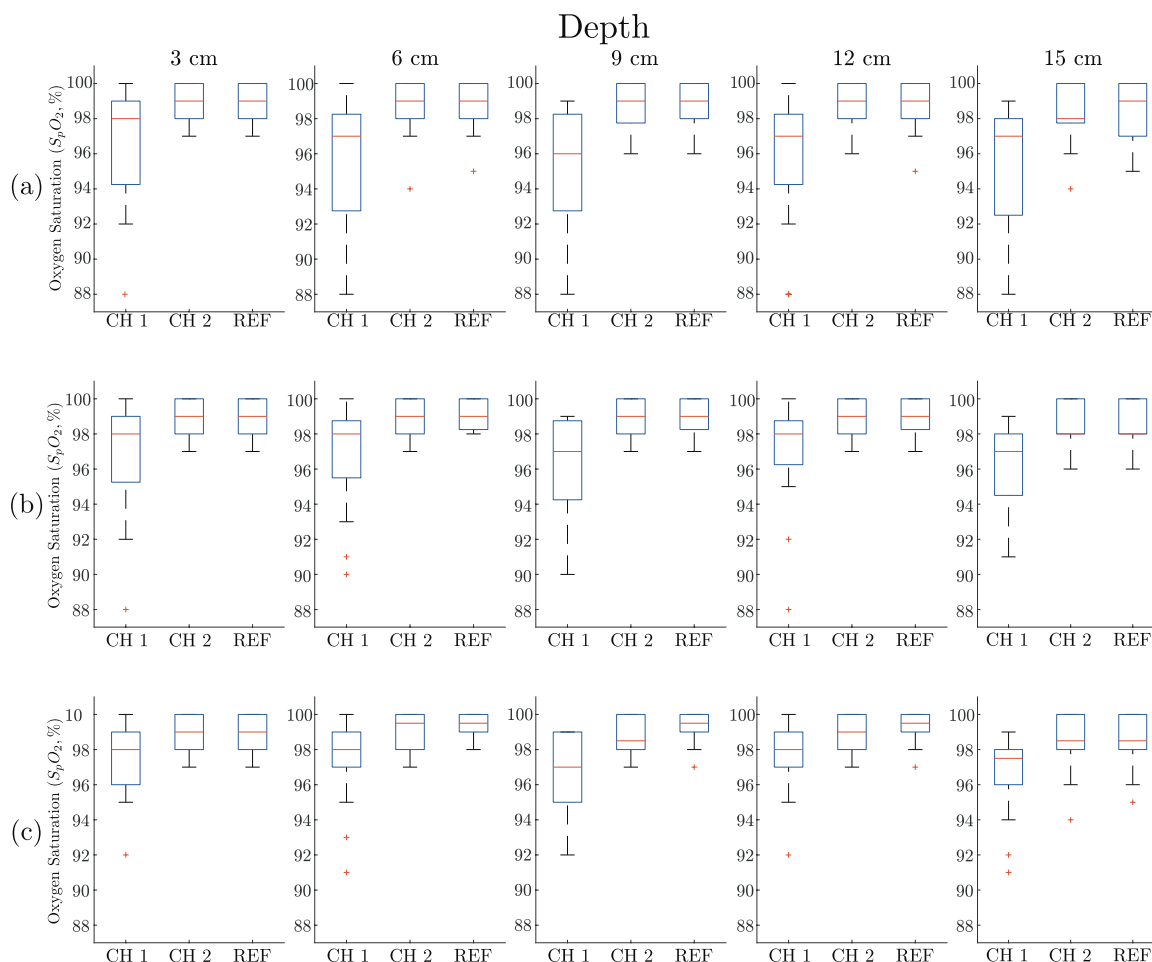


Figure 9.5 Oxygen saturation (S_pO_2) represented as box plots, where CH1, CH2 and REF corresponds to S_pO_2 's using the intraluminal optical sensor, the optically identical sensor and a commercial pulse oximeter respectively. (a) All cases (referring to Figure 9.4(a)) where Study 6, 11 and 19 were reduced to a window size of 10 s. (b) Initial correction (referring to Figure 9.4(b)) where Study 6 and 19 were excluded and Study 1, 5 and 18 were reduced to a window size of 10 s. (c) Final correction where Study 1 is excluded from the overall data set.

Amplitudes Figure 9.6(a) depicts typical IR ac PPG traces from the CR at each depth with reference to the rectum. Figure 9.6(b) depicts typical R ac PPG traces from the CR at each depth with reference to the rectum. Comparison of the ac PPG amplitude changes at different depths were made, where the overall mean and standard deviation ($\overline{M}_{ac} \pm \overline{SD}_{ac}$) was calculated for each of the five depths, as shown in Figure 9.7.

SNR To quantify the quality of the PPG signals obtained from each wavelength, the signal-to-noise ratio (SNR) was calculated using the signal against the background noise as described in Section 10. For comparisons, the overall mean of the SNR of the ac PPG signals (\overline{M}_{SNR}) were obtained for each of the five depths. Figure 9.8 presents the $\overline{M}_{SNR} \pm \overline{SD}_{SNR}$ for IR and R ac PPGs from the CR.

SpO₂ For the estimation of S_pO_2 , the methods described in Section 10 were performed. Similarly, the comparisons of S_pO_2 against the depths were obtained by calculating the overall mean and standard deviation ($\overline{M}_{S_pO_2} \pm \overline{SD}_{S_pO_2}$) for the five depths within the CR. Table 9.3 presents the estimated S_pO_2 calculated for the developed PPG sensors which were placed within the CR and finger. Additionally, the S_pO_2 from the routinely used PO by RLH are presented as the gold standard reference values.

Table 9.3 Overall mean and standard deviation of the blood oxygen saturation ($\overline{M}_{S_pO_2} \pm \overline{SD}_{S_pO_2}$) estimated at different depths within the colorectum. The results present the overall mean and standard deviation of blood oxygen saturation from the colon, finger and reference pulse oximeter. Note that the finger PPG sensor and the reference pulse oximeter was kept in contact with the patients' finger.

Depth (cm)	$\overline{M}_{S_pO_2} \pm \overline{SD}_{S_pO_2}(\%)$		
	Colon	Finger	Reference
3	97 ± 2	99 ± 1	99 ± 1
6	97 ± 2	99 ± 1	99 ± 1
9	97 ± 2	99 ± 1	99 ± 1
12	97 ± 2	99 ± 1	99 ± 1
15	97 ± 2	98 ± 2	98 ± 2

Figure 9.9 is a Bland-Altman plot of the differences between the CR and reference values, obtained from the routinely used PO values, against their mean. Plots at each of the five depths are presented, where the limits of agreements and mean difference \pm SD were calculated and annotated on each graph.

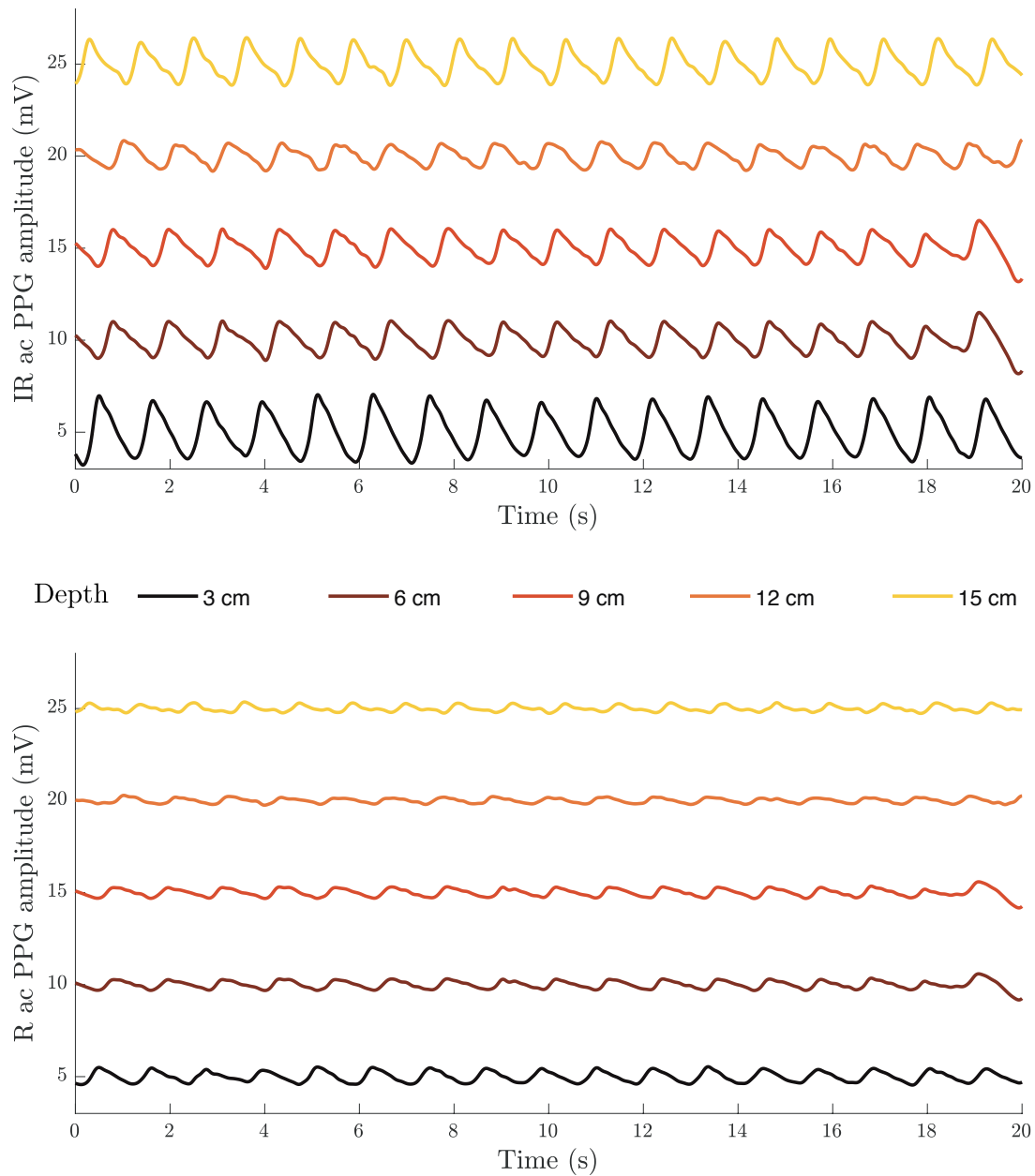


Figure 9.6 First reported colorectum (CR) photoplethysmography (PPG) signals using a custom-made intraluminal optical sensor. Twenty seconds of typical PPG signals at different depths within the CR are presented, where the minimum and maximum depth, with respect to the back passage was 3 cm and 15 cm, respectively. (a) presents the infrared PPG signals, whilst, (b) presents the red PPG signals. For visualisation purposes, five signals are equally spaced with a 5 mV offset; as the offset increases, the separation increases.

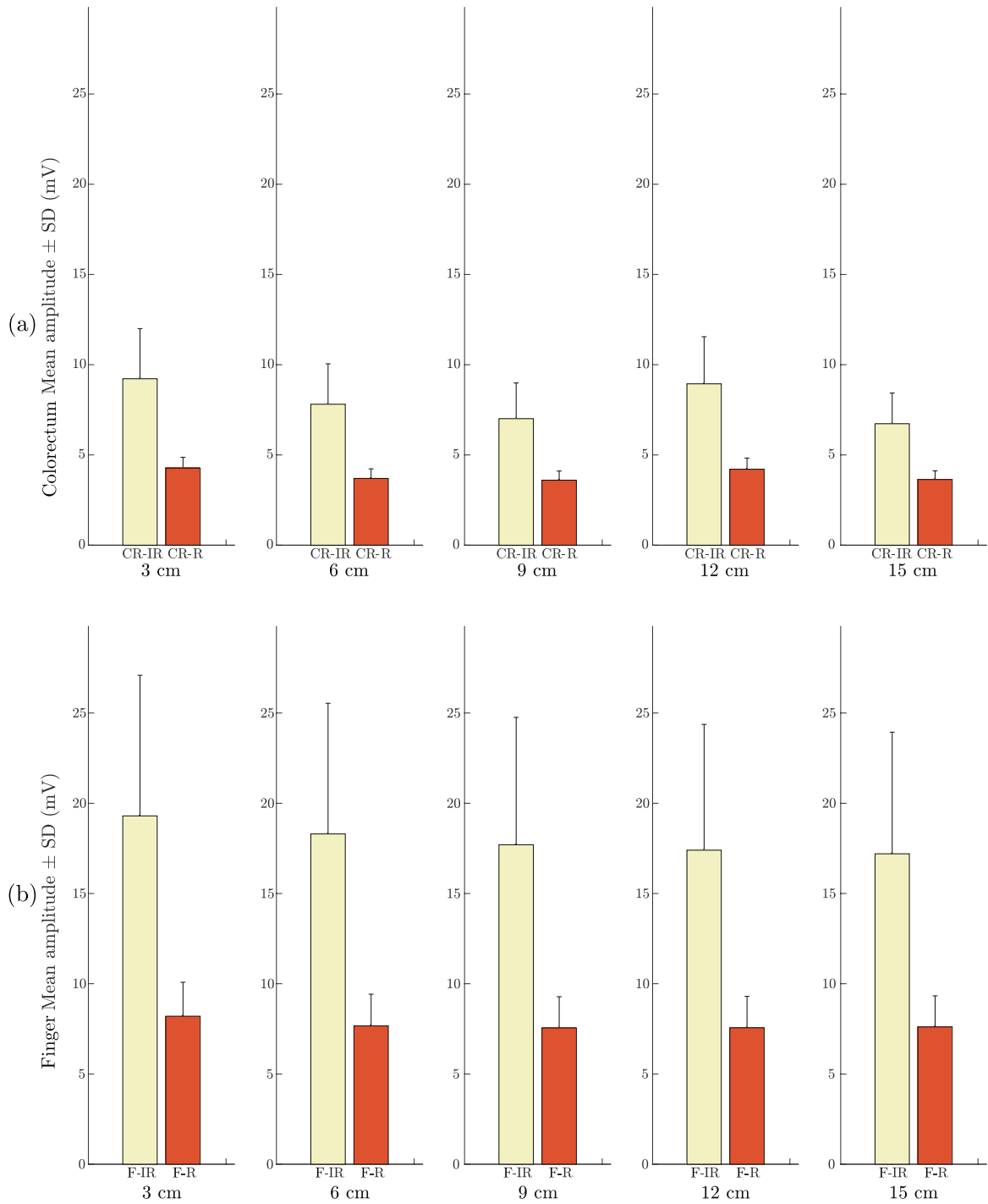


Figure 9.7 Overall mean and standard deviation of the ac photoplethysmography (PPG) amplitudes ($\overline{M}_{ac} \pm \overline{SD}_{ac}$) at different depths within the colorectum. The results present the overall mean ac PPG amplitudes and standard deviation from (a) the colorectum (CR) and (b) finger (F) using red (R, red) and infrared (IR, yellow) wavelengths. Note, that the finger PPG sensor was kept in contact with the patients' finger.

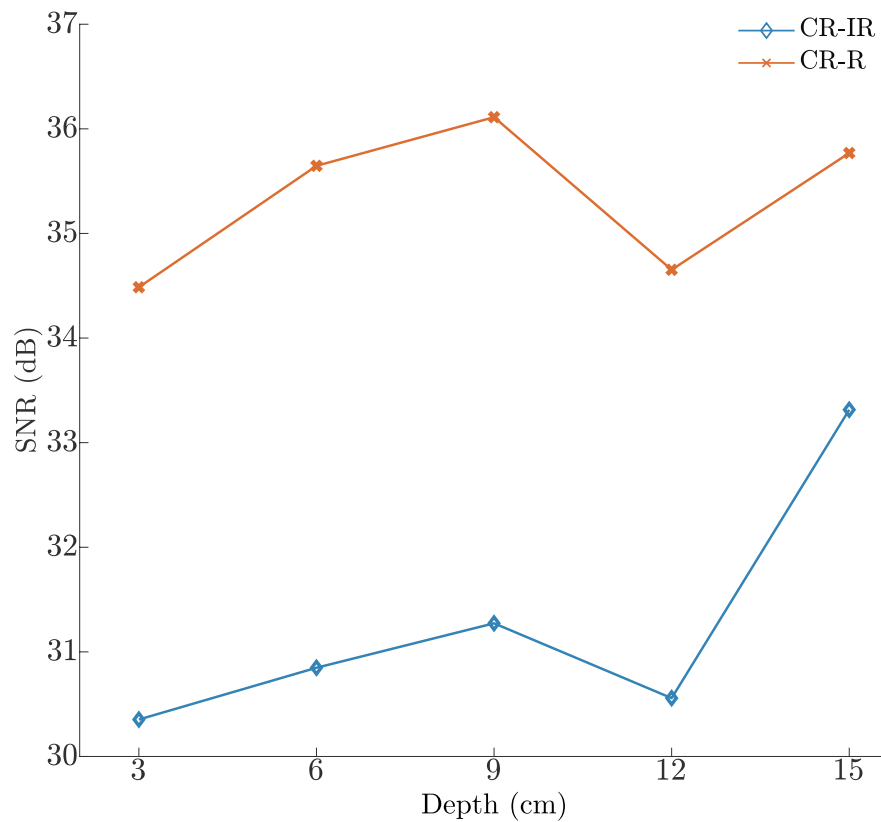


Figure 9.8 Overall mean of the signal-to-noise ratio (\overline{M}_{SNR}) within the colorectum (CR) at different depths at the two wavelengths, infrared ($-\diamond-$, blue) and red ($-\times-$, red).

9.2 Data analysis and statistics

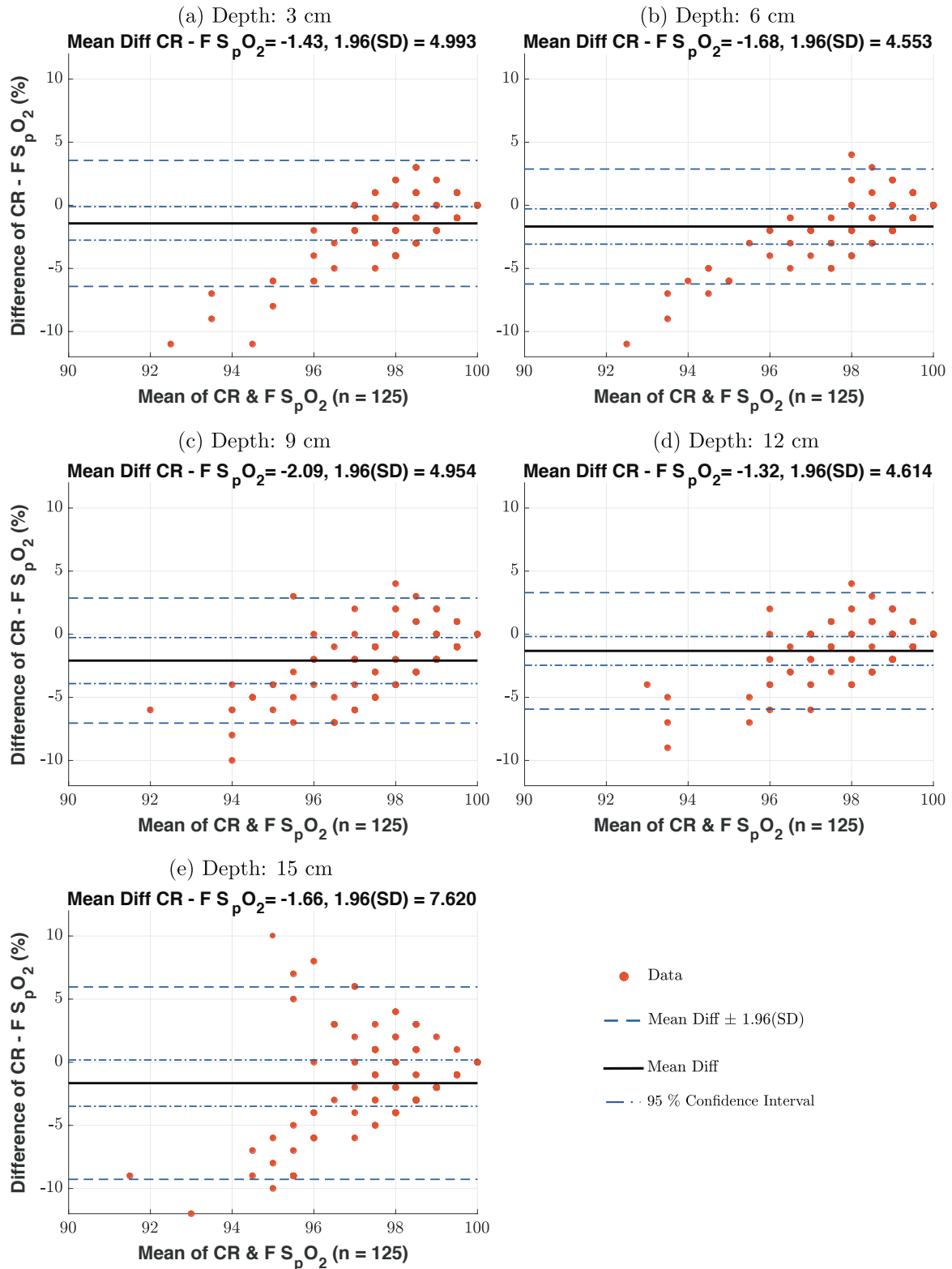


Figure 9.9 Comparisons of oxygen saturation (S_pO_2) values from the intraluminal optical sensor (CR) and the commercial pulse oximeter (F) using the Bland-Altman analysis. Note, 125 data points are presented, however, due to discrete S_pO_2 values, the data points overlap.

Clinical evaluation on healthy tissue regions within the colorectum

Further analysis The KS test described in Section 6.8.3 was used to validate the normality of the \overline{M}_{ac} , \overline{M}_{SNR} , at each wavelength and the $\overline{M}_{S_pO_2}$. With values found to have a normal distribution, the ANOVA, described in Section 6.8.3 tested for statistical significance between the \overline{M} from the CR from two related depths, for example, 9 mm versus 12 mm depth. Table 9.4 is a multiple comparison table presenting the p-values from the post-hoc Bonferroni correction of the paired tests on each depth pair. Tests that were unable to reject the null hypothesis are highlighted in red.

Table 9.4 One-way analysis of variance (ANOVA) tested for statistical significance between the overall mean of ac photoplethysmography signals (\overline{M}_{ac}), signal-to-noise ratio (\overline{M}_{SNR}) and estimated oxygen saturation ($\overline{M}_{S_pO_2}$) from two related depths within the colorectum. The table presents the p-values of the post-hoc Bonferroni correction of the paired test on each depth pair (first and second column). Bonferroni correction was tested where the null hypothesis could not be rejected are highlighted in red.

Depth (cm)		p-values				
		Amplitude (mV)		SNR (dB)		S_pO_2 (%)
		IR	R	IR	R	
3	vs. 6	> 0.05	> 0.05	> 0.05	> 0.05	> 0.05
	vs. 9	> 0.05	> 0.05	> 0.05	> 0.05	> 0.05
	vs. 12	> 0.05	> 0.05	> 0.05	> 0.05	> 0.05
	vs. 15	> 0.05	> 0.05	> 0.05	> 0.05	> 0.05
6	vs. 9	> 0.05	> 0.05	> 0.05	> 0.05	> 0.05
	vs. 12	> 0.05	> 0.05	> 0.05	> 0.05	> 0.05
	vs. 15	> 0.05	> 0.05	> 0.05	> 0.05	> 0.05
9	vs. 12	> 0.05	> 0.05	> 0.05	> 0.05	> 0.05
	vs. 15	> 0.05	> 0.05	> 0.05	> 0.05	> 0.05
12	vs. 15	> 0.05	> 0.05	> 0.05	> 0.05	> 0.05

Observation from the investigation PPGs were obtained from the CR at various depths in reference to the anal verge. At the two wavelengths, IR and R, Figure 9.6 corresponds to PPG signals obtained from the CR. At each depth, the PPG amplitude and morphology visually remains consistent.

Similar trends were observed in Figure 9.7 when comparing the \overline{M}_{ac} between the IR and R PPG signals within the CR. For the IR PPGs, the ANOVA test indicated no statistical significance within the five \overline{M}_{ac} obtained at each depth [$F = 0.62$, $p = 0.6533$ ($p < 0.05$)]. Furthermore, the Bonferroni correction presented in Table 9.4 showed the multiple comparison of the \overline{M}_{ac} R had no significant differences at each depth [$F = 0.24$, $p = 0.9167$ ($p < 0.05$)].

Referring to Figure 9.8, high SNRs were observed at both wavelengths where the SNR ranged between 30 dB and 37 dB. At a depth of 12 cm within the CR, there is a drop in SNR at both wavelengths. Although this change in SNR presents a large reduction, Table 9.4 indicated the multiple comparison had no significant difference for the SNR of IR [$F = 0.35$, $p = 0.8401$ ($p < 0.05$)] and SNR of R [$F = 0.30$, $p = 0.8785$ ($p < 0.05$)].

Table 9.3 shows a large agreement between the developed sensors, in addition to the developed finger PPG sensor being in full agreement with the reference PO. Comparisons of the S_pO_2 within the CR were made, where Table 9.4 indicates no significant difference between each depth [$F = 0.43$, $p = 0.7847$ ($p < 0.05$)]. Referring to Figure 9.9, the S_pO_2 's were within the limits of agreement, indicating the intraluminal PPG sensor and reference PO could be used interchangeably when monitoring S_pO_2 from the healthy rectum.

9.3 Summary

This chapter demonstrated the investigation of feasibly acquiring raw PPGs within the inner walls of the colorectum. The study is the first quantitative report of PPG within the human colorectum at different depths, with the use of a custom-made intraluminal optical system. At all depths, PPG amplitudes were of good quality and remained consistent for the two wavelengths. The obtained PPGs from the colorectum and S_pO_2 indicates the feasibility to directly measure bowel tissue viability parameters from the colorectal wall using the intraluminal reflectance PPG system.

Chapter 10

Discussion

This thesis addresses the needs for continuous monitoring of bowel viability from the clinical aspect (Chapter 2) and the current technological solutions (Chapter 3). To overcome the limitations of current techniques in assessing bowel viability, the thesis proposes the use of an intraluminal optical device based on the principles of photoplethysmography (PPG) and pulse oximetry (PO) (Chapter 4) within the colorectum (CR). The intraluminal device was designed and developed based on the outcomes of probabilistic simulations (Chapter 5), physical restrictions and work previously presented [128, 126, 8]. With the anatomical structures of the CR taken into consideration, the optical device was developed to be placed within the lumen of the CR through the back passage, also known as the anal verge and connected to a PPG processing system (Chapter 6). Evaluations of the sensors functionality were carried out both *in-vitro* and *in-vivo* (Chapter 7 and 8), prior to a clinical pilot study carried out on human participants (Chapter 10). In this chapter, each stage of the work presented will be contextualised and discussed, leading up to the conclusion.

Current state of the art The causes of gastrointestinal tract (GIT) complications such as anastomotic leaks are multi-factorial, where the major risk factor is the blood supply to the anastomosis [286]. Fortunately, the risk factor of colonic ischaemia is one which clinicians could assess and minimise, by intervening at the correct time. Chapter 3 presented several techniques that have attempted to assess and identify colon ischaemia. The techniques were categorised into four groups based on their underlying principle which were: (i) mechanical patency, (ii) tonometry, (iii) imaging modalities and, (iv) optics.

Discussion

Having several techniques addressed in this chapter highlights the struggle clinicians are facing to assess colonic ischaemia. With mechanical patency remaining as the gold standard technique, there has been no advancement in monitoring and identifying early signs of colon ischaemia in the past 50 years [286]. The attempted techniques are seen as experimental findings rather than a routine assessment, due to the lack of accessibility of the measurement site, complexity, reproducibility and equipment cost. For a method to be clinically appropriate, it must not only be able to provide accurate results, but to also have easy implementation, minimal user dependency and minimal subjectivity.

Design of the intraluminal optical sensor According to the colon physiology (Chapter 2) and findings from previous experiments (Chapter 3), to be successful in identifying early signs of ischaemia, it is crucial to assess the viability of the mucosa, as the serosa could remain well perfused [192]. Thus, the current research proposed to develop an optical sensor which would be placed in the lumen of the colon, in close proximity to the mucosa to measure blood oxygen saturation (S_pO_2). The intraluminal approach was also considered, as ischaemia is more common in the distal colon, where surgeons have reduced visibility of the colon whilst operating [31]; therefore allowing easy insertion and removal of the sensor, when necessary. With this current proposal, curiosity arose in whether the sensor could provide additional information in the form of continuous, quantitative measurements, to that already perceived by the surgeon through visual observations. As mentioned in Section 3.4, S_pO_2 measurements from the mucosa were achieved with the use of an inflating balloon on a Foley catheter. The current research attempted to design a balloon-less optical sensor, as a balloon design may inadvertently cause pressure-related complications.

Computational simulations of light-tissue interaction PPG and PO have remained questionable techniques for assessing colon ischaemia. Previous studies such as Vahl [128] and Koga et al. [126] address the lack of understanding of the tissue volume being interrogated by the optical sensor, where they believe the sensor obtains measurements from neighbouring tissues or organs. To address this, Chapter 5 presented the development of a multi-layered tissue model for a reflectance mode sensor to simulate light propagating through a colon tissue. Furthermore, the limited literature for modelling the application of PPG within the colon was a driving factor for the computational evaluation. Monte Carlo (MC) simulations have been previously used

to understand and explain the light-tissue interaction in generic tissues such as the brain and finger, whilst simulations related to the colon have focused on light-tissue interactions with individual constituents of the colon, such as the layers of the muscularis and mucosa. With no study evaluating light interactions with all four layers of the colon, the results presented in this thesis provides information that is crucial for the knowledge on the light-tissue behaviour, such as the optical path, penetration depth and the distribution of absorption and scattering.

The multi-layered MC model was developed in such a way, for easy adaptation for any tissue, providing the number of layers and optical parameters are known. Different types of optical sources with a detector replicating a photodetector component with an active area of 0.66 m^2 was incorporated. A fixed source-detector separation of 5 mm was chosen since small separations used in PPG interrogates the micro-circulation in a vascular tissue bed [260]. Furthermore, to simulate the application of PPG, typical wavelengths for PO such as red (R) and infrared (IR), corresponding to 660 nm and 880 nm respectively. Prior to modelling the colon, the developed model was validated against previous simulations. By comparing the model with pre-validated data, confidence was built on the accuracy and functionality of the model. To model the colon, efforts were made to closely replicate the tissue by careful selections of all parameters from published literature.

For the modelling of light-tissue behaviour within the colon during changes of perfusion, a perfused colon was simulated. Absorbers such as HbO_2 and Hb within the mucosal layer were introduced whilst varying the blood volume. Referring to the development of the MC model (Section 5.2) and Figure 5.6, photons moved to random positions with a step size, followed by events of scattering and absorption. As shown in Figure 5.8, a higher absorbance event was seen in R compared to IR, whilst both wavelengths showed an increase in the mean weight absorbed with an increase in blood volume. The main findings from the study showed that regardless of the changes in perfusion within the colon, photons of both wavelengths were confined within the colon layers, where the photons penetrated no further than the muscularis layer. Thus, the investigation of the effects of different perfusion states of the colon and the photon penetration depth provides confidence that light photons solely interrogates the colon and does not provide information from neighbouring tissues or organs.

Development of the intraluminal optical system The intraluminal optical sensor was developed in Chapter 6, following the custom simulations of light-tissue

interactions. Based on PPG and PO, the intraluminal sensor was developed to acquire continuous measurements of S_pO_2 within the colon in a minimally invasive manner. In order to acquire PPG signals from the CR, a reflectance PPG sensor was designed, along with an optically identical finger PPG sensor as a reference. The optical components within the optical sensors included light sources of R (660 nm), IR (660 nm) and a photodiode with an active area of 0.66 m^2 , as described in the MC modelling (Chapter 5). The optical components were soldered and encapsulated by a casing, which was suitable for clinical use within a 26 FG (French Gauge) rectal catheter.

The research PPG instrumentation unit (ZenPPG) was assembled to operate in conjunction with a virtual instrument (VI) developed in LabVIEW. The ZenPPG was used to acquire raw PPG signals from the developed optical sensors, provide control of the LEDs light intensities and to record all acquired signals for post-processing. The ZenPPG was able to drive two channels of dual wavelength PPG sensors, as in the intraluminal sensor and the finger sensor. Furthermore, the VI allowed for the continuous acquisition and display of all signals from the instrumentation unit and algorithms were included for the estimation of S_pO_2 and monitoring of the electrical parameters of the ZenPPG.

Evaluations of the intraluminal optical system Evaluations of the intraluminal optical system through *in-vitro* and *in-vivo* experiments were demonstrated in Chapter 7. *In-vitro* thermal tests were carried out on a section of pigs' intestine, whilst an *in-vivo* thermal test was conducted on the mucosal lining of the inner cheek of a healthy human participant, to determine the effect of thermal radiation emitted by the LEDs onto the surrounding tissue. The risk of thermal injury was shown to be negligible as neither the sensor or tissue exceeded the temperature of $38\text{ }^\circ\text{C}$.

An *in-vivo* evaluation of the intraluminal optical system was designed to validate the functionality of the system and confirm the ability to acquire raw PPG signals and S_pO_2 from an endocavity setting, such as the buccal mucosa. The R and IR PPG signals were acquired from both the buccal mucosa and the left index finger using the developed optical sensors, along with a commercial PO placed on a finger as a gold standard reference. The offline analysis developed in Section 6.8, demonstrated its semi-automated capability of filtering (Figure 7.5) and calculating parameters from the ac and dc PPG signals, such as the amplitude and signal-to-noise ratio (SNR). The results presented in Figure 7.6, show that good quality ac PPG signals at both wavelengths can be obtained from endocavities such as the mouth, using the developed

intraluminal optical system. The quality of the signals was quantified by calculating the SNR for each developed optical sensor, where the intraluminal sensor acquired signals with a SNR of 25.6 dB and 23.4 dB, for IR and R, respectively. Furthermore, the finger sensor acquired signals with a SNR of 25.1 dB and 24.6 dB, for IR and R respectively. Statistical comparisons using the Pearson's correlation shows a strong correlation between both developed sensors ($r^2 = 0.80$) and between the finger sensor and commercial PO ($r^2 = 0.82$).

The effects of optical sensor-tissue separation The assessment of non-contact PPG within the colon has not been attempted. It should be noted that non-contact PPG is described as monitoring PPG within an area of tissue from the classical PPG method in a contact-less way, rather than the use of imaging [287]. By the suggestion of the surgical team involved, the intraluminal optical sensor did not include a design to hold the sensor in direct contact with the mucosa, such as the balloon described in Chapter 3. With this exclusion, it was necessary to investigate the influence of direct contact versus no contact PPG measurements between the sensor and tissue surface on the acquisition and quality of endocavitary PPGs. The difficulty to assess the colon for controlled studies has hindered the ability to analyse the sensor for the given problem. Therefore, an *in-silico* (Section 5.4) investigation simulated the light-tissue propagation within the colon and an *in-vivo* (Chapter 8) investigation was undertaken in the buccal mucosa.

Further modelling of the light-tissue interaction within the colon was performed, where an air gap was introduced between the sensor and tissue. The non-contact modelling was used for a comparative analysis between the two operating wavelengths of the optical source by estimating variables such as the penetration depth and detected intensity. The distribution of scattering for both R and IR was shown when a sensor-tissue separation was introduced (Figure 5.10). Whilst the sensor-tissue separation increased; a visual observation could be made on the wide spread of photon being detected by the detector. To visualise the photon propagation clearer within the colon model, Figure 5.11 presented the scattering distribution within the tissue, excluding the air gap. Due to the different scattering coefficients of the mucosa and submucosa, a prominent band with high number of scattering events could be observed. The mean weight detected (Figure 5.12(b)) corresponds to the detected intensity of photons. Thus, as expected, increasing the sensor-tissue separation resulted in a decrease in detected intensity, due to the photons experiencing greater scattering and absorbance

Discussion

events. Additionally, the R photons overall were detected less than the IR, which is due to the R photons encountering larger scattering and absorbance events compared to IR, resulting in less photons reaching the detector.

Interestingly, the PD did not match the hypothesis, where it was believed that the PD would decrease whilst increasing the sensor-tissue separation. As seen in Figure 5.12(d), the PD had a gradual increase as the sensor-tissue separation increased. It is unknown why such effects occurred, however a suggested explanation can be given. Given that the photons shown in the distribution of scattering account only for the photons detected, and that the photons enter the tissue in a very specific range of angles of incidence, it could be assumed that only photons travelling in such angles would eventually circle back to the detector. While it could not be assured, one could explain the behaviour of PD by the allowed angles of incidence of the photons with the tissue. In greater sensor-tissue separation, the angles of incidence could be closer to the normal of the tissue surface; probably aiding in the penetration of the photons in the tissue. It is unknown why such effects on the PD occurred and requires further investigation from researchers within the light-tissue modelling community. Aside from the unexpected PD trend, the main finding from the investigation suggests that the photons lost the most energy within the submucosa layer, corresponding to a tissue depth between 0.7 mm and 1.5 mm. This is reassuring, as the submucosa is supplied by the pulsating arterioles (Section 2.3). Thus, along as the light is penetrating within the submucosa, the arterioles would contribute in the pulsatile signal captured in the PPG.

To physically evaluate the feasibility of acquiring non-contact endocavitary PPGs, an *in-vivo* investigation on twenty healthy volunteers presented in Chapter 8 was performed. The developed intraluminal sensor, finger sensor and a commercial PO were placed within the mouth and left hand. The protocol consisted of acquiring PPG signals from the mouth and finger at different sensor-tissue separation. The buccal mucosa (mouth) was chosen as a surrogate tissue of the colon mucosa. Non-contact endocavitary PPGs were obtained for the first time and presented in Figures 8.3 - 8.6. Similar results obtained from the model were seen with the acquired PPGs, where the overall trend displayed a decrease in signal amplitude as the sensor-tissue separation increased. As the ac component of the PPG signal is considerably smaller than the dc, the ac should be maximised by increasing the light intensity. This was demonstrated, where the increase of light intensity visually enhanced the signal amplitude and morphology. By increasing the light intensity by two folds, the amplitudes for both wavelengths

approximately doubled. Referring to the model simulated, the increase in amplitude is due to the increase in the number of photons emitted in order to penetrate the tissue; similarly increasing the number of returning photons to the photodetector, therefore resulting in a larger PPG amplitude.

Bearing in mind S_pO_2 is a global variable, the values should not change from different positions, such as the mouth and finger, in a healthy participant. With reference to the S_pO_2 values obtained when the sensor was in contact with the tissue, there was a reduction in S_pO_2 which was mainly due to the reduction in amplitude and quality of the signal. Sensor placement in non-contact PPG is essential for the quality of the signal as shown in the SNR for each wavelength (Figure 8.10). High SNRs from both tissue sites, were observed up to distances of 5 mm. Exceeding 5 mm led to a substantial reduction in the SNR, which contributes to the accuracy of determining the S_pO_2 values. Although the amplitude of the ac PPG signal and SNR could be improved by the increase in light intensity, the reflection from the tissue surface must be kept to a minimum to avoid over saturation of the photodetector. Furthermore, and most importantly, increasing the light intensity, which is altered by the increase in driving current within the instrumentation unit, could contribute to thermal effects to the tissue. This could lead to discomfort or thermal damage to the delicate mucosal layer, if used for a long duration. Having the ability to acquire non-contact PPG signals of high amplitude and quality up to 5 mm is reassuring for cases of sensor-tissue separation within the colon.

Clinical pilot investigation Following the experimental investigations, sufficient confidence was acquired to commence to the first *in-vivo* investigation of the intraluminal optical system on twenty human participants undergoing CR surgery (Chapter 9). The clinical study was conducted in accordance with the principles of Good Clinical Practice (GCP) and granted ethical approval by the UK Health Research Authority (HRA), Research Ethics Committee (REC). The protocol involved the acquisition of CR PPG signals within healthy sections of the CR, prior to the surgery commencing. The intraluminal optical sensor was designed to be used with a FG 26 rectal catheter and inserted via the transanal route to a depth of 15 cm, in reference to the back passage. At five depths, at least one-minute raw PPG recordings were simultaneously taken from the CR and finger, using the intraluminal optical sensor and developed finger PPG sensor respectively. S_pO_2 values from a commercial PO were also manually

Discussion

recorded, as commercial PO do not provide the ability to store the raw PPG signals used to calculate the S_pO_2 values.

As prior attempts could not confirm the direction of the PO sensor within the lumen of the CR, efforts were made within the clinical study to place the sensor in the same orientation. With the sensor wire marked, all measurements were obtained whilst facing the antimesentery for reproducibility. Figure 9.6 presented the first in-human CR PPGs using a custom-made intraluminal optical system with R and IR wavelengths. For all spot measurements, the PPG amplitude and morphology visually remained consistent and were statistically analysed with the ANOVA test, comparing the mean amplitude of each wavelength at each depth. The results from the ANOVA test (Table 9.4), indicated no statistical significance was found for amplitudes within R [$F = 0.24$, $p = 0.9167$ ($p < 0.05$)] and IR [$F = 0.62$, $p = 0.6533$ ($p < 0.05$)]. Additionally, the PPGs obtained from the CR and finger are differential, as the CR PPGs were approximately half the amplitudes obtained from the finger.

Initial analysis of the recorded data was assessed with the semi-automated offline signal analyser presented in Section 6.8. Referring to Table 9.5, preliminary estimations of the S_pO_2 from the developed finger PPG sensor and the commercial PO were in agreement. In comparison, observations of the spectrogram of the recorded data and the estimated S_pO_2 from the CR showed discrepancies with large variations. As the clinical pilot study assessed the intraluminal optical system within healthy regions of the CR, the S_pO_2 values were expected to be within the normal range (95 % to 100 %) [288]. The CR S_pO_2 values appeared to be an underestimation in comparison to the commercial PO placed on the finger. Based on prior attempts utilising PPG and PO, such as Ouriel et al. [257], La Hei and Shun [42] and Abdollahi et al. [8], S_pO_2 ranged between 80 % to 100 %. There are several justifications for the underestimation of the S_pO_2 , including:

1. The S_pO_2 calculations were derived from the methods described in Section 4.3. It must be noted, that commercial PO devices do not use the same method and additional data manipulation may be undertaken to correct artefacts.
2. The intraluminal optical system is an uncalibrated system within the CR. Instead, S_pO_2 estimations were calculated using Equation (4.27), which is an empirically derived calibration equation for a finger PO.
3. With the presence of the venous circulation in the vascular bed under the optical sensor, morphological alterations in the signal and erroneous S_pO_2 estimation can

occur [289]. As seen in Figure 2.3, the venules are found at the luminal surface of the mucosa and the larger veins begin within the submucosa. Unfortunately, this cannot be minimised unless a transmission PPG sensor is used, where a pressure is exerted onto the tissue to minimise the venous pulsation.

Limitations of the clinical pilot study will be discussed further in Chapter 11, however the variation of bowel preparation conducted and visual observations of the catheter once fully withdrawing from the participant must be addressed. Referring to the steps of CR surgeries (Section 2.5), bowel preparation has typically been performed preoperatively to reduce faecal contamination [290]. Since bowel preparation has not been shown to influence postoperative complications, there has been a recent trend to exclude bowel preparations and chosen as a preference [31]. As bowel preparation requires long duration of preoperative starvation, this could lead to electrolyte imbalance and dehydration, which are additional factors which may lead to higher rates of postoperative complications [31]. Within the clinical pilot study, there were two techniques for bowel cleansing: (i) a laxative, 24 hours prior surgery, or (ii) a saline wash, minutes prior to surgery. In addition, the catheter was visually inspected and categorised based on the cleanliness upon removal from the participant, as seen in Table 9.1. The assessments were noted to observe whether such factor would affect the quality of the PPG signals. Although the sample size was small, excluding bowel preparation suggests to affect the quality of the PPG. This can be observed, where the excluded participants (studies 1, 6 and 19) were either cleansed with a laxative (study 1) or no cleansing was provided (studies 6 and 19). With the assumption that the laxative would cleanse the bowel, the catheter was found to be soiled, resulting in the catheter to be of low opacity. For the excluded participants, the SNR was calculated, as shown in Table 9.2. The SNR for the excluded participants were lower compared to the SNR of the remaining participants. In addition to movement artefacts, which may have been introduced during the measurement, the presence of stool in the lumen could reduce the quality of the signal obtained. Depending on the composition of the stool, the opacity would also vary, therefore limiting light to propagate sufficiently from the sensor to the tissue.

Concluding the discussion of the current research, the intraluminal optical system shows potential to continuously monitor intestinal viability through S_pO_2 estimations within the lumen of the CR. The developments of the system, software and the evaluations carried out, have provided major contributions, which will be summarised in the concluding chapter (Chapter 11).

Chapter 11

Conclusions and future work

A new approach of a well-known optical technique, photoplethysmography (PPG), has been utilised to design and develop an intraluminal optical system. The system is capable of interrogating the colorectum for real-time, continuous measurements of bowel viability. This thesis presented the different stages of such development, from the technical specifications, modelling of light-tissue propagation and concluding with a proof of concept clinical study within the colon. Several controlled *in-vitro* and *in-vivo* feasibility evaluations were carried out, followed by an *in-vivo* clinical pilot study in an attempt to prove the capability of monitoring intestinal viability within a clinical setting. This chapter presents the major contributions, which highlights the key findings and conclusion. Furthermore, the limitations will be presented, leading to suggestions for further research.

11.1 Major contributions

- Initiating a thorough exploration of the literature on the physiology and pathology of the CR, followed by the techniques attempting to assess intestinal viability, in effort of indicating early signs of ischaemia. Each technique was critically discussed with its working principles, evidence of use within the CR and highlighting the techniques' limitations.
- Developing a multi-layer tissue model to be easily adapted to any tissue composition. The model was used to simulate the colon and the proposed intraluminal optical sensor with varying parameters, to understand the light-tissue interactions specifically within the colon. The varying parameters are additional features

Conclusions and future work

within the model, allowing the simulations of non-contact light-tissue interactions and the variation of perfusion states within a chosen tissue layer.

- Designed, developed and evaluated a dual wavelength intraluminal optical sensor to be used within the lumen of the CR. Combined with the research groups' instrumentation unit (ZenPPG), the optical sensor works on the principles of PPG to continuously monitor the blood oxygen saturation (S_pO_2) within the inner walls of the CR.
- Developed a semi-automated offline signal analyser which allows users to manually extract signal segments and provides S_pO_2 calculations within a 2 second window. Additional features include filtering the signals and calculating parameters such as the amplitude and signal-to-noise ratio (SNR).
- Demonstrated the acquisition of non-contact PPGs within hollow cavities such as the colon and mouth. The acquisition of non-contact capabilities within the colon were demonstrated with the use of the multi-layer model, whilst a physical non-contact measurement was evaluated within the buccal mucosa of human participants.
- The first acquisition of CR PPG signals utilising the custom-made intraluminal optical sensor within a clinical pilot study. By inserting the sensor through the back passage of the participants, the sensor was positioned at several depths within the CR. The sensor has demonstrated the ability to obtain raw PPG signals, provide continuous S_pO_2 and the ease of insertion and withdrawal.

11.2 Major conclusions

The major conclusions are considered:

- The blood supply to the colon is major contributing factor in the most feared complication of CR cancer surgeries, resulting in anastomotic leaks. Fortunately, the colonic blood supply is a factor surgeons have some influence over, where early indicators of colon ischaemia can be identified and intervened appropriately. Despite the awareness of the effects of colon ischaemia, the assessment of bowel viability remains unreliable, where the gold standard assessment relies mainly on visual inspection. To qualitatively monitor the early signs of colon ischaemia, it

is crucial to assess the viability from the inner wall of the colon, corresponding to the mucosa. The mucosa is the furthest tissue layer from the major arteries, thus, the first to be affected by the lack of oxygenated blood.

- The use of PPG and PO within the CR was a questionable technique for assessing colon ischaemia due to the lack of understanding of the tissue volume being interrogated by the PO. Modelling the colon whilst simulating an optical sensor in contact with the inner wall of the intestine demonstrated the feasibility of using PPG within an intraluminal environment. By changing the perfusion state of the mucosal layer through variations of blood volume, the simulation provides reassurance that a PPG sensor interrogates the colon tissue only, where the light penetrates up to the muscularis layer.
- A dual wavelength intraluminal optical sensor was successfully developed with the aim to be used within the lumen of the CR. Feasibility studies were performed prior further investigations of the sensor and clinical pilot study. The feasibility studies included both an *in-vitro* and *in-vivo* thermal evaluations, confirming the sensors usability with negligible risks of thermal injury. Furthermore, an *in-vivo* evaluation of the intraluminal system validated the ability to obtain, record and analyse raw PPG signals from the buccal mucosa, which was chosen as a surrogate tissue to the colon mucosa.
- The investigation of the influence of direct contact versus non-contact PPG measurements was evaluated through computational models and an *in-vivo* study. The non-contact simulations demonstrated the possible light-tissue interactions occurring within the colon, where there was reassurance that light enters the colon tissue and is able to propagate through the tissue with sufficient energy to return to the detector. Furthermore, the simulations suggest that light remains in the tissue, where the light photons lost most of its energy within the submucosa, which is a suitable layer consisting of pulsating arterioles which would contribute to the pulsatile signal captured in the PPG. The investigation was extended into an *in-vivo* study, where non-contact PPG signals within the buccal mucosa and finger were presented. The results displayed a decrease in PPG amplitude along with SNR as the sensor-tissue separation increased. For large amplitudes and high-quality signals, the sensor-tissue separation must not exceed 5 mm. Both investigations presented the importance of sensor positioning, where the signal quality can affect the S_pO_2 estimations.

- The results from the *in-vivo* clinical pilot study has demonstrated, for the first time, that a developed system is capable of acquiring good quality PPG within the lumen of the bowel.

11.3 Limitations

The research carried out within this thesis allowed to investigate the proposed aims, however, some limitations existed and should be acknowledged. The limitations presented are highlighted to introduce possible future research.

Signal amplification Once obtaining CR PPG signals within the lumen, the signals were noticeably small in amplitude. There are two approaches to increase the amplitude of the signal: (i) increasing the light intensity via the driving currents of the light sources, or (ii) increasing the trans-impedance amplifier gain in the instrumentation unit (ZenPPG). Increasing the driving current results in the sensor temperature to increase. Since the optical sensor operated at a driving current of 40 mA, where the typical operating current ranges between 20 mA to 50 mA, the better alternative is to increase the gain of the trans-impedance amplifier.

Signal quality of the colon During the clinical pilot study, the CR PPG signals were particularly hindered due to motion artefact during the surgery preparation and artefacts from the core temperature management system. In addition, there were two limitations which may have contributed to the decrease in signal quality: (i) the choice of bowel preparation and, (ii) the handling of the sensor.

Choice of bowel preparation As discussed in Chapter 10, signals which were excluded came from participants who were provided a laxative to clear the lumen of the intestine a day before the surgery, or no preparation was chosen. Although the study sample was too small to correlate the relationship between the choice of bowel preparation and signal quality, there is a possibility of such a relation. The presence of stool in the lumen could reduce the quality of the signal obtained as the opacity of the stool could vary, depending on the stool composition. Changes in opacity could lead to the decrease of light propagation from the sensor to the colon, and alternatively reduce the ability for light to be captured by the photodetector.

Handling of the sensor As measurements within the CR were taken for at least one-minute, the surgeons were holding the optical sensor during the acquisition period. The clinician required a steady hand, where movements introduced motion artefact which affected the signals quality. In discussion with the clinicians involved in this research, as the sensor would be in use for longer measurement periods, the intraluminal optical sensor would not require the clinician to hold the sensor. Alternatively, the sensor would be attached to the buttocks or thigh of the participant with an adhesive, such as medical tape.

11.4 Suggestions for further research

The following suggestions for further research do not necessarily address the problems stated within the limitations, however, provide further extension to the research.

- As the computational modelling was simplified to understand the light-tissue interaction within the colon, the tissue geometry was modelled as a rectangle. Given the anatomical structure of the colon, it would be interesting to model the colon with a cylindrical geometry. The computational modelling could be further extended to evaluate additional wavelengths, additional PPG channels within a single sensor and to simulate colon ischaemia.
- Improvement of the sensor design could be performed, where modifications to the sensor casing could be undertaken. The primary aim would be to manufacture either a single-use optical sensor or a reusable sensor, where there is no longer a need for a rectal catheter.
- The sensor was not evaluated on patients with compromised bowel viability, however, the results presented would justify a thorough clinical investigation. As the manipulation of the circulation and termination of the collateral vessels cannot be conducted ethically in human participants, an animal study should be considered. Such studies would allow further evaluation of the intraluminal sensors ability to respond to the changes in oxygenation, and investigate the corresponding changes in the PPG amplitudes.
- The sensor in its current configuration may provide as a useful tool for surgeons for monitoring bowel viability at three given situations: (i) pre-surgical baseline measurements, (ii) intraoperative during a resection, and (iii) postoperative

Conclusions and future work

within the 48 hour observation time. A large study to evaluate the intraluminal optical system at each stage should be performed, which may lead to further improvements on the sensor design and analysis techniques.

Closing statement In this work, the lack of reliable continuous monitoring techniques for the assessment of bowel viability was presented. To understand the problem further, the anatomical physiology and biomedical engineering techniques were taken into consideration. This work proposes an intraluminal optical system, where the principle of photoplethysmography is used to provide continuous monitoring capabilities of the blood oxygen saturation, whilst positioned within the lumen of the colorectum. Throughout the current research, several investigations, including computational modelling, have been performed to evaluate the feasibility of the system within an inaccessible location, such as the colorectum.

The work presented in this thesis contributes new knowledge for the use of photoplethysmography in an intraluminal environment. Surgeons are still assessing intestinal viability through visual inspections including the assessment of colour, muscle contraction and air leaks. The developed intraluminal optical sensor could allow clinicians to have quantitative measurements of the blood oxygen saturation which can aid as an additional tool to their decision making through visual inspections. Furthermore, due to the ease of insertion and withdrawal through the back passage, the sensor could be further extended and incorporated in preoperative and postoperative measurements.

References

- [1] L. L. Azzouz and S. Sharma. *Physiology, Large Intestine*. StatPearls Publishing, 2019.
- [2] N. H. Hyman. Managing anastomotic leaks from intestinal anastomoses. *The Surgeon*, 7(1):31–35, 2009.
- [3] UK Cancer Research. Bowel cancer incidence statistics, 2016. URL <http://www.cancerresearchuk.org/health-professional/cancer-statistics/>.
- [4] M. D. Jafari, K. H. Lee, W. J. Halabi, S. D. Mills, J. C. Carmichael, M. J. Stamos, and A. Pigazzi. The use of indocyanine green fluorescence to assess anastomotic perfusion during robotic assisted laparoscopic rectal surgery. *Surgical Endoscopy*, 27(8):3003–3008, 2013.
- [5] T. P. Kingham, H. L. Pachter, G. Brisinda, S. Vanella, F. Cadeddu, and P. Mazzeo. Colonic Anastomotic Leak: Risk Factors, Diagnosis, and Treatment. *Journal of the American College of Surgeons*, 208(2):269–278, 2009.
- [6] E. S. Lee, A. Bass, F. R. Arko, M. Heikkinen, E. J. Harris, C. K. Zarins, P. van der Starre, and C. Olcott. Intraoperative Colon Mucosal Oxygen Saturation During Aortic Surgery. *Journal of Surgical Research*, 136(1):19–24, 2006.
- [7] M. D. Jafari, S. D. Wexner, J. E. Martz, E. C. McLemore, D. A. Margolin, D. A. Sherwinter, S. W. Lee, A. J. Senagore, M. J. Phelan, and M. J. Stamos. Perfusion assessment in laparoscopic left-sided/anterior resection (PILLAR II): A multi-institutional study. *Journal of the American College of Surgeons*, 220(1): 82–92.e1, 2015.
- [8] Z. Abdollahi, M. A. Thaha, P. A. Kyriacou, and J. P. Phillips. Performance of a novel optical sensor for intraoperative assessment of intestinal viability - ‘proof of principle’ study. *Gut*, 64, 2015.
- [9] R. J. Nicholls and R. R. Dozois. *Surgery of the colon & rectum*. Churchill Livingstone, New York, 1 edition, 1997.
- [10] J. T. Collins and M. Badireddy. *Anatomy, Abdomen and Pelvis, Small Intestine*. StatPearls Publishing, 2019.
- [11] G. E. Weissengruber. Topographic-anatomical description of the ventriculus, intestinum tenue, intestinum crassum and their arteries of the mara (Dolichotis patagonum Desmarest 1820). *Anatomia, Histologia, Embryologia: Journal of Veterinary Medicine Series C*, 29(2):87–95, 2000.

References

- [12] J.C. Slieker. *Improving quality in colorectal surgery*. Phd, Erasmus University Rotterdam, 2014.
- [13] P. Kahai and S. Lobo. *Anatomy, Abdomen and Pelvis, Large Intestine*. StatPearls Publishing, 2019.
- [14] M. Hickey, N. Samuels, N. Randive, R. M. Langford, and P. A. Kyriacou. Development and evaluation of a photometric fibre-optic sensor for monitoring abdominal organ photoplethysmographs and blood oxygen saturation. *Proceedings of SPIE*, 7503, 2009.
- [15] M. Rutegård and J. Rutegård. Anastomotic leakage in rectal cancer surgery: The role of blood perfusion. *World journal of gastrointestinal surgery*, 7(11): 289–92, 2015.
- [16] A. J. Pappano and W. G Wier. The Microcirculation and Lymphatics. In *Cardiovascular Physiology*, chapter 8, pages 153–170. Philadelphia, 10 edition, 2013. ISBN 9780323086974. doi: 10.1016/B978-0-323-08697-4.00008-3.
- [17] E. Fait, W. Malkusch, and S. H. Gnoth. Microvascular Patterns of the Human Large Intestine: Morphometric Studies of Vascular Parameters in Corrosion Casts. *eCM Journal*, 12(4):641, 1998.
- [18] D. N. Granger, P. R. Kvietys, R. J. Korthuis, and A. J. Premen. Microcirculation of the intestinal mucosa. In *Comprehensive Physiology*, pages 1405–1474. John Wiley & Sons, Inc., Hoboken, NJ, USA, 2011.
- [19] H. Gray. The Veins: The Portal System of Veins, 1918. URL <http://www.bartleby.com/107/174.html>.
- [20] K. B. Corbin. The advanced degree in graduate medical education. *Journal of medical education*, 30(5):270–4, 1955.
- [21] P. R. Kvietys. Gastrointestinal Circulation and Mucosal Pathology I: Ischemia/Reperfusion. In Morgan & Claypool Life Sciences, editor, *The Gastrointestinal Circulation*, chapter 10. Morgan & Claypool Life Sciences, 2010.
- [22] C. Washington and J. Carmichael. Management of ischemic colitis. *Clinics in Colon and Rectal Surgery*, 25(4):228–235, 2012.
- [23] C. Corke and K. Glenister. Monitoring intestinal ischaemia. *Critical care and resuscitation: Journal of the Australasian Academy of Critical Care Medicine*, 3(3):176–80, 2001.
- [24] J. Hopkins. Stage I Colorectal Surgery, 2008. URL <http://www.hopkinscoloncancercenter.org>.
- [25] J. Pickleman, W. Watson, J. Cunningham, S. G. Fisher, and R. Gamelli. The failed gastrointestinal anastomosis: An inevitable catastrophe? *Journal of the American College of Surgeons*, 188(5):473–482, 1999.

-
- [26] N. Komen. *New approaches towards risk assessment , diagnosis and prevention strategies of colorectal anastomotic leakage*. PhD thesis, Erasmus University, Rotterdam, 2014.
- [27] F. Goulder. Bowel anastomoses: The theory, the practice and the evidence base. *World Journal of Gastrointestinal Surgery*, 4(9):208–213, 2012.
- [28] C. Wheelless and J. Smith. A comparison of the flow of iodine 125 through three different intestinal anastomoses: Standard, Gambee, and Stapler. *Obstetrics & Gynecology*, 62(4):513–518, 1983.
- [29] N. A. Hirst, J. P. Tiernan, P. A. Millner, and D. G. Jayne. Systematic review of methods to predict and detect anastomotic leakage in colorectal surgery. *Colorectal Disease*, 16(2):95–109, 2014.
- [30] L. Urbanavičius, P. Pattyn, D. Putte, and D. Venskutonis. How to assess intestinal viability during surgery: A review of techniques. *World Journal of Gastrointestinal Surgery*, 3(5):59–69, 2011.
- [31] W. M. Chambers and N. J. Mortensen. Postoperative leakage and abscess formation after colorectal surgery. *Best Practice & Research Clinical Gastroenterology*, 18(5):865–880, 2004.
- [32] S. Nachiappan, A. Askari, A. Currie, R. H. Kennedy, and O. Faiz. Intraoperative assessment of colorectal anastomotic integrity: A systematic review. *Surgical Endoscopy*, 28(9):2513–2530, 2014.
- [33] A. Karliczek, D. A. Benaron, C. J. Zeebregts, T. Wiggers, and G. M. van Dam. Intraoperative Ischemia of the Distal End of Colon Anastomoses as Detected With Visible Light Spectroscopy Causes Reduction of Anastomotic Strength. *Journal of Surgical Research*, 152(2):288–295, 2009.
- [34] R. Fröjse. *Exploring Intestinal Ischemia: An experimental study*. PhD thesis, Umea, 2005.
- [35] T. Abay. *Investigation of Non-Invasive Optic Techniques in the Assessment of Forearm Tissue Perfusion during Cuff-Induced Vascular Occlusion in Healthy Volunteers*. Mphil thesis, City University London, 2013.
- [36] M. Hickey. *A new fibre optic photoplethysmographic sensor for the assessment of splanchnic organ perfusion*. PhD thesis, City University London, 2009.
- [37] T. Zaman. *Optical sensors for the in vivo assessment of flap perfusion in plastic surgery*. PhD thesis, City University London, 2013.
- [38] T. Abay. *Reflectance Photoplethysmography for Non-invasive Monitoring of Tissue Perfusion*. PhD thesis, City, University of London, 2016.
- [39] R. J. Strand-Amundsen, J. O. Høgetveit, H. M. Reims, F. P. Reinholt, T. E. Ruud, R. Yang, and T. I. Tønnessen. Ischemia/reperfusion injury in porcine intestine - Viability assessment. *World Journal of Gastroenterology*, 24(18), 2009.

References

- [40] J. B. Bussemaker and J. Lindeman. Comparison of Methods to Determine Viability of Small Intestine. *Annals of Surgery*, 176(1):97–101, 1972.
- [41] P. J. Orland, G. A. Czi, J. L. Semmlow, M. T. Reddell, and R. E. Brodin. Determination of Small Bowel Viability Using Myoelectric and Colour Analysis. *Journal of Surgical Research*, 55(6):581–587, 1993.
- [42] E. R. La Hei and A. Shun. Intra-operative pulse oximetry can help determine intestinal viability. *Pediatric surgery international*, 17(2-3):120–1, 2001.
- [43] E. N. Yilmaz, A. C. Vahl, G. Van Rij, S. H. M. Nauta, H. L. F. Brom, and J. A. Rauwerda. Endoluminal pulse oximetry of the sigmoid colon and the monitoring of the colonic circulation. *Cardiovascular Surgery*, 7(7):704–709, 1999.
- [44] A. W. Hewlett. The Significance of Pulse Form. *Journal of the American Medical Association*, 67(16):1134–1136, 1916.
- [45] J. F. Moran. Pulse. In HK Walker, WD Hall, and JW Hurst, editors, *Clinical Methods: The History, Physical, and Laboratory Examinations*, chapter 17. Boston: Butterworths, 3 edition, 1990. ISBN 040990077X.
- [46] A. Raabe, J. Beck, R. Gerlach, M. Zimmermann, and V. Seifert. Near-infrared Indocyanine Green Video Angiography: A New Method For Intraoperative Assessment of Vascular Flow. *Neurosurgery*, 52(1):132–139, 2003.
- [47] D. Lawson, I. Norley, G. Korbon, R. Loeb, and J. Ellis. Blood Flow Limits and Pulse Oximeter Signal Detection. Technical Report 4, University of Virginia Medical Center, 1987.
- [48] M. Erikoglu, A. Kaynak, E. A. Beyatli, and H. Toy. Intraoperative Determination of Intestinal Viability: A Comparison with Transserosal Pulse Oximetry and Histopathological Examination. *Journal of Surgical Research*, 128(1):66–9, 2005.
- [49] S. Petterson, C. Kuchta, and L. Snyder-Mackler. Aerobic Metabolism during Exercise. In Robert Donatelli, editor, *Sports-Specific Rehabilitation*, chapter 4, pages 65–85. Churchill Livingstone, 1 edition, 2007. ISBN 9780443066429.
- [50] S. C. Dennis and T. D. Noakes. Exercise: Metabolic Requirements, 2003.
- [51] F. W. Blaisdell. The pathophysiology of skeletal muscle ischemia and the reperfusion syndrome: a review. *Cardiovascular surgery*, 10(6):620–30, 2002.
- [52] H. W. Wallmann. Muscle Fatigue. In Robert Donatelli, editor, *Sports-Specific Rehabilitation*, chapter 5, pages 87–95. Churchill Livingstone, 1 edition, 2007. ISBN 9780443066429.
- [53] L. L. Spriet. Anaerobic metabolism in human skeletal muscle during short-term, intense activity. *Canadian journal of physiology and pharmacology*, 70(1):157–65, 1992.
- [54] A. Theodoropoulou and I. Koutroubakis. Ischemic colitis: Clinical practice in diagnosis and treatment. *World Journal of Gastroenterology*, 14(48):7302–7308, 2008.

-
- [55] A. T. Stearns and J. T. Jenkins. Assessing Anastomotic Integrity and Perfusion. In Christopher Schlachta and Patricia Sylla, editors, *Current Common Dilemmas in Colorectal Surgery*, chapter 31, pages 355–367. Springer, Cham, 1 edition, 2018. ISBN 9783319701172.
- [56] Y. Mendelson and B. D. Ochs. Noninvasive pulse oximetry utilizing skin reflectance photoplethysmography. *IEEE Transactions on Biomedical Engineering*, 35(10):798–805, 1988.
- [57] R. E. Brolin, P. J. Orland, G. Cazi, J. L. Semmlow, and C. Bibbo. Comparison of Blood Flow and Myoelectric Measurements in Two Chronic Models of Mesenteric Ligation. *Archives of Surgery*, 130(2):147–152, 1995.
- [58] D. J. Glotzer, A. H. Villegas, S. Anekamaya, and R. S. Shaw. Healing of the intestine in experimental bowel infarction. *Annals of Surgery*, 155(2):183–90, 1962.
- [59] T. F. Gorey. The recovery of intestine after ischaemic injury. *British Journal of Surgery*, 67(10):699–702, 1980.
- [60] S. D. Shah and C. A. Andersen. Prediction of Small Bowel Viability Using Doppler Ultrasound. *Annals of Surgery*, 194(1):97–99, 1981.
- [61] R. E. Brolin, J. L. Semmlow, J. W. Mackenzie, and M. T. Reddell. Quantitative myoelectric determination of bowel viability. *Journal of Surgical Research*, 41(6):557–562, 1986.
- [62] J. L. Semmlow and R. Brolin. Instrumentation for quantitative assessment of intestinal viability. *IEEE Transactions on Biomedical Engineering*, 35(10):888–892, 1988.
- [63] S. S. Hegde, S. A. Seidel, J. K. Ladipo, L. A. Bradshaw, S. Halter, and W. O. Richards. Effects of Mesenteric Ischemia and Reperfusion on Small Bowel Electrical Activity. *Journal of Surgical Research*, 74(1):86–95, 1998.
- [64] M. Sethi, J. Zagzag, K. Patel, M. Magrath, E. Somoza, M. S. Parikh, J. K. Saunders, A. Ude-Welcome, B. F. Schwack, M. S. Kurian, G. A. Fielding, and C. J. Ren-Fielding. Intraoperative leak testing has no correlation with leak after laparoscopic sleeve gastrectomy. *Surgical Endoscopy*, 30(3):883–891, 2016.
- [65] J. T. Maple, S. Banerjee, B. A. Barth, Y. M. Bhat, D. J. Desilets, K. T. Gottlieb, P. R. Pfau, D. K. Pleskow, U. D. Siddiqui, J. L. Tokar, A. Wang, L. W. K. Song, and S. A. Rodriguez. Methods of luminal distention for colonoscopy. *Gastrointestinal Endoscopy*, 77(4):519–525, 2013.
- [66] S. L. Klein, J. E. Israel, and R. T. Kronengold. New burst test method for comparing strengths of blood vessel repairs. *Microsurgery*, 16(2):118–21, 1995.
- [67] A. H. Davies, D. C. Bartolo, A. E. Richards, C. D. Johnson, and N. J. McC Mortensen. Intra-operative air testing: an audit on rectal anastomosis. *Annals of the Royal College of Surgeons of England*, 70(6):345–7, 1988.

References

- [68] Z. Wu, R. C. J. van de Haar, C. L. Sparreboom, Geesien S. A. Boersema, Z. Li, J. Ji, J. Jeekel, and J. F. Lange. Is the intraoperative air leak test effective in the prevention of colorectal anastomotic leakage? A systematic review and meta-analysis. *International Journal of Colorectal Disease*, 31(8):1409–1417, 2016.
- [69] S. Kwon, A. Morris, R. Billingham, J. Frankhouse, K. Horvath, M. Johnson, S. Mcnevin, A. Simons, R. Symons, S. Steele, R. Thirlby, M. Whiteford, D. R. Flum, D. Kwon, F. Horvath, and M. Symons. Routine Leak Testing in Colorectal Surgery in the Surgical Care and Outcomes Assessment Program. *Archives of Surgery*, 147(4):345–351, 2012.
- [70] D. A. Sherwinter, J. Gallagher, and T. Donkar. Intra-operative transanal near infrared imaging of colorectal anastomotic perfusion: a feasibility study. *Colorectal Disease*, 15(1):91–96, 2012.
- [71] T. Kamal, A. Pai, V. R. Velchuru, M. Zawadzki, J. J. Park, S. J. Marecik, H. Abcarian, and L. M. Prasad. Should anastomotic assessment with flexible sigmoidoscopy be routine following laparoscopic restorative left colorectal resection? *Colorectal Disease*, 17(2):160–164, 2015.
- [72] S. Y. Yang, J. Han, Y D. Han, M. S. Cho, H. Hur, K. Y. Lee, N. K. Kim, and B. S. Min. Intraoperative colonoscopy for the assessment and prevention of anastomotic leakage in low anterior resection for rectal cancer. *International Journal of Colorectal Disease*, 32(5):709–714, 2017.
- [73] S. Smith, W. McGeehin, R. A. Kozol, and D. Giles. The efficacy of intraoperative methylene blue enemas to assess the integrity of a colonic anastomosis. *BMC surgery*, 7(1):15, 2007.
- [74] J. D. Beard, M. L. Nicholson, R. D. Sayers, D. Lloyd, and N. W. Everson. Intraoperative air testing of colorectal anastomoses: A prospective, randomized trial. *British Journal of Surgery*, 77(10):1095–1097, 1990.
- [75] R. Yalin, A. O. Aktan, C. Yeğen, H. Döşlüoğlu, and N. Okboy. Importance of testing stapled rectal anastomoses with air. *The European journal of surgery*, 159(1):49–51, 1993.
- [76] Y. Sakanoue, K. Nakao, Y. Shoji, H. Yanagi, M. Kusunoki, and J. Utsunomiya. Intraoperative colonoscopy. *Surgical Endoscopy*, 7(2):84–87, 1993.
- [77] F. Lazorthes and P. Chiotassol. Stapled colorectal anastomoses: peroperative integrity of the anastomosis and risk of postoperative leakage. *International Journal of Colorectal Disease*, 1(2):96–98, 1986.
- [78] C. D. Griffith and J. D. Hardcastle. Intraoperative testing of anastomotic integrity after stapled anterior resection for cancer. *Journal of the Royal College of Surgeons of Edinburgh*, 35(2):106–8, 1990.
- [79] J. M. D. Wheeler and J. M. Gilbert. Controlled intraoperative water testing of left-sided colorectal anastomoses: are ileostomies avoidable? *Annals of The Royal College of Surgeons of England*, 81(2):105–108, 1999.

-
- [80] R. Ricciardi, P. L. Roberts, P. W. Marcello, J. F. Hall, T. E. Read, and D. J. Schoetz. Anastomotic Leak Testing After Colorectal Resection. *Archives of Surgery*, 144(5):407, 2009.
- [81] S. Ishihara, T. Watanabe, and H. Nagawa. Intraoperative colonoscopy for stapled anastomosis in colorectal surgery. *Surgery Today*, 38(11):1063–1065, 2008.
- [82] C. L. Sparreboom, Z. Wu, J. Ji, and J. F. Lange. Integrated approach to colorectal anastomotic leakage: Communication, infection and healing disturbances. *World Journal of Gastroenterology*, 22(32):7226, 2016.
- [83] J. M. Gilbert and J. E. Trapnell. Intraoperative testing of the integrity of left-sided colorectal anastomoses: a technique of value to the surgeon in training. *Annals of the Royal College of Surgeons of England*, 70(3):158–160, 1988.
- [84] R. Schwab, S. Weßendorf, A. Gutcke, and H. Becker. Early bursting strength of human colon anastomoses – an in vitro study comparing current anastomotic techniques. *Langenbeck’s Archives of Surgery*, 386(7):507–511, 2002.
- [85] B. Middleton. *Physics in Anaesthesia*. Scion Pub. Ltd, 1 edition, 2012. ISBN 9781904842989.
- [86] W. H. Pearce, D. N. Jones, G. H. Warren, E. J. Bartle, T. A. Whitehill, and R. B. Rutherford. Identifying Early Intestinal Ischemia. *Archives of Surgery*, 122(3):308–310, 1986.
- [87] A. Ntelezos, F. Guarato, and J. F. C. Windmill. The anti-bat strategy of ultrasound absorption: the wings of nocturnal moths (Bombycoidea: Saturniidae) absorb more ultrasound than the wings of diurnal moths (Chalcosiinae: Zygaenoidea: Zygaenidae). *Biology Open*, 6(1):109–117, Jan 2017.
- [88] T. G. Lynch, R. W. Hobson, J. C. Kerr, D. A. Brousseau, D. G. Silverman, C. A. Reilly, and H. Tseng. Doppler ultrasound, laser Doppler, and perfusion fluorometry in bowel ischemia. *Archives of Surgery*, 123(4):483–486, 1988.
- [89] V. Crabtree. *Non-invasive vascular assessment using photoplethysmography*. PhD thesis, Loughborough University, 2003.
- [90] M. Cooperman, W. G. Pace, E. W. Jr. Martin, B. Pflug, L. M. Jr. Keith, W. E. Evans, and L. C. Carey. Determination of viability of ischemic intestine by Doppler ultrasound. *Surgery*, 83(6):705–710, 1978.
- [91] G. Maconi, V. Imbesi, and G. Bianchi Porro. Doppler ultrasound measurement of intestinal blood flow in inflammatory bowel disease. *Scandinavian Journal of Gastroenterology*, 31(6):590–593, 1996.
- [92] G. B. Bulkley, G. D. Zuidema, S. R. Hamilton, C. S. O’Mara, P. G. Klacsmann, and S. D. Horn. Intraoperative determination of small intestinal viability following ischemic injury: a prospective, controlled trial of two adjuvant methods (Doppler and fluorescein) compared with standard clinical judgment. *Annals of Surgery*, 193(5):628–37, 1981.

References

- [93] M. Cooperman, E. W. Martin, W. E. Evans, and L. C. Carey. Doppler Malformation. *Annals of Surgery*, 190(1):24–26, 1979.
- [94] R. W. Hobson, C. B. Wright, N. M. Rich, and G. J. Collins. Assessment of colonic ischemia during aortic surgery by Doppler ultrasound. *Journal of Surgical Research*, 20(3):231–235, 1976.
- [95] M. Ando, M. Ito, Z. Nihei, and K. Sugihara. Assessment of intestinal viability using a non-contact laser tissue blood flowmeter. *American Journal of Surgery*, 180(3):176–180, 2000.
- [96] H. D. Zacho and J. Abrahamsen. Chronic intestinal ischaemia: Diagnosis. *Clinical Physiology and Functional Imaging*, 28(2):71–75, 2008.
- [97] A. J. Crerar-Gilbert, P. A. Kyriacou, D. P. Jones, and R. M. Langford. Assessment of photoplethysmographic signals for the determination of splanchnic oxygen saturation in humans. *Anaesthesia*, 57(5):442–445, 2002.
- [98] A. Lima and J. Bakker. Noninvasive monitoring of peripheral perfusion. *Intensive Care Medicine*, 31(2):1316–1326, 2005.
- [99] M. Siegemund, J. Van Bommel, and C. Ince. Assessment of regional tissue oxygenation. *Intensive Care Medicine*, 25(1):1044–1060, 1999.
- [100] P. J. Sheffield. Measuring tissue oxygen tension: a review. *Undersea & hyperbaric medicine: Journal of the Undersea and Hyperbaric Medical Society*, 25(3):179–88, 1998.
- [101] J D Whitney. The measurement of oxygen tension in tissue. *Nursing Research*, 39(4):203–206, 1990.
- [102] J. Webster. *Design of Pulse Oximeters*. Taylor & Francis Ltd, New York, 1 edition, 1997. ISBN 9780750304672.
- [103] H. B. Kram and W. C. Shoemaker. Method for intraoperative assessment of organ perfusion and viability using a miniature oxygen sensor. *American Journal of Surgery*, 148(3):404–7, 1984.
- [104] B. Vallet, N. Lund, S. E. Curtis, D. Kelly, and S. M. Cain. Gut and muscle tissue PO₂ in endotoxemic dogs during shock and resuscitation. *Journal of Applied Physiology*, 76(2):793–800, 1994.
- [105] C. Piasecki. A new method for the assessment of gut viability. *British Journal of Surgery*, 68(5):319–322, 1981.
- [106] M. Haisjackl, G. Luz, H. Sparr, R. Germann, N. Salak, B. Friesenecker, E. Deusch, S. Meusburger, and W. Hasibeder. The Effects of Progressive Anemia on Jejunal Mucosal and Serosal Tissue Oxygenation in pigs. *Anesthesia and Analgesia*, 84(3):538–544, 1997.

-
- [107] M. Haisjackl, R. Germann, W. Hasibeder, B. Schwarz, N. Salak, W. Pajk, J. Bonatti, W. Nussbaumer, G. Klima, W. Kox, and N. Mutz. Mucosal tissue oxygenation of the porcine jejunum during normothermic cardiopulmonary bypass. *British Journal of Anaesthesia*, 82(5):738–745, 1999.
- [108] K. Armbruster, G. F. Nöldge-Schomburg, I. M. Dressler, A. J. Fittkau, J. Haberstroh, and K. Geiger. The effects of desflurane on splanchnic hemodynamics and oxygenation in the anesthetized pig. *Anesthesia and Analgesia*, 84(2):271–7, 1997.
- [109] Å. Mellström, P. Månsson, K. Jönsson, and M. Hartmann. Measurements of Subcutaneous Tissue PO₂ Reflect Oxygen Metabolism of the Small Intestinal Mucosa during Hemorrhage and Resuscitation. *European Surgical Research*, 42(2):122–129, 2009.
- [110] W. Pajk, K. Stadlbauer, A. Kleinsasser, O. Kotzinger, H. Ulmer, W. Hasibeder, and H. Knotzer. The impact of endotoxin on jejunal tissue oxygenation. *Microcirculation*, 24(6):e12379, 2017.
- [111] W. G. Sheridan, R. H. Lowndes, and H. L. Young. Tissue oxygen tension as a predictor of colonic anastomotic healing. *American Society of Colon and Rectal Surgeons*, 30:867–871, 1987.
- [112] T. Koch, S. Geiger, and M. J. Ragaller. Monitoring of organ dysfunction in sepsis/systemic inflammatory response syndrome: novel strategies. *Journal of the American Society of Nephrology*, 12(1):S53–9, 2001.
- [113] P. U. Reber, M. Peter, A. G. Patel, E. Stauffer, G. Printzen, D. Mettler, H. Hakki, and H. W. Kniemeyer. Ischaemia/Reperfusion Contributes to Colonic Injury Following Experimental Aortic Surgery. *European Journal of Vascular and Endovascular Surgery*, 21(1):35–39, 2001.
- [114] C. A. Jacobi, H. U. Zieren, J. Zieren, and J. M. Müller. Is tissue oxygen tension during esophagectomy a predictor of esophagogastric anastomotic healing? *Journal of Surgical Research*, 74(2):161–4, 1998.
- [115] A. Thorén, A. Nygren, E. Houltz, and S. E. Ricksten. Cardiopulmonary bypass in humans - Jejunal mucosal perfusion increases in parallel with well-maintained microvascular hematocrit. *Acta Anaesthesiologica Scandinavica*, 49(4):502–509, 2005.
- [116] S. McGuinness, A. Mckee, and D. Sidebotham. *Cardiothoracic Critical Care*. Elsevier, 1 edition, 2007. ISBN 9780750675727.
- [117] N. Rémi, J. Chagnon, T. Jean-Louis, V. Benoit, and W. Francis. Small intestine intramucosal PCO₂ and microvascular blood flow during hypoxic and ischemic hypoxia. *Critical Care Medicine*, 30(2):379–384, 2002.
- [118] R. G. Fiddian-Green. Remote sensing tonometric catheter apparatus and method, 2001.

References

- [119] R. G. Fiddian-Green. *Yearbook of Intensive Care and Emergency Medicine 1993*. Springer Berlin Heidelberg, Berlin, Heidelberg, 1993. ISBN 978-3-540-56463-8.
- [120] A. B. J. Groeneveld and J. J. Kolkman. Splanchnic tonometry: a review of physiology, methodology, and clinical applications. *Journal of Critical Care*, 9(3):198–210, 1994.
- [121] R. G. Fiddian-Green. Prediction of the Development of Sigmoid Ischemia on the Day of Aortic Operations. *Archives of Surgery*, 121(6):654, 1986.
- [122] L. J. D. van Dijk, L. M. G. Moons, D. van Noord, A. Moelker, H. J. M. Verhagen, M. J. Bruno, and E. V. Rouwet. Persistent symptom relief after revascularization in patients with single-artery chronic mesenteric ischemia. *Journal of Vascular Surgery*, 68(3):779–785, 2018.
- [123] J. J. Tenhunen, H. Kosunen, E. Alhava, L. Tuomisto, and J. A. Takala. Intestinal luminal microdialysis: A new approach to access gut mucosal ischemia. *Anesthesiology*, 91(12):1807–1807, 1999.
- [124] M. E. Campbell, J. E. Van Aerde, P. Y. Cheung, and D. C. Mayes. Tonometry to estimate intestinal perfusion in newborn piglets. *Archives of Disease in Childhood - Fetal and Neonatal Edition*, 81(2):F105–F109, 1999.
- [125] R. Fröjse, S. Lehtipalo, O. Winsö, G. Johansson, B. Biber, and C. Arnerlöv. Assessment of Graded Intestinal Hypoperfusion and Reperfusion Using Continuous Saline Tonometry in a Porcine Model. *European Journal of Vascular and Endovascular Surgery*, 28(1):79–88, 2004.
- [126] I. Koga, H. Stiernström, and L. Wiklund. Sigmoid colonic reflectance pulse oximetry and tonometry in a porcine experimental hypoperfusion shock model. *Acta Anaesthesiologica Scandinavica*, 46(10):1212–1216, 2002.
- [127] M. Björck and B. Hedberg. Early detection of major complications after abdominal aortic surgery: Predictive value of sigmoid colon and gastric intramucosal ph monitoring. *British Journal of Surgery*, 81(1):25–30, 1994.
- [128] A. C. Vahl. Endoluminal pulse oximetry combined with tonometry to monitor the perfusion of the sigmoid during and after resection of abdominal aortic aneurysm. *Cardiovascular Surgery*, 5(1):65–70, 1997.
- [129] J. J. Kolkman, J. A. Otte, and A. B. Groeneveld. Gastrointestinal luminal PCO₂ tonometry: an update on physiology, methodology and clinical applications. *British Journal of Anaesthesia*, 84(1):74–86, 2000.
- [130] J. Pascual-Ramírez, L. G. Collar Viñuelas, J. Martín, G. Bernal, A. Bosque Castro, and N. García-Serrano. Mucosal Tonometry as Early Warning of Gastrojejunal Leak in Laparoscopic Roux-en-y Gastric Bypass. *Obesity Surgery*, 22(5):843–846, 2012.

-
- [131] H. Ozawa, Y. Imanishi, F. Ito, Y. Watanabe, T. Kato, H. Nameki, K. Isobe, and K. Ogawa. PiCO₂ Monitoring of Transferred Jejunum Perfusion Using an Air Tonometry Technique After Hypopharyngeal Cancer Surgery. *Medicine*, 94(11):e632, 2015.
- [132] S. Höhne and V. Hesse. Standard values for gas-perfusion manometry of the esophagus. *Medicine*, 97(8):e9910, 2018.
- [133] E. Bennett-Guerrero, M. H. Panah, C. A. Bodian, B. J. Methikalam, J. R. Alfarone, M. DePerio, and M. G. Mythen. Automated detection of gastric luminal partial pressure of carbon dioxide during cardiovascular surgery using the Tonocap. *Anesthesiology*, 92(1):38–45, 2000.
- [134] J. Creteur, D. De Backer, and J. L. Vincent. Does gastric tonometry monitor splanchnic perfusion? *Critical Care Medicine*, 27(11):2480–2484, 1999.
- [135] F. Daams, Z. Wu, and H. Cakir. Identification of anastomotic leakage after colorectal surgery using microdialysis of the peritoneal cavity. *Techniques in Coloproctology*, 18:65–71, 2014.
- [136] S. Hsi-Lin and S. Hsi-Lin Chang. *Clinical evaluation of a new optical fibre method of measuring oxygen saturation using photoplethysmograph signals reflected from internal tissues*. PhD thesis, Queen Mary University of London, 2013.
- [137] M. K. Wax. The role of the implantable Doppler probe in free flap surgery. *The Laryngoscope*, 124:S1–S12, 2014.
- [138] F. Daams. Colorectal anastomotic leakage: Aspects of prevention, detection and treatment. *World Journal of Gastroenterology*, 19(15):2293, 2013.
- [139] R. Johansson. Microdialysis probe, 2004.
- [140] G. H. Hochmuth and R. Mischler. Microdialysis catheter and process for manufacture, 2009.
- [141] N. Högberg, P. Carlsson, L. Hillered, A. Stenbäck, and H. E. Lilja. Intraluminal intestinal microdialysis detects markers of hypoxia and cell damage in experimental necrotizing enterocolitis. *Journal of Pediatric Surgery*, 47(9):1646–1651, 2012.
- [142] L. Pynnönen, M. Minkkinen, A. Perner, S. Rätty, I. Nordback, J. Sand, and J. Tenhunen. Validation of Intraluminal and Intraperitoneal microdialysis in ischemic small intestine. *BMC Gastroenterology*, 13(170):1–8, 2013.
- [143] M. Jansson, K. and Jansson, M. Andersson, A. Magnuson, U. Ungerstedt, and L. Norgren. Normal values and differences between intraperitoneal and subcutaneous microdialysis in patients after non-complicated gastrointestinal surgery. *Scandinavian Journal of Clinical and Laboratory Investigation*, 65(4):273–281, 2005.

References

- [144] J. Ungerstedt, G. Nowak, B. Ericzon, and U. Ungerstedt. Intraperitoneal microdialysis (IPM): a new technique for monitoring intestinal ischemia studied in a porcine model. *Shock (Augusta, Ga.)*, 20(1):91–6, 2003.
- [145] T. Sommer and J. F. Larsen. Intraperitoneal and intraluminal microdialysis in the detection of experimental regional intestinal ischaemia. *British Journal of Surgery*, 91(7):855–861, 2004.
- [146] H. Birke-Sorensen and N. T. Andersen. Metabolic markers obtained by microdialysis can detect secondary intestinal ischemia: An experimental study of ischemia in porcine intestinal segments. *World Journal of Surgery*, 34(5):923–932, 2010.
- [147] M. E. Pedersen, N. Qvist, C. Bisgaard, U. Kelly, A. Bernhard, and S. M. Pedersen. Peritoneal Microdialysis. Earlydiagnosis of Anastomotic Leakage after Low Anterior Resection for Rectosigmoid Cancer. *Scandinavian Journal of Surgery*, 98(3):148–154, 2009.
- [148] E. C. Wright, P. Connolly, M. Vella, and S. Moug. Peritoneal fluid biomarkers in the detection of colorectal anastomotic leaks: a systematic review. *International Journal of Colorectal Disease*, 32(7):935–945, 2017.
- [149] M. Hellan, G. Spinoglio, A. Pigazzi, and J. A. Lagares-Garcia. The influence of fluorescence imaging on the location of bowel transection during robotic left-sided colorectal surgery. *Surgical Endoscopy and Other Interventional Techniques*, 28(5):1695–1702, 2014.
- [150] B. Seeliger, M. Barberio, A. D. Urso, V. Agnus, F. Longo, P. Mascagni, J. Marescaux, D. Mutter, and M. Diana. Fluorescence in rectal cancer surgery. *Annals of Laparoscopic and Endoscopic Surgery*, 47(3):1–10, 2018.
- [151] C. Lim, A. Malek, R. Martins, S. Petillon, G. Boulate, H. Hentati, N. De’Angelis, F. Brunetti, C. Salloum, A. Laurent, P. Compagnon, and D. Azoulay. Real-time assessment of intestinal viability using indocyanine green fluorescent imaging (with video). *Journal of Visceral Surgery*, 152(1):71–72, 2015.
- [152] M Miwa. The Principle of ICG Fluorescence Method. *The Open Surgical Oncology Journal*, 2:26–28, 2010.
- [153] L. Boni, G. David, A. Mangano, G. Dionigi, S. Rausei, S. Spampatti, E. Cassinotti, and A. Fingerhut. Clinical applications of indocyanine green (ICG) enhanced fluorescence in laparoscopic surgery. *Surgical Endoscopy*, 29(7):2046–2055, 2015.
- [154] J. A. Solís-lemus. *Segmentation and Shape Tracking of Overlapping Macrophages in Fluorescent Microscopy Images*. Phd thesis, City, University of London, 2018.
- [155] J. Paral, F. Cecka, and M. Chobola. Fluorescein dye and ultraviolet light technique in diagnosis of small bowel ischaemia. *Journal of surgery*, 80(10):762–3, 2010.
- [156] J. Rittscher, R. Machiraju, and S. T. C. Wong. *Microscopic image analysis for life science applications*. Artech House, 2008. ISBN 1596932376.

-
- [157] F. Ris, R. Hompes, C. Cunningham, I. Lindsey, R. Guy, O. Jones, B. George, R. A. Cahill, and N. J. Mortensen. Near-infrared (NIR) perfusion angiography in minimally invasive colorectal surgery. *Surgical Endoscopy and Other Interventional Techniques*, 28(7):2221–2226, 2014.
- [158] D. R. C. James, F. Ris, T. M. Yeung, R. Kraus, N. C. Buchs, N. J. Mortensen, and R. J. Hompes. Fluorescence angiography in laparoscopic low rectal and anorectal anastomoses with pinpoint perfusion imaging- a critical appraisal with specific focus on leak risk reduction. *Colorectal Disease*, 17:16–21, 2015.
- [159] Y. Shimada, T. Okumura, T. Nagata, S. Sawada, K. Matsui, R. Hori, I. Yoshioka, T. Yoshida, R. Osada, and K. Tsukada. Usefulness of blood supply visualization by indocyanine green fluorescence for reconstruction during esophagectomy. *Esophagus*, 8:259–266, 2011.
- [160] D. A. Sherwinter. Transanal near-infrared imaging of colorectal anastomotic perfusion. *Surgical Laparoscopy, Endoscopy & Percutaneous Techniques*, 22(5):433–6, 2012.
- [161] L. Boni, A. Fingerhut, A. Marzorati, S. Rausei, G. Dionigi, and E. Cassinotti. Indocyanine green fluorescence angiography during laparoscopic low anterior resection: results of a case-matched study. *Surgical Endoscopy*, 31(4):1836–1840, 2017.
- [162] R. Blanco-Colino and E. Espin-Basany. Intraoperative use of ICG fluorescence imaging to reduce the risk of anastomotic leakage in colorectal surgery: a systematic review and meta-analysis. *Techniques in Coloproctology*, 22(1):15–23, 2018.
- [163] F. W. Prinzen and J. B. Bassingthwaite. Blood flow distributions by microsphere deposition methods. *Cardiovascular Research*, 45(1):13–21, 2000.
- [164] T. Wada, K. Kawada, R. Takahashi, M. Yoshitomi, K. Hida, S. Hasegawa, and Y. Sakai. ICG fluorescence imaging for quantitative evaluation of colonic perfusion in laparoscopic colorectal surgery. *Surgical Endoscopy*, 31(10):4184–4193, 2017.
- [165] M. Diana, E. Noll, P. Diemunsch, B. Dallemagne, M. A. Benahmed, V. Agnus, L. Soler, B. Barry, I. J Namer, N. Demartines, A. Charles, B. Geny, and J. Marescaux. Enhanced-Reality Video Fluorescence. *Annals of Surgery*, 259(4):700–707, 2014.
- [166] S. Kudzus, C. Roesel, A. Schachtrupp, and J. J. Höer. Intraoperative laser fluorescence angiography in colorectal surgery: a noninvasive analysis to reduce the rate of anastomotic leakage. *Langenbeck’s Archives of Surgery*, 395(8):1025–1030, 2010.
- [167] R. Weigert, M. Sramkova, L. Parente, and A. Masedunskas. Intravital microscopy: a novel tool to study cell biology in living animals. *Histochemistry and Cell Biology*, 133(5):481–491, 2010.

References

- [168] A. Masedunskas, O. Milberg, N. Porat-Shliom, and M. Sramkova. Intravital microscopy: A practical guide on imaging intracellular structures in live animals. *BioArchitecture*, 2(5):143–157, 2012.
- [169] J. Secklehner, C. L. Celso, and L. M. Carlin. Intravital microscopy in historic and contemporary immunology. *Immunology and Cell Biology*, 95(6):506–513, 2017.
- [170] D. Fiole and J. N. Tournier. Intravital microscopy of the lung: minimizing invasiveness. *Journal of Biophotonics*, 9(9):868–878, 2016.
- [171] R. Düchs and T. Foitzik. Possible pitfalls in the interpretation of microcirculatory measurements: A comparative study using intravital microscopy, spectroscopy and polarographic pO₂ measurements. *European Surgical Research*, 40(1):47–54, 2008.
- [172] S. Y. Yuan and R. R. Rigor. Structure and function of exchange microvessels. In *Regulation of Endothelial Barrier Function*, chapter 2. Morgan & Claypool Life Sciences, 2010.
- [173] T. Kurata, Z. Li, S. Oda, H. Kawahira, and H. Haneishi. Impact of vessel diameter and bandwidth of illumination in sidestream dark-field oximetry. *Biomedical Optics Express*, 6(5):1616–31, 2015.
- [174] U. Kubitscheck. *Fluorescence Microscopy*. Wiley-VCH Verlag GmbH & Co. KGaA, Weinheim, Germany, 2017. ISBN 9783527687732.
- [175] T. Fukuhara, Y. Ueda, Y. Kamioka, K. Okazaki, and T. Kinashi. P030 Intravital observation system of the colon by two photon excitation microscopy. In *Journal of Crohn's and Colitis*, page S108, 2018.
- [176] K. Goto, G. Kato, I. Kawahara, Y. Luo, K. Obata, H. Misawa, T. Ishikawa, H. Kuniyasu, J. Nabekura, and M. Takaki. In Vivo Imaging of Enteric Neurogenesis in the Deep Tissue of Mouse Small Intestine. *PLoS ONE*, 8(1):e54814, 2013.
- [177] S. Hashimoto, M. Honda, T. Takeichi, M. Sakisaka, Y. Narita, D. Yoshii, K. Uto, S. Sakamoto, and Y. Inomata. Intravital imaging of neutrophil recruitment in intestinal ischemia-reperfusion injury. *Biochemical and Biophysical Research Communications*, 495(3):2296–2302, 2018.
- [178] R. Diller, U. Stratmann, T. Helmschmied, G. Bäumer, R. Bahde, E. Minin, and H. U. Spiegel. Microcirculatory Dysfunction in Endotoxemic Bowel Anastomosis: The Pathogenetic Contribution of Microcirculatory Dysfunction to Endotoxemia-Induced Healing Impairment. *Journal of Surgical Research*, 150(1):3–10, 2008.
- [179] I. Farquhar, C. M. Martin, C. Lam, R. Potter, C. G. Ellis, and W. J. Sibbald. Decreased Capillary Density in Vivo in Bowel Mucosa of Rats with Normotensive Sepsis 1. *Journal of Surgical Research*, 61:190–196, 1996.

-
- [180] P. Biberthaler and S. Langer. Comparison of the New OPS Imaging Technique with Intravital Microscopy: Analysis of the Colon Microcirculation. *European Surgical Research*, 34(1-2):124–128, 2002.
- [181] A. F. J. de Bruin and V. Kornmann. Sidestream dark field imaging of the serosal microcirculation during gastrointestinal surgery. *Colorectal Disease*, 18(3):O103–O110, 2016.
- [182] E. C. Boerma and K. Kaiferova. Rectal microcirculatory alterations after elective on-pump cardiac surgery. *Minerva Anestesiologica*, 77(7):698–703, 2011.
- [183] Z. Turek, V. Cerný, and R. Parížková. Noninvasive in vivo assessment of the skeletal muscle and small intestine serous surface microcirculation in rat: sidestream dark-field (SDF) imaging. *Physiological Research*, 57(3):365–71, 2008.
- [184] A. Andersson, M. Rundgren, S. Kalman, O. Rooyackers, O. Brattstrom, A. Oldner, S. Eriksson, and R. Frithiof. Gut microcirculatory and mitochondrial effects of hyperdynamic endotoxaemic shock and norepinephrine treatment. *British Journal of Anaesthesia*, 108(2):254–261, 2012.
- [185] S. D. Hurcombe, B. R. Welch, J. M. Williams, E. S. Cooper, D. Russell, and M. C. Mudge. Dark-field microscopy in the assessment of large colon microperfusion and mucosal injury in naturally occurring surgical disease of the equine large colon. *Equine Veterinary Journal*, 46(6):674–680, 2014.
- [186] C. Lehmann, I. Abdo, H. Kern, L. Maddison, D. Pavlovic, N. Sharawi, J. Starkopf, R. Hall, P. Johnson, L. Williams, and V. Cerny. Clinical evaluation of the intestinal microcirculation using sidestream dark field imaging-Recommendations of a round table meeting. *Clinical Hemorheology and Microcirculation*, 57(2):137–146, 2014.
- [187] E. C. Boerma, P. H.J. Van Der Voort, P. E. Spronk, and C. Ince. Relationship between sublingual and intestinal microcirculatory perfusion in patients with abdominal sepsis. *Critical Care Medicine*, 35(4):1055–1060, 2007.
- [188] J. D. Wayne, J. Aisenberg, and P. H. Rubin. Advanced Imaging Techniques. In *Practical Colonoscopy*, chapter 18, pages 178–185. John Wiley & Sons, Ltd, 1 edition, 2013.
- [189] A. Barbieri, M. L. Barretta, D. Rea, C. Picone, O. Fabozzi, G. Palma, L. Antonio, A. Federico, S. Bimonte, F. Setola, E. De Lutio Di Castelguidone, M. Castellano, A. G. D’Errico, M. Caraglia, and C. Arra. Intraluminal gel ultrasound and eco-color doppler: new tools for the study of colorectal cancer in mice. *In vivo (Athens, Greece)*, 27(4):443–50, 2013.
- [190] J. D. Wayne, J. Aisenberg, and P. H. Rubin. The Endoscopy Unit, Colonoscope, and Accessories. In *Practical Colonoscopy*, chapter 1, pages 3–15. John Wiley & Sons, Ltd, New York, NY, 2013.
- [191] S. Lee, Y. Park, D. Lee, and K. Kim. Colonoscopy procedural skills and training for new beginners. *World journal of gastroenterology*, 20(45):16984–95, 2014.

References

- [192] J. Baixauli. Investigation and management of ischemic colitis. *Cleveland Clinical Journal of Medicine*, 70(11), 2003.
- [193] D. R. Tobergte and S. Curtis. The endoscopic spectrum of colonic mucosal injury following aortic aneurysm resection. *Journal of Chemical Information and Modeling*, 53(9):1689–1699, 2013.
- [194] A. Sciuto, G. Merola, G. D. D. Palma, M. Sodo, F. Pirozzi, U. M. Bracale, and U. Bracale. Predictive factors for anastomotic leakage after laparoscopic colorectal surgery. *World Journal of Gastroenterology*, 24(21):2247–2260, 2018.
- [195] R. D. Fanelli. Intraoperative endoscopy: An important adjunct to gastrointestinal surgery. *Techniques in Gastrointestinal Endoscopy*, 15(4):184–190, 2013.
- [196] E. Lieto, M. Orditura, P. Castellano, M. Pinto, A. Zamboli, F. De Vita, C. Pignatelli, and G. Galizia. Endoscopic Intraoperative Anastomotic Testing May Avoid Early Gastrointestinal Anastomotic Complications. A Prospective Study. *Journal of Gastrointestinal Surgery*, 15(1):145–152, 2011.
- [197] S. Sujatha-Bhaskar and M. Jafari. An endoscopic mucosal grading system is predictive of leak in stapled rectal anastomoses. *Surgical Endoscopy*, 32:1769–1775, 2018.
- [198] Andreas Shamiyeh, Kornel Szabo, Wolfgang Ulf Wayand, and Joerg Zehetner. Intraoperative endoscopy for the assessment of circular-stapled anastomosis in laparoscopic colon surgery. *Surgical Laparoscopy, Endoscopy & Percutaneous Techniques*, 22(1):65–67, 2012.
- [199] M. Lanthaler, M. Biebl, R. Mittermair, D. Öfner, and H. Nehoda. Intraoperative Colonoscopy for Anastomosis Assessment in Laparoscopically Assisted Left-Sided Colon Resection: Is It Worthwhile? *Journal of Laparoendoscopic & Advanced Surgical Techniques*, 18(1):27–31, 2008.
- [200] O. Schmidt, S. Merkel, and W. Hohenberger. Anastomotic leakage after low rectal stapler anastomosis: significance of intraoperative anastomotic testing. *European Journal of Surgical Oncology (EJSO)*, 29(3):239–243, 2003.
- [201] M. S. Thomas and D. A. Margolin. Management of Colorectal Anastomotic Leak. *Clinics in Colon and Rectal Surgery*, 29(2):138–44, 2016.
- [202] V. V Simianu, A. Basu, R. Alfonso-Cristancho, R. C. Thirlby, A. D. Flaxman, and D. R. Flum. Assessing Surgeon Behavior Change after Anastomotic Leak in Colorectal Surgery. *Journal of Surgical Research*, 205(2):378–383, 2016.
- [203] J. D. Waye, J. Aisenberg, and P. H. Rubin. Teaching and Training in Colonoscopy. In *Practical Colonoscopy*, chapter 16, pages 167–174. John Wiley & Sons, Ltd, 2013.
- [204] H. Alsaadi and J. Delanghe. *A new High Sensitive Functional Nephelometrical Assay for Assaying C-reactive protein in Serum Based on Phosphocholine Interaction*. PhD thesis, Ghent University Hospital, 2013.

-
- [205] I. S. Reynolds, M. R. Boland, F. Reilly, A. Deasy, M. H. Majeed, J. Deasy, J. P. Burke, and D. A. McNamara. C-reactive protein as a predictor of anastomotic leak in the first week after anterior resection for rectal cancer. *Colorectal Disease*, 19(9):812–818, 2017.
- [206] A. Alam, A. Ahmed, R. Kumar, and R. G. Baxla. Role of C-Reactive Protein (CRP) in the Prediction of Anastomotic Leakage Following Gastrointestinal Surgery. *International Journal of Science and Research*, 6(1):21–31, 2017.
- [207] B. Clyne and J. S. Olshaker. The C-reactive Protein. *Journal of Emergency Medicine*, 17(6):1019–1025, 1999.
- [208] T. Komoriya, N. Inoue, and K. Yoshimune. Use of a highly sensitive latex reagent with amino acid spacer for determination of C-reactive protein concentration in a variety of liver diseases. *Journal of Bioscience and Bioengineering*, 114(5):560–563, 2012.
- [209] J. Jun Li and C. Fang. C-reactive protein is not only an inflammatory marker but also a direct cause of cardiovascular diseases. *Medical Hypotheses*, 62:499–506, 2004.
- [210] A. B. Almeida, G. Faria, H. Moreira, J. Pinto-de Sousa, P. Correia-da Silva, and J. C. Maia. Elevated serum C-reactive protein as a predictive factor for anastomotic leakage in colorectal surgery. *International Journal of Surgery*, 10(2):87–91, 2012.
- [211] P. P. Singh, I. S. L. Zeng, S. Srinivasa, D. P. Lemanu, A. B. Connolly, and A. G. Hill. Systematic review and meta-analysis of use of serum C-reactive protein levels to predict anastomotic leak after colorectal surgery. *British Journal of Surgery*, 101(4):339–346, 2014.
- [212] O. Facy, B. Paquette, D. Orry, N. Santucci, P. Rat, P. Rat, C. Binquet, and P. Ortega-Deballon. Inflammatory markers as early predictors of infection after colorectal surgery: the same cut-off values in laparoscopy and laparotomy? *International Journal of Colorectal Disease*, 32(6):857–863, 2017.
- [213] S. R. Smith, P. Pockney, R. Holmes, F. Doig, J. Attia, E. Holliday, R. Carroll, and B. Draganic. Biomarkers and anastomotic leakage in colorectal surgery: C-reactive protein trajectory is the gold standard. *ANZ Journal of Surgery*, 88(5):440–444, 2018.
- [214] M. Mik, M. Berut, L. Dziki, and A. Dziki. Does C-reactive protein monitoring after colorectal resection with anastomosis give any practical benefit for patients with intra-abdominal septic complications? *Colorectal Disease*, 18(7):O252–O259, 2016.
- [215] C. Riva, B. Ross, and G. B. Benedek. Laser Doppler measurements of blood flow in capillary tubes and retinal arteries. *Investigative Ophthalmology*, 11(11):936–44, 1972.
- [216] L. Y. Orekhova and A. A. Barmasheva. Doppler flowmetry as a tool of predictive, preventive and personalised dentistry. *EPMA Journal*, 4(1):21, 2013.

References

- [217] C. Limjeerajarus. Laser Doppler flowmetry: Basic Principle, Current Clinical and Research Applications in Dentistry. *Chulalongkorn University Dental Journal*, 37:123–136, 2014.
- [218] A Humeau, W. Steenbergen, H. Nilsson, and T. Strömberg. Laser Doppler perfusion monitoring and imaging: Novel approaches. *Medical and Biological Engineering and Computing*, 45:421–435, 2007.
- [219] N. Boyle, D. Manifold, M. Jordan, and R. Mason. Intraoperative Assessment of Colonic Perfusion Using Scanning Laser Doppler Flowmetry. *Journal of American College of Surgeons*, 191(5):504–510, 2000.
- [220] C. M. Choi and R. G. Bennett. Laser Dopplers to determine cutaneous blood flow. *Dermatologic Surgery*, 29(3):272–80, 2003.
- [221] I. Fredriksson, C. Fors, and J. Johansson. Laser Doppler Flowmetry - a Theoretical Framework. Technical report, Linköping University, 2007.
- [222] Y. Hirano, K. Omura, Y. Tatsuzawa, J. Shimizu, Y. Kawaura, and G. Watanabe. Tissue oxygen saturation during colorectal surgery measured by near-infrared spectroscopy: Pilot study to predict anastomotic complications. *World Journal of Surgery*, 30(3):457–461, 2006.
- [223] K. Seike, K. Koda, N. Saito, K. Oda, C. Kosugi, K. Shimizu, and M. Miyazaki. Laser Doppler assessment of the influence of division at the root of the inferior mesenteric artery on anastomotic blood flow in rectosigmoid cancer surgery. *International Journal of Colorectal Disease*, 22(6):689–697, 2007.
- [224] H. Ahn, J. Lindhagen, G. E. Nilsson, E. G. Salerud, M. Jodal, and O. Lundgren. Evaluation of laser Doppler flowmetry in the assessment of intestinal blood flow in cat. *Gastroenterology*, 88(4):951–7, 1985.
- [225] A. J. Avino, W. A. Oldenburg, P. Gloviczld, V. M. Miller, L. J. Burgart, and E. J. Atkinson. Inferior mesenteric venous sampling to colonic ischemia: A comparison with laser Doppler flowmetry and photoplethysmography. *Journal of Vascular Surgery*, 22(3):271–279, 1995.
- [226] H. Kashiwagi. The lower limit of tissue blood flow for safe colonic anastomosis: An experimental study using laser doppler velocimetry. *Surgery Today*, 23(5): 430–438, 1993.
- [227] R. S. Chung, D. C. Hitch, and D. N. Armstrong. The role of tissue ischemia in the pathogenesis of anastomotic stricture. *Surgery*, 104(5):824–9, 1988.
- [228] G P Gardner, W W LaMorte, E T Obi-Tabot, and J O Menzoian. Transanal intracolonic pulse oximetry as a means of monitoring the adequacy of colonic perfusion., 1994.
- [229] A. Thorén, S. E. Ricksten, S. Lundin, B. Gazelius, and M. Elam. Baroreceptor-mediated reduction of jejunal mucosal perfusion, evaluated with endoluminal Laser Doppler flowmetry in conscious humans. *Journal of the Autonomic Nervous System*, 68(3):157–163, 1998.

-
- [230] A. Vignali, L. Gianotti, M. Braga, G. Radaelli, L. Malvezzi, and V. Di Carlo. Altered microperfusion at the rectal stump is predictive for rectal anastomotic leak. *Diseases of the Colon and Rectum*, 43(1):76–82, 2000.
- [231] L. Boni, G. David, G. Dionigi, S. Rausei, E. Cassinotti, and A. Fingerhut. Indocyanine green-enhanced fluorescence to assess bowel perfusion during laparoscopic colorectal resection. *Surgical Endoscopy*, 30(7):2736–2742, 2016.
- [232] E. J. Corbett. Laser Doppler flowmetry is useful in the clinical management of small bowel transplantation. *Gut*, 47(4):580–583, 2000.
- [233] Z. Abdollahi. *Intra-operative optical monitoring of bowel tissue viability based on photoplethysmography and laser doppler flowmetry*. PhD thesis, City University London, 2014.
- [234] B. J. Bain. *Blood cells: a practical guide*. John Wiley & Sons, Ltd, Chichester, UK, 5 edition, 2014. ISBN 9781118817322.
- [235] D. Kim, H. Han, Y. Yoon, J. Y. Cho, Y. Choi, J. Y. Jang, and H. Choi. Postoperative white blood cell counts change after pancreatoduodenectomy: Early sign for pancreatic fistula. *Korean Journal of Clinical Oncology*, 11(2):95–100, 2015.
- [236] R. Warschkow, I. Tarantino, M. Torzewski, F. Näf, J. Lange, and T. Steffen. Diagnostic accuracy of C-reactive protein and white blood cell counts in the early detection of inflammatory complications after open resection of colorectal cancer: a retrospective study of 1,187 patients. *International Journal of Colorectal Disease*, 26(11):1405–1413, 2011.
- [237] E. E. Morse, A. Nashed, and L. Spilove. Automated Differential Leukocyte Counts. *Annals of Clinical and Laboratory Science*, 19(3):155–160, 1989.
- [238] M. Brown and C. Wittwer. Flow Cytometry: Principles and Clinical Applications in Hematology. *Clinical Chemistry*, 46(8):1221–1229, 2000.
- [239] C. F. Bellows, L. S. Webber, D. Albo, S. Awad, and D. H. Berger. Early predictors of anastomotic leaks after colectomy. *Techniques in Coloproctology*, 13(1):41–47, 2009.
- [240] C. L. Verdant, M. Chierago, V. De Moor, R. Chamlou, J. Creteur, J. De Dieu Mutijima, P. Loi, M. Gelin, A. Gullo, J. Vincent, and D. De Backer. Prediction of Postoperative Complications After Urgent Laparotomy by Intraperitoneal Microdialysis A Pilot Study. *Annals of Surgery*, 244(6):994–1002, 2006.
- [241] P. A. Kyriacou, K. Budidha, and T. Abay. Optical Techniques for Blood and Tissue Oxygenation. In *Encyclopedia of Biomedical Engineering*, volume 3, pages 461–472. Elsevier, 2019. ISBN 9780128048290.
- [242] S. Friedland, R. Soetikno, and D. Benaron. Reflectance spectrophotometry for the assessment of mucosal perfusion in the gastrointestinal tract. *Gastrointestinal Endoscopy Clinics of North America*, 14:539–553, 2004.

References

- [243] P. G. Maxim, J. J. L. Carson, D. A. Benaron, B. W. Loo, L. Xing, A. L. Boyer, and S. Friedland. Optical Detection of Tumors In Vivo by Visible Light Tissue Oximetry. *Technology in Cancer Research & Treatment*, 4(3):227–234, 2005.
- [244] W. Pajk, B. Schwarz, H. Knotzer, B. Friesenecker, M. Dünser, W. Hasibeder, A. Mayr, and M. Du. Jejunal tissue oxygenation and microvascular flow motion during hemorrhage and resuscitation. *American Journal of Physiology - Heart and Circulatory Physiology*, 283(6):H2511–7, 2002.
- [245] F. C. Ramirez, S. Padda, S. Medlin, H. Tarbell, and F. W. Leung. Reflectance spectrophotometry in the gastrointestinal tract: limitations and new applications. *American Journal of Gastroenterology*, 97(11):2780–4, 2002.
- [246] S. L. Wang, D. Y. Sze, and M. D. Drake. Continuous gastrointestinal mucosal oximetry during endovascular procedures carrying risk of ischemia. In *SIR Annual Scientific Meeting Conference Phoenix*, Phoenix, AZ, 2004.
- [247] A. Karliczek, D. A. Benaron, P. C. Baas, C. J. Zeebregts, A. Van Der Stoel, T. Wiggers, J. T. M. Plukker, and G. M. Van Dam. Intraoperative assessment of microperfusion with visible light spectroscopy for prediction of anastomotic leakage in colorectal anastomoses. *Colorectal Disease*, 12:1018–1025, 2009.
- [248] B. Temmesfeld-wollbrück, A. Szalay, K. Mayer, H. Olschewski, W. Seeger, and F. Grimminger. Abnormalities of Gastric Mucosal Oxygenation in Septic Shock. *American Journal of Respiratory and Critical Care Medicine*, 157(5):1586–1586–92, 1998.
- [249] F. W. Leung, S. K. Lo, Q. Q. Phan, J. W. C. Leung, G. S. Yanni, and J. Jing. Factors influencing reflectance spectrophotometric measurements of gastrointestinal mucosal blood flow. *Gastrointestinal Endoscopy*, 41(1):18–24, 1995.
- [250] K. Budidha and P. A. Kyriacou. The Human Ear Canal : Investigation of its suitability for monitoring photoplethysmographs and arterial oxygen saturation. *Physiological Measurement*, 35(2):111–128, 2014.
- [251] J. M. May. *Investigation of fontanelle photoplethysmographs and oxygen saturations in intensive care neonates and infants utilising miniature photometric sensors*. PhD thesis, City University London, 2013.
- [252] P. A. Kyriacou, M. Hickey, and J. P. Phillips. Pulse oximetry of body cavities and organs. *Proceedings of the Annual International Conference of the IEEE Engineering in Medicine and Biology Society, EMBS*, pages 2664–2667, 2013.
- [253] M. Hickey, N. Samuels, N. Randive, R. Langford, and P. A. Kyriacou. A new fibre optic pulse oximeter probe for monitoring splanchnic organ arterial blood oxygen saturation. *Computer Methods and Programs in Biomedicine*, 108(3): 883–888, 2012.
- [254] Z. Türkyilmaz, K. Sönmez, A. Can Baçaklar, B. Demiroğullari, V. Numanoğlu, G. Ekingen, A. Dursun, M. Ali Altin, and N. Kale. Assessment of anastomotic reliability with pulse oximetry in graded intestinal ischemia: An experimental study in dogs. *Journal of Pediatric Surgery*, 1997.

-
- [255] D. F. J. Tollefson, D. J. Wright, D. J. Reddy, and E. B. Kintanar. Intraoperative determination of intestinal viability by pulse oximetry. *Annals of Vascular Surgery*, 9(4):357–360, 1995.
- [256] J. DeNobile, P. Guzzetta, and K. Patterson. Pulse oximetry as a means of assessing bowel viability. *Journal of Surgical Research*, 48(1):21–23, 1990.
- [257] K. Ouriel, W. M. Fiore, and J. E. Geary. Detection of occult colonic ischemia during aortic procedures: Use of an intraoperative photoplethysmographic technique. *Journal of Vascular Surgery*, 7(1):5–9, 1988.
- [258] E. L. Servais, N. P. Rizk, L. Oliveira, V. W. Rusch, M. Bikson, and P. S. Adusumilli. S008 – Real-time intraoperative detection of tissue hypoxia in gastrointestinal surgery by Wireless Pulse Oximetry (WiPOX) HHS Public Access. *Surgical Endoscopy*, 25(5):1383–1389, 2011.
- [259] L. Wang, S. L. Jacques, and L. Zheng. MCML - Monte Carlo modeling of light transport in multi-layered tissues. *Computer methods and programs in biomedicine*, 47:131–146, 1995.
- [260] S. Chatterjee. *Monte Carlo investigation of light-tissue interaction in photoplethysmography*. Phd, City, University of London, 2018.
- [261] K. Budidha. *Investigation of inner ear oximetry under conditions of compromised peripheral perfusion*. PhD thesis, City University London, 2015.
- [262] Y. Sun and N. Thakor. Photoplethysmography Revisited: From Contact to Non-contact, from Point to Imaging. *IEEE Transactions on Biomedical Engineering*, 63(3):463–477, 2016.
- [263] J. Allen. Photoplethysmography and its application in clinical physiological measurement. *Physiological Measurement*, 28(3):R1–R39, 2007.
- [264] K. Gerard Humphreys, T. E. Ward, and C. M. Markham. *An Investigation of Remote Non-Contact Photoplethysmography and Pulse Oximetry*. Phd, National University of Ireland, 2007.
- [265] L. Wang and S. L. Jacques. *Monte Carlo Modeling of Light Transport in Multi-layered Tissues in Standard C*. Phd, University of Texas, 1992.
- [266] A. N. Bashkatov, E. A. Genina, and V. I Kochubey. Optical properties of human colon tissues in the 350 - 2500 nm spectral range. *Quantum Electronics*, 44(8):779–784, 2014.
- [267] F. M. Castro-Poças, M. Dinis-Ribeiro, T. P. Araújo, and I. Pedroto. Echoendoscopic characterization of the human colon. Technical report, University of Porto, 2015.
- [268] L. Oliveira, I. Carneiro, S. Carvalho, R. Henrique, and V. V. Tuchin. Optical properties of colorectal muscle in visible/NIR range. In Jürgen Popp, Valery V. Tuchin, and Francesco S. Pavone, editors, *Biophotonics: Photonic Solutions for Better Health Care VI*, volume 10685, page 122. SPIE, 2018. ISBN 9781510618961.

References

- [269] D. Hidović-Rowe and E. Claridge. Modelling and validation of spectral reflectance for the colon. *Physics in Medicine and Biology*, 50(6):1071–1093, 2005.
- [270] S. A. Prahl. *Light transport in tissue*. PhD thesis, The University of Texas, 1988.
- [271] D. Jurovata, J. Kurnatova, S. Ley, D. Laqua, P. Vazan, and P. Husar. Simulation of Photon Propagation in Tissue Using Matlab. *Research Papers Faculty of Materials Science and Technology Slovak University of Technology*, 21:31–36b, 2013.
- [272] S. Chatterjee. *Computational Modelling of Light Propagation in Biological Tissue using Monte Carlo technique*. Mphil thesis, City, University of London, 2016.
- [273] Z. Patel, S. Chatterjee, M. A. Thaha, and P. A. Kyriacou. A multilayer Monte Carlo model for the investigation of optical path and penetration depth at different perfusion states of the colon. In *Proceedings of the Annual International Conference of the IEEE Engineering in Medicine and Biology Society, EMBS*, Berlin, Germany, 2019. IEEE.
- [274] N. Bosschaart, G. J. Edelman, M. C. G. Aalders, Ton G. Van Leeuwen, and D. J. Faber. A literature review and novel theoretical approach on the optical properties of whole blood. *Lasers in Medical Science*, 29(2):453–479, 2014.
- [275] M. Hickey and P. A. Kyriacou. Optimal spacing between transmitting and receiving optical fibres in reflectance pulse oximetry. *Journal of Physics: Conference Series*, 85:012030, 2007.
- [276] P. H. Charlton, T. Bonnici, L. Tarassenko, D. A. Clifton, R. Beale, and P. J. Watkinson. An assessment of algorithms to estimate respiratory rate from the electrocardiogram and photoplethysmogram. *Physiological Measurement*, 37(4): 610–626, 2016.
- [277] P. A. Kyriacou. Direct pulse oximetry within the esophagus, on the surface of abdominal viscera, and on free flaps. *Anesthesia and Analgesia*, 117(4):824–833, 2013.
- [278] F. J. Massey. The Kolmogorov-Smirnov Test for Goodness of Fit. *American Statistical Association*, 46(253):68–78, 1951.
- [279] R. V. Hogg and J. Ledolter. *Engineering Statistics*. MacMillan, New York, 1987.
- [280] J. Neter and M. H. Kutner. *Applied Linear Statistical Models*. Irwin Press, 4 edition, 1996.
- [281] M. Armstrong and R. A. Moore. *Anatomy, Patient Positioning*, 2019.
- [282] M. Hickey, N. Samuels, N. Randive, R. M. Langford, and P. A. Kyriacou. An in vivo investigation of photoplethysmographic signals and preliminary pulse oximetry estimation from the bowel using a new fiberoptic sensor. *Anesthesia and Analgesia*, 112(5):1104–1109, 2011.

-
- [283] Z. Patel, M. A. Thaha, and P. A. Kyriacou. The effects of optical sensor-tissue separation in endocavitary photoplethysmography. *Physiological Measurement*, 39(7), 2018.
- [284] R. Inghin, L. Brugger, D. Candinas, and D. Eberli. Bioengineering of Colo-Rectal Tissue. In *Tissue engineering for tissue and organ regeneration*, volume 1, pages 271–284. InTech, 2011. doi: 10.5772/57353. URL <https://www.intechopen.com/books/advanced-biometric-technologies/liveness-detection-in-biometrics><http://www.intechopen.com/books/trends-in-helicobacter-pylori-infection/floating-drug-delivery-systems-for-eradication-of-helicobacter-pylori-in-treatment-of-peptic-ulcer>
- [285] P. A. Kyriacou. Pulse oximetry in the oesophagus. *Physiological Measurement*, 27(1):R1–R35, 2006.
- [286] G. Armstrong, J. Croft, N. Corrigan, J. M. Brown, V. Goh, P. Quirke, C. Hulme, D. Tolan, A. Kirby, R. Cahill, P. R. O’Connell, D. Miskovic, M. Coleman, and D. Jayne. IntAct: intra-operative fluorescence angiography to prevent anastomotic leak in rectal cancer surgery: a randomized controlled trial. *Colorectal Disease*, 20(8):O226–O234, 2018.
- [287] P. Shi. *Photoplethysmography in noninvasive cardiovascular assessment*. PhD thesis, Loughborough University, 2009.
- [288] WHO. Pulse oximetry, 2019. URL https://www.who.int/patientsafety/safesurgery/pulse_oximetry/en/.
- [289] T. Abay, K. Shafqat, and P. A. Kyriacou. Perfusion Changes at the Forehead Measured by Photoplethysmography during a Head-Down Tilt Protocol. *Biosensors*, 9(2):71, 2019.
- [290] D. Beck. Bowel Preparation for Colonoscopy. *Clinics in Colon and Rectal Surgery*, 23(01):010–013, 2010.

Appendix A

Instrumentation unit and data acquisition

The instrumentation unit and the data acquisition functionalities will be discussed further in this appendix.

A.1 Instrumentation unit

ZenPPG, is a portable, battery-operated instrumentation unit allowing the operation of two PPG sensors. In context to the research, the dual-channels allow the acquisition of PPGs using the intraluminal PPG sensor (Channel 1) and the finger PPG sensor (Channel 2). The main functions of ZenPPG is to acquire raw PPG signals consisting of both PPG components (ac and dc) and operating the LEDs with the ability to adjust the light intensities. Both channels are electronically identical, therefore, the explanation of ZenPPG will be referring to a single channel. Within a rectangular enclosure ($16.0\text{ cm} \times 10.3\text{ cm} \times 5.6\text{ cm}$, ($l \times w \times h$)), there are five independent modules interconnected through a double sided system bus, allowing the removal or modification of modules without altering the entire system as shown in Figure A.1.

Instrumentation unit and data acquisition

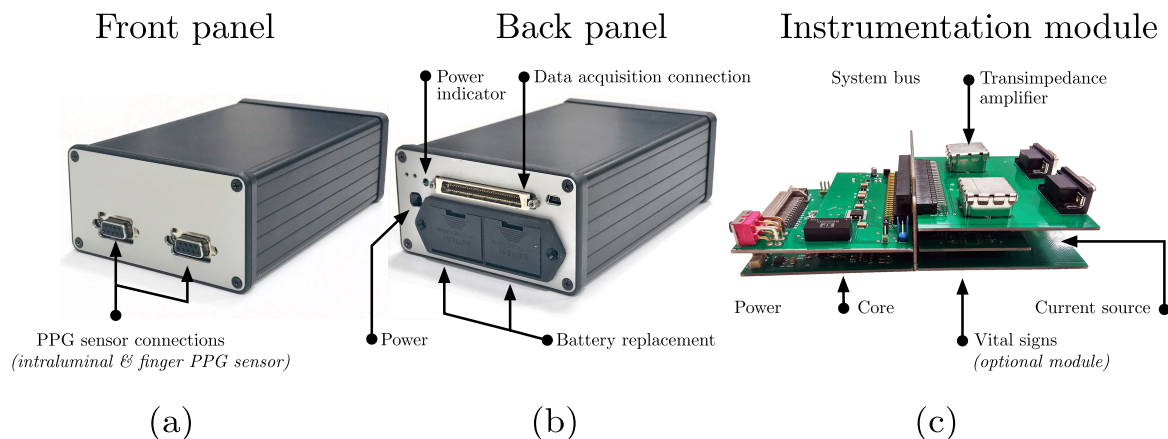


Figure A.1 Photographs of the instrumentation unit, also referred as ZenPPG. The enclosed system allows (a) connections of the intraluminal and finger photoplethysmography (PPG) sensor on the front panel; (b) connections for the data acquisition and battery replacements and, (c) ZenPPG modules within the enclosure holding all the instrumentation electronics. The modular system allows additional modules to be interconnected via a double-sided system bus, such as the vital signs module (removed in the current application).

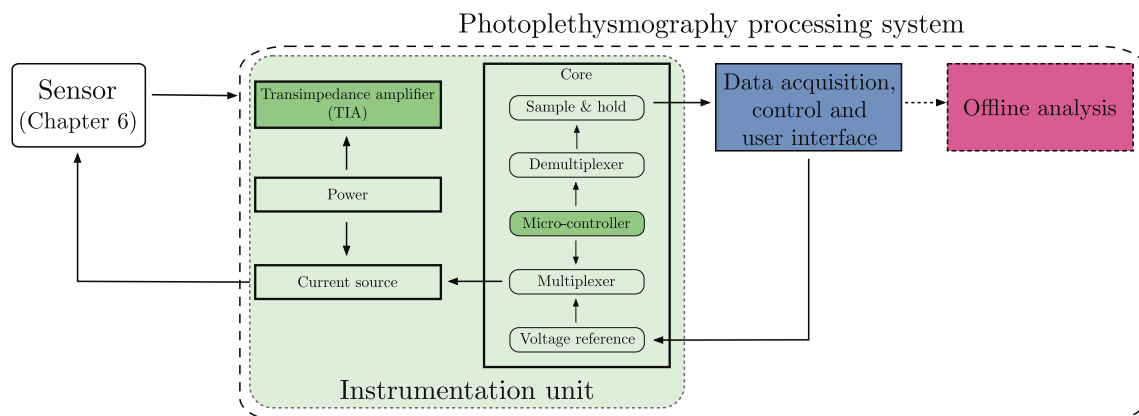


Figure A.2 Detailed block diagram of the instrumentation unit within the processing system. As the instrumentation unit is an available research tool, minor alterations were required. The modules requiring the alterations are highlighted in dark green, such as the trans-impedance amplifier and the micro-controller.

As previously stated, ZenPPG is a research tool developed with the aim to standardise all PPG based research within RCBE. Minor alterations were implemented for this research, including the removal of the vital signs module. Figure A.2 illustrates the interconnected modules used within this research. For each module, the functions will be mentioned, where further explanation will be given to altered modules or units which are highlighted in Figure A.2.

Power module The instrumentation unit is battery-operated, where two 9 V batteries are enclosed within the rectangular enclosure. The main function of the power module is to regulate the batteries for multiple DC power rails required within ZenPPG. DC power rails such as ± 5 V are used for components within the current source module and the micro-controller in the core module.

Core module The core module consists of many units, however for the purpose of this research, the micro-controller code was altered. By altering the code, two units within the core module are affected; (i) multiplexer and (ii) demultiplexer. To understand these effects, three units within the core module will be explained further: (i) voltage reference, (ii) multiplexer and (iii) demultiplexer.

Voltage reference There are two voltage reference circuits within ZenPPG to independently control the light intensities of each LED within a single channel. Channel 2 which operates the finger PPG sensor has a constant 1 V on-board regulator and attenuator circuits to generate voltage references between 0 V to 1 V (ICPOS0) and -1 V - 0 V (ICNEGO) for the infrared (IR) and red (R) LED respectively. Light intensities for Channel 2 are adjusted manually with the use of attenuators consisting of variable resistors, resulting in alterations in the attenuating gains. The light intensities for LEDs in the intraluminal PPG sensor, operating on Channel 1, are digitally controlled through a VI using LabVIEW. Configured within the VI, digital voltage references ranging between 0 V to 5 V (A01) and -5 V - 0 V (A02) are generated for the IR and R LED respectively. For Channel 1 to have the same voltage reference ranges as Channel 2 (± 1 V), the voltage references undergo further attenuation with the use of on-board attenuators.

Multiplexer To obtain signals from each LED independently within a PPG sensor, the LEDs require ZenPPG to alternate the LED operating times. By alternating the on and off time of each LED, independent sampling of detected light at each wavelength is achieved with the use of multiplexers. The multiplexer works by receiving the positive and negative voltage references, to produce a signal output varying between ± 1 V. With reference to the truth table as shown in Figure A.3, two multiplexing clocks (CMUX0 and CMUX1) were generated from the micro-controller to determine which input would be passed on to the output in a single channel. Switching off both LEDs was not required, therefore CMUX0 was set to alternate between logic 0 and 1, whilst

Instrumentation unit and data acquisition

CMUX1 was set to a constant logic 0. As illustrated in Figure A.3, providing the multiplexer output is positive, one LED is switched on and when negative, the second LED switches on. With a sampling frequency of 800 Hz, each emitter was switched on every 1250 μs for a duration of 625 μs .

Demultiplexer With the photodetector continuously detecting back-scattered light, the output of the photodetector is a mixed signal of both wavelengths. To differentiate between the signals from the two LED wavelengths, a demultiplexer is used. Contrary to the multiplexer, the demultiplexer works by receiving a single input and separating into multiple outputs, depending on three demultiplexing clocks (MUX0, MUX1 and SMP_INH0) from the micro-controller. Ideally, by synchronising the multiplexing and demultiplexing clocks, signals would be separated accordingly; however, this is not the case due to a switching noise produced by the LEDs. To eliminate the switching noise from the demultiplexed signals, ZenPPG uses a time window, where a slight delay between the multiplexing and demultiplexing clocks are introduced.

Referring to Figure A.4, with such delay, the photodetector is sampled in the middle of the photodetector output, where the output has reached a plateau, representing the true light level of the detected light intensity. By sampling within the region of plateau eliminates the need for sampling dark light, where both LEDs remain switched off.

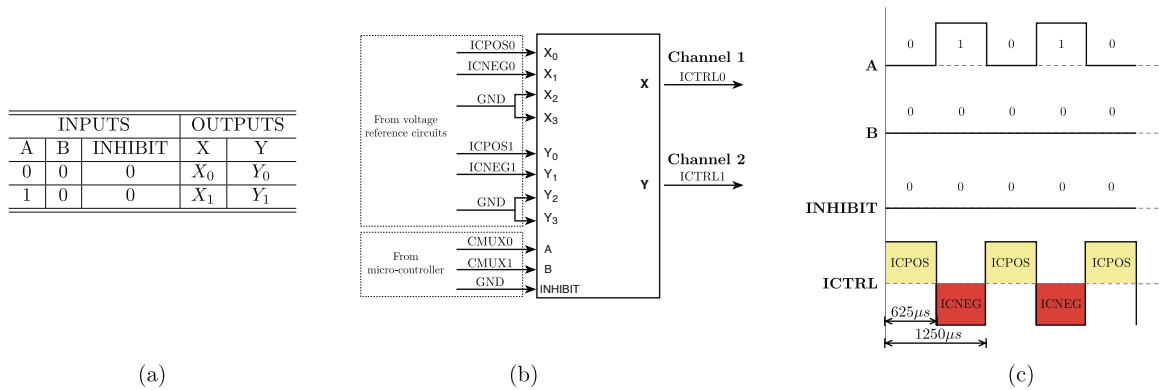


Figure A.3 Functional diagram of the multiplexer module. The truth table (a) was required to programme the micro-controller clocks, for the switching of the light emitting diodes for each channel. The functional diagram (b) illustrates the configuration used with the instrumentation unit, whilst (c) presents the two clock configuration with the corresponding output, ICTRL. For each channel, the two light emitting diodes alternate their operating time every 625 μs . Image redrawn from Budidha [261].

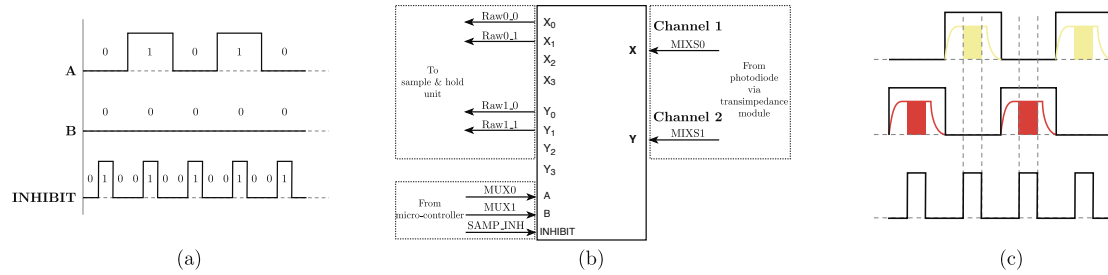


Figure A.4 Functional diagram of the demultiplexer module. Three clocks were generated (a) for the demultiplexer to separate the mixed photoplethysmography (PPG) signals (MIXS0 and MIXS1) into raw PPG signals (Raw0 and Raw1) corresponding to the two wavelengths, for each channel. (c) illustrates the timing window used to sample the signals from the two wavelengths. The signals were sampled during the LED switched on and at a plateau to avoid sampling the switching noise. Image redrawn from Budidha [261].

Current source module There are two identical current driver circuits operating the LEDs on each channel. The current driver circuits consist of a modified Howland current source which linearly converts the switching voltage signal from the multiplexer to current. Recalling that the output of the multiplexer is an alternating square wave depending on the voltage reference chosen by the user, as shown in Figure A.3, the voltage reference has a maximum value of ± 1 V. By converting the voltage into current, a maximum current of ± 1 A would be produced, large enough to burn the LEDs. Therefore, within the current source module, further voltage attenuation with a gain of 10 is performed to ensure the maximum current is limited to ± 10 mV. The current source module has an additional function where the current across each LED is continuously monitored and displayed in the user interface (ui) in the VI which will be discussed in Section A.2.

Trans-impedance amplifier module The trans-impedance amplifier module is required to convert the light photons detected by the photodetector into a voltage for the ZenPPG to process. The module consists of two female D-Sub 9 connectors to allow the PPG sensors to be connected to the instrumentation unit. The connector and pin configuration used are similar to the commercial probes as shown in Figure A.5. Within the module, there are two identical trans-impedance amplifiers for each channel. ZenPPG was designed to allow easy alteration to this module, as different research applications require different gains to enhance the PPG signal. As the acquisition of PPG signals within the human colorectum is novel, no literature was found suggesting

Instrumentation unit and data acquisition

the values of amplification required for adequate signals. ZenPPG allows the trans-impedance amplifier to have a gain between 100k and 1M. With the understanding that the colorectum has an extensive network of collateral blood supply and signals have been acquired previously from the outer surface of the intestine [21], a low-medium gain of 330 k was chosen. This gain value was decided as the light intensity of the LEDs could be adjusted until an adequate voltage is achieved. Within the trans-impedance amplifier design, a phase compensation capacitor parallel to the gain resistor was included to provide stability to the circuit. The phase-compensating capacitor (C_f) was calculated using the following equation,

$$C_f = \sqrt{\frac{C_{PD} + C_{icm}}{2\pi R_f G_{BW}}} \quad (\text{A.1})$$

where R_f is the feedback resistance (330 k Ω), G_{BW} is the op-amp gain bandwidth (90 M), C_{PD} is the photodiodes capacitance (10 pF) and C_{icm} is the common mode input capacitance of the op-amp (4.1 pF). Although the C_f was calculated to be 27 pF, 68 pF was used as it increased the stability of the output of the trans-impedance amplifier.

Based on the way the instrumentation unit was used for the research, ZenPPG provided eleven (11) signals, consisting of PPGs from each channel and electrical monitoring parameters of ZenPPG. The output will be discussed further in the following section (Section A.2).

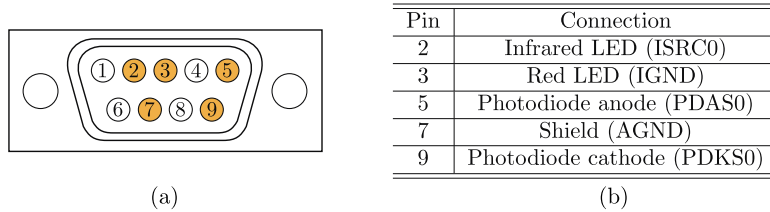


Figure A.5 Pin configuration for the D-Sub 9 connector. This allows the electrical communication between the developed sensors and the processing system, through the instrumentation unit. The pins are highlighted in orange (a) which are used for the current research, and (b) reflects the corresponding connections to the sensor and the instrumentation unit.

A.2 Data acquisition, control and user interface

The set-up parameters for data to be acquired and converted from analogue to digital signals will be discussed further. In addition, a detailed explanation of the user control and online analysis developed in LabVIEW will be presented.

Analogue-to-digital conversion The resultant analogue signals from the instrumentation unit were digitised with a National Instrument (NI) digital acquisition card (DAQ, *NI-PcIe 6321 DAQ, National Instruments, USA*). The connection of the DAQ between the instrumentation unit and VI will be described.

- **DAQ set-up** The DAQ connects to the instrumentation unit through a shielded 64-pin NI connector (*SCH68-68-EPM, National Instruments*). The DAQ has a 16-bit resolution with the ability to accommodate sixteen analogue input (AI) and two analogue output (AO) channels. The DAQ communicates with the laptop through a USB connection via a set of drivers called NI-DAQmx. A laptop was chosen due to its portability and ability to operate with an internal battery, compared to a device connected to the mains supply which is a risk to the subject under investigation.
- **DAQ initialisation** Through NI-DAQmx, the DAQ parameters were initialised, including the channels requiring sampling, the input range of the signal and sampling mode. For PPG acquisition, the DAQ parameters were set to have a $\pm 5\text{ V}$ input range and a sampling rate of 1 kHz to ensure all fundamental frequencies of the PPGs and their residual harmonics were adequately sampled. Continuous sampling of all eleven (11) ZenPPG outputs were digitised and assigned to a physical channel that could be read by the VI to determine its corresponding channel.

Table A.1 presents the outputs from the instrumentation unit and their corresponding physical channel for the VI. Following the DAQ initialisation, the developed VI using LabVIEW could communicate with the DAQ bidirectional, by sending digital signals to be converted to analogue signals for the instrumentation unit to interpret. With this capability, the user has the ability to control the voltage reference of the LEDs which will now be explained.

Voltage reference user control Acquiring PPG signals through LabVIEW is advantageous due to its capability in allowing user control of certain parameters. This

Instrumentation unit and data acquisition

Table A.1 Pin configuration of the data acquisition card (DAQ), in order to acquire data incoming from the instrumentation unit, into digital signals. The analogue data from the instrumentation unit (ZenPPG) enter the DAQ through analogue input (AI) pins, whilst the analogue output (AO) pins transfers data from the user interface and control module to control the light intensity of one developed sensor. Each AI is assigned a DAQ physical output, which is recognised by the virtual instrument for storage and online analysis.

ZenPPG outputs	Description	DAQ physical outputs
AI0	Channel 1, raw infrared mixed signal (IR)	0
AI1	Channel 1, raw red mixed signal (R)	1
AI2	Channel 2, raw infrared mixed signal (IR)	2
AI3	Channel 2, raw red mixed signal (R)	3
AI4	Channel 1, ac PPG from infrared (IR_{zac})	4
AI5	Channel 1, ac PPG from red (R_{zac})	5
AI6	Channel 2, ac PPG from infrared (IR_{zac})	6
AI7	Channel 2, ac PPG from red (R_{zac})	7
AI10	ZenPPG power supply monitoring (PSVMON)	10
AI11	Channel 1, LED current monitoring (ISENSE0)	8
AI12	Channel 2, LED current monitoring (ISENSE1)	9
AO0	Channel 1, user controlled infrared voltage reference	-
AO1	Channel 1, user controlled red voltage reference	-

is achieved by designing a ui on LabVIEW, which is visible to the user on the front panel window. As mentioned in Section A.1, the instrumentation unit was designed to allow user control of the light intensities of the LEDs for Channel 1. The choice of operating the intraluminal PPG sensor digitally was to ensure no harm was inflicted to the subject under investigation. In an event of device failure, the laptop would terminate the operation of the entire channel. Recalling from Section 6.6, the ZenPPG current source module receives the voltage references to supply a directly proportional current to operate the LEDs. The DAQ was configured through the DAQmx to allow AO's within a voltage range of ± 5 V, which generates two digital voltage references (AO0 and AO1) between 0 V - 5 V (ICPOS1) and -5 V - 0 V (ICNEG1) for the IR and R LED respectively in the intraluminal PPG sensor. Within the front panel, the user has the ability to change the voltage references.

Online analysis Another advantage of using LabVIEW is for allowing acquired physiological measurements to be analysed and displayed continuously in real-time. Prior to either functions, the incoming digitised signals from both PPG channels

A.2 Data acquisition, control and user interface

require separation into independent data lines corresponding to the physical channels initialised within the ADC.

- **Filters:** From both channels, the raw PPGs were digitally filtered using a band-pass filter with a pass-band between 0.5 Hz - 10 Hz. Additional digital low pass filters with a cut-off frequency of 0.05 Hz were included to separate the dc PPG components from both channels, resulting in the ac and dc constituents.
- **Continuous estimation of oxygen saturation:** To provide an indication of the quality of PPGs acquired, blood oxygen saturation (S_pO_2) for both channels were continuously estimated using the equations commonly used by pulse oximeters (Equation 4.27). PPG signals were continuously collected every 2 s for the estimations of S_pO_2 . Within this time frame, the mean peak-to-peak amplitudes of the ac and mean value of dc signals were calculated.

Appendix B

Access for research documentation

This includes documentations of the letter of access for research and certification for Good Clinical Practice (GCP).

Our ref: LOA-UR

Zaibaa Patel
PhD Researcher
City University
Northampton Square
London
EC1V 0HB

Tel: 020 7882 7274

Fax: 020 7882 7276

Email: [REDACTED]@bartshealth.nhs.uk

10th November 2016

Dear Miss Patel

Letter of access for research

This letter confirms your right of access to conduct research through Barts Health NHS Trust for the purpose and on the terms and conditions set out below. This right of access commences with immediate effect and ends on 9th November 2019 unless terminated earlier in accordance with the clauses below.

You have a right of access to conduct such research as confirmed in writing in the letter of permission for research from this NHS organisation. Please note that you cannot start the research until the Principal Investigator for the research project has received a letter from us giving permission to conduct the project.

The information supplied about your role in research at Barts Health NHS Trust has been reviewed and you do not require an honorary research contract with this NHS organisation. We are satisfied that such pre-engagement checks as we consider necessary have been carried out.

You are considered to be a legal visitor to Barts Health NHS Trust premises. You are not entitled to any form of payment or access to other benefits provided by this NHS organisation to employees and this letter does not give rise to any other relationship between you and this NHS organisation, in particular that of an employee.

While undertaking research through Barts Health NHS Trust, you will remain accountable to City University but you are required to follow the reasonable instructions of Mr Mohammed Thaha, Consultant in this NHS organisation or those given on his/her behalf in relation to the terms of this right of access.

Where any third party claim is made, whether or not legal proceedings are issued, arising out of or in connection with your right of access, you are required to co-operate fully with any investigation by this NHS organisation in connection with any such claim and to give all such assistance as may reasonably be required regarding the conduct of any legal proceedings.

You must act in accordance with Barts Health NHS Trust policies and procedures, which are available to you upon request, and the Research Governance Framework.

You are required to co-operate with Barts Health NHS Trust in discharging its duties under the Health and Safety at Work etc Act 1974 and other health and safety legislation and to take reasonable care for the health and safety of yourself and others while on Barts Health NHS Trust premises. You must observe the same standards of care and propriety in dealing with patients, staff, visitors, equipment and premises as is expected of any other contract holder and you must act appropriately, responsibly and professionally at all times.

You are required to ensure that all information regarding patients or staff remains secure and *strictly confidential* at all times. You must ensure that you understand and comply with the requirements of the NHS Confidentiality Code of Practice and the Data Protection Act 1998. Furthermore you should be aware that under the Act, unauthorised disclosure of information is an offence and such disclosures may lead to prosecution.

You should ensure that, where you are issued with an identity or security card, a bleep number, email or library account, keys or protective clothing, these are returned upon termination of this arrangement. Please also ensure that while on the premises you wear your ID badge at all times, or are able to prove your identity if challenged. Please note that this NHS organisation accepts no responsibility for damage to or loss of personal property.

We may terminate your right to attend at any time either by giving seven days' written notice to you or immediately without any notice if you are in breach of any of the terms or conditions described in this letter or if you commit any act that we reasonably consider to amount to serious misconduct or to be disruptive and/or prejudicial to the interests and/or business of this NHS organisation or if you are convicted of any criminal offence. Your substantive employer is responsible for your conduct during this research project and may in the circumstances described above instigate disciplinary action against you.

Barts Health NHS Trust will not indemnify you against any liability incurred as a result of any breach of confidentiality or breach of the Data Protection Act 1998. Any breach of the Data Protection Act 1998 may result in legal action against you and/or your substantive employer.

If your current role or involvement in research changes, or any of the information provided in your Research Passport changes, you must inform your employer through their normal procedures. You must also inform your nominated manager in this NHS organisation.

Yours sincerely

[Redacted signature]

[Redacted name]

[Redacted title]

cc:

[Redacted recipient names]

The Faculty of Pharmaceutical Medicine has accredited this course for 6 Continuing Professional Development credits.

GCP web-based training course designed and developed by **INFONETICA**



Certificate Of Achievement

ICH GCP adapted for the UK in English

This is to certify that
Zaibaa Patel
of City University London

has successfully passed web-based examination covering all aspects of Good Clinical Practice as laid down in the International Conference on Harmonisation Guidelines, the EU GCP Directives (2001/20 & 2005/28) and the UK Clinical Trials Regulations 2004 (SI 1031) and amendments of 2006 (SI 1928 & 2984), 2008 (SI 941) and 2009 (SI 1164 & 3063)

22 November 2016

Certificate No: 35595-33-42575

(Recommended renewal date: 22 November 2018)

It takes about 6 hours to complete the training depending on the level of experience.

Nick Deaney, C.Sc.,
International Course Director

Appendix C

Clinical physics documentation

This includes documentations approved by the Clinical Physics department at The Royal London Hospital, UK. This includes the approval of the intraluminal PPG system as a medical device for research and the risk assessment form.



1. Clinical Investigation Details	
Title:	An indwelling optical sensor for monitoring large bowel tissue perfusion
Clinical Physics & Study Ref No.:	RD2017-012; REX Reference No.: 17/LO/0010
Principle Investigator/researchers:	Professor Panayiotis Kyriacou, Zaibaa Patel & Mohamed Thaha

2. Medical Device Details		
Asset ID:	Not assigned (EST Test record ref: ZENPPG)	
Device type:	Intraluminal PPG sensor	
Location of use:	Department of Colorectal Surgery, Royal London Hospital, Barts Health NHS Trust	
Manufacturer:	Research Centre for Biomedical Engineering, School of Engineering and Mathematical Sciences, City University London	
Model:	ZENPPG	
Serial number:	ZENPPG V1.1	
Additional information:	N/A	

3. Medical Devices Regulation	
CE marking present:	No – research device
MHRA No Objection Letter Ref:	N/A. This is Clinical study of a non-CE marked device for use within the institution, where commercialisation is not intended
Risk assessment details:	 RiskAssessmentFina Signed.pdf See attached

4. Comments for the Principal Investigator
<p>Clinical Physics has no objection to the use the medical device(s) and accessories listed in Section 2 for research or as part of a clinical investigation. The Principal Investigator should ensure that the following provisions are in place before the medical device(s) are put into use:</p> <ul style="list-style-type: none"> • Have an indemnity agreement in place. • Equipment training for all users. • Have control measures to manage risk identified from risk assessment. • Where appropriate, visibly label the device ‘Exclusively for Clinical Investigation’ or ‘For research only.’” <p>Approval is limited to the medical devices listed in section 2. Separate approval must be sought for other medical devices involved or for any amendments made to the study protocol.</p>



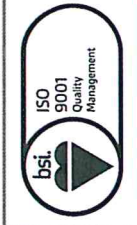
Clinical Physics

Approval of Medical Devices for Research



Barts Health
NHS Trust

Name(s) of Assessor(s):	[REDACTED]
Position(s):	[REDACTED]
Contact Details:	[REDACTED]
Assessment Date:	13 th February 2018



This form is to be used to document particular risks associated with the equipment concerned, rather than all possible risks that would be considered generically e.g. by a harmonised standard. Risk rating shall be carried out according to Trust Risk Management Policy in the format of Likelihood/Consequence. This simultaneously informs users of all residual risks.

Medical Equipment Details:
Intraluminal optical sensor probe, finger sensor and instrumentation unit (ZenPPG V1.1)

Location
Department of Colorectal Surgery, Royal London Hospital, Barts Health NHS Trust

Assessor(s):
Clinical Physics, Barts Health NHS Trust: Gursharan Kalsi (GK), Allan Wilkins (AW)
Study Investigator (s): Panayiotis Kyriacou (PK), Zaibaa Patel (ZP), Mohamed Thaha (MT)

1.0 GENERAL HAZARDS	Risk grading before control		Recommended control measures	Risk grading after control		Person(s) responsible	Sign	
	Likelihood	Consequence		Risk Score	Likelihood			Consequence
1.1 Using non-CE marked equipment as a medical device to diagnose, prevent, monitor, treat or alleviate disease, injury or handicap.	4	5	20	1	5	5	PK MT ZP	

Likelihood*	Definition Rating	Unlikely (expected to occur for years)			Possible (expected to occur monthly)			Likely (expected to occur at least weekly)			Almost certain (expected to occur at least daily)		
		1	2	3	3	4	5	4	5	5	5		
Consequence*	Insufficient (minimal injury, loss/interruption of > 1 hour, <£10K finance loss, potential for public concern)	Minor (minor injury/illness, loss /interruption of > 8 hours, financial loss between £10K and < £50K, local medal coverage, short term public concern)	Moderate (Moderate injury, loss/interruption > 1 day, financial loss between £50K and £500K, local media coverage Long term reduction in public confidence)	Major (Major injury leading to long term incapacity/disability, loss/interruption > 1 week, financial loss between 500K and 1M, National Media coverage, service well below reasonable public expectation)	Catastrophic (Death multiple permanent or irreversible health effects, Permanent loss of service or facility, financial losses >5M, National media coverage, MP Concern, total loss of public confidence)								

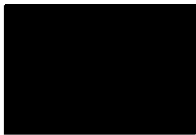


2.0 ENERGY HAZARDS	Risk grading before control		Recommended control measures	Risk grading after control		Person(s) responsible	Sign
	Likelihood	Consequence		Risk Score	Likelihood		
2.1 Electric shock hazard presented by non-CE marked equipment in use in a patient environment.	4	4	16	1	4	PK MT ZP AW GK	
			<ul style="list-style-type: none"> The entire system i.e. the laptop, ZenPPG and sensors will be operated by battery. During use, the laptop will be battery operated. The instruction for use strictly indicates the laptop should not be connected to the mains during use. System and sensors are optically isolated from laptop. Event of device failure, there is no risk as the laptop would stop the equipment from operating the intraluminal sensor. Laptop is recognised as Class II equipment and the sensor has been identified as Type BF, however system was tested as Type CF as intraluminal sensor is invasive (imposing stricter limits). System (laptop, control boxes and both sensors) were electrically safety tested using Tester 068584; Equipment passed all tests. Records are stored under Ref ZENPPG. 				

Likelihood*	Definition Rating	Rare (not expected to occur for years)			Possible (expected to occur monthly)			Likely (expected to occur at least weekly)			Almost certain (expected to occur at least daily)		
		1	2	3	4	5	6	7	8	9	10	11	12
Consequence*	Definition Rating	1	2	3	4	5	6	7	8	9	10	11	12
		Insignificant (minimal injury, loss/interruption of > 1 hour, <£10K finance loss, potential for public concern)	Minor (minor injury/illness, loss /interruption of > 8 hours, financial loss between £10K and < £50K, local medial coverage, short term public concern)	Moderate (Moderate injury, loss/interruption > 1 day, financial loss between £50K and £500K, local media coverage Long term reduction in public confidence)	Major (Major injury leading to long term incapacity/disability, loss/interruption > 1 week, financial loss between 500K and 1M; National Media coverage, service well below reasonable public expectation)	Catastrophic (Death multiple permanent or irreversible health effects, Permanent loss of service or facility, financial losses >5M, National media coverage, MP Concern, total loss of public confidence)							

*As defined in the Barts Health NHS Trust Risk Assessment Policy (Ref: COR/POL/004/2015-001)



2.2	Electrocution from SpO2 probes (intraluminal optical sensor and finger).	4	4	16	<ul style="list-style-type: none"> All components (active and non-active) have been isolated from patient contact with the medical graded epoxy and the intraluminal sensor has an added barrier of the sterile plastic sheath/tubing that covers the whole sensor. Isolation device in place separating SpO2 power source from laptop power source. Device physically limited to an absolute maximum output of 100mA functional current. ZenPPG, including the laptop will be battery operated during the trials. As the device is optically isolated, there are no foreseen situations where current appears on the equipment enclosure even under fault conditions. The medical epoxy dielectric strength (insulation breakdown) is 500 V/Mil (Mil = 25.4µm) and thermal limit of 150°C, based on Dymax Standard test methods. 	1	4	4	PK ZP	
-----	--	---	---	----	---	---	---	---	----------	--

Likelihood*	Definition Rating	Rare (not expected to occur for years)	Unlikely (expected to occur at least annually)	Possible (expected to occur monthly)	Likely (expected to occur at least weekly)	Almost certain (expected to occur at least daily)
Consequence*	Definition Rating	1 <i>Insignificant</i> (minimal injury, loss/interruption of > 1 hour, <£10K finance loss, potential for public concern)	2 <i>Minor</i> (minor injury/illness, loss /interruption of > 8 hours, financial loss between £10K and < £50K, local medial coverage, short term public concern)	3 <i>Moderate</i> (Moderate injury, loss/interruption > 1 day, financial loss between £50K and £500K, local media coverage Long term reduction in public confidence)	4 <i>Major</i> (Major injury leading to long term incapacity/disability, loss/interruption > 1 week, financial loss between 500K and 1M, National Media coverage, service well below reasonable public expectation)	5 <i>Catastrophic</i> (Death multiple permanent or irreversible health effects, Permanent loss of service or facility, financial losses >5M, National media coverage, MP Concern, total loss of public confidence)

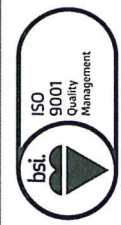
*As defined in the Barts Health NHS Trust Risk Assessment Policy (Ref: COR/POI/004/2015-001)



2.3	Burn from optical components on SpO2 probes (intra luminal optical sensor and finger)	4	4	16	<ul style="list-style-type: none"> LEDs are current limited, therefore in the unlikely event of device failure, the LEDs would not output more than the equivalent of 0.2 W of power. Isolation device in place, separating SpO₂ power source from the laptop power source. Device physically limited to an absolute maximum output of 100 mA functional current. Furthermore, insulation of LEDs by medical epoxy. Thermal safety test was conducted in a water bath at 36°C (documentation available). Temperature of the optical sensor increased with an approximate temperature difference of 0.32°C. Additional thermal test on a tissue (pig's intestines) resulted in a temperature difference of 0.23°C. As the temperature did not exceed 38°C, it was concluded that there was negligible risk of thermal damage to any tissue using the optical sensor. 	1	4	4	PK ZP	[Redacted]
-----	---	---	---	----	---	---	---	---	----------	------------

Likelihood*	Definition Rating	Rare (not expected to occur for years)	Unlikely (expected to occur at least annually)	Possible (expected to occur monthly)	Likely (expected to occur at least weekly)	Almost certain (expected to occur at least daily)
Consequence*	Definition	1 <i>Insignificant</i> (minimal injury, loss/interruption of > 1 hour, <£10K finance loss, potential for public concern)	2 <i>Minor</i> (minor injury/illness, loss/interruption of > 8 hours, financial loss between £10K and < £50K, local media coverage, short term public concern)	3 <i>Moderate</i> (Moderate injury, loss/interruption > 1 day, financial loss between £50K and £500K, local media coverage Long term reduction in public confidence)	4 <i>Major</i> (Major injury leading to long term incapacity/disability, loss/interruption > 1 week, financial loss between 500K and 1M, National Media coverage, service well below reasonable public expectation)	5 <i>Catastrophic</i> (Death multiple permanent or irreversible health effects, Permanent loss of service or facility, financial losses >5M, National media coverage, MP Concern, total loss of public confidence)
Rating	Rating	1	2	3	4	5

*As defined in the Barts Health NHS Trust Risk Assessment Policy (Ref: COR/POL/004/2015-001)



2.4	Fluid ingress to instrumentation ("ZenPPG" control box, isolation DAQ device) causing electrical shorts)	4	4	16	<ul style="list-style-type: none"> For this study, the measurement time expected for the intraluminal sensor is a maximum of 30 minutes, where data recording will be obtained for 5 minutes per distances (5 distances, 15, 12, 9, 6 and 3 cm) "ZenPPG" control box sealed against minor splashes/spills, device openings for maintenance on bottom of device, all ports on the side panels. DAQ isolation card completely passive and sealed. IPX rating – unknown, however, manufacturers of the instrumentation enclosure have been contacted for the additional information. If provided, the clinical physics team will be notified with this information. ZENPPG is not anticipated to come into contact with fluids during use. 	1	4	4	PK ZP	[Redacted]
2.5	System will be used in the operating theatre – potential for electromagnetic interference with other CE-marked medical equipment or	4	4	16	<ul style="list-style-type: none"> No significant ferromagnetic components are included. The device will not be connected to external electrical supplies during use. 	1	4	4	PK ZP	[Redacted]

Definition Rating	Rare (not expected to occur for years)	Unlikely (expected to occur at least annually)	Possible (expected to occur monthly)	Likely (expected to occur at least weekly)	Almost certain (expected to occur at least daily)
Definition	Insignificant (minimal injury, loss/interruption of > 1 hour, <£10K finance loss, potential for public concern)	Minor (minor injury/illness, loss /interruption of > 8 hours, financial loss between £10K and < £50K, local medial coverage, short term public concern)	Moderate (Moderate injury, loss/interruption > 1 day, financial loss between £50K and £500K, local media coverage Long term reduction in public confidence)	Major (Major injury leading to long term incapacity/disability, loss/interruption > 1 week, financial loss between 500K and 1M, National Media coverage, service well below reasonable public expectation)	Catastrophic (Death multiple permanent or irreversible health effects, Permanent loss of service or facility, financial losses >5M, National media coverage, MP Concern, total loss of public confidence)
Rating	1	2	3	4	5

*As defined in the Barts Health NHS Trust Risk Assessment Policy (Ref: COR/POL/004/2015-001)



	other equipment may interfere with the investigational device			<ul style="list-style-type: none"> Reciprocal interference effects have been minimised using earthed metallic (aluminium) casing. ZenPPG enclosure incorporates EMI shielding (metal casing) and additional internal earthed metal cases around sensitive individual components. There are possibilities of CE-marked equipment such as the diathermy, interfering with ZenPPG. Data will only be recorded when diathermy is not in operation, although the intraluminal sensor may be in situ in the rectum during diathermy but will be switched off. Alternatively, the consequence of interference with the ZenPPG would result to partial data collection. Laptop – will be placed outside the patient environment (1.2m) 					
--	---	--	--	--	--	--	--	--	--

Likelihood*	Definition Rating	Rare (not expected to occur for years)	Unlikely (expected to occur at least annually)	Possible (expected to occur monthly)	Likely (expected to occur at least weekly)	Almost certain (expected to occur at least daily)
Consequence*	Rating	1	2	3	4	5
Definition	Rating	1	2	3	4	5
	Definition	1	2	3	4	5

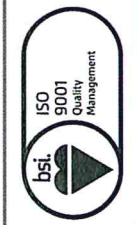
*As defined in the Barts Health NHS Trust Risk Assessment Policy (Ref: COR/POL/004/2015-001)



3.0 BIOLOGICAL AND CHEMICAL HAZARDS	Risk grading before control		Recommended control measures	Risk grading after control		Person(s) responsible	Sign	
	Likelihood	Consequence		Risk Score	Likelihood			Consequence
3.1 Infection risk if equipment is not adequately cleaned/decontaminated	4	4	<ul style="list-style-type: none"> Intraluminal sensor will be placed within a single use, sterile plastic sheath/tubing. The sheath will cover the whole of the sensor and will be replaced after every use. Intraluminal sensor and associated equipment will be cleaned and disinfected between uses as per the Trust's Infection Prevention and Control (IPC) policies and procedure and using products recommended by the Trust's IPC Team. 	1	4	4	PK MT ZP	[Redacted]
3.2 Potential biological risk due to device being incompatible with tissue.	3	4	<ul style="list-style-type: none"> All materials used are of similar materials used with pulse oximetry devices. The plastic sheath/tubing is sterile, latex-free, biocompatible and clinically approved. They are single use materials packed within sealed pouches. This plastic sheath/tubing would be the only material in contact with the tissue. The developed sensor will be fully encapsulated within the 	1	3	3	PK ZP MT	[Redacted]

Likelihood*	Definition Rating	Rare (not expected to occur for years)			Unlikely (expected to occur at least annually)			Possible (expected to occur monthly)			Likely (expected to occur at least weekly)			Almost certain (expected to occur at least daily)		
		1	2	3	1	2	3	1	2	3	1	2	3	1	2	3
Consequence*	Definition	Insignificant (minimal injury, loss/interruption of > 1 hour, <£10K finance loss, potential for public concern)	Minor (minor injury/illness, loss /interruption of > 8 hours, financial loss between £10K and < £50K, local medial coverage, short term public concern)	Moderate (Moderate injury, loss/interruption > 1 day, financial loss between £50K and £500K, local media coverage Long term reduction in public confidence)	Major (Major injury leading to long term incapacity/disability, loss/interruption > 1 week, financial loss between 500K and 1M, National Media coverage, service well below reasonable public expectation)	Catastrophic (Death multiple permanent or irreversible health effects, Permanent loss of service or facility, financial losses >5M, National media coverage, MP Concern, total loss of public confidence)										
	Rating	1	2	3	1	2	3	1	2	3	1	2	3	1	2	3

*As defined in the Barts Health NHS Trust Risk Assessment Policy (Ref: COR/POL/004/2015-001)



4.2	Perforation of colon by intraluminal sensor or the indwelling cable can snap causing perforation.	3	4	12	<ul style="list-style-type: none"> the second channel of the box (finger sensor). During use, current will be limited to 20-40mA. Patient is electrically and thermally isolated by the medical epoxy and sterile plastic sheath/tubing. All corners of the intraluminal sensor have been rounded. Medical epoxy sealant has been placed over the main electronic components of the intraluminal sensor that greatly reduce the effect of the components abrasiveness on tissue surfaces. As the sensor will be placed within medically approved, sterile plastic sheath/tubing, these materials are of smooth surfaces. Insertion of the sensor by the surgeon will be under direct vision through the anal canal into the rectum, aided by a proctoscope. Evaluation of the intraluminal sensor will be in the normal left 	1	4	4	<p>PK ZP MT</p>
4.3	Device will be used whilst patient is undergoing colon	3	3	9	<ul style="list-style-type: none"> the second channel of the box (finger sensor). During use, current will be limited to 20-40mA. Patient is electrically and thermally isolated by the medical epoxy and sterile plastic sheath/tubing. All corners of the intraluminal sensor have been rounded. Medical epoxy sealant has been placed over the main electronic components of the intraluminal sensor that greatly reduce the effect of the components abrasiveness on tissue surfaces. As the sensor will be placed within medically approved, sterile plastic sheath/tubing, these materials are of smooth surfaces. Insertion of the sensor by the surgeon will be under direct vision through the anal canal into the rectum, aided by a proctoscope. Evaluation of the intraluminal sensor will be in the normal left 	1	3	3	<p>PK ZP</p>

Likelihood*	Definition Rating	1	2	3	4	5
Consequence*	Definition Rating	1	2	3	4	5
		Rare (not expected to occur for years)	Unlikely (expected to occur at least annually)	Possible (expected to occur monthly)	Likely (expected to occur at least weekly)	Almost certain (expected to occur at least daily)
		Insignificant (minimal injury, loss/interruption of > 1 hour, <£10K finance loss, potential for public concern)	Minor (minor injury/illness, loss /interruption of > 8 hours, financial loss between £10K and < £50K, local medial coverage, short term public concern)	Moderate (Moderate injury, loss/interruption > 1 day, financial loss between £50K and £500K, local media coverage Long term reduction in public confidence)	Major (Major injury leading to long term incapacity/disability, loss/interruption > 1 week, financial loss between 500K and 1M, National Media coverage, service well below reasonable public expectation)	Catastrophic (Death multiple permanent or irreversible health effects, Permanent loss of service or facility, financial losses >5M, National media coverage, IMP Concern, total loss of public confidence)

*As defined in the Barts Health NHS Trust Risk Assessment Policy (Ref: COR/POL/004/2015-001)



Risk Assessment Form

	surgery. Risk of device interfering/disrupting surgery.			colon and rectum of patients undergoing right-sided bowel surgery or small bowel surgery. <ul style="list-style-type: none"> Measurements are obtained away from the field of surgery and pathology, therefore no adverse events or direct impact on patients' care is anticipated. 				MT	[Redacted]
4.4.	Risk of equipment failure	3	3	9	<ul style="list-style-type: none"> Failure of any system components (including intraluminal sensor) is not expected to cause harm as the system will switch off. All software used in clinical trial is industry standard. Windows 10, LabVIEW (National Instruments) The software is for data logging and rudimentary display of raw signals to the investigator only. For the clinical trial, the consequence would be the result of partial data collection. 	1	2	2	PK ZP
4.5	Equipment failure due to lack of service/maintenance	3	3	9	<ul style="list-style-type: none"> Service/maintenance will be inspected always, before and after studies by the study investigator. The intraluminal sensor has been evaluated with the buccal 	1	3	3	PK ZP

Likelihood*	Definition Rating	Rare (not expected to occur for years)	Unlikely (expected to occur at least annually)	Possible (expected to occur monthly)	Likely (expected to occur at least weekly)	Almost certain (expected to occur at least daily)
Consequence*	Definition	1	2	3	4	5
Rating	Rating	1	2	3	4	5
		Insignificant (minimal injury, loss/interruption of > 1 hour, <£10K finance loss, potential for public concern)	Minor (minor injury/illness, loss /interruption of > 8 hours, financial loss between £10K and < £50K, local media coverage, short term public concern)	Moderate (Moderate injury, loss/interruption > 1 day, financial loss between £50K and £500K, local media coverage Long term reduction in public confidence)	Major (Major injury leading to long term incapacity/disability, loss/interruption > 1 week, financial loss between 500K and 1M, National Media coverage, service well below reasonable public expectation)	Catastrophic (Death multiple permanent or irreversible health effects, Permanent loss of service or facility, financial losses >5M, National media coverage, MP Concern, total loss of public confidence)

*As defined in the Barts Health NHS Trust Risk Assessment Policy (Ref: COR/POL/004/2015-001)



Risk Assessment Form

4.6	Device used by researchers without specialist training resulting in incorrect use – who will train users?	4	4	16	<p>mucosa (inner cheek) with reference to the periphery (finger). The blood oxygen saturation was determined using the empirically derived calibration equation ($110 - 25R$), where R is the ratio of ratio of the signal amplitudes obtained from the dual wavelengths of the optical components.</p> <ul style="list-style-type: none"> The blood oxygen saturation results were found to be in close agreement, with a correlation coefficient (r^2) of 0.80 ($p < 0.05$). This can be found in the published conference paper provided. Strictly one device, one user policy. Only investigators and researchers assigned to the research/trial will be using the device. Surgeon (MT) is trained to insert the device. Study investigator (ZP) will control the software and hardware components of the system. 	1	4	4	<p>PK ZP MT</p>
-----	---	---	---	----	--	---	---	---	-------------------------

Likelihood*	Definition Rating	Rare (not expected to occur for years)	Unlikely (expected to occur at least annually)	Possible (expected to occur monthly)	Likely (expected to occur at least weekly)	Almost certain (expected to occur at least daily)
Consequence*	Definition	1 <i>Insignificant</i> (minimal injury, loss/interruption of > 1 hour, <£10K finance loss, potential for public concern)	2 <i>Minor</i> (minor injury/illness, loss /interruption of > 8 hours, financial loss between £10K and < £50K, local medial coverage, short term public concern)	3 <i>Moderate</i> (Moderate injury, loss/interruption > 1 day, financial loss between £50K and £500K, local media coverage Long term reduction in public confidence)	4 <i>Major</i> (Major injury leading to long term incapacity/disability, loss/interruption > 1 week, financial loss between 500K and 1M, National Media coverage, service well below reasonable public expectation)	5 <i>Catastrophic</i> (Death multiple permanent or irreversible health effects, Permanent loss of service or facility, financial losses >5M, National media coverage, MP Concern, total loss of public confidence)
Rating	Rating	1	2	3	4	5

*As defined in the Barts Health NHS Trust Risk Assessment Policy (Ref: COR/POL/004/2015-001)



Risk Assessment Form

5.0 INFORMATION HAZARDS	Risk grading before control		Recommended control measures	Risk grading after control		Person(s) responsible	Sign
	Likelihood	Consequence		Risk Score	Likelihood		
5.1 Lack of appropriate instructions on device use	3	3	<ul style="list-style-type: none"> Instructions for use available. 	1	1	PK ZP	

Completed By:

Signed:

Date:

13/02/2018

Likelihood*	Definition Rating	Rare (not expected to occur for years)		Unlikely (expected to occur at least annually)		Possible (expected to occur monthly)		Likely (expected to occur at least weekly)		Almost certain (expected to occur at least daily)	
		1	2	3	4	5	6	7	8	9	
Consequence*	Definition	1	2	3	4	5	6	7	8	9	10
		<p><i>Insignificant</i> (minimal injury, loss/interruption of > 1 hour, <£10K finance loss, potential for public concern)</p>	<p><i>Minor</i> (minor injury/illness, loss /interruption of > 8 hours, financial loss between £10K and < £50K, local media coverage, short term public concern)</p>	<p><i>Moderate</i> (Moderate injury, loss/interruption > 1 day, financial loss between £50K and £500K, local media coverage Long term reduction in public confidence)</p>	<p><i>Major</i> (Major injury leading to long term incapacity/disability, loss/interruption > 1 week, financial loss between 500K and 1M, National media coverage, service well below reasonable public expectation)</p>	<p><i>Catastrophic</i> (Death multiple permanent or irreversible health effects, Permanent loss of service or facility, financial losses >5M, National media coverage, MP Concern, total loss of public confidence)</p>					

*As defined in the Barts Health NHS Trust Risk Assessment Policy (Ref: COR/POL/004/2015-001)

Appendix D

Health Research Authority (HRA) documentation

Professor Panayiotis Kyriacou
City, University of London
Northampton Square
London
EC1V 0HB
p.kyriacou@city.ac.uk

Email: hra.approval@nhs.net

16 June 2017 **[Re-issued 28 June 2018 – to correct version control on documentation and confirmation that MHRA is not required for the device being used in the study]**

Dear Professor Kyriacou,

Letter of HRA Approval

Study title:	An indwelling optical sensor for monitoring large bowel tissue perfusion.
IRAS project ID:	213233
Protocol number:	RCBE-ZP-16/01
REC reference:	17/LO/0010
Sponsor	City, University of London

I am pleased to confirm that **HRA Approval** has been given for the above referenced study, on the basis described in the application form, protocol, supporting documentation and any clarifications noted in this letter.

Participation of NHS Organisations in England

The sponsor should now provide a copy of this letter to all participating NHS organisations in England.

Appendix B provides important information for sponsors and participating NHS organisations in England for arranging and confirming capacity and capability. **Please read *Appendix B* carefully**, in particular the following sections:

- *Participating NHS organisations in England* – this clarifies the types of participating organisations in the study and whether or not all organisations will be undertaking the same activities
- *Confirmation of capacity and capability* - this confirms whether or not each type of participating NHS organisation in England is expected to give formal confirmation of capacity and capability. Where formal confirmation is not expected, the section also provides details on the time limit given to participating organisations to opt out of the study, or request additional time, before their participation is assumed.
- *Allocation of responsibilities and rights are agreed and documented (4.1 of HRA assessment criteria)* - this provides detail on the form of agreement to be used in the study to confirm capacity and capability, where applicable.

Further information on funding, HR processes, and compliance with HRA criteria and standards is also provided.

It is critical that you involve both the research management function (e.g. R&D office) supporting each organisation and the local research team (where there is one) in setting up your study. Contact details and further information about working with the research management function for each organisation can be accessed from www.hra.nhs.uk/hra-approval.

Appendices

The HRA Approval letter contains the following appendices:

- A – List of documents reviewed during HRA assessment
- B – Summary of HRA assessment

After HRA Approval

The document “*After Ethical Review – guidance for sponsors and investigators*”, issued with your REC favourable opinion, gives detailed guidance on reporting expectations for studies, including:

- Registration of research
- Notifying amendments
- Notifying the end of the study

The HRA website also provides guidance on these topics, and is updated in the light of changes in reporting expectations or procedures.

In addition to the guidance in the above, please note the following:

- HRA Approval applies for the duration of your REC favourable opinion, unless otherwise notified in writing by the HRA.
- Substantial amendments should be submitted directly to the Research Ethics Committee, as detailed in the *After Ethical Review* document. Non-substantial amendments should be submitted for review by the HRA using the form provided on the [HRA website](#), and emailed to hra.amendments@nhs.net.
- The HRA will categorise amendments (substantial and non-substantial) and issue confirmation of continued HRA Approval. Further details can be found on the [HRA website](#).

Scope

HRA Approval provides an approval for research involving patients or staff in NHS organisations in England.

If your study involves NHS organisations in other countries in the UK, please contact the relevant national coordinating functions for support and advice. Further information can be found at <http://www.hra.nhs.uk/resources/applying-for-reviews/nhs-hsc-rd-review/>.

If there are participating non-NHS organisations, local agreement should be obtained in accordance with the procedures of the local participating non-NHS organisation.

User Feedback

The Health Research Authority is continually striving to provide a high quality service to all applicants and sponsors. You are invited to give your view of the service you have received and the application procedure. If you wish to make your views known please use the feedback form available on the HRA website: <http://www.hra.nhs.uk/about-the-hra/governance/quality-assurance/>.

HRA Training

We are pleased to welcome researchers and research management staff at our training days – see details at <http://www.hra.nhs.uk/hra-training/>

Your IRAS project ID is **213233**. Please quote this on all correspondence.

Yours sincerely

██████████
Assessor

Email: hra.approval@nhs.net

Copy to: *Miss Zaibaa Patel, City, University of London [Student]*
zaibaa.patel.1@city.ac.uk
██████████, *City, University of London [Sponsor Contact]*
██████████ [@city.ac.uk](mailto:██████████@city.ac.uk)
██████████ *Barts Health NHS Trust [Lead NHS R&D Contact]*
██████████ [@bartshealth.nhs.uk](mailto:██████████@bartshealth.nhs.uk)

Appendix A - List of Documents

The final document set assessed and approved by HRA Approval is listed below.

<i>Document</i>	<i>Version</i>	<i>Date</i>
Contract/Study Agreement [Schedule of Events]	1	17 May 2017
Contract/Study Agreement [Statement of Activities]	1	17 May 2017
Evidence of Sponsor insurance or indemnity (non NHS Sponsors only) [Insurance]		Issued on 07 August 2015
IRAS Checklist XML [Checklist_17022017]		17 February 2017
Other [Principal Investigator CV]	1	17 November 2016
Participant consent form	2	01 February 2017
Participant information sheet (PIS)	2	17 February 2017
REC Application Form [REC_Form_16022017]		16 February 2017
Research protocol or project proposal [Final protocol]	1	15 November 2016
Summary CV for Chief Investigator (CI) [Prof Kyriacou CV]		15 November 2016
Summary CV for student [Student CV]		15 November 2016
Summary CV for supervisor (student research) [Prof Kyriacou CV]		15 November 2016

Appendix B - Summary of HRA Assessment

This appendix provides assurance to you, the sponsor and the NHS in England that the study, as reviewed for HRA Approval, is compliant with relevant standards. It also provides information and clarification, where appropriate, to participating NHS organisations in England to assist in assessing and arranging capacity and capability.

For information on how the sponsor should be working with participating NHS organisations in England, please refer to the, *participating NHS organisations, capacity and capability and Allocation of responsibilities and rights are agreed and documented (4.1 of HRA assessment criteria)* sections in this appendix.

The following person is the sponsor contact for the purpose of addressing participating organisation questions relating to the study:

Name: Mr Mohamed Thaha

Tel: 0207 882 8747

Email: m.a.thaha@qmul.ac.uk

HRA assessment criteria

Section	HRA Assessment Criteria	Compliant with Standards	Comments
1.1	IRAS application completed correctly	Yes	The REC Form has been submitted instead of IRAS Form. IRAS [A36] has been left blank.
2.1	Participant information/consent documents and consent process	Yes	The applicant has confirmed that the research team form members of the clinical care team who will make the initial contact with prospective participants. Following REC review, the applicant submitted updated participant information sheet and consent form to bring them in line with HRA Standards (e.g. inclusion of IRAS ID).
3.1	Protocol assessment	Yes	No comments
4.1	Allocation of responsibilities and rights are agreed and	Yes	The sponsor has provided statement of activities and schedule of events.

Section	HRA Assessment Criteria	Compliant with Standards	Comments
	documented		The sponsor has confirmed that no other agreement will be used, or is required.
4.2	Insurance/indemnity arrangements assessed	Yes	IRAS [A76-3] should indicate that NHS Indemnity Scheme applies to the conduct of the study. Where applicable, independent contractors (e.g. General Practitioners) should ensure that the professional indemnity provided by their medical defence organisation covers the activities expected of them for this research study.
4.3	Financial arrangements assessed	Yes	The study will not receive any external funding.
5.1	Compliance with the Data Protection Act and data security issues assessed	Yes	No comments
5.2	CTIMPS – Arrangements for compliance with the Clinical Trials Regulations assessed	Not Applicable	No comments
5.3	Compliance with any applicable laws or regulations	Yes	No comments
6.1	NHS Research Ethics Committee favourable opinion received for applicable studies	Yes	REC Favourable Opinion was issued by London –City & East Research Ethics Committee on 24 February 2017.
6.2	CTIMPS – Clinical Trials Authorisation (CTA) letter received	Not Applicable	No comments
6.3	Devices – MHRA notice of no objection received	Not Applicable	MHRA have confirmed notice of no objection is not required for the device being used in the study.
6.4	Other regulatory approvals and authorisations received	Not Applicable	No comments

Participating NHS Organisations in England

This provides detail on the types of participating NHS organisations in the study and a statement as to whether the activities at all organisations are the same or different.

There is one site type participating in this study. All research activities are the same as described in the study protocol.

The Chief Investigator or sponsor should share relevant study documents with participating NHS organisations in England in order to put arrangements in place to deliver the study. The documents should be sent to both the local study team, where applicable, and the office providing the research management function at the participating organisation. For NIHR CRN Portfolio studies, the Local LCRN contact should also be copied into this correspondence. For further guidance on working with participating NHS organisations please see the HRA website.

If chief investigators, sponsors or principal investigators are asked to complete site level forms for participating NHS organisations in England which are not provided in IRAS or on the HRA website, the chief investigator, sponsor or principal investigator should notify the HRA immediately at hra.approval@nhs.net. The HRA will work with these organisations to achieve a consistent approach to information provision.

Confirmation of Capacity and Capability

This describes whether formal confirmation of capacity and capability is expected from participating NHS organisations in England.

Participating NHS organisations in England **will be expected to formally confirm their capacity and capability** to host this research.

- The sponsor should ensure that participating NHS organisations are provided with a copy of this letter and all relevant study documentation, and work jointly with NHS organisations to arrange capacity and capability whilst the HRA assessment is ongoing.
- Further detail on how capacity and capability will be confirmed by participating NHS organisations, following issue of the Letter of HRA Approval, is provided in the *Participating NHS Organisations and Allocation of responsibilities and rights are agreed and documented (4.1 of HRA assessment criteria)* sections of this appendix.

The [Assessing, Arranging, and Confirming](#) document on the HRA website provides further information for the sponsor and NHS organisations on assessing, arranging and confirming capacity and capability.

Principal Investigator Suitability

This confirms whether the sponsor position on whether a PI, LC or neither should be in place is correct for each type of participating NHS organisation in England and the minimum expectations for education, training and experience that PIs should meet (where applicable).

The sponsor has confirmed that a Local Principal Investigator is required at participating NHS sites, and has already been identified.

GCP training is not a generic training expectation, in line with the [HRA statement on training expectations](#).

Appendix E

Clinical trial approval and protocol

This includes documentations of the clinical trial decision letter and selected sections of the study protocol. The selected sections includes a summary of the clinical trial and the inclusion and exclusion criteria for participants.



Health Research Authority

London - City & East Research Ethics Committee

Bristol Research Ethics Committee Centre
Whitefriars
Level 3, Block B
Lewins Mead
Bristol
BS1 2NT

Telephone: 02071048033/53

Please note: This is the favourable opinion of the REC only and does not allow you to start your study at NHS sites in England until you receive HRA Approval

24 February 2017

Miss Zaibaa Patel
PhD Research Student
City, University of London
Northampton Square
London EC1V 0HB

Dear Miss Patel

Study title: An indwelling optical sensor for monitoring large bowel tissue perfusion.
REC reference: 17/LO/0010
Protocol number: RCBE-ZP-16/01
IRAS project ID: 213233

Thank you for your submission of 16 February 2017, responding to the Committee's request for further information on the above research and submitting revised documentation.

The further information was considered in correspondence by a Sub-Committee of the REC. A list of the Sub-Committee members is attached.

We plan to publish your research summary wording for the above study on the HRA website, together with your contact details. Publication will be no earlier than three months from the date of this opinion letter. Should you wish to provide a substitute contact point, require further information, or wish to make a request to postpone publication, please contact hra.studyregistration@nhs.net outlining the reasons for your request.

Confirmation of ethical opinion

On behalf of the Committee, I am pleased to confirm a favourable ethical opinion for the above

research on the basis described in the application form, protocol and supporting documentation as revised, subject to the conditions specified below.

Conditions of the favourable opinion

The REC favourable opinion is subject to the following conditions being met prior to the start of the study.

1. *The Committee was satisfied with the addition of the sentence "The study may increase the duration of the entire procedure by approximately 5 minutes." However it takes 30 minutes to do the test: so it should be briefly explained why it only adds 5 minutes to the procedure*

You should notify the REC once all conditions have been met (except for site approvals from host organisations) and provide copies of any revised documentation with updated version numbers. Revised documents should be submitted to the REC electronically from IRAS. The REC will acknowledge receipt and provide a final list of the approved documentation for the study, which you can make available to host organisations to facilitate their permission for the study. Failure to provide the final versions to the REC may cause delay in obtaining permissions.

Management permission must be obtained from each host organisation prior to the start of the study at the site concerned.

Management permission should be sought from all NHS organisations involved in the study in accordance with NHS research governance arrangements. Each NHS organisation must confirm through the signing of agreements and/or other documents that it has given permission for the research to proceed (except where explicitly specified otherwise).

Guidance on applying for NHS permission for research is available in the Integrated Research Application System, www.hra.nhs.uk or at <http://www.rdforum.nhs.uk>.

Where a NHS organisation's role in the study is limited to identifying and referring potential participants to research sites ("participant identification centre"), guidance should be sought from the R&D office on the information it requires to give permission for this activity.

For non-NHS sites, site management permission should be obtained in accordance with the procedures of the relevant host organisation.

Sponsors are not required to notify the Committee of management permissions from host organisations

Registration of Clinical Trials

All clinical trials (defined as the first four categories on the IRAS filter page) must be registered on a publically accessible database within 6 weeks of recruitment of the first participant (for medical device studies, within the timeline determined by the current registration and publication trees).

There is no requirement to separately notify the REC but you should do so at the earliest opportunity e.g. when submitting an amendment. We will audit the registration details as part of the annual progress reporting process.

To ensure transparency in research, we strongly recommend that all research is registered but for non-clinical trials this is not currently mandatory.

If a sponsor wishes to request a deferral for study registration within the required timeframe, they should contact hra.studyregistration@nhs.net. The expectation is that all clinical trials will be registered, however, in exceptional circumstances non registration may be permissible with prior agreement from the HRA. Guidance on where to register is provided on the HRA website.

It is the responsibility of the sponsor to ensure that all the conditions are complied with before the start of the study or its initiation at a particular site (as applicable).

Ethical review of research sites

NHS sites

The favourable opinion applies to all NHS sites taking part in the study, subject to management permission being obtained from the NHS/HSC R&D office prior to the start of the study (see "Conditions of the favourable opinion" below).

Non-NHS sites

The Committee has not yet completed any site-specific assessment (SSA) for the non-NHS research site(s) taking part in this study. The favourable opinion does not therefore apply to any non-NHS site at present. We will write to you again as soon as an SSA application(s) has been reviewed. In the meantime no study procedures should be initiated at non-NHS sites.

Approved documents

The final list of documents reviewed and approved by the Committee is as follows:

<i>Document</i>	<i>Version</i>	<i>Date</i>
Evidence of Sponsor insurance or indemnity (non NHS Sponsors only) [Insurance]	1	17 November 2016
Other [Principle Investigator CV]	1	17 November 2016
Participant consent form [Consent form]	1.1	17 November 2016
Participant information sheet (PIS) [Tracked changes PIS]	2	17 February 2017
REC Application Form [REC_Form_16022017]		16 February 2017
Research protocol or project proposal [Final protocol]	1.1	17 November 2016
Summary CV for Chief Investigator (CI) [Prof Kyriacou CV]	1	15 November 2016
Summary CV for student [Student CV]	1	15 November 2016
Summary CV for supervisor (student research) [Prof Kyriacou CV]	1	15 November 2016

Statement of compliance

The Committee is constituted in accordance with the Governance Arrangements for Research Ethics Committees and complies fully with the Standard Operating Procedures for Research

Ethics Committees in the UK.

After ethical review

Reporting requirements

The attached document “*After ethical review – guidance for researchers*” gives detailed guidance on reporting requirements for studies with a favourable opinion, including:

- Notifying substantial amendments
- Adding new sites and investigators
- Notification of serious breaches of the protocol
- Progress and safety reports
- Notifying the end of the study

The HRA website also provides guidance on these topics, which is updated in the light of changes in reporting requirements or procedures.

User Feedback

The Health Research Authority is continually striving to provide a high quality service to all applicants and sponsors. You are invited to give your view of the service you have received and the application procedure. If you wish to make your views known please use the feedback form available on the HRA website:

<http://www.hra.nhs.uk/about-the-hra/governance/quality-assurance/>

HRA Training

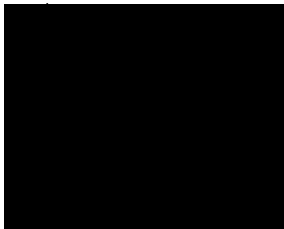
We are pleased to welcome researchers and R&D staff at our training days – see details at <http://www.hra.nhs.uk/hra-training/>

17/LO/0010

Please quote this number on all correspondence

With the Committee’s best wishes for the success of this project.

Yours sincerely



pp 
Chair

Email:nrescommittee.london-cityandeast@nhs.net

Study Summary

Title	An indwelling optical sensor for monitoring large bowel tissue perfusion.
Short Title	Intraluminal optical monitoring of large bowel tissue perfusion.
Protocol Version and Number	Version 1, RCBE-ZP-16/01
Sponsor	City, University of London Northampton Square, London, EC1V 0HB, United Kingdom
Funder	City, University of London PhD studentship
Methodology	Proof of principle
Study duration	Expected to take approximately 6 months for data collection.
Study site	Operating Theatres, The Royal London Hospital, Barts Health NHS Trust
Study Design	A single centre prospective series.
Objectives	<p>The aim of this study is to evaluate a novel intraluminal optical sensor, based on photoplethysmography/ (PPG), for the assessment of large bowel perfusion in humans. The study specifically aims to investigate the feasibility of reliably obtaining physiological signals using the newly developed sensor applied from within the colon/rectum. The study will also assess patient acceptability and ability to recruit.</p> <p>A novel intraluminal optical sensor has been developed. The probe will be inserted under vision through the anal canal into the rectum aided by a proctoscope. This allows continuous monitoring and assessment of the perfusion status and blood oxygen saturation from the bowel.</p> <p>The study aims to evaluate the new intraluminal optical sensor in the normal left colon and rectum of patients undergoing either right-sided bowel surgery, left-sided bowel surgery excluding for rectal diseases, small bowel surgery, diagnostic laparoscopy for abdominal conditions but excluding rectal disease or anorectum examination for diagnostic purposes for perianal disease. Since the measurements are obtained from the left side of the colon (specifically from the rectum); away from the field of surgery and pathology, no significant adverse events or direct impact on patient's care is anticipated.</p>
Sample Size	30
Participant Time	Maximum 30 minutes of measurement time.
Study Population	Patients undergoing either right-sided large bowel surgery, left-sided large bowel surgery but excluding rectal surgery, diagnostic laparoscopy for abdominal conditions but excluding disease of the rectum, surgery to the small bowel or examination of anorectum for diagnostic purposes.
Study Parameters	The following measurements will be obtained from the large bowel tissue:

	<ol style="list-style-type: none"> 1. AC and DC PPG components at two wavelengths, red and infrared. 2. Arterial oxygen saturation estimated by two-wavelength pulse oximetry. 3. Perfusion index estimated by infrared PPG. 4. Estimation of tissue oxygenation index estimated by optical reflectance spectroscopy.
Data Analysis	<p>The following post hoc measurements will be taken from the recorded data:</p> <ul style="list-style-type: none"> • Mean amplitude of PPG signals at two wavelengths, at different positions. • Arterial oxygen saturation values at all monitoring positions. • The percentage of time the data could be obtained that is useful for bio signal interpretation and processing. • The percentage of total time with no signal and/or signal artefacts. • Analysis of variance (e.g. t-test) comparing paired measured variables at different measurement sites.
Safety Analysis	<p>Adverse events and vital signs for each subject will be tabulated and summarised in the case report form.</p>

Time and Events Table

	Pre-Screening Visit	Trial Day (in operating theatre)
Patient Information Sheet	X	
Informed Consent Form Signed	X	
Vital Signs		Baseline and during measurements (30 mins)
Height / Weight / BMI	X	
Concomitant Meds		X
PPG Measurements		Spot measurements from distal most left colon (recto-sigmoid junction) and rectum. The intraluminal optical sensor would be inserted through the anal canal; advancing to a maximum distance of 15 cm from the back passage. Incrementally withdrawing the intraluminal optical sensor by 3 cm, repeated measurements lasting for up to 5 minutes would be taken. Therefore, the position of the intraluminal optical sensor would be at 15, 12, 9, 6 and 3 cm, from the back passage. Each measurement lasting a maximum of 5 minutes, with a total time of study for each individual taking no longer than 30 minutes. Average actual measurement time at each level would be for 1 minute after 1 minute of stabilisation period.

Patient Population

All patients will be recruited from the Department of Colorectal Surgery at the Royal London Hospital, Barts Health NHS Trust surgical lists prior to their surgical procedure by the study investigators. The study will be carried out on 30 patients undergoing either right-sided large bowel surgery, left sided large bowel surgery but excluding surgery for the rectum, surgery to the small bowel, diagnostic laparoscopy for abdominal conditions but excluding for rectum or anorectum examinations for diagnostic purposes of perianal conditions.

Patients will be clearly informed that participation in the study is voluntary and that refusal to participate will in no way disadvantage them.

The patients will be provided with a full explanation of the nature, purpose and requirements of the study including Patient Information Sheet (PIS) and will sign an Informed Consent Form (ICF). The patients will be given more than 24 hours to consider their participation in the study once they have been introduced to the study. The patient consent form will be countersigned by researchers only when satisfied that the patient has understood the patient information sheet and is willing to give informed written consent to participate in the study, and that the patient understands that it is their right to withdraw from the trial at any time without the need to explain their reasons for doing so and without prejudice to their future treatment.

No patients will be recruited if they lack capacity and if it is deemed that capacity is lost during the trial period. If so, the patient will be removed from the trial and all information relating to them will be destroyed.

Inclusion Criteria

In order to be eligible for inclusion in the study, the participants must meet the following criteria:

- Adult patients aged (≥ 18 years) from whom full written informed consent will be sought.
- Patients who fall into the American Society of Anaesthesiologists scoring system of ASA I–IV.
- Patients with no known clotting abnormalities.
- Patients undergoing right-colonic, transverse colonic and left colonic (descending colon and sigmoid colon) surgery.
- Patients undergoing surgery to their small bowel.
- Patients undergoing appendicectomy surgery.
- Diagnostic laparoscopy for abdominal conditions but excluding for conditions relating to the rectum
- Examination of anorectum for diagnostic purposes of perianal conditions (perianal skin, anal sphincter and anal canal).
- Patients who have not had previous major left-sided large bowel surgery.
- Patients who do not have rectal disorders or disease.
- Patients without anatomical abnormalities of the lower gastro–intestinal tract.
- Potential participants would be approached only if they have a good understanding of spoken and written English.

Exclusion Criteria

Patients will not be included in the study if they meet any of the following exclusion criteria:

- Patients who decline consent.
- Patients requiring emergency surgery where obtaining informed consent is not possible.
- Patients with a known clotting abnormality.
- Patients with anatomical abnormalities of the lower gastro-intestinal tract.
- Patients in whom surgery carries unusually high risk.
- Patients who have serious underlying conditions or are moribund.
- Patients who previously had rectal disorder or disease.
- Patients who have had previous major bowel surgery in the left colon and or rectum.
- Patients who cannot give consent (dementia, unconscious, etc.).
- Pregnant women.
- Patients with a latex allergy.
- Patients whom any member of the surgical or anaesthetic team is unhappy with their participation in the trial.